UNIVERSITY OF LIVERPOOL

Modelling sediment storage times in alluvial floodplains

Thesis submitted in accordance with the requirements of the University of Liverpool for the degree of Doctor of Philosophy

by

Christopher John Feeney

April 2020

Abstract

Soil erosion rates are accelerating worldwide as climate change effects and human population pressures, including agricultural expansion, degrade the land surface. Fluvial systems transfer sediments from uplands to depositional landforms and basins downstream. However, only a fraction of eroded material will ultimately transfer to catchment outlets – a phenomenon termed, “the sediment delivery problem”. Thus, sediment fluxes to the coast are declining in many river catchments, as a result of storage behind dams and within landforms such as floodplains and alluvial terraces. Storage time allows us to measure the timescale of storage and removal of sediments from floodplains, which, given their spatial extent (8×10^5 to 2×10^6 km^2 of all land area), are significant in interrupting the transmission of soil erosion fluxes downstream. While sediment storage times in alluvial floodplains have been quantified before, this thesis presents the first attempts to model the impacts of various environmental and experimental conditions on sediment storage behaviour using the CAESAR-Lisflood landscape evolution model. The thesis tests the following hypotheses: i) Removal rates from storage decline with increasing floodplain age; ii) the distribution of sediment storage times is sensitive to reach-specific characteristics, vegetation cover types and changes, changing river flows, and measurement frequency; and iii) a non-linear function can be fitted to the distribution and parameterised using readily quantifiable variables.

A detailed literature review synthesised our current understanding of sediment storage times, including variables that have been quantified or hypothesised as possible controls. This culminated in a conceptual model of major controls and their interactions which was used to support the development of experiments tested in this thesis. A review of quantification techniques, including “black-box”, one-dimensional mass balance modelling approaches, and methods that calculate storage times directly from timings of geomorphic changes, justified adopting a landscape evolution modelling approach.

CAESAR-Lisflood was applied to conduct this research, as it can simulate variable channel widths, divergent flow, and both braided and meandering planforms – capturing a wider range of channel-floodplain evolution processes

than models previously used to simulate storage times. Ten 1 km-long reaches of river valleys from the north of England were used to calibrate the model, test the transferability of calibrated parameters, and verify the accuracy of simulated historical channel changes against mapped reconstructions. These simulations replicated mapped erosion, deposition and lateral migration rates reasonably well overall. Floodplain turnover times, estimated by extrapolating erosion rates, increased confidence that calibrated parameters were representative over longer timescales and revealed that all sediments stored in the floodplain would undergo exchange with the channel within 1000 years.

Using CAESAR-Lisflood, an ensemble of 9 simulations, incorporating 3 of the 10 calibrated reaches and 3 vegetation cover scenarios (forest, grass and unvegetated) – each spanning 1000 years of river channel changes – was run. Together with measuring channel changes over four different frequencies (10, 20, 50 and 100 years), a total of 36 storage time distributions was modelled, with the age and storage times of floodplain sediments calculated from timings of deposition and erosion. This was done to test whether distributions were best fit by either an exponential or a heavy-tailed decay function, with the former indicating constant erosion rates over space and time, while the latter implies that removal rates from storage decay with increasing deposit age. As well as uniform vegetation conditions, a further 15 simulations, incorporating changes in vegetation cover or flow magnitudes over time, were run, to test how storage time dynamics respond to disturbance.

This thesis demonstrates that sediment erosion rates decline with increasing floodplain age in most cases, with the strength of this relationship dependent on reach, floodplain erodibility and frequency of recorded measurements. A lognormal function can be fitted to distributions of sediment storage times in most cases, and it is possible to parameterise this function using the median storage time and measurement time-step. Coupling this storage time function with a model of stochastic sediment transport could generate predictions of decontamination times for a valley corridor enriched with polluted sediments (e.g. from mining). However, some environmental disturbances can be great enough to invalidate this storage time model – a challenge that merits further attention before application to practical environmental management contexts.

Acknowledgements

The positive experience I have had over the past 4 years producing this thesis in large part stems from the advice and support of many colleagues and friends. My special thanks go to Richard Chiverrell for his excellent ideas and guidance throughout the last couple of years since he took over as my lead supervisor. His support has been invaluable, and the regular and detailed feedback he provided on my work will have no doubt improved my thesis and submitted journal papers immensely. I would also like to thank Hugh Smith for his enthusiastic support and ideas throughout my PhD. Our early discussions about the project in January 2015, and his help with my application to become a PhD student at the University of Liverpool, really engaged me early on, and his support as my lead supervisor until February 2018 has been incredible. I am delighted that his close involvement and interest in my research continued even after he left the university to take on a job in New Zealand. I also owe a huge thank you to my other supervisors, James Cooper and Janet Hooke, for their helpful suggestions and feedback throughout – often providing alternative perspectives and ideas that had not occurred to me previously.

My supervisors have provided me with excellent opportunities in teaching and research, including as a research assistant analysing soil and sediment samples (including from termite mounds of all things!) in the lab, and as a student demonstrator in undergraduate field, lab and computer practical classes. I am grateful to Mike O'Connor and Jenny Bradley for their patient explanations of different lab procedures and help with equipment while I was working as a research assistant. My thanks also go to John Boyle, Rachel Smedley, James Lea, Kim Peters and Jonny Higham for providing me with the chance to build my teaching skills with them. I am sure that these experiences, as well as the advice and encouragement from my supervisors on my thesis, will have been instrumental if I do go on to forge an academic career.

Completing my PhD would not have been possible without the funding and training I received from the Natural Environment Research Council and the Earth, Atmosphere and Oceans Doctoral Training Programme. In particular, I would like to thank the DTP administrator, Julie Samson for all the fantastic

workshops, meet-ups and opportunities – including a public outreach event with NERC Into the Blue at Manchester Airport – she has organised over the years. In addition, fellow students I have met on the DTP at both Liverpool and Manchester Universities, and in the Roxby Building have made my time as a PhD student very enjoyable. I especially wish to thank Rachael and Ai, who I first shared an office with, for helping me to settle in and their advice early on in my PhD, and to Hannah and Hazel, for their support and being such a pleasure to now share an office with (and their patience with my untidiness!). It has also been a pleasure to work alongside past and present PhD students: Alice, Amy, Ben, Cai, Celestine, Charlotte, Chris, Connor, Fiona, Grace, Karen, Maddy, Onema, Phil, Sam, Siôn, Simon, Soeren, Thea and Veronica.

I am grateful to Dr. Rob Duller and Prof. Tom Coulthard for examining my PhD *viva voce* defence on the 21st January 2020. Their comments have helped to improve my thesis and (hopefully!) future publications. In addition, I would also like to thank Tom for the great opportunity to attend the British Society for Geomorphology postgraduate workshop in Windsor in December 2015, and as an organiser of the BSG conference that year, the chance for me to present a poster on my PhD research, in one of my first conference experiences, at Hull University in September 2017.

This PhD has not been without challenges during my personal life. My father very sadly passed away at the end of November 2017. As somebody who had completed a PhD himself, he was a regular source of encouragement and advice, and his loss was particularly difficult to come to terms with. I would like to thank my supervisors, Rich, Hugh, James and Janet, for their kindness, patience and immense support over the past 2 years. My friends within the university, Thea, Veronica, Michael and Louise, and outside, Jim, Milly, Nathan, and my partner, Liam, in particular, have been a huge source of support for me. Most of all, I am grateful to my mother, grandparents and my brothers, Nick and Alex, for all of their love and support, especially during a time when I know it was enormously difficult to do so. I am immensely grateful and indebted to all of these people, who without their help and kindness, I would have found it impossible to complete this thesis.

Contents

List of Tables

List of Figures

CHAPTER 1:

Introduction

1.1. Background and motivation for the research

As human population pressures and economic development have impacted global environmental change, some have argued that we may be living in a new geological epoch in Earth's history – the Anthropocene (e.g. Zalasiewicz et al. 2008; Syvitski & Kettner 2011). Intensification of the global hydrological cycle by anthropogenically driven climate warming (Huntington 2006) is manifested as observed increases in the average magnitude and variability of flood events of river systems worldwide (Déry et al. 2009; Gloor et al. 2013). Compounding this, as land-use change associated with agriculture and settlement expansion has proliferated, the Earth's land surface has become primed for accelerated rates of soil erosion – to the extent that anthropogenically driven erosion rates are estimated to exceed natural sediment production rates by an order of magnitude (Zalasiewicz et al. 2008 and references therein). These accelerated soil erosion rates are evident in sedimentary deposits (e.g. Chiverrell, Foster, Marshall, et al. 2009; Chiverrell, Foster, Thomas, et al. 2009; Hoffmann et al. 2009), and affect water quality, by driving the transmission of sediment-bound contaminants through river networks (Whitehead et al. 2009). Fine sediments enriched with heavy metals from mining activity for instance, that are present in the sediment sequences of floodplain terraces (e.g. Brewer & Taylor 1997) and lake basins (Boyle et al. 2015 and references therein), reflect the long-term consequences of accelerated sediment production rates that characterise the Anthropocene (Syvitski & Kettner 2011). Given their large spatial coverage – 8×10^5-2×10^6 km^2 of the Earth's land surface – (Leopold et al. 1964; Tockner & Stanford 2002; Mitsch & Gosselink 2015) and adjacency to stream channels, floodplains potentially accumulate significant volumes of contaminated sediments and retain these for vast periods of time (e.g. Dennis et al. 2009). Developing our understanding of sediment storage and transmission through river networks – particularly storage times in landforms such as floodplains – is required in order to better understand and manage the long-term effects of the afore-mentioned global environmental changes in the future (Slaymaker et al. 2009).

Fluvial systems act as conduits for the transfer of sediments from source to sink (Schumm 1977). These transfers are controlled in large part by the balance of impelling forces (i.e. the erosivity of stream flows, which varies under changing flow discharge and stream slope) and resisting forces (i.e. sediment erodibility, which depends on the sedimentology of channel boundaries and the types of catchment land-use and local riparian vegetation cover) acting within the fluvial system (Fryirs & Brierley 2013). This can be conceptualised as a spectrum, with systems characterised by high-energy flows and low channel boundary resistance as efficient conveyors of sediment, and systems with low-energy flows and high resistance, the opposite (Trimble 2010). Research into catchment sediment fluxes has revealed that only a fraction of the material that is mobilised upstream will ultimately transfer to catchment outlets and be quantifiable as sediment yield – a phenomenon termed, “the sediment delivery problem”, owing to the black-box nature of the processes operating within the fluvial system to drive this disparity between upstream erosion rates and downstream sediment fluxes (Walling 1983). In many cases, sediment yield may be a function predominantly of sediment storage, rather than reflecting contemporary soil erosion rates in the upper reaches of river catchments (Trimble 1975). As sediment is transported, it undergoes exchange with surrounding landforms such as the channel bed and floodplains, in what Ferguson characterises as a “jerky conveyor belt” (Ferguson 1981). For example, while soil erosion rates may be accelerating globally (as mentioned previously), fluxes to the coastal zone are declining in many river catchments as a result of storage behind dams and within landforms such as floodplains and alluvial terraces (Syvitski 2003). We therefore need an approach that allows us to quantify these patterns of sediment fluxes over space and time.

Catchment-scale sediment fluxes can be conceptualised in the form of a sediment budget, detailing present volumes of eroded sediment from multiple locations, where these volumes are transported to, and where these are stored (e.g. Trimble 1983; Fryirs & Brierley 2001). Despite providing broad details of internal process structure (e.g. the sources of erosion and their relative contributions to total sediment fluxes within the catchment) that sediment yield

measurements alone fail to capture (Schumm 1977), Walling (1983) critiqued this approach, arguing that sediment budgets represent total volumes aggregated across all sediment erosion and storage processes over a specific timeframe. To overcome this spatial and temporal clumping, additional frameworks that specify the provenance and changes in erosion, deposition and yield rates in greater spatio-temporal detail have emerged. The concept of "(dis)connectivity" defines the water-mediated flux of material between two different parts of the fluvial system (Jain & Tandon 2010; Fryirs 2013). As Jain and Tandon (2010) explain, connectivity can either manifest between two physically connected compartments (i.e. landform to landform coupling such as hillslope-channel) (e.g. Harvey 2002) or between two physically separate (decoupled) compartments, such as coarse sediment transfers between channel bars (e.g. Hooke 2003). (Dis)Connectivity describes how the efficiency of sediment flux relationships is restricted by any limiting factor in one or more of the following dimensions: laterally, longitudinally, vertically (by landforms termed buffers, barriers and blankets, respectively) and temporally (Fryirs et al. 2007). As Fryirs (2013) notes, most sediment budget flow diagrams contract from river source to mouth, reflecting quantities of sediment (re)entering storage and indicating where sediment transport has been interrupted (e.g. at tributary junctions) over a defined period of time (see also de Vente et al. 2007). What is missing however, are timescales of sediment storage and ultimate delivery to the catchment outlet.

River catchments can be conceptualised as a "sediment-routing system" that integrates all the sediment "trajectories" (unique transport pathways including storage zones) a particle can travel along from source to sink (Allen 2008). In theory, such a model could be used to simulate the distribution of sediment delivery times through a river network to predict how long it would take for a polluted system to eventually decontaminate (Malmon et al. 2003). What is unclear however, is the role of temporary storage within floodplains in lagging sediment signals delivered from upstream (Pizzuto et al. 2017) or "shredding" them altogether (see Jerolmack & Paola 2010). That is the motivation for this research: to investigate the sediment storage times in floodplains under different environmental conditions. While multiple attempts have been made

to model storage times in floodplains (e.g. Lauer 2012; Bradley & Tucker 2013; Torres et al. 2017), the types of models employed to date have only captured single-thread meandering channels, neglecting other lateral erosion processes such as avulsions and formation of braided channel patterns. Further, these did not investigate the effect of environmental controls, such as the effects of the type and abundance of riparian vegetation on the erodibility of floodplain surfaces, or changes in the magnitudes of streamflow or rates of sediment supply on the stability of channel patterns. By quantifying the effects of these various impelling and resisting forces on floodplain evolution, this research offers a significant but hitherto untested contribution to constrain timescales of sediment storage in alluvial floodplains.

1.2. Main aim, objectives and research questions

The primary aim of this thesis is to quantify the length of time sediment remains stored in alluvial floodplains under different environmental conditions. This will be addressed by developing a method that incorporates simulating river channel changes over multi-centennial timescales and using the timings of sediment deposition and erosion to record the ages and storage times of sediment in specific locations of the floodplain. CAESAR-Lisflood is a model capable of simulating geomorphic change and sediment dynamics at catchment and reach scales (Coulthard & Van De Wiel 2006; Van De Wiel et al. 2007; Coulthard et al. 2013), and previous research is replete with applications of this model to quantify the effects of varying environmental conditions on sediment dynamics (e.g. Van De Wiel & Coulthard 2010; Coulthard & Van De Wiel 2013, 2017). Unlike most other models, it is capable of simulating both multi-thread and single-thread channel planforms (Coulthard & Van De Wiel 2006), allowing a wider range of floodplain forms and processes – including sediment storage times – to be simulated. This thesis tests a procedure that calculates the ages and storage times of sediment in floodplain surface areas from a 2D planimetric river channel change time-series simulated in CAESAR-Lisflood. Three reach-scale river systems from the north of England are chosen as the primary test sites. These reaches are highly dynamic, exhibiting significant lateral adjustment in the

position and morphology of their channels (including some evidence of braiding as well as meandering planforms) over multi-decadal time scales. Reconstructions from the overlapping historical map and daily flow record were used to calibrate parameters governing erosion rates in CAESAR-Lisflood for ten sites, and to evaluate the accuracy of simulated channel changes based on direct comparison with mapped historical changes. Calibrated parameter values, in conjunction with a synthetic flow series and parameter settings for various vegetation cover scenarios, were used to drive an ensemble of simulations of river channel change – spanning 1000 years each. A series of R scripts were developed to automate the age and storage time calculation procedure and to derive a probability density function of storage times. Deriving a probability density function of sediment storage times is important for parameterising stochastic models of particle trajectories through valley floors and predict the distribution of delivery times of sediment to catchment outlets. As catchment systems may be subject to a multitude of disturbance events, it is also important to test how the distribution of storage times may evolve in response to changing environmental conditions. If storage time distributions are sensitive to environmental perturbations, this will pose significant challenges to predicting delivery times in catchment-scale sediment-routing models, with implications for monitoring contaminant fluxes and interpreting the stratigraphic record of depocentres such as lakes.

The thesis structure is framed around the following research questions:

1) What approaches can be used to quantify sediment storage behaviour in river floodplains and the effects of environmental controls on storage times?

Rationale: Floodplains are some of the most spatially extensive sedimentary reservoirs in fluvial systems, spanning $8 \times 10^5 – 2 \times 10^6$ km^2 of the Earth's land surface (Leopold et al. 1964; Tockner & Stanford 2002; Mitsch & Gosselink 2015). Depending on the size and erosion rates of floodplains, turnover time (the time for all sediments in storage to be exchanged with the channel) may span timescales of multiple decades to several millennia. Hence, the impact of floodplain storage on delivery times through catchment sediment-routing

systems will be significant. While attempts have been made to investigate how floodplains interrupt sediment delivery to catchment outlets, storage time quantification remains a poorly understood area of research. Here a comprehensive review is undertaken of the current state of fluvial sediment storage time research, including effects of environmental controls and potential quantification methods. The review examines how afore-mentioned impelling and resisting forces (*sensu* Fryirs & Brierley 2013) interact to control the longevity of storage and delivery times in fluvial systems, how different techniques can quantify storage time distributions and the impact of controls/process interactions, and how these ultimately feed into predictions of sediment delivery times from source to sink. In this review, particular attention is drawn to the need for future work on recording storage times directly from the timings of deposition and erosion processes over the timescales of long-term channel-floodplain evolution. Developing and applying a methodology that combines long-term simulations of river channel changes with a procedure for calculating the ages and storage times of floodplain deposits is a key objective underpinning this thesis.

2) To what extent can a landscape evolution model accurately reconstruct recent historical 2D planimetric channel dynamics of reach-scale valley floor systems?

Rationale: The accumulation and subsequent removal of sediments from valley floor environments has been characterised as a “fast in, slow out” process, whereby floods supply a great pulse of sediment to the reach that is removed gradually over time as the channel migrates laterally across its full valley width (Trimble 2010). Constraining the processes and rates of river channel dynamics is therefore key to modelling the lifetime of sediment storage in the adjoining floodplain. River channel changes are reconstructed along ten 1 km-long reaches from rivers in the north of England. The time period for channel change reconstruction covers the timeframe when historical maps and aerial imagery overlaps with the daily flow record (which was used to drive simulations). These reconstructions provide data on processes such as mean annual rates of lateral migration, floodplain erosion and deposition, and changes to planform morphology of the channel over time. Evaluating the

extent to which these reconstructed changes can be replicated accurately by a landscape evolution model (LEM) through direct comparison with mapped historical changes is a major objective of this thesis. If successful, it will increase confidence that the model can be used to simulate longer-term dynamics including sediment storage behaviour.

3) How can a LEM be applied to quantify the distributions of sediment ages and storage times?

Rationale: Floodplain turnover times typically range from multi-decadal to multi-millennial timescales. Our ability to measure over these timescales directly in the field is compromised by factors such as human longevity, and limitations with radiometric dating (e.g. half-life, lack of suitable samples, such as organic material in the case of ^{14}C). While available map and aerial image records allow us to reconstruct the timings of erosion and deposition processes necessary for age and storage time calculation, these records tend to go back only as far as ~150 years and only include a few survey dates. Landscape evolution modelling has the key advantage of control over boundary conditions, such as spatial and temporal scales and resolution, including the ability to quantify processes over much longer timeframes than historical monitoring records. However, these types of model have tended to be avoided when modelling floodplain sediment storage dynamics because of their high data demands (Lauer 2012). The LEM chosen to address Research Question 2, once calibrated and evaluated, will be used to simulate river channel changes over timescales typical of estimated floodplain turnover times. These channel changes will record the timings of erosion and deposition at specific locations of the floodplain over the duration of the model runs. The timings of these processes will form the basis of sediment age and storage time calculation. Over a long enough period, there should be a enough calculated ages and storage times to model their distributions and gain insight into the sensitivity of storage times to conditions including vegetation cover and the geomorphology of different river valley floor reaches.

4) How sensitive are reach-scale channel-floodplain systems to various environmental conditions in terms of sediment storage duration?

Rationale: Environmental variability, such as changes in streamflow magnitudes and differences in channel pattern, are known to influence floodplain turnover rates and sediment storage times (e.g. Beechie et al. 2006; Miller & Friedman 2009). Channel-floodplain systems that have been monitored over several years have been shown to exhibit age and storage time distributions that change shape in response to geomorphic disturbances (Moody 2017). However, it remains unclear to what extent this response is manifested when ages and storage times are recorded over different temporal frequencies. Changes in vegetation cover and flow magnitude, reflecting reconstructions from the British Isles over the Holocene (e.g. Fyfe et al. 2013) and projections of future streamflow (Centre for Ecology and Hydrology 2015), make up an ensemble of scenarios with which to quantify the effects of sudden and gradual-onset environmental changes on floodplain sediment storage. The response of these environmental changes should register as switches in the curvature of age and storage time distributions, between concave (dominance of lower values in the distribution) and convex (dominance of higher values) forms. This is an important research area to test as it may provide further insight into how sediment pulses affect reach-scale rates of sediment accumulation and removal (James 2018). Furthermore, catchment-scale sediment-routing models require a probability density function of storage times to generate predictions of sediment delivery times from source to sink.

1.3. Thesis outline

This thesis is formatted as a series of journal articles. Thus, it comprises a set of self-contained manuscripts (albeit with occasional cross-referencing between chapters in the thesis). Figure 1.1 shows the overall structure of the thesis, including brief summary points of what each chapter covers and how these chapters connect to each other. Chapters 2 and 3 have previously been submitted for peer review, while Chapters 4 and 5 are prepared for imminent submission to international peer-reviewed journals. Chapter 2 is a literature review of the current state of understanding of sediment storage and delivery timescales in reach-scale channel-floodplain systems, including process controls and potential quantification techniques. Chapter 3 details the process

of parameterising a model to simulate 2D planimetric river channel changes accurately based on direct comparison with mapped historical changes. Results from this chapter sets up the experimental modelling of sediment storage behaviour under different environment conditions that make up the core of this thesis (Chapters 4 and 5).

Chapter 2: *Timescales of sediment storage and delivery in channel-floodplain systems: Developments in understanding, controls and implications*. This was originally titled: *Sediment residence times in fluvial systems: Significance, techniques and applications* (submitted to Earth-Science Reviews, May 2018). However, this manuscript was rejected in July 2018 and subsequently revised to the new version based on peer reviewer comments. This chapter provides a comprehensive literature review of the dynamics of sediment storage and delivery timescales in channel-floodplain systems. It outlines physical controls on the accumulation and removal of sediments from landforms within the sediment-routing system (focussing on floodplains in particular), evaluating proxies of and approaches to quantifying storage times at reach-scale and how these might be fed into models of sediment delivery times at reach to catchment scales. Implications for landscape evolution, modelling of contaminant and biogeochemical fluxes, and delivery of sediments to the stratigraphic record are discussed, with suggestions of future research questions outlined.

Chapter 3: *Modelling reach-scale river channel and floodplain turnover dynamics with CAESAR-Lisflood* (Feeney et al. 2020: published online early-access in Earth Surface Processes and Landforms, January 2020). Ten study sites from across the north of England were chosen, and an overview of how channel changes are reconstructed, for the period covering when the daily flow record overlaps with historical maps, to provide a dataset for evaluating model accuracy is described. The CAESAR-Lisflood LEM was selected for use in the thesis, and this chapter describes in detail how this model operates at reach-scale and its advantages over other models. To date, few attempts have been made to comprehensively evaluate the ability of CAESAR-Lisflood to simulate 2D channel-floodplain dynamics at reach-scale – a gap that this manuscript aims to address. Here, a methodology is described and undertaken to:

i. Calibrate model parameters with appropriate values.

ii. Select the single “best-fitting” combination of parameter values for each site from an ensemble of calibration trial runs.

iii. Evaluate the overall accuracy of the model by assessing how completely recent historic geomorphic changes are reconstructed through direct comparison with mapped 2D planimetric historical changes. These direct comparisons between model results and mapped datasets are based on four key metrics: lateral migration rate, erosion rate, deposition rate and the successful matchup between modelled and mapped landform areas.

Chapter 4: *Modelling the distribution and behaviour of sediment storage times in alluvial floodplains*. A methodology for quantifying the dynamics of sediment storage times in river floodplain surface areas is presented. Three reaches, using calibrated model parameters determined in Chapter 3, are used to simulate a series of experimental environmental change scenarios in CAESAR-Lisflood and their effects on the distribution of sediment storage times. The ages and storage times of floodplain surface area deposits are calculated based on the timings and 2D spatial extents of erosion and deposition processes. Other proxies, such as the erosion hazard (the probability a floodplain surface will erode based on its age) and changes in the mean age and mean storage time through time provide insight into the floodplain (re)occupation behaviour of the channel. Factors that may potentially influence results including the time step for recording channel changes (e.g. every 10 years vs every 100 years) and vegetation cover are tested, and results compared across the three reaches. Results of these simulations are used to determine a best-fit probability density function using non-linear regression, and details on how to estimate the parameter values of this non-linear function are outlined.

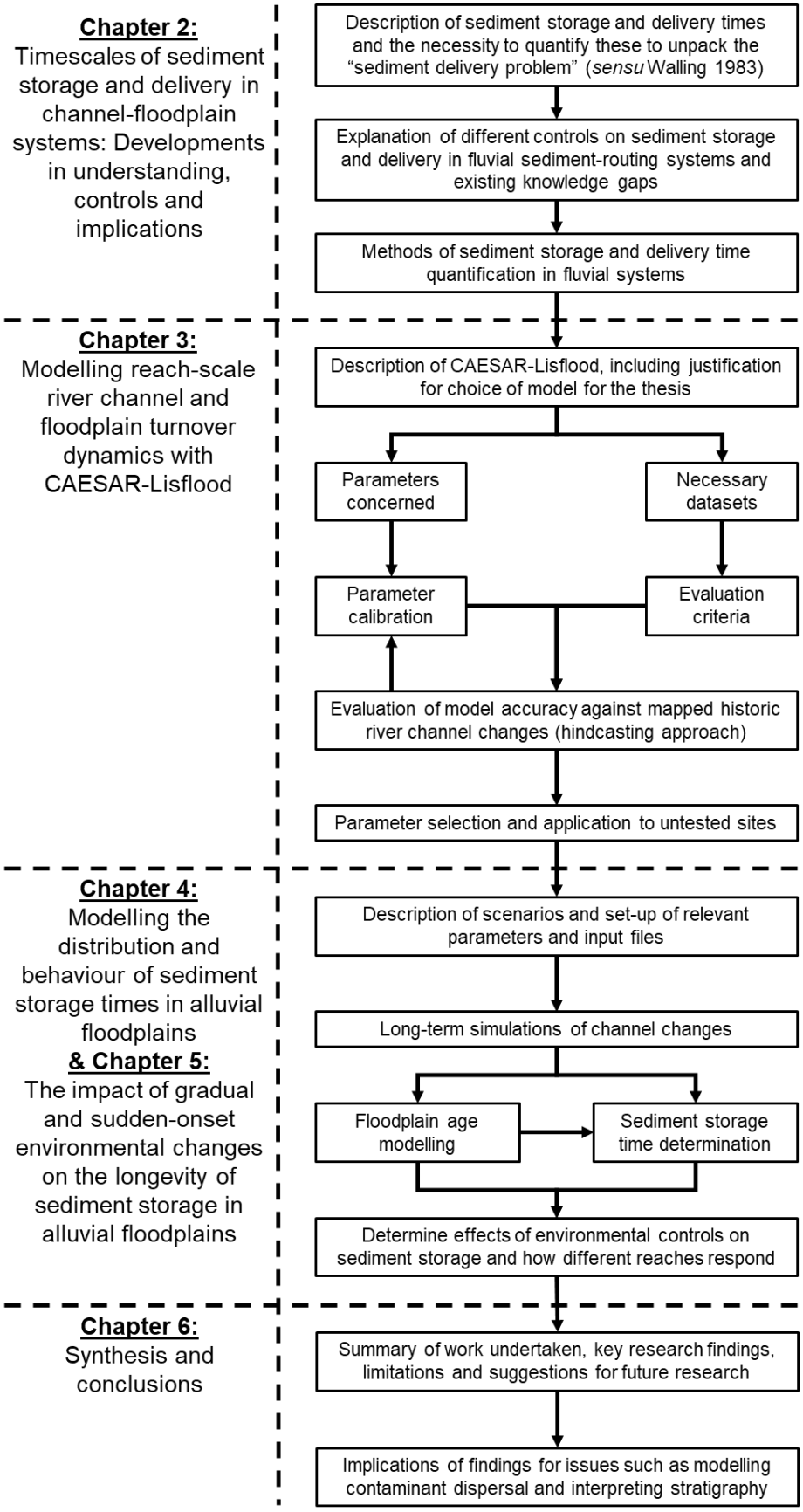

Figure 1.1: Outline of the thesis structure including the titles and contents of chapters. Arrows show where / how different parts of the thesis link together.

Chapter 5: *The impact of gradual and sudden-onset environmental changes on the longevity of sediment storage in alluvial floodplains*. Results from a second set of experimental scenarios run in CAESAR-Lisflood, are presented. These scenarios incorporate either a gradual change in daily flow magnitudes over time or an instantaneous change in vegetation cover halfway through the simulation. The rationale for these scenarios and their descriptions are provided. Sediment storage behaviour is quantified using the same proxies as in Chapter 4. The non-linear function derived in Chapter 4 is applied to the results of the simulations presented here to demonstrate how effectively this model holds when a disturbance occurs.

Chapter 6: This chapter provides an extended discussion that brings together the findings from the review chapter (Chapter 2), CAESAR-Lisflood model evaluation chapter (Chapter 3) and the sediment storage time modelling results chapters (Chapter 4 and 5), and addresses the key research questions outlined here in Chapter 1. Key limitations to the research conducted in this thesis are discussed and a number of future research avenues are suggested.

1.4. Status of manuscripts and author contributions

At the time of submission, the status of the four manuscripts is as follows:

Chapter 2

Feeney, C. J., Smith, H. G., Chiverrell, R. C., Cooper, J. R. and Hooke, J. M. (Aim for potential submission to Progress in Physical Geography) Timescales of sediment storage and delivery in channel-floodplain systems: Developments in understanding, controls and implications.

Author contribution:

Feeney, C. J. – Main author, conducted the literature review and wrote the manuscript.

Smith, H. G. – Originally led in-depth discussions and detailed manuscript review (after the first half of the PhD, Chiverrell, R. C. became the primary supervisor)

Chiverrell, R. C. – Later led in-depth discussions and detailed manuscript review.

Cooper, J. R. – Contributed to in-depth discussion and detailed manuscript review.

Hooke, J. M. – Contributed to in-depth discussion and detailed manuscript review.

1st submission: 29 May 2018 to Earth-Science Reviews (rejected: July 2018).

Chapter 3

Feeney, C. J., Chiverrell, R. C., Smith, H. G., Cooper, J. R. and Hooke, J. M. (Manuscript published online in Earth Surface Processes and Landforms) Modelling reach-scale river channel and floodplain turnover dynamics with CAESAR-Lisflood (Feeney et al. 2020). Available open-access from ESP&L at: https://onlinelibrary.wiley.com/doi/full/10.1002/esp.4804 (last accessed on 23/02/20).

Feeney, C. J. – Main author, wrote the manuscript and collected, processed and interpreted the data.

Chiverrell, R. C. – Led detailed discussions and thorough manuscript review.

Smith, H. G. – Led detailed discussions and thorough manuscript review.

Cooper, J. R. – Contributed to in-depth discussion and detailed manuscript review.

Hooke, J. M. – Contributed to in-depth discussion and detailed manuscript review.

1st submission: 29 May 2019 (reviewer feedback received: 6 August 2019: Major revisions).

2nd submission: November 2019 (reviewer feedback received: early December 2019: Moderate revisions).

3rd submission: December 2019 (accepted for publication later in the month and published online early-access on 20 January 2020).

Chapter 4

Feeney, C. J., Chiverrell, R. C., Smith, H. G., Cooper, J. R. and Hooke, J. M. (Manuscript for submission to either Geomorphology or Earth Surface Processes and Landforms) Modelling the distribution and behaviour of sediment storage times in alluvial floodplains.

Feeney, C. J. – Main author, wrote the manuscript and collected, processed and interpreted the data.

Chiverrell, R. C. – Led detailed discussions and thorough manuscript review.

Smith, H. G. – Next biggest contributor to discussions and manuscript review.

Cooper, J. R. – Contributed to in-depth discussion and detailed manuscript review.

Hooke, J. M. – Contributed to in-depth discussion and detailed manuscript review.

Chapter 5

Feeney, C. J., Chiverrell, R. C., Smith, H. G., Cooper, J. R. and Hooke, J. M. (Manuscript for submission to either Geomorphology or Earth Surface Processes and Landforms) The impact of gradual and sudden-onset environmental changes on the longevity of sediment storage in alluvial floodplains.

Feeney, C. J. – Main author, wrote the manuscript and collected, processed and interpreted the data.

Chiverrell, R. C. – Led detailed discussions and thorough manuscript review.

Smith, H. G. – Next biggest contributor to discussions and manuscript review.

Cooper, J. R. – Contributed to in-depth discussion and detailed manuscript review.

Hooke, J. M. – Contributed to in-depth discussion and detailed manuscript review.

CHAPTER 2:

Timescales of sediment storage and delivery in channel-floodplain systems: Developments in understanding, controls and implications

Summary and linkages to other thesis chapters

Sediment yield, measured at catchment outlets, has been linked to processes, such as soil erosion rates, to inform land management practices. Good understanding of these processes helps to inform management strategies of issues such as poor water quality in rivers. However, only a fraction of material that is eroded passes from one part of the landscape, via river networks, to another and is recorded as sediment yield. This is because sediments, as they are transported in channels, undergo repeated exchange with the surrounding floodplain, where they become stored for long periods of time. When this storage effect is aggregated over entire river catchments – especially large ones like the Amazon or the Ganges – a fraction of eroded material may not be recorded as sediment yield until millions of years after being eroded initially. Recognising this, several authors (reviewed in this chapter) have attempted to quantify the longevity of sediment storage in floodplains. However, our understanding of the processes that control sediment storage is limited. Further, relatively few methods have been applied to either infer or directly quantify sediment storage times, and these exclude certain processes of channel-floodplain evolution such as the formation of braided channel patterns. Thus, this thesis aims to quantify storage times using an approach that considers the spectrum of channel-floodplain evolutionary processes, and controls upon these.

This chapter aims to address Research Question 1: “What approaches can be used to quantify sediment storage behaviour in river floodplains and the effects of environmental controls on storage times?” Here, current understanding of channel-floodplain evolutionary processes is reviewed, including the roles of intrinsic and extrinsic controls over space and time. Methods, arranged from simple, black-box model calculations to more complex approaches that integrate multiple geomorphic processes into the quantification of sediment storage and delivery times, are synthesised. Advantages and limitations to each of these approaches are discussed, and a series of potential research questions are outlined, to justify the methodological design, aims and objectives of the succeeding thesis chapters (Chapters 3, 4 and 5).

2.1. Introduction

Fluvial systems are important for transferring sediments through river catchments from hillslopes to seas and lakes (Schumm 1977). However, only a fraction of what is mobilised upstream will transfer to catchment outlets and be quantifiable as sediment yield – a principle termed, “the sediment delivery problem” (Walling 1983). Sediment yield, especially following disturbances – defined as extreme events such as wildfires, floods and earthquakes, or anthropogenic activities such as deforestation and dam construction, which initiate a change in the energy conditions of a river system that produces a measurable geomorphic response such as increased sediment erosion rates (Owens et al. 2010) – may be a function predominantly of sediment storage rather than contemporary upland erosion rates (Trimble 1975). As Syvitski (2003) highlights, while soil erosion rates are accelerating globally, fluxes to the coastal zone are declining in many places because of storage within floodplains and behind dams.

The disruption of sediment delivery from sources of erosion to the catchment outlet (and by extension, the stratigraphic record) has important implications for reconstructing environmental change. The mobilisation of sediments in fluvial systems depends strongly on external forcing (e.g. climate and land-use change), internal forcing (e.g. flow conditions) and the configuration of river catchments (e.g. catchment size, length of channel networks and landform coupling) (Hoffmann et al. 2007, 2009). For example, in the Rhine basin, slope-channel coupling varied over the course of the Holocene. As a result, climatic impacts were only recorded in floodplain alluvium when both the landscape was sensitive enough (e.g. following deforestation) and energy thresholds for gullying (i.e. rainfall intensity) were breached (Lang et al. 2003). This meant that during the Neolithic period (when deforestation extents were restricted spatially), sediment derived from agriculturally driven soil erosion was retained mostly in colluvial storage. Subsequently, from the Iron Age onwards, widespread recording of soil erosion in floodplain alluvium occurred as agriculture expanded (Lang et al. 2003). When boundary conditions such as climate or vegetation cover change significantly (as in the example of the Rhine catchment), geomorphic systems adjust, with a lag in this adjustment

referred to as the “response time” (Brunsden & Thornes 1979). Determining the response time of geomorphic systems to external forcing, in terms of the transmission of sediments, therefore requires the quantification of landform coupling or “(dis)connectivity” within the sediment cascade (Jain & Tandon 2010; Fryirs 2013).

Storage times, also known as transit times or waiting times (Bolin & Rodhe 1973), of sediments in various catchment landforms provide an effective timeframe of sediment (dis)connectivity in fluvial systems (Hoffmann 2015). Reanalysis by Hoffmann (2015) of a long-term sediment budget from the Aufsess river catchment in Germany (Fuchs et al. 2011) demonstrated that the prolonged storage of sediments on hillslopes (~800 to ~4000 years) buffered the catchment response to the onset of agricultural land use. Elsewhere, storage time calculations provide potential constraints on the longevity of contaminant storage in various sediment stores. For example, using volumes of floodplain sediment (estimated by multiplying areas of mapped floodplain units by the maximum depths of cores extracted at these sites) and suspended sediment transport rates constrained by previous sediment budget analyses (Walling & Owens 2003; Walling et al. 2003), mean storage times of approximately 5000 years for lead and zinc enriched sediments were calculated for the Swale catchment, UK (Dennis et al. 2009). In the South River, Virginia, sedimentary deposits associated with large woody debris, termed “fine-grained channel margin” (FGCM) deposits, were found to be significant reservoirs of mercury-enriched suspended sediments, storing equivalent to 17 to 43% of the annual suspended sediment load (Skalak & Pizzuto 2010). Radiometric dating revealed the ages (B.P.) of these deposits ranged from 1 to 60 years (Skalak & Pizzuto 2010).

River catchments can be conceptualised as a “sediment-routing system” whereby individual sediment particles will have a unique trajectory from eroded source to a sink and a unique set of timescales pertaining to storage within landforms and ultimate delivery to the catchment outlet (Allen 2008). Taking floodplains as an example, vertical accretion allows sedimentation rates to be governed predominantly by sediment supply (e.g. via large floods or the transmission of sediment slugs) such that vast quantities may accumulate over

decades or centuries (Trimble 2010). As sediment removal occurs predominantly via channel erosion, it may take millennia – especially where floodplains are wide – for sediment to leave storage (Trimble 2010). This temporal disparity between accumulation and removal rates drives storage as a lagging mechanism of sediment erosion signals by delaying their ultimate delivery to catchment outlets and prolongs the storage of any sediment-bound contaminants entering the river network.

While attempts have been made to quantify timescales of sediment storage within channel-floodplain systems (e.g. Lancaster & Casebeer 2007; Skalak & Pizzuto 2010; Bradley & Tucker 2013), several outstanding questions have been posed in the literature, including:

1) What are the sediment storage times for different river segments and sedimentary landforms (see Syvitski 2003)?

2) How do potential complexities, including unbalanced sediment budgets, sediment grainsize distributions, inputs from tributaries, temporal variability in environmental conditions (e.g. climate and land-use), and spatial variations in valley morphology (e.g. slope and confinement) affect sediment storage and delivery times within valley corridors (see Pizzuto et al. 2017)?

3) What role does sediment storage time play in biogeochemical cycles (see Rodhe 2000; Aufdenkampe et al. 2011; Sutfin et al. 2016)?

4) How can multiple delivery times be integrated to determine how river systems will buffer disturbance-induced sediment flux signals (see Allen 2008)?

While this review does not seek to answer these above questions, it does aim to discuss many of the processes underpinning these questions, and the possible methods which one could apply to attempt to answer these questions. Thus, the aims of this chapter are to (i) review current knowledge of sediment storage in channel-floodplain systems, including processes and controls; (ii) synthesise and review approaches to quantify timescales of sediment storage

in various landforms within the channel-floodplain system and delivery through valley floor corridors; and (iii) discuss the importance of storage in sediment-routing models and wider implications for quantifying and managing environmental change. The first two aims are pertinent to acquiring answers to the first and second questions. The third aim seeks to illuminate potential gaps in understanding of sediment storage timescales, concluding with a discussion on the implications for biogeochemical cycling and environmental change reconstruction.

The following section of this review focusses on conceptualising timescales of sediment storage within channel-floodplain systems, including processes and controls (Section 2.2). Addressing the first aim, the diversity of landforms associated with the channel-floodplain system is introduced, providing a detailed discussion of the different processes that shape these landforms and the spatially and temporally varying drivers of these processes. This is followed by a review of different techniques for quantifying storage and delivery timescales (Section 3). Simple one-dimensional mass balance modelling is discussed first, before introducing increasingly complex approaches that include inferring the distribution of storage times from ages, and quantifying storage times directly from the timings of erosion and particle mobilisation. This is followed by a discussion of the importance of storage time distributions for parameterising models of probabilistic sediment transfer to predict sediment delivery times. While several quantification methods exist, this review will not attempt to discuss them all and will focus exclusively on reach scale channel-floodplain systems to address the second aim. Section 3 also contains discussion of the different shapes of storage time distributions and what these mean in terms of sediment storage behaviour, with the objective of discussing further how disturbances may influence storage timescales. Finally, in relation to the third aim, the importance of channel-floodplain storage on sediment routing and delivery timescales is discussed. Here, outstanding gaps in current understanding of controls on storage timescales are outlined with suggestions of ideas to direct future research. In particular, these directed suggestions are focussed in the context of the four

questions outlined earlier and the wider implications these questions may have for the Earth Sciences.

2.2. Sediment trajectories through river corridors

2.2.1. Reservoirs and transport pathways in river systems

Mass fluxes, associated with Earth surface processes acting across the terrestrial environment, are characterised by the constant redistribution of particulate sediment and solutes (Allen 2008). The sediment-routing system – a complex series of transport pathways (or "trajectories") punctuated with temporary storage zones – connects the erosional engine of upland regions with depocentres at the coast, and facilitates the delivery of sediment from source to sink (Schumm 1977; Castelltort & Van Den Driessche 2003; Figure 2.1). If we imagine that a mass of sediment (e.g. a million particles) is "released" into the river network, each individual particle would follow a unique trajectory from source to sink and by extension, a unique delivery time that has been modulated to some degree by transient storage in a landform such as a floodplain or channel bed (Pizzuto 2014; Pizzuto et al. 2017). The integration of sediment trajectories defines a sediment-routing system (Allen 2008) and, were it possible to obtain this, the distribution of sediment delivery times would provide information on the capacity of a sediment-routing system to buffer sediment flux signals generated by climatic and tectonic forcing processes (Armitage et al. 2011, 2013, 2015).

The buffering of sediment fluxes manifests itself in various ways, including lagging delivery times to catchment outlets and attenuating the amplitude of input signals. For example, analysis of nearly 100 rivers reveals that river networks >300 km long will buffer sediment disturbance input signals with 10^4-10^5-year periods (Castelltort & Van Den Driessche 2003). Pizzuto et al. (2017) found that sediment signals with a period of 10 years were delayed by a factor of 12.6 and damped by a factor of 380, with the form of the sediment signal transformed from a Dirac delta function to a power-law function, meaning that storage, not in-channel transport time controls delivery times. As a result, any attempts to engineer short-term sediment signals that can be transmitted

rapidly downstream via best management practices (e.g. Chesapeake Bay Program 2014) will be difficult to evaluate as current catchment modelling does not account for sediment storage times (Pizzuto et al. 2017).

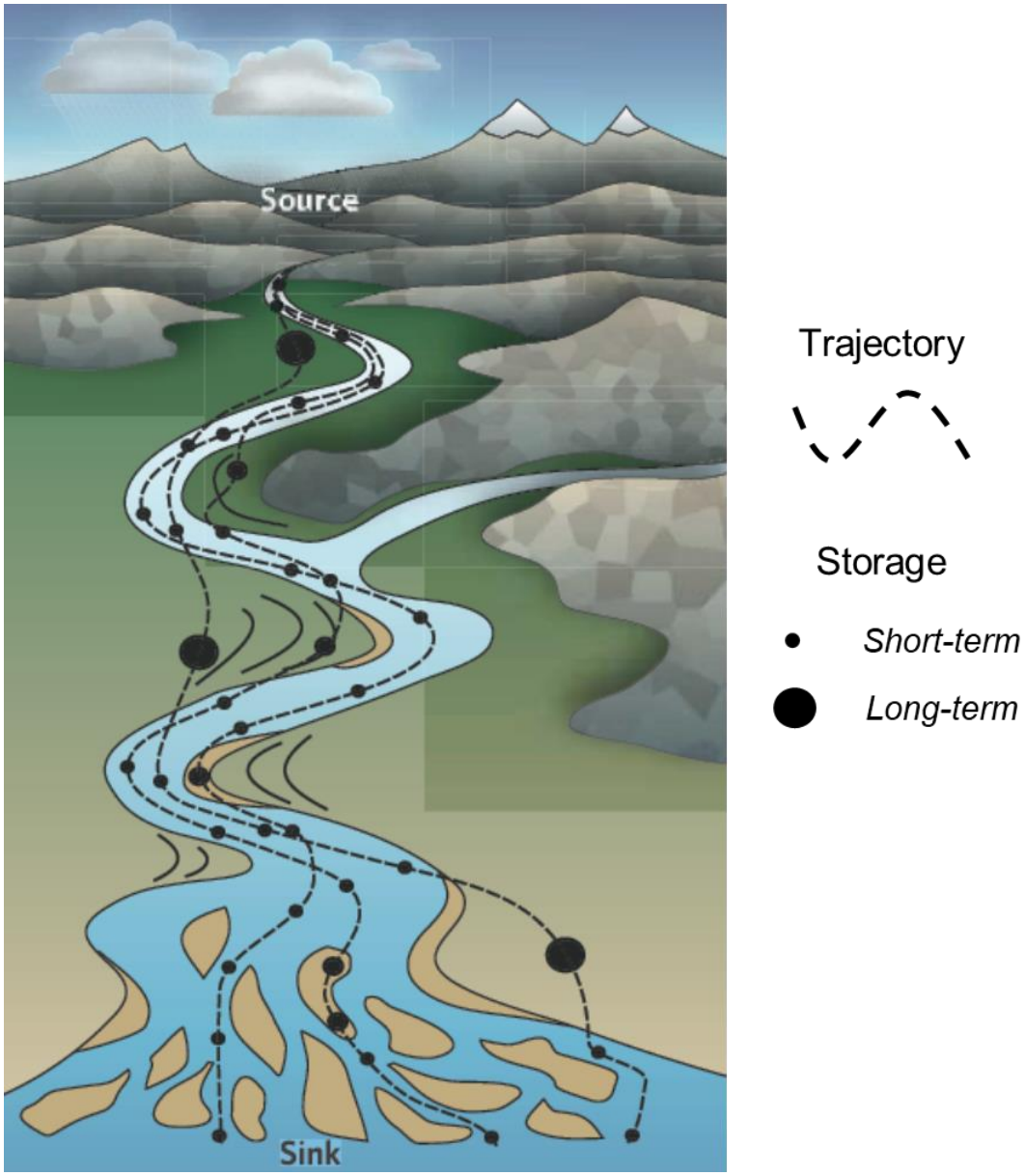

Figure 2.1: The sediment-routing system concept. Sediment is "released" from an initial source region via erosion, and transfers to a sink region at the catchment outlet along one of a multitude of pathways or "trajectories" (indicated by the dashed black lines). Some trajectories are characterised by short delivery times, with brief periods of storage in the sediment-routing system (small circles). Other trajectories entail lengthy delivery times with prolonged periods of storage (large circles) (adapted from Allen 2008).

A key control of the buffering of sediment fluxes is the length of the river network (Castelltort & Van Den Driessche 2003; Pizzuto et al. 2014, 2017). In part, this is due to the fact that the probability a particle will enter into at least one episode of storage increases as a function of transport length (Pizzuto et al. 2017). Another factor is the degree of (dis)connectivity in the sediment-routing system (Fryirs et al. 2007; Fryirs 2013). One way of conceptualising the fluvial system is to divide it up into three broad sub-systems: a source zone, transfer zone and accumulation zone (Schumm 1977). Each of these zones is characterised by a set of longitudinal, vertical and lateral (hillslope-channel or channel-floodplain) linkages (Figure 2.2). These linkages however, can become interrupted at various points in space and time by different types of "blockages": buffers (which impede lateral fluxes), barriers (affecting longitudinal transfers) and blankets (which disrupt vertical exchanges) (Fryirs et al. 2007). In an idealised fluvial system, the source zone will be characterised by high levels of longitudinal and lateral connectivity between hillslopes and channels and efficient sediment transfer; a transfer zone with efficient longitudinal transfer and decreasing hillslope-channel connectivity; and an accumulation zone where vertical and channel-floodplain connectivity are high and longitudinal transfer is inefficient (Figure 2.2). Further, the role of different landforms in sediment storage will change – from hillslopes and channel beds dominating storage upstream to floodplains retaining sediment over long timescales downstream (Fryirs & Brierley 2013).

Sediment (dis)connectivity – and by extension, storage and delivery timescales – varies across catchment systems. Previous literature have documented how factors such as valley confinement and slope (Kuo & Brierley 2013), variations in stream competence and sediment supply over space and time (Hooke 2003), the removal of riparian trees and in-stream wood (Florsheim et al. 2011), and climatic oscillations (Hoffmann 2015) can all impact on particle trajectories through sediment-routing systems. To discuss these controls in more detail, including how these affect storage and delivery timescales, it is necessary to examine processes of sediment storage and removal from different landforms.

Figure 2.2: Linkages in an idealised catchment. Between source, transfer and accumulation zones, longitudinal, lateral and vertical linkages vary in type and strength as a result of different blockages (see text). Lateral and longitudinal linkages weaken and vertical linkages strengthen downstream. Downstream, sediment storage capacity and duration increase (adapted from Fryirs 2013).

2.2.2. Processes of sediment storage and removal and their controls

In the context of channel-floodplain systems, sediment storage times are controlled by the continuum of different stream types. This continuum is itself arranged along a gradient, from high-energy and low-resistance, which are conducive to high erosion rates and inherent disequilibrium in the system, to low-energy and high-resistance conditions that lead to low erosion rates and inherent stability within the system (Figure 2.3). As derivatives of their adjoining channel systems, floodplain forms and processes also tend to be arranged along this energy/resistance gradient (Nanson & Croke 1992). At the high-energy/low-resistance end of the continuum (Figure 2.3), sediment storage and flux in river systems tend to be highly episodic, with highly mobile channel boundary and valley floor sediments flushed out readily by infrequent, but large erosion events such as floods (Trimble 2010). On the other side of the continuum (Figure 2.3), channel-floodplain systems exhibit less change. These tend to be typified by single-thread channels, flowing through a wide valley with well-defined, fine-textured and vegetated channel banks (Trimble 2004, 2010). Sediment deposition and erosion are approximately equal in terms of their mass and rates over space and time, often occur simultaneously, and typify the steady-state channel-floodplain systems that much of the storage time quantification literature focus on (Lauer & Parker 2008; Trimble 2010).

Channel-floodplain systems operate and evolve (and by extension, sediment is sequestered into and liberated from storage) as a function of river slope and discharge versus sediment grain size and supply – the “Lane Balance” (Lane 1955). Under steady-state conditions, the supply of sediment will equal the capacity of the channel to transport the supply, resulting in no net geomorphic change occurring. For example, as a channel laterally migrates into its floodplain, the mass of material eroded from the cut-bank will be balanced through a combination of lateral accretion on point bars along the inside of the bend, overbank deposition and deposition within abandoned channel courses (Lauer & Parker 2008). However, if channel-floodplain systems are overloaded with supply, deposition rates may exceed erosion rates, leading to net aggradation. Conversely, if the channel is starved of sediment supply, it will

have excess capacity and (assuming there is plenty of readily mobile material in the valley floor) erosion rates will exceed deposition rates, leading to net degradation (Trimble 2010).

Systems that have undergone some form of disturbance, such as an extreme wildfire and flood event (e.g. Moody 2017), a change in sediment supply and grain size distribution in response to historical mining activity (e.g. Macklin & Lewin 1989; Rowan et al. 1995; Rowan & Franks 2002), or land clearance associated with the expansion of agriculture and human settlements (e.g. Florsheim et al. 2011; Donovan et al. 2015), are characterised by imbalances in supply and capacity. Under these conditions, the channel-floodplain system is in disequilibrium and may undergo a dramatic change in planform morphology, such as from meandering to braided, known as “active transformation” (Miller 1997). In other cases, an aggradation-degradation episode may occur, whereby the elevation of the valley floor surface rises as floodplain alluviation occurs, followed by channel incision and subsequent transformation of the channel-floodplain morphology (James 2018). Figure 2.4 illustrates how an aggradation-degradation episode manifests in two hypothetical valley floor environments. These types of events are significant in buffering catchment disturbance. A burst of sediment may fill a valley over multiple years or decades, but the subsequent removal of deposited material may take centuries or millennia on average to remove, creating a regime of sediment exchanges that is described as “fast in, slow out” (Trimble 2010). This “fast in, slow out” dynamic is evident in valley floor systems worldwide, where changes in climate and land-use over the course of the Holocene have altered the balance of sediment supply and channel capacity to cause abandonment of floodplain surfaces via channel incision. Terrace deposits in UK river systems for instance may date back as far as centuries to the Late Pleistocene in age (e.g. Hooke et al. 1990; Lewin et al. 2005; Chiverrell et al. 2009; Foster et al. 2009), demonstrating just how long some sediments may remain stored in the fluvial system before eventual delivery.

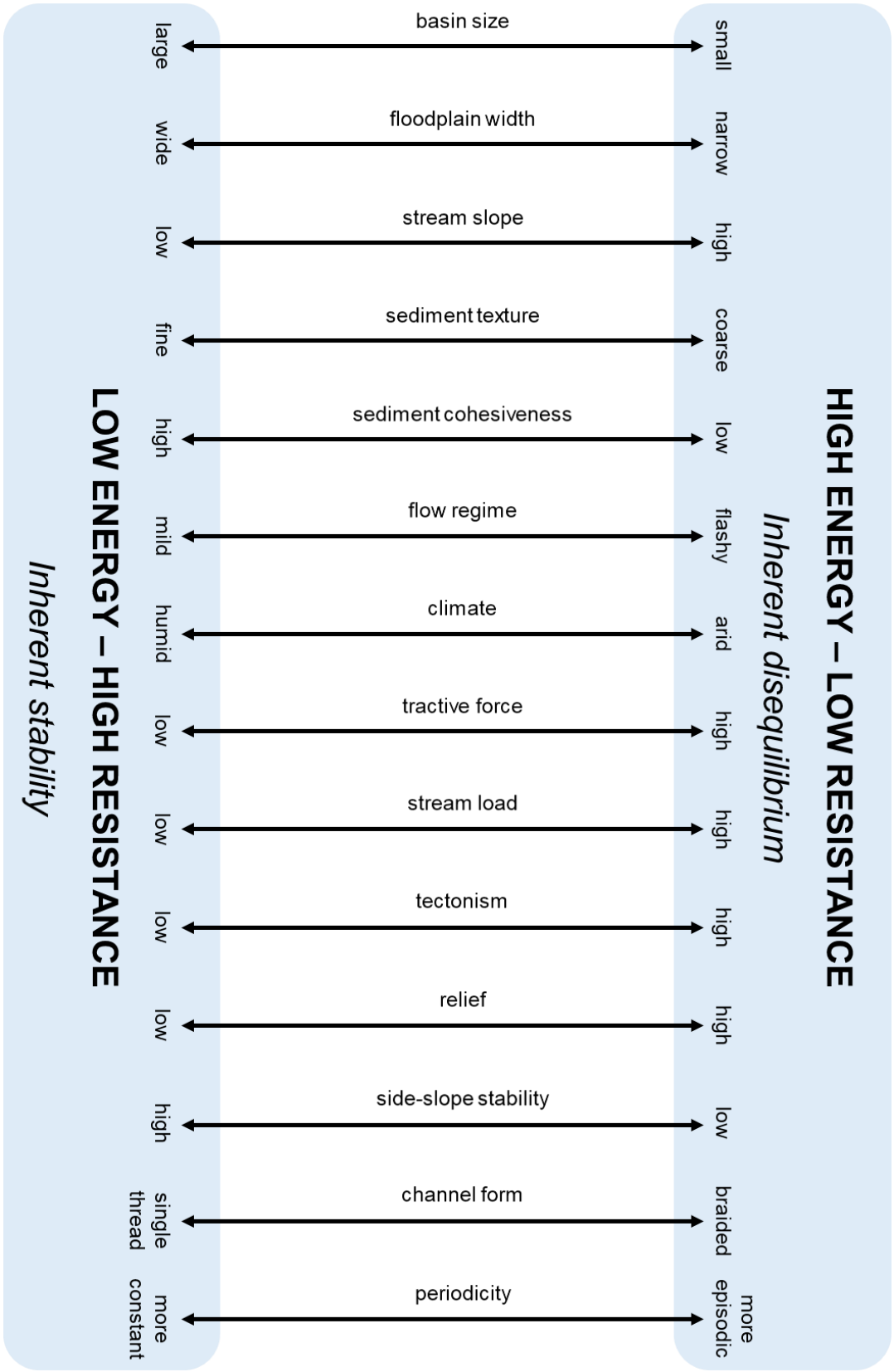

Figure 2.3: The continuum of stream types and controlling variables (adapted from Trimble 2010). Variables are generalised and the figure is not deterministic. For most systems, multiple variables would control behaviour.

Another way to conceptualise fluvial system behaviour is as a balance between impelling and resisting forces (Fryirs & Brierley 2013). Impelling forces drive geomorphic changes in the channel system as a function of discharge and slope, while resisting forces reduce flow energy via friction and control the capacity of a channel to convey sediment of a given volume and grain size distribution (Fryirs & Brierley 2013). Sediment cohesiveness along the channel bed and banks, blockages, such as large boulders, accumulations of in-stream wood and other forms described in Figure 2.2, and vegetation within the channel and in the riparian zone all contribute to resisting forces (see also Figure 2.3). In a similar vein to the three states of the Lane Balance (supply is equal to, greater than or less than capacity), the balance between impelling and resisting forces has implications for geomorphic process rates and hence, the timescales of storage and delivery through sediment-routing systems.

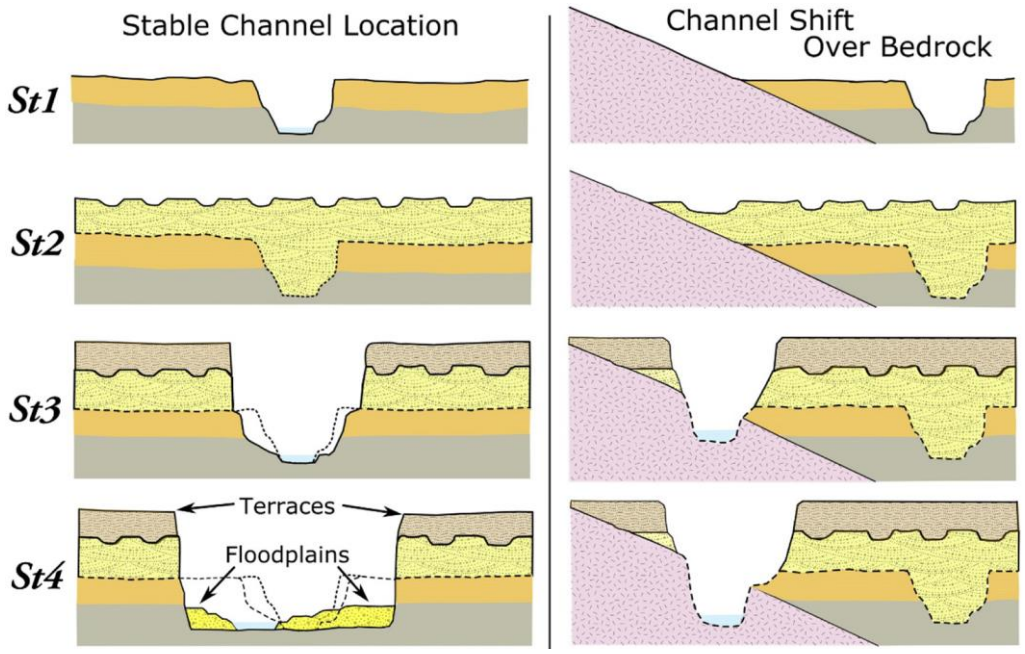

Figure 2.4: Four stages of aggradation-degradation episodes in two hypothetical valley floor systems following floodplain alluviation (St2), incision following reduced sediment supply (St3), and a phase of channel-floodplain transformation (St4). Left: The channel reoccupies its original position, widens and develops a new floodplain during St4. Right: The channel avulses and incises into the bedrock to form a steep, narrow gorge (after James 2018).

As impelling forces increase relative to resisting forces, erosion and transport rates will increase. This has been shown to decrease sediment delivery times as well. Bonniwell et al. (1999) for example, demonstrated that at peak flows, sediments entering the river network would travel 60 km at peak flows, with delivery times of 1.6 days on average. Along a reach of the Little Missouri River, USA, Miller & Friedman (2009) correlated declining mean annual flow rates with mean annual floodplain erosion rates. From their analysis, they interpreted that the distribution of sediment storage times must take a power law form, implying very long periods of storage for a small proportion of deposits (Miller & Friedman 2009). In Carnation Creek, Canada, higher virtual velocities of sediment – defined as the total distance of sediment transit divided by the time taken to travel that distance and integrates episodes of storage (Voepel et al. 2013; Parsons et al. 2018) – measured over distances of ~100 m, corresponded with greater dominant peak discharge, stream power and scour depths (Haschenburger & Church 1998). Given that sediment delivery or storage times can be estimated by dividing the travel distance of a particle by its virtual velocity (Martin & Church 2004; see also Table 2.1 for a definition), this would imply that storage/delivery times were reduced as well.

When resisting forces increase relative to impelling forces, erosion and transport rates tend to decrease, and deposition rates increase. For example, the amount of geomorphic work that will be expended along channel boundaries varies widely between different types of vegetation cover (see Trimble 2004 and references therein). Riparian forest not only increases the resistance of floodplain surfaces to erosion, it provides a significant supply of large woody debris (LWD) to the channel. In-channel LWD interacts with streamflow and the surrounding floodplain to impede sediment transport rates and increase delivery times, affect planform channel morphology, and alter the rates of turnover in different parts of the floodplain (Collins et al. 2012; Wohl 2013). In the Ducktrap River, Maine, transport-limited reaches associated with frequent LWD blockages, exhibited longer residence times (>100 days) for fine sediments (<2 mm in diameter), than supply-limited zones (<100 days) (Fisher et al. 2010). Approximately 17-43% of the suspended sediment load in the South River, Virginia, USA, was estimated to be stored in sediment deposits

downstream of LWD accumulations, with 10% of sediment retained for over 60 years (Skalak & Pizzuto 2010). Elsewhere, several studies have documented how riparian vegetation and LWD have driven long-term floodplain turnover dynamics (e.g. Gottesfeld & Johnson Gottesfeld 1990; Konrad 2012; Nakamura et al. 2017).

In the context of sediment storage within floodplains specifically, an important process that needs to be considered is lateral erosion of the river channel. Natural channels are seldom perfectly straight lines and typically have a planform sinuosity (channel length divided by straight-line length between two points in the valley) that is greater than 1. As a result, the channel takes on a somewhat asymmetric cross-sectional profile, with shallower and slower flows along one side of the channel and a “thalweg” (area of fastest flow within the channel) along the opposite, apex side (Figure 2.5). As water flows through the channel it piles up at the apexes of the bends, which creates a pressure gradient across the channel cross-section whereby water and sediment transfer to the inside of the bends via secondary currents (Howard & Hemberger 1991). Deposited sediments along the inside of bends form point bars (Figure 2.5). As these point bars develop and bank erosion continues, the bends get tighter, causing a positive feedback that accelerates lateral migration (see Hickin & Nanson 1975; Nanson & Hickin 1983; Begin 1986 for further discussion of the relationship between radius of curvature and migration rate). Eventually, a cut-off forms across the neck of the meander bend (or across the necks of multiple meander bends simultaneously or in quick succession) via progressive lateral erosion of the floodplain or following a large flood event (Hooke & Harvey 1983). The resultant cut-off meander bend remains on the floodplain as an oxbow lake (and later, a palaeochannel), along with the point bar deposits that have accumulated at the inside of the old bend (Figure 2.5). The storage times of these floodplain deposits can be defined as the timeframe that spans from the initial deposition/abandonment of these features by the channel to their eventual erosion and remobilisation of their constituent sediments (cf. Bradley & Tucker 2013).

While our understanding of the full suite of controlling processes (and their interactions) on lateral erosion remain incomplete, one hypothesis is the

balance of impelling and resisting forces (*sensu* Fryirs & Brierley; Figure 2.3). Several studies have contributed to this hypothesis, including linking lateral erosion rates to declining streamflow magnitudes (e.g. Miller & Friedman 2009), changes in sediment supply (e.g. Constantine et al. 2014; Ahmed et al. 2019), different types of riparian vegetation cover (e.g. Micheli & Kirchner 2002; Trimble 2004), and anthropogenic influences such as the breaching of colonial mill dams (e.g. Pizzuto & O'Neal 2009).

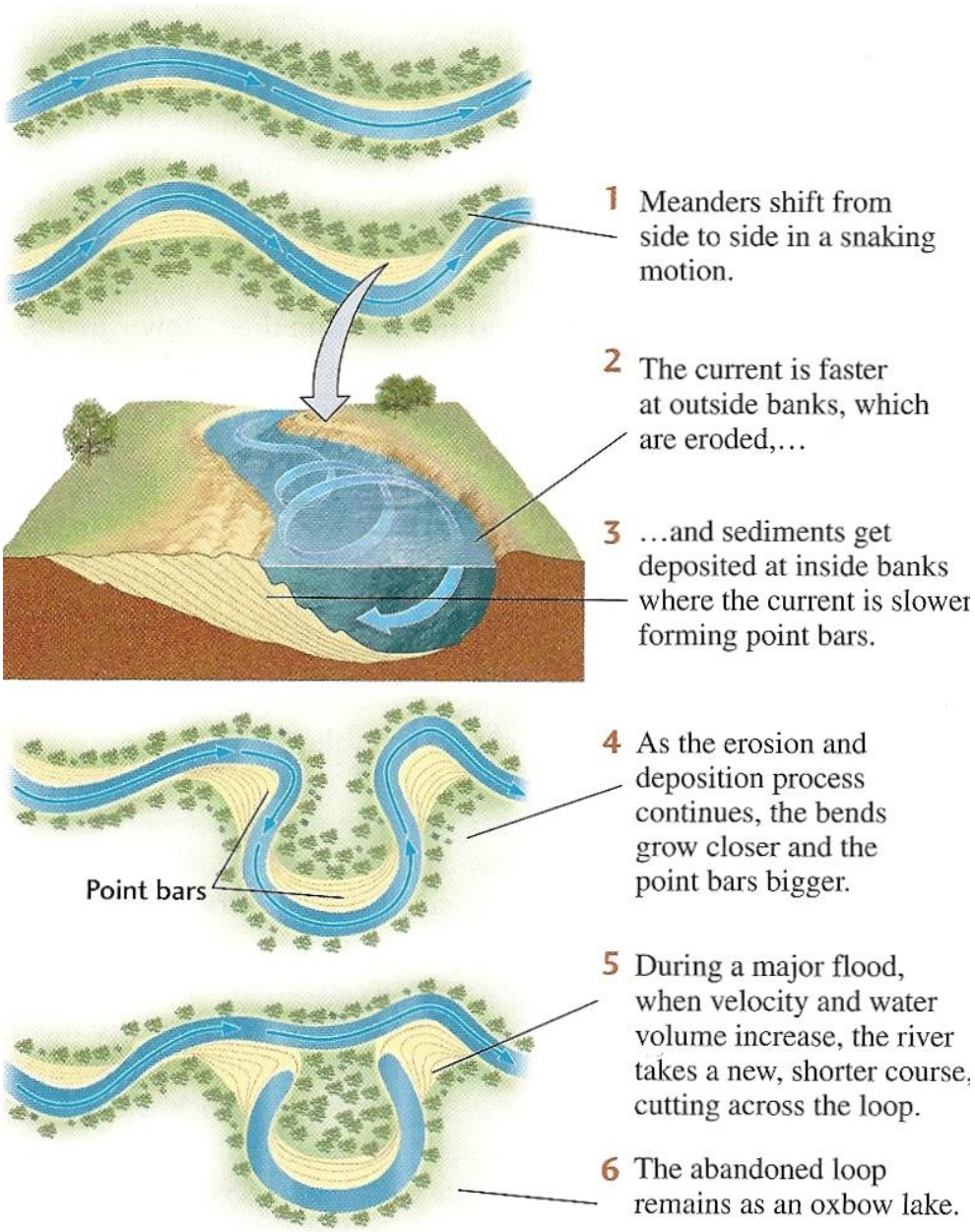

Figure 2.5: Lateral migration of river channels and the development of meanders and oxbow lakes (Grotzinger & Jordan 2010).

Other papers have pointed to internal process mechanisms as a major driver of lateral erosion dynamics. For example, some meander bends may take a form similar to semi-circles, while others may arrange into asymmetric Kinoshita waveforms with high levels of bend curvature and amplitude (Parker & Andrews 1986). At the whole catchment-scale, Fonstad and Marcus (2003) derived power-law relationships between the frequency of bank failures and their magnitudes, which may be interpreted as the spatial signal of self-organised criticality (SOC). If true, local instabilities generate wider-scale order and local alterations to the system will not change the criticality of the whole system (Fonstad & Marcus 2003), implying that internal process mechanisms are the primary driver of lateral erosion, not the balance of impelling and revisiting forces. Similar SOC-type behaviour has been identified for other lateral erosion processes, including channel width adjustments (e.g. Phillips 1991) and river meandering (e.g. Stolum 1996; Hooke 2004).

2.3. Quantifying timescales of storage and removal

2.3.1. Reservoir theory and key terminology

Determining timescales of particle storage and removal has been attempted throughout the environmental sciences, with early applications including ecology, hydrology and atmospheric chemistry (see Bolin & Rodhe 1973; Eriksson 1961, 1971), and later, geomorphology (Dietrich & Dunne 1978). Reservoir theory provides a useful framework for defining the sediment age, storage time, residence time and turnover time.

Reservoir theory describes the exchange of particles between one reservoir and another (Eriksson 1961, 1971; Bolin & Rodhe 1973). Usually, this assumes steady-state conditions, i.e. the total mass and statistical distributions of particles under consideration (e.g. sediment) remains constant over time (Bolin & Rodhe 1973).

Determining the storage times of individual particles is often difficult; hence, quantification focusses on bulk populations. Following Bolin & Rodhe (1973), by assuming that the age, τ, of sediment represents the time since initial entry

into a reservoir, the cumulative mass function of ages, $M(\tau)$, can be calculated as the mass of sediment that is equal to or younger than τ. From $M(\tau)$, it follows that the mass frequency function, $\psi(\tau)$, of the sediment with respect to age (the age distribution of stored sediment) is defined by:

$$\psi(\tau) = \frac{1}{M_0}\frac{dM(\tau)}{d\tau} \qquad (1)$$

where M_0 is the total mass in storage. As each particle can be distinguished by its age, the storage time (termed the "transit time" in the original literature) function can be resolved from the age of the cumulative mass of sediment exiting storage over a given timespan, $Q(\tau)$, and the steady state flux into and out of storage, Q_0. The storage time frequency function, $\phi(\tau)$, or the age distribution of material leaving storage, is given as:

$$\phi(\tau) = \frac{1}{F_0}\frac{dF(\tau)}{d\tau} \qquad (2)$$

Thus, the average age, τ_a, and the average transit time, τ_t, are given as:

$$\tau_a = \frac{1}{M_0}\int_0^\infty \tau dM(\tau) \qquad (3)$$

$$\tau_t = \int_0^\infty \tau\phi(\tau)dt \qquad (4)$$

Under steady-state conditions, the age distribution within storage remains constant such that the flux out of the reservoir that is older than τ must be balanced by the mass reaching an age of τ within the reservoir (Bolin & Rodhe 1973). Turnover time is defined as the ratio of mass in storage to the total flux, which is equal to the mean storage time (also termed the residence time) of particles under steady state (Bolin & Rodhe 1973):

$$\frac{M_0}{Q_0} \qquad (5)$$

The reservoir theory concept has often been applied to fluvial systems, with this inherent steady-state assumption, to estimate residence times and storage time distributions from sediment ages in storage (e.g. Malmon et al. 2002, 2003, 2005). However, Hoffmann (2015) notes that many geomorphic systems are out of equilibrium with respect to their environmental drivers,

particularly over 10^3-10^4-year timescales. Thus, these assumptions cannot apply in systems that are out of equilibrium. If one can determine if the system is degrading (i.e. mean age > residence time) or aggrading (mean age < residence time), then alternative storage time frequency functions can be calculated (see Bolin & Rodhe 1973 and Hoffmann 2015). One such example was applied to millennial-scale sediment budgets of agricultural catchments in Central Europe and paraglacial mountain catchments in the Canadian Rockies. In the case of the former, sediment delivery ratios were linked to the storage times of eroded sediments, i.e. time since the onset of agriculture and associated land cover change. In the latter, paraglacial sediment flux response times were 100-400 kyr, exceeding the return intervals of major glaciations (Hoffmann 2015).

Table 2.1 describes a number of key terms related to the quantification of sediment storage timescales. Throughout this chapter, the use of terms will be based strictly on the definitions described in Table 2.1. Delivery times (also called travel or export times) are a measure of the total timescale of sediment delivery from original erosion source to ultimate sink, and can be thought of as the accumulation of time across all individual episodes of storage and transit (Figure 2.1; Pizzuto et al. 2017). Sediment storage behaviour may evolve over time, for example, from age-dependent to age-independent erosion patterns. The time required for this transition is the crossover time, with one example including the transition from transient state to equilibrium conditions in channel bed elevation fluctuations (Voepel et al. 2013). Transport length has been described as the distance particles travel in a single flow event (Bonniwell et al. 1999) and to illustrate that sediments may undergo multiple phases of storage before leaving a river system (Torres et al. 2017).

Table 2.1: Definitions of key terms in sediment storage time literature.

Term	Definition	Example references
Age (often termed depositional age)	The time elapsed since a particle first entered storage until the time of measurement.	Eriksson (1961, 1971); Almond et al. (2007); Miller & Friedman (2009); Lauer (2012); Hoffmann (2015)

Storage / transit / waiting time	The length of time that a particle will reside in a defined system or reservoir, from initial entry to eventual removal. Equals the sum of age and time required to erode sediment.	Bolin & Rodhe (1973); Bradley & Tucker (2013); Pizzuto et al. (2017)
	Storage and transit times have been defined as separate entities, with the former referring to time elapsed in storage for an individual deposition/erosion interval, and the latter the total time accumulated across all these events.	(see Torres et al. 2017)
Residence time	The mean storage / transit / waiting time value.	Bolin & Rodhe (1973); Rodhe (2000); Hoffmann (2015)
Turnover time	The time required to completely replace all particles within an individual store or sink. Under steady-state conditions, turnover time equals the residence time.	Beechie et al. (2006); Collins et al. (2012); Wohl (2013)
Delivery / travel / export time	The total timescale of sediment delivery to ultimate sink from original source. Essentially, integrates the storage / transit times of all storage and transport events of a sediment particle.	Pizzuto et al. (2017); Croissant et al. (2017)
Crossover time	Time required to transition from one form of storage / transit / waiting time behaviour to another form.	Voepel et al. (2013)
Transport length	A characteristic length scale sediment travels before being re-deposited.	Bonniwell et al. (1999); Pizzuto (2014); Torres et al. (2017)
Virtual velocity	The total distance travelled by a particle divided by a measurement time interval, which includes periods of rest and transit.	Haschenburger & Church (1998); Ferguson & Wathen (1998); Voepel et al. (2013); Parsons et al., (2018)

2.3.2. Methods

As interest in understanding sediment trajectories and storage times in fluvial systems has grown, so too has the range of techniques with which to quantify them. Some methods have been applied to investigate environmental issues such as determining the spatial and temporal scale of floodplain contamination (e.g. Macklin & Lewin 1989; Miller 1997). Recently, other methods have emerged specifically for quantifying storage times and have been applied, for example, to estimate timescales of particle trajectories through valley floor

corridors and within sediment stores (e.g. Malmon et al. 2002, 2003, 2005), and variations in sediment age in response to environmental drivers (e.g. Dosseto et al. 2008a, 2008b). Each of these approaches, including their advantages and limitations, are reviewed below.

2.3.2.1. One-dimensional mass balance modelling

In the context of reach-scale fluvial systems, a simple one-dimensional mass balance approach can be applied to estimate the longevity of sediment storage. This procedure involves defining a reservoir mass (e.g. a floodplain area, volume or width) and dividing this by a representative flux rate (e.g. surface areal erosion, incision or lateral migration rate) (Dietrich & Dunne 1978; Dietrich et al. 1982). Under steady-state conditions, this value equals the turnover time – the time required to completely recycle the population of stored particles (in this case, sediment) within a reservoir (Table 2.1).

Turnover times have been estimated from average valley floor widths and lateral migration rates (Figure 2.6). For example, a turnover time of approximately 1000 years was calculated for a lowland reach of the Strickland River, Papua New Guinea, based on a floodplain width of ~10 km and mean lateral migration rate of 5.1 m yr^{-1} (Aalto et al. 2008). Floodplain turnover times ranged widely from ~100 to ~7000 years across several sites in the UK, depending on whether long-term lateral migration rates approximated calculated mean or maximum values (Hooke 1980). Turnover times for more than 20 rivers in western Canada, estimated using published lateral migration rates (Nicoll & Hickin 2010), ranged widely between ~70 and ~3750 years, with a mean of just under 900 years (Figure 2.6). Assuming steady-state conditions, calculated turnover times should equal the residence time (Bolin & Rodhe 1973). These calculations, however, assume that channel migration will span the entire valley width and calculated migration rates will not significantly deviate over time. This is very often not the case as the discussions in sections 2.3.2.2 and 2.3.2.3 elaborate.

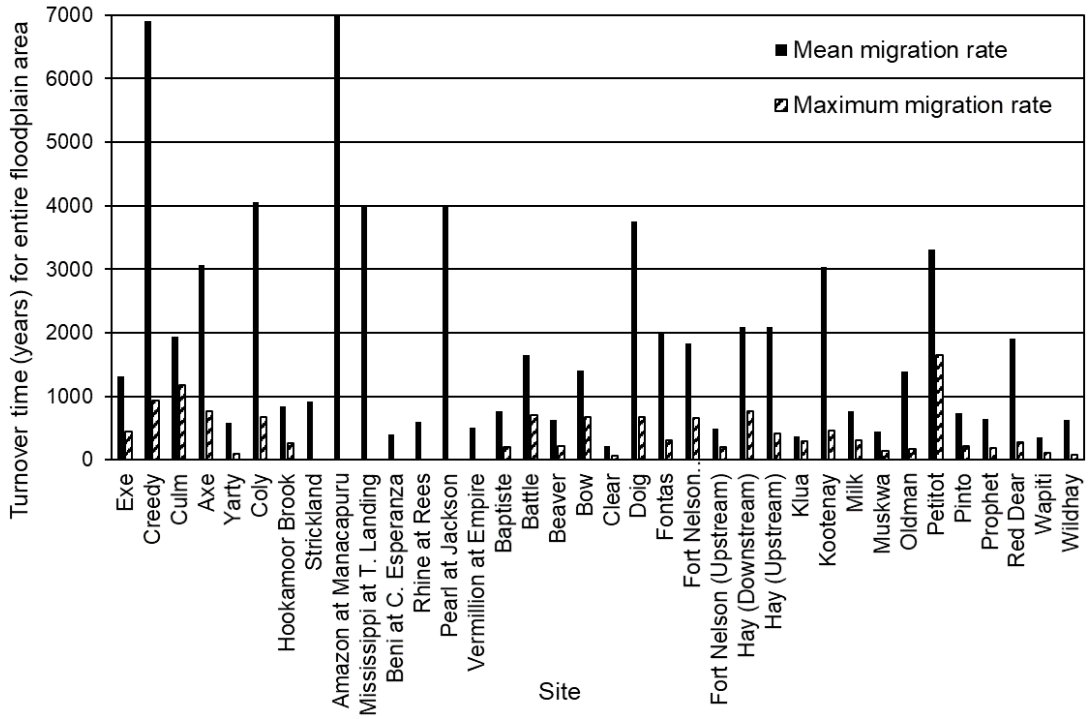

Figure 2.6: Published data on calculated floodplain turnover times for the Exe, Creedy, Culm, Axe, Yarty, Coly, Hookamoor Brook (Hooke 1980), Strickland (Aalto et al. 2008), Amazon, Mississippi, Beni, Rhine, Pearl, Vermillion Rivers (Wittmann & von Blanckenburg 2009 and references therein), and confined meandering river systems from 22 locations in western Canada (Nicol & Hickin 2009). Floodplain turnover times for these river systems were estimated by dividing valley widths (meander-belt widths in the case of the Canadian rivers) by lateral migration rates.

Konrad (2012) proposes three alternate models – linear, exponential and power law – of floodplain occupation dynamics by the channel. Floodplain turnover times, estimated using an average (or other single value) of lateral migration rate (Figure 2.6), imply that the cumulative area of the floodplain occupied by the channel will increase linearly over time (Figure 2.7a). For a linear model, the probability that an abandoned floodplain area will be re-occupied by the channel increases over time (Figure 2.7b), as the fraction of abandoned area remaining unoccupied decreases at a constant rate until reaching 0 (Figure 2.7c). The other models, exponential and power law, reflect

the skewed age distributions of floodplain surfaces (Everitt 1968; Nakamura & Kikuchi 1996).

Under the exponential model, the cumulative area of floodplain occupied by the channel, $C(t)$, increases according to:

$$C(t) = V(1 - e^{-rt}) \qquad (6)$$

where r is the probability of occupation over time, t (years) and V is the valley area (Konrad 2012; Figure 2.7a). The probability of the reoccupation of abandoned areas by the channel is assumed spatially uniform across the floodplain, and hence locations will be reoccupied in proportion to the fraction of the area that has been occupied previously (Figure 2.7b). The fraction of abandoned area remaining unoccupied decreases exponentially, and like the linear model, eventually approaches 0. Examples of this occurring in nature include the Little Missouri River, USA (Everitt 1968), Saru River in Japan (Nakamura & Kikuchi 1996), and along the Fraser, Grand and Bella Coola Rivers in Canada (Martin & Church 2004).

However, as several other studies have demonstrated, the probability that a channel will occupy a given area is not spatially uniform, i.e. floodplain areas that are closest to the channel are the most likely to be (re)occupied (e.g. Gottesfeld & Johnson Gottesfeld 1990; O' Connor et al. 2003; Miller & Friedman 2009). A power law function accounts for the decreasing probability of reoccupation over time (Figure 2.7b). Both the exponential and power law functions account for a decreasing rate of floodplain occupation over time as a result of reoccupation. However, the occupation rate initially decreases at a faster rate under the power law model than under the exponential model (Figure 2.7c). This reflects the preferential reoccupation of the most recently abandoned area under power law conditions versus the spatially uniform probability of reoccupation under exponential conditions (Konrad 2012). When historical channel-floodplain dynamics of five US rivers were reconstructed, Konrad (2012) found that in all cases, the power law model captured best the rates of floodplain (re)occupation by the channel. On average, an area of floodplain abandoned in the past decade was 10 times more likely to become

reoccupied by the channel than an area abandoned 30 years ago (Konrad 2012).

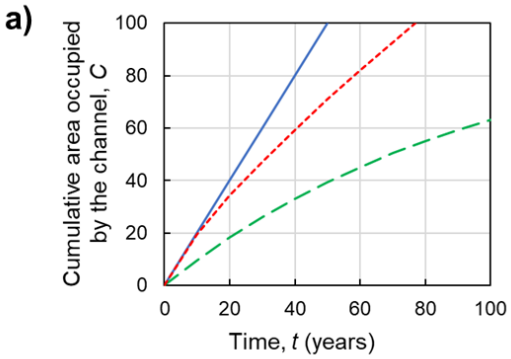

$$C(t) = 2t$$
$$C(t) = 3.1t^{0.8}$$
$$C(t) = 100\left(1 - e^{-0.01t}\right)$$

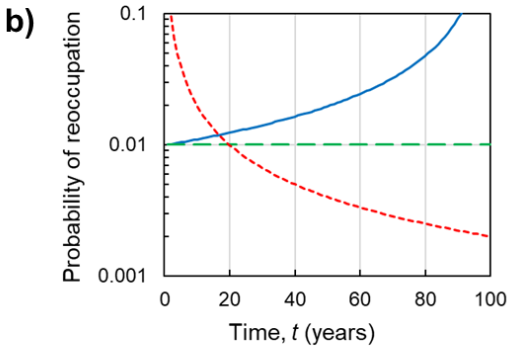

$$Pr(reoccupation) = \frac{2\Delta t}{200 - 2(t - t_i)}$$
$$Pr(reoccupation) = 1 - \frac{(t + \Delta t)^{0.8} - (t + \Delta t - t_i)^{0.8}}{t^{0.8} - (t - t_i)^{0.8}}$$
$$Pr(reoccupation) = 0.01$$

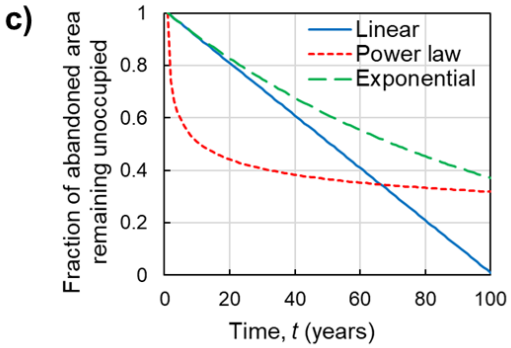

$$Proportion = 1 - \frac{2(t - t_i)}{200}$$
$$Proportion = \left(\frac{t}{t_i}\right)^{0.8} - \left(\frac{t}{t_i} - 1\right)^{0.8}$$
$$Proportion = e^{-0.01(t - t_i)}$$

Figure 2.7: a) Hypothetical examples of modelled cumulative area of floodplain occupation by the channel (expressed as linear, exponential and power law functions of time); b) The probability that a floodplain area will be reoccupied by the channel as a function time since previous occupation (i.e. floodplain age), expressed for the three models; c) The fraction of floodplain area that remains unoccupied as a function of time since the previous occupation for the three models (adapted from Konrad 2012).

The distinction between exponential and power law functions of floodplain (re)occupation has important ramifications for the distributions of sediment ages and storage times. Under the power law model, parts of the floodplain would remain uneroded for significantly longer than the one-dimensional mass balance approach of M_0/Q_0 would predict (Bolin & Rodhe 1973). If this is the case and the floodplain turnover time was calculated as M_0/Q_0, storage times would be under-estimated for areas of the floodplain unvisited by the channel, and over-estimated in areas where high rates of reoccupation of the youngest floodplain areas by the channel occurs (Miller & Friedman 2009). Depending on the floodplain in question, these under- and over-estimates could be at the scale of multiple orders of magnitude of the true values. Therefore, it is important to utilise techniques that allows one to model the full distribution of sediment ages and storage times within the floodplain or other sedimentary reservoir in question.

2.3.2.2. Modelling storage time distributions from age populations

A variety of proxies can be used to derive estimates of sediment storage time from deposit ages and landscape evolution processes. Several sources of evidence and techniques are summarised and displayed on a temporal scale-resolution matrix grid (Figure 2.8). This review focusses primarily on techniques and sources of evidence that have been employed in some effort to quantify or at least describe storage time behaviour. Hence, the use of erosion pins, lichenometry and terrestrial photogrammetry are not discussed in this review. However, these approaches (Figure 2.8) could be applied to quantify storage times at reach scale in conjunction with techniques that cover longer temporal scales, such as sediment deposit dating. The advantages and limitations of these alternative techniques have been reviewed previously (e.g. Lawler 1993; Barker et al. 1997; Čufar 2007; Black et al. 2010; Belmont et al. 2014).

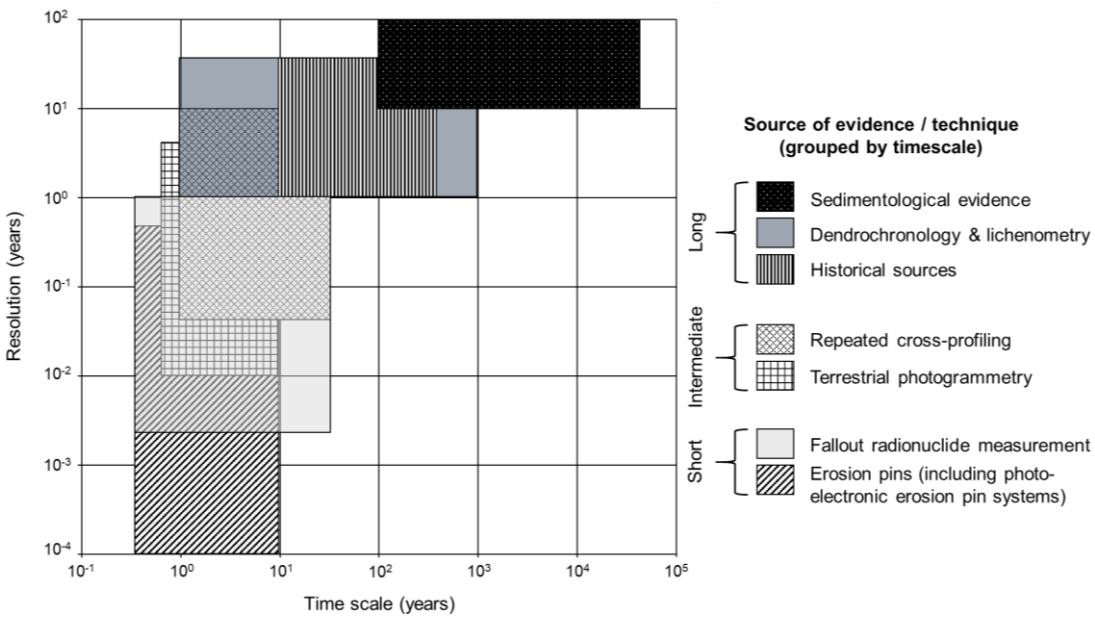

Figure 2.8: Potential techniques, including typical applicable time scales and resolutions, for measuring bank erosion, channel migration and quantifying sediment storage times at reach scale (modified from Lawler 1993).

Deriving storage times of sedimentary reservoirs from ages requires the determination of formative (depositional) and destructive (erosional) processes that drive rates and extents of sediment turnover. Preserved sediments in fluvial landforms, such as floodplains, terraces and deposits within the channel, provide a record of sediment deposition from which the age and rate of sediment accumulation can be resolved using a suite of chronometric techniques and proxies. Yet so far, there remain few attempts to derive estimates of sediment storage times from the stratigraphic record.

Storage times have been calculated from age populations using reservoir theory (Bolin & Rodhe 1973). Assuming ages have been constrained accurately (i.e. as close to the "true" ages of the deposited sediment/landform as possible – a significant challenge with chronometric techniques such as radiocarbon dating and dendrochronology), the workflow (Figure 2.9) involves the calculation of the cumulative distribution of ages, which are rearranged to determine the corresponding probability density function (PDF) and then evaluated at (or close to, if not possible) time 0 to obtain the residence time.

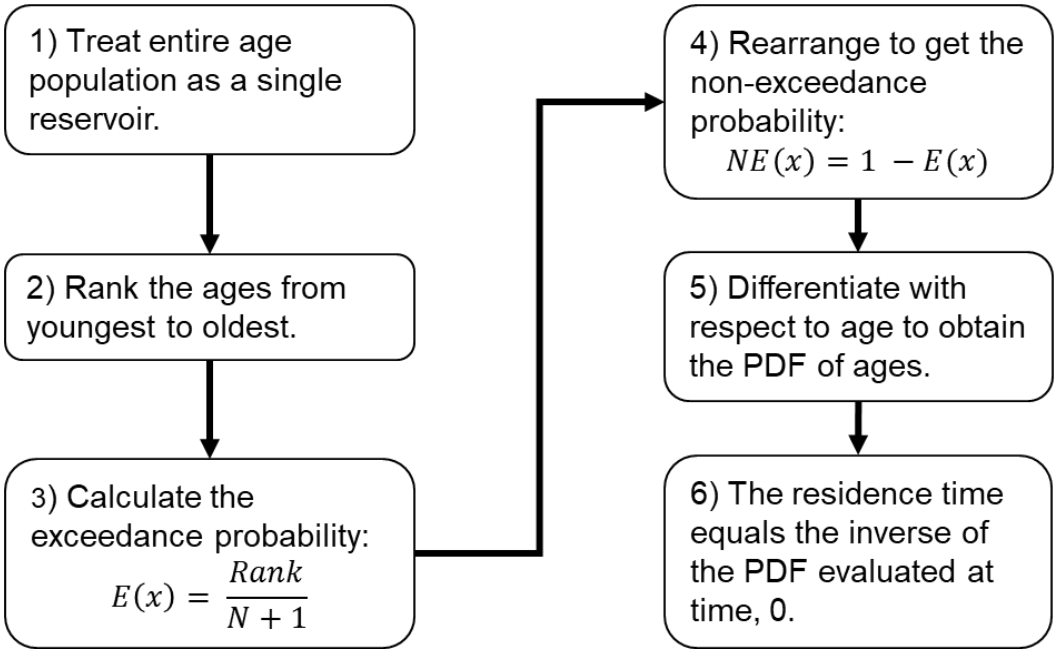

Figure 2.9: Workflow to estimate residence time from constrained sediment ages (based on the methods in Lancaster et al. 2007; Skalak & Pizzuto 2010).

In a study of two reaches in the Bear Creek Basin, Oregon, radiocarbon measurements were used to produce age estimates of sediments from channel bank and debris-flow deposits from which storage times could be inferred (Lancaster & Casebeer 2007). In the downstream reach, where sediment evacuation was dominated by fluvial erosion, a residence time of 1.22 x 10^3 ^{14}C yr (radiocarbon years) was calculated and an exponential storage time distribution was derived, implying sediment removal from landforms was age-independent (Lancaster & Casebeer 2007). Conversely in the upstream reach, where evacuation was dominated by debris flow processes, the residence time was 4.43 x 10^2 ^{14}C yr, with a power-law storage time distribution for sediment older than 100 ^{14}C yr, indicating preferential retention of older deposits here (Lancaster & Casebeer 2007). In a later study in the same region, storage times inferred from ^{14}C age estimates of terrace, channel bank and bed sediments taken from a debris-flow dominated confluence were compared with samples from a fluvial-process dominated confluence (Lancaster et al. 2010). Tributary deposits at both sites showed similar means (1370 ± 2240 yr and 1660 ± 2130 yr for the debris-flow

dominated and fluvial-process dominated sites, respectively), with right-skewed power-law storage time distributions (Lancaster et al. 2010). However, when comparing the main channel adjacent to the debris flow with that next to the terraces, the channel next to the debris flow exhibited much faster sediment removal (and with more equal probability across sediment ages) than the site next to the terraces where long-term preservation was much more likely (Lancaster et al. 2010). Both examples imply that not only are storage times variable by location within the drainage network, but also by antecedent sediment redistribution processes.

At a finer temporal scale, in the South River, Virginia, radiocarbon and radionuclide derived age populations were used to infer storage times of mercury-enriched fine-grained channel margin deposits (Skalak & Pizzuto 2010). Here, power-law storage time distributions, with a median of 1.75 years, implied that while the majority of sediments in these deposits were remobilised rapidly, a fraction could be retained chronically (10% for over 60 years), with potentially lasting water quality implications (Skalak & Pizzuto 2010). Similar patterns were noted for the adjoining floodplain, albeit with a much larger residence time of 2930 years (Skalak et al. 2015).

There are two key limitations to this type of approach. First, uncertainties and sources of error are associated with the dating-techniques themselves (see Bronk Ramsey 2008 and Thrasher et al. 2009 for a review of radiocarbon dating and optically stimulated luminescence dating limitations, respectively). Second, ages relate only to remnant material, which are then used to infer a distribution of storage times (i.e. the ages of the no longer present material). The accuracy of an age population-inferred storage time distribution has yet to be evaluated, and to explicitly quantify storage times, ages of the material must be determined directly at the point of erosion.

Reconstruction of historical river channel changes using alluvial valley mapping techniques offers a means of quantifying directly the processes that determine the age distribution of deposited sediments. Alluvial valley floor mapping using geographical information systems and remote sensing has been widely applied in fluvial geomorphology, especially at a reach scale. Past

applications include monitoring contaminated sediment dispersal within valley floors (e.g. Miller 1997), quantifying the contribution of sediments from recent historical and older “legacy” deposits within American piedmont streams (e.g. Donovan et al. 2015), and reconstructing historical channel migration patterns (e.g. Hooke 1980). Quantifying valley floor sediment storage times using geographical information systems and remote sensing has also been previously explored.

Miller & Friedman (2009) digitised polygons of channel position into separate planimetric measures of floodplain formation and destruction to produce a map of surface patch ages for a reach of the Little Missouri River. They used a linear regression of patch ages and area to infer the nature of the storage time distribution. A negative relationship indicated exponential decay, because the probability of floodplain reoccupation would be age-independent and hence, older material would occupy the smallest area of land due to longer exposure times to erosion (see Konrad 2012; Bradley & Tucker 2013). A positive relationship indicated age-dependent sediment retention, reflecting preservation of older material, and preferential reworking of younger material. Their analysis revealed that decreasing lateral erosion rates, in response to a century-long decline in mean annual discharge, yielded a positive age-area trend (Miller & Friedman 2009). Field and aerial survey of floodplain deposits of the Saru River, Japan revealed exponential decreases in the proportion of eroded area with increasing floodplain age (Nakamura & Kikuchi 1996). Phillips et al. (2007) however, critiqued this approach, arguing that the Saru River study assumed steady-state conditions and unrealistically extrapolated determined transport rates backwards in time. Their own study determined a surface area-age relationship for the entire valley floor of a reach of the Waipaoa River, New Zealand, and trialled different regressions to determine the best-fit distribution equation (Phillips et al. 2007). The equation of the resulting logarithmic distribution was then rearranged to estimate times of 310, 30,610 and 96,510 years for 50, 90 and 100% removal of the floodplain, respectively (Phillips et al. 2007).

The historical record of maps and aerial imagery for river channel change reconstruction is relatively short (several decades) compared to estimated

floodplain turnover times (centuries to millennia in many cases – see Figure 2.6). However, even relatively short-timescale reconstructions of river channel changes can reveal useful information about the sediment storage time distribution of a floodplain. Consider the example of two river systems – the Little Missouri River in North Dakota and the Beaver River in Alberta (Figure 2.10). Both reaches are similar in valley length (~2-3 km) and river channel changes have been reconstructed over a similar timeframe (the past ~50-65 years). The Little Missouri River reach shows signs of floodplain areas that were occupied by the channel previously being re-eroded (Figure 2.10a). In the circled area of Figure 2.10a, a cut-off formed across two bends at some time between 1958 and 1966 (red polygon). Since that time, the channel has started to reform these two bends, with the most upstream of these bends migrating in a northeast direction and the downstream bend in a southwest direction. As migration progressed, the channel eroded more of its recently occupied floodplain areas than areas of the floodplain that have not been occupied by the channel before – i.e. the pre-1939 floodplain (grey polygon). It is likely here that the probability of reoccupation of floodplain by the channel decays as a power law function of floodplain age (see Figure 2.7b) and the resulting storage time distribution of floodplain sediment is heavy tailed. By contrast, digitisation of historical channel centrelines along the Beaver River displays a different form of behaviour (Figure 2.10b). In this system, the channel does not develop cut-offs (or any other avulsions) and the meander bends migrate downstream as a coherent waveform along the central valley axis (Nicoll & Hickin 2010). As a meander bend migrates, its former position within the valley floor eventually becomes occupied by the neighbouring upstream meander bend. The probability of floodplain reoccupation by the channel will therefore likely be uniform (Figure 2.7b) and as a result the distribution of sediment storage times will decay exponentially.

More often than not, historical maps and aerial imagery do not cover the timescales necessary to measure the long-term dynamics of floodplain-channel sediment exchanges. This limitation restricts the application of this approach to only the most actively changing and extensively monitored systems. Thus, some storage time quantification studies have relied on

dendrochronology – the method of constraining arboreal or other woody material ages from the analysis of tree growth patterns (Everitt 1968) – as an alternative or supplementary technique to extend historical age reconstructions.

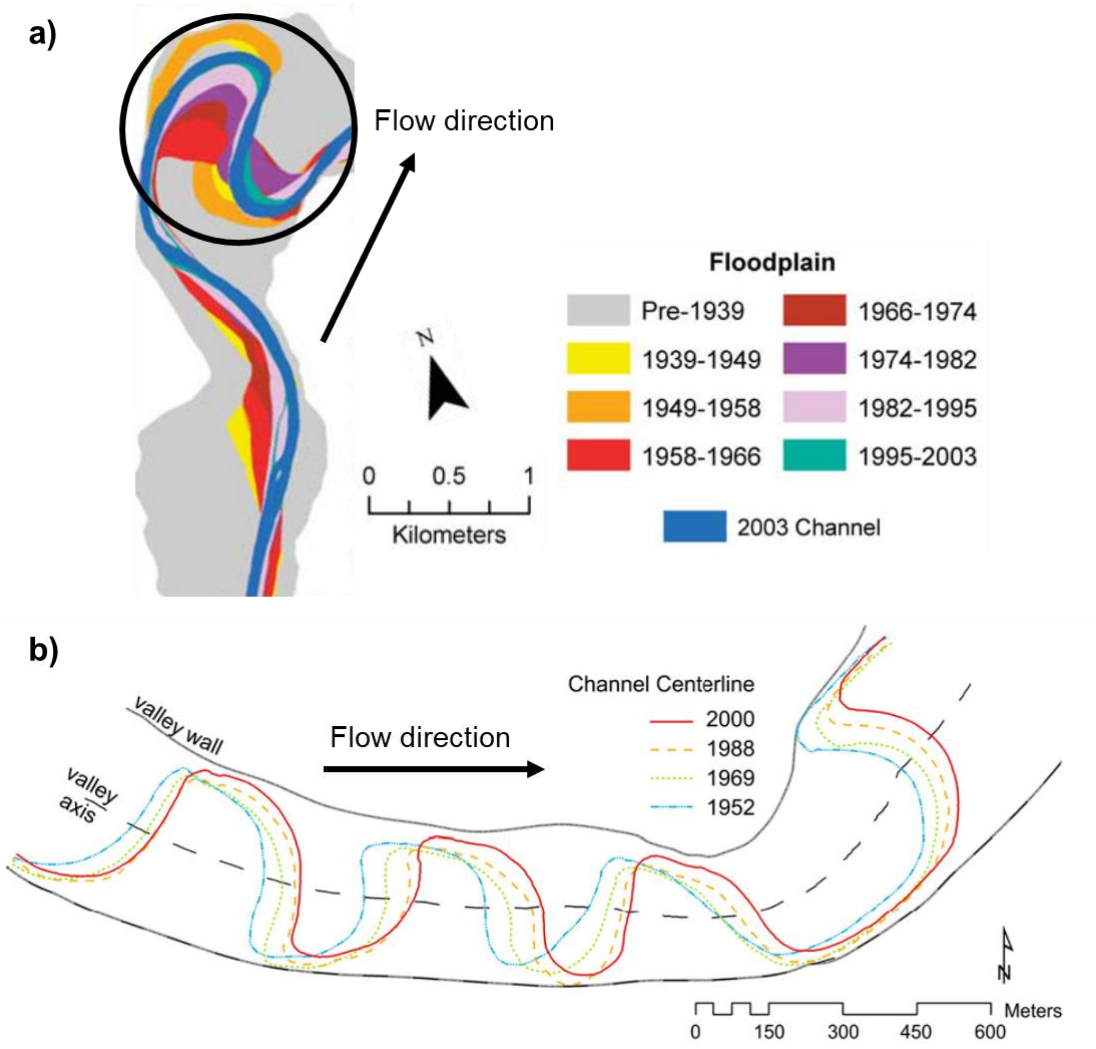

Figure 2.10: a) Intervals of floodplain formation and the resulting age map (in planform) of the Little Missouri River, USA (modified from Miller & Friedman 2009). The black circle indicates where the channel appears to be eroding areas that it previously occupied during the reconstructed historical record at a higher rate than areas that have not been occupied by the channel before the reconstruction period (pre-1939). b) Successive channel centrelines of the Beaver River in western Canada illustrating planimetric lateral channel migration over 50 years (adapted from Nicoll & Hickin 2010).

Determining the ages of vegetation on the floodplain relies on the premise that vegetation age directly reflects the history of sediment transport – i.e. the age distribution of vegetation is equivalent to the age distribution of the floodplain deposits they occupy (Nakamura & Kikuchi 1996) – and thus, the continuous reworking of sedimentary landforms drives the distribution of different vegetation species and age patterns. Thus, the ages of the oldest riparian vegetation may provide a realistic estimate of the minimum age of the colonised sediments in question (Everitt 1968; Nanson & Beach 1977). Beechie et al. (2006) estimated floodplain turnover times using tree stand ages derived from crown diameter measurements in aerial photographs and related this to four different channel pattern types (straight, meandering, braided and anabranching) for rivers in forested mountain valleys. Braided systems were found to rework their floodplains in as little as 8 years on average, increasing to 33, 60 and 89 years for anabranching, meandering and straight reaches, respectively (Beechie et al. 2006).

Dendrochronology is limited by several factors. First, unless an approach like Beechie et al. (2006) is adopted, spatial scales may be limited to reaches of up to a few kilometres at most. Second, the time scale that can be reconstructed is limited by the life span of the vegetation species, which may be much shorter than the lifetime of some sedimentary deposits such as older floodplains and terraces. Third, dating inaccuracies can arise with the presence of double rings or missing rings in sampled cores or disks (Malik 2006). Fourth, there is often a lag time between initial sediment deposition and vegetation colonisation, and thus deposit age estimates can be off by decades or more (e.g. Everitt 1968; Nanson & Beach 1977; Malik 2006). Care should also be taken when inferring sediment storage time behaviour directly from age distributions of the local vegetation. Miller & Friedman (2009) determined that sediment patch ages reconstructed from channel changes did not correlate with the exponentially distributed forest ages in the Little Missouri River valley identified by Everitt (1968). Thus, using vegetation as the only proxy for quantifying sediment storage behaviour could be problematic, and therefore should be applied in conjunction with other proxies and techniques.

2.3.2.3. Recording ages and storage times directly from spatial and temporal patterns of erosion and deposition

Storage time determination for individual grains in the channel bed is difficult and, in some cases, direct measurement periods are constrained by human lifetimes. Therefore, storage time probability distributions of the wider population of sediments are inferred theoretically from a smaller dataset of measured storage times. In the rare case that direct measurements can be obtained, these distributions are inferred from transport characteristics such as transport distance, the timings of sediment mobilisation and sediment virtual velocity (Voepel et al. 2013), or from depositional evidence such as age-constrained material and elevation changes (Moody 2017).

Voepel et al. (2013) constructed a high-resolution time-series of fluctuations in channel bed elevation using sonar transducer measurements of two different flume experiments. The first experiment focussed on well-sorted grains with no bedforms, with elevation measurements taken every 3 seconds; the second focussed on poorly sorted grains with bedforms present, and elevations measured every 10 seconds. These data were combined with an empirical model, that equated time of deposition with bed elevation increase, and time of entrainment with elevation decrease, resulting in storage times calculated for the entire bed thickness under different conditions. Under “semi-infinite” conditions, where the bed could fluctuate in thickness from 0 (bedrock level) to ∞, power-law distributions emerged; conversely exponential distributions emerged for “finite” conditions, where bed elevations were bounded above by sediment, flow and hydraulic drag conditions, as well as bedrock below (Voepel et al. 2013). In both experiments, they found that the storage time distribution was best fitted by a power law function initially, before adjusting to an exponential one as sufficient time elapsed (Voepel et al. 2013). While this crossover to exponential conditions took less than 1 minute in both flume experiments, it is noted that for field examples, where large-scale fluctuations in flow, sediment supply, vegetation and bedform morphologies are much more complex and, this crossover time could be on the order of days to years (Voepel et al. 2013).

In another example, age and storage time distributions were constrained from a time series of cross-sectional elevation changes along a “sediment superslug” – defined as a large body of clastic sediment deposited following disturbance, resulting from catchment-scale sediment supply and producing major valley-floor adjustment (see Nicholas et al. 1995) – that was deposited during a major flood event following wildfire in the Colorado Front Range (Moody 2017). Like Voepel et al. (2013), increases in elevation were recorded as deposition and decreases as erosion (Moody 2017). Due to the complex shapes of the age and storage time distributions, which could not be fitted with either an exponential or a power law function, they were instead fitted with two-parameter Weibull probability distribution functions. In both cases, the scale parameter approximated the median of each distribution and the shape parameter increased linearly with the time since the extreme flood that originally deposited the superslug (Moody 2017). These distributions changed shape at each cross-section with time, reflecting changes in the prevalence of major geomorphic processes (Figure 2.11a). For example, when the age distribution displayed overall concave curvature, stored deposits consisted predominantly of younger aged material, reflecting the rapid accumulation of new deposits during the early aggradation phase (Figure 2.11). Subsequent incision changed the age distribution to a convex form (Figure 2.11c), with significant reductions in the rate of accumulation of new deposits, but also reflecting the relatively high retention of older aged material along the valley margins and at the greatest depths of the sediment superslug (Figure 2.11b). Likewise, the storage time distribution also switched to convex curvature (Figure 2.11d). This is because during aggradation, the channel would have eroded the youngest deposits for the most part, as these were closest to the channel. When rates of sediment supply fell and incision was initiated as a result, channel erosion reached greater depths and with it, a wider range of deposit ages could be sampled, creating a storage time distribution that was skewed towards larger values (Moody 2017). As the superslug stabilised, and the channel eroded only its closest (and therefore youngest aged) deposits, the age distribution retained its convex curvature (Figure 2.11c) while the storage time distribution switched back to concave curvature (Figure 2.11d).

These studies represent the few attempts to constrain, and model the distributions of, storage times using cross-sectional measurements of the channel bed. This dearth of storage time calculations in the literature may reflect the paucity of channel bed elevation time-series data arising from the time constraints associated with monitoring, such as human longevity (particularly if multi-decadal or longer timeframes are required for analysis). Nevertheless, existing studies demonstrate this approach can provide insights into the evolution of channel beds in response to hydrological and geomorphological controls, such as flood frequency and magnitude, and sediment supply over sub-annual to multi-decadal timescales.

Modelling geomorphological processes offers a means of overcoming data limitations and restrictions on temporal scale and resolution. Many existing models can be applied at a range of scales, from whole river basins to field plots. In the context of sediment storage dynamics, the choice of model (see Coulthard 2001; Tucker & Hancock 2010 for reviews) and the scale of application (see Coulthard et al. 2007) will depend primarily on the research question itself and the variables to be tested including the size of the sedimentary reservoir. Models can simulate the effects of environmental drivers on sediment exchanges over a range of timescales from minutes to millions of years. They provide a virtual laboratory where the choice of boundary conditions and inputs can be controlled carefully (Van De Wiel et al. 2011). This approach could elucidate what controls sediment storage times and potentially be used to reconstruct past behaviour or generate predictions of the future (Tucker & Hancock 2010).

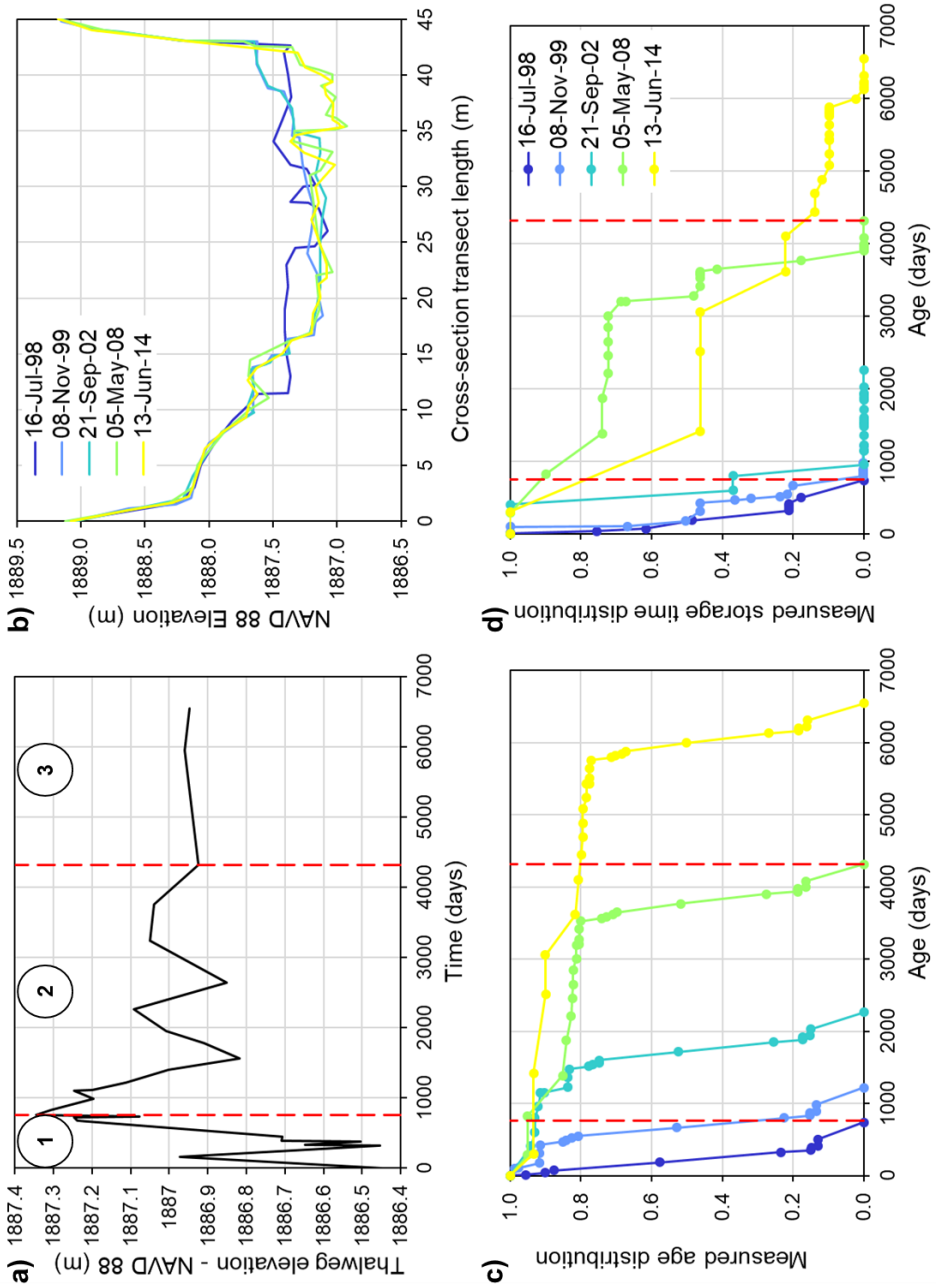

Figure 2.11: a) Three phases in the evolution of a superslug deposited following a wildfire in the Front Range Mountains, Colorado (1. Aggradation, 2. Incision, 3. Stabilisation). Thalweg elevations of the superslug at XS0341 (see Moody 2017) are plotted following the extreme flood on 12 July 1996 (~510 m^3 s^{-1} or ~24 m^3 s^{-1} km^{-2}). Red dashed lines mark the boundaries between the phases of dominant processes in the evolution of the superslug. b) Changes in the cross-sectional profile at XS0314 for five dates over ~18 years. c) Measured age distributions and d) measured storage time distributions for the same dates as in b) at XS0341. Plots were generated using data from: http://doi.org/10.5066/F757196C (last accessed 10/10/19).

Landscape evolution models (LEMs) simulate morphological changes, including processes that (re)distribute sediments within the landscape (Tucker & Hancock 2010). The CAESAR model for example, has simulated changes in metal-contaminated sediment storage and flux patterns in the Swale catchment in Yorkshire (Coulthard & Macklin 2003), reach scale channel changes (e.g. Coulthard & Van De Wiel 2006; Van De Wiel et al. 2007), and catchment responses to environmental change (e.g. Coulthard & Macklin 2001; Coulthard et al. 2005). Yet, LEM-based attempts to determine sediment storage times remain relatively unexplored.

One of the few LEM-based attempts at storage time quantification has been undertaken using the CHILD model (Tucker et al. 2001) in a study by Bradley & Tucker (2013). Lateral migration of a synthetic channel was simulated over 100 ka using a topographic steering model (Lancaster & Bras 2002). The floodplain developed over time via lateral migration, with the channel position recorded at each time interval using a static grid of distributed nodes over an imported triangulated irregular network used in previous meander evolution studies (see Clevis et al. 2006). Storage times were calculated as the interval between a channel departing from a node and its subsequent return, creating a mosaic of floodplain ages (Figure 2.12a), with the oldest ages representing the longest time since a node was last occupied (Bradley & Tucker 2013). They observed an age distribution that did not conform to the exponential model (Figure 2.12b) and a power-law storage time distribution (Figure 2.12c). Further, the mean age exceeded the mean storage time consistently (Figure 2.12d), suggesting erosion favoured younger material – a fact which was supported when calculated “erosion hazards” (the probability of removal from storage based on age) correlated negatively with age (Figure 2.12e). Using similar methods along a reach of the Strickland River, Papua New Guinea, the recorded floodplain age distribution after ~6000 years was exponential (Lauer 2012), indicating the erosion hazard/probability of reoccupation was uniform across ages (Bradley & Tucker 2013; Konrad 2012).

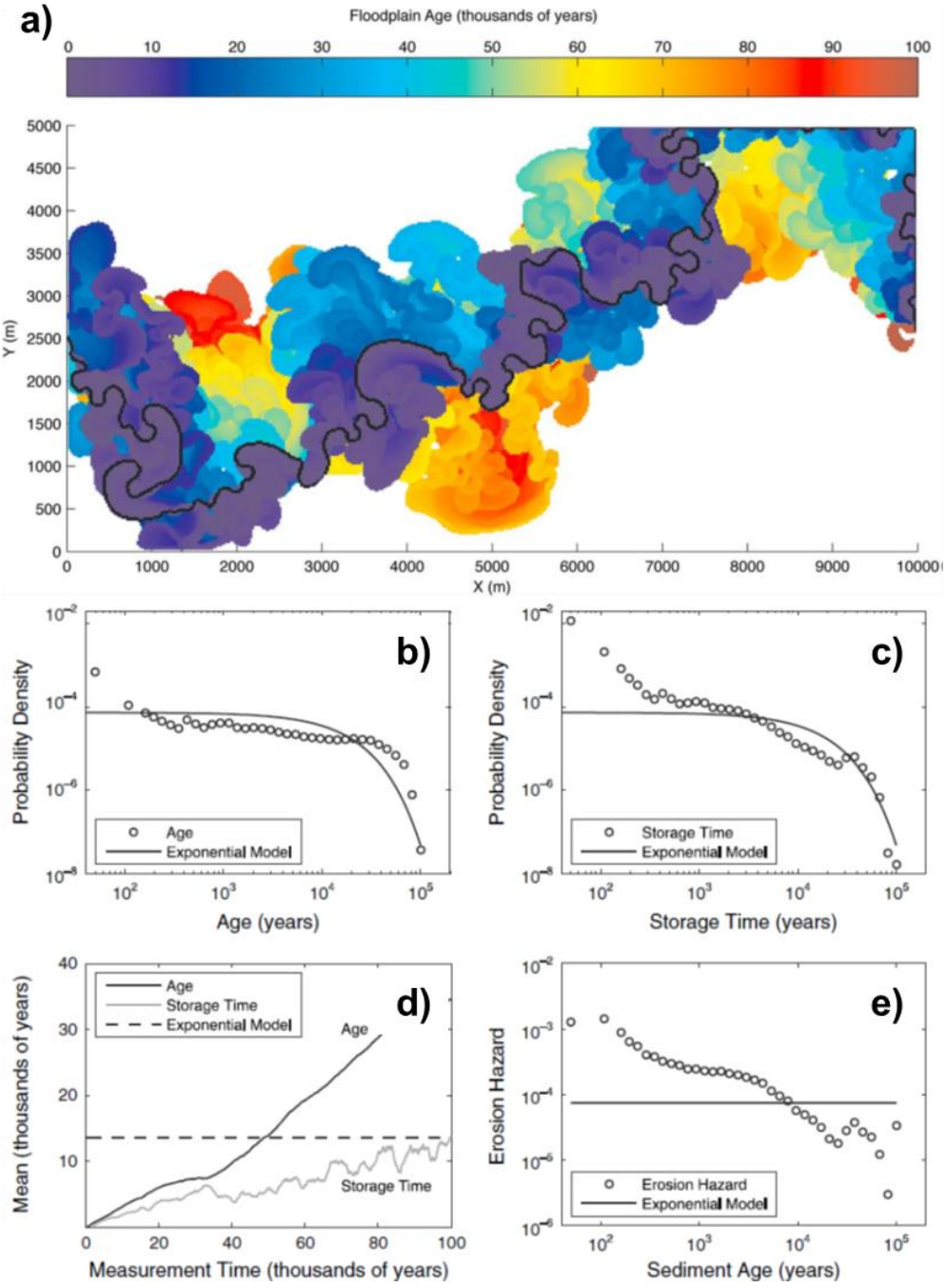

Figure 2.12: a) Floodplain age map after 100,000 years of simulated channel changes using CHILD (black line marks the channel position at the end of the simulation). b) the recorded age distribution (circles) with the exponential model produced if floodplain area (M_0) is divided by the mean erosion rate (Q_0) – black line. c) the storage time distribution with the exponential function predicted from M_0/Q_0. d) Changes in mean age and mean storage time over time. e) Erosion hazard for each of the age bins, with the uniform erosion hazard line – $Q_0/M_0 = 7.36 \times 10^{-5}$ – assuming the distribution of ages and storage times decayed exponentially (adapted from Bradley & Tucker 2013).

Recent work has produced some useful insights into the storage dynamics of landslide-derived sediment in valley floors. A 2D LEM, tested on the Sun Koshi River, revealed that landslide sediment delivery times were dramatically reduced (from 37-600 years to 4.4-8.5 years) as the channel adjusted through self-organisation to a narrower form with increased transport capacity (Croissant et al. 2017). This insight, along with results from storage time calculations from monitored geomorphic changes (see Moody 2017), has important implications for monitoring downstream sedimentation and associated hazards. Using a particulate organic carbon cycling model, that combined lateral channel change with atmosphere-biosphere carbon exchanges, it was shown that floodplain sedimentary carbon storage can have a significant impact on carbon cycling over 10^0 – 10^6 year scales (Torres et al. 2017).

While LEMs possess many advantages for simulating storage times and their controls, there are some important limitations. These include prohibitively long run times, especially if very long timescales (several thousands of years) and a high spatial resolution are chosen, meaning a compromise of spatio-temporal detail is inevitable (Coulthard 2001; Tucker & Hancock 2010). Models may need to be parameterised and evaluated based on measured datasets, which can be time-consuming and difficult to achieve. Torres et al. (2017) for example, evaluated their model results by comparison with datasets of measured riverine particulate organic matter radiocarbon content. Many simulations cover often very long timescales, so model evaluation may be limited to short and/or scarce historical datasets. Furthermore, many LEMs, despite using simplified equations to drive Earth surface processes, may still have large data requirements, which may have to be derived from sample points that are aggregated or interpolated over wider spatial scales (Van De Wiel et al. 2011). Given the simulation timeframes necessary to adequately capture reservoir turnover (e.g. at least $10^{2\text{-}3}$ years for many floodplains – see Figure 2.6), modelling storage times may focus more on exploratory than predictive/retrodictive applications.

2.3.2.4. Stochastic modelling of sediment routing through valley floor corridors

A sediment mass balance can determine net changes in storage in different reservoirs by subtracting sediment outputs past a defined outlet from total inputs of sediment upstream and from lateral sources such as hillslopes and channel banks (Dietrich & Dunne 1978). The technique has been applied previously to calculate catchment sediment budgets and describe (dis)connectivity within the sediment cascade (Fryirs 2013). Several studies have focussed primarily on hillslope-channel coupling in mountain basins (e.g. Bennett et al. 2014), while others have investigated how storage and transport of suspended sediments are conditioned by channel length, and by extension, catchment area (e.g. Keeler et al. 2015; Pizzuto et al. 2014, 2017). Successions of these mass balances can also provide estimates of sediment storage times in different stores by dividing the mass in storage by the average rate of flux over a given time interval (Dietrich & Dunne 1978).

At reach scale, the focus is on the probabilistic transfer of sediments between the channel and floodplain (Lauer & Willenbring 2010; Malmon et al. 2002, 2003, 2005; Wittmann & von Blanckenburg 2009). The rationale for this focus is that hillslope sediment supplied to channel networks, as well as storage and transport processes within alluvial valley floors are described by some authors as stochastic in nature (Dietrich & Dunne 1978; Kelsey et al. 1987; Benda & Dunne 1997). At reach scale, the valley floor can be represented as a Markov chain, consisting of multiple connected reaches, with each reach subdivided into separate floodplain and channel compartments (Figure 2.13a). Sediment particles have multiple possible fates, the probability of these being determined from a sediment budget, equations governing erosion, deposition and transport, and a probability density function of sediment storage times (Kelsey et al. 1987; Pizzuto et al. 2017). A particle in the channel of an upstream reach may be temporarily remobilised and then resettle in the same store; transfer to the floodplain of the same reach; transfer to either the channel or the floodplain of a downstream reach; or transfer out of the system to a defined “absorbing state” such as a lake or sea (see Malmon et al. 2003 for more details). Subsequent studies (e.g. Lauer & Willenbring 2010) have

built upon this model by including additional lateral inputs from tributaries, as well as removal from the system via deep burial (Figure 2.13b).

There have been numerous applications of this approach to calculate sediment delivery times. Delivery times and possible trajectories of ^{137}Cs-enriched fluvial sediments in the Los Alamos Canyon were modelled using calculated sediment budgets, ^{137}Cs inventories and estimates of upstream input history for parameterisation (Malmon et al. 2002, 2005). Half of the original 38,500 metric tons of presently stored sediments were predicted to be evacuated in 12-18 years, 90% in 82-87 years, and 99% in 126-211 years (Malmon et al. 2002). Malmon et al. (2005) revised the Markov chain model in Figure 2.13a to simulate bedload transfers between channel reservoirs and fine sediments between floodplain reservoirs. They found that coarse sediment storage within channel reservoirs spanned 15.5 years before reaching the absorbing state, while for floodplains, the delivery time of fine sediment was 58 years on average (Malmon et al. 2005). Pizzuto et al. (2017) modelled sediment delivery times over different transport distances. Over 25 km, few particles entered storage, resulting in median delivery times of 0.2 years, while over 1000 km, the effect of storage was much more significant, producing median delivery times of 2.6 million years (Pizzuto et al. 2017). In a model of reaches of the Amazon and Beni Rivers, the floodplain was divided into a number of compartments and residence times calculated by dividing channel belt width by lateral migration rate (Wittmann & von Blanckenburg 2009). Sediment residence times of approximately 400 and 7000 years were calculated for the floodplains of the Beni and Amazon Rivers, respectively (Wittmann & von Blanckenburg 2009). In a study of the Neuse River, USA, sediment exchanges were modelled laterally (via channel migration mainly) and vertically (via burial and incision) (Lauer & Willenbring 2010; Figure 2.13b). Although storage times were not reported, for floodplains with long residence times, meteoric fallout and cosmogenic production allowed radioactive tracer concentrations to increase down-valley (Lauer & Willenbring 2010).

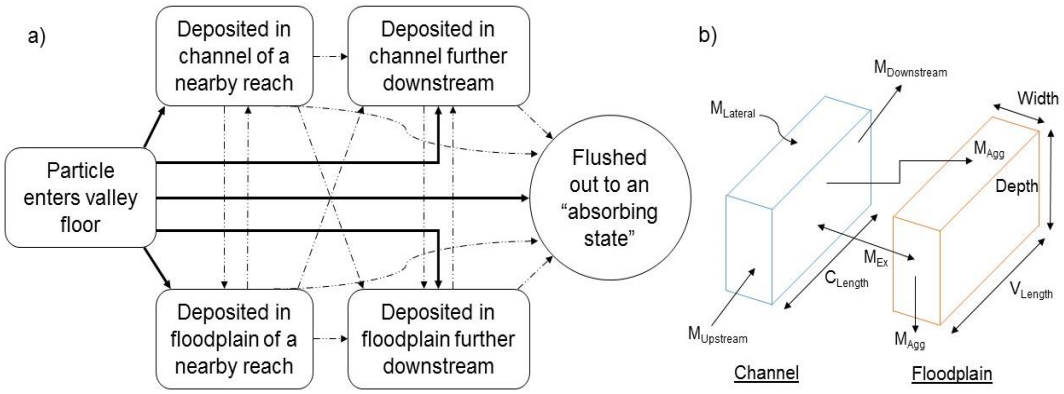

Figure 2.13: Reach-scale sediment mass balance representations: a) Example Markov chain model of stochastic sediment fluxes and delivery times. Bold arrows represent initial pathways for sediments and dashed arrows represent secondary pathways if sediment is deposited before exiting the reach. Pathways have transition probabilities derived from a sediment budget and equations governing erosion, transport and deposition (schematic based on Malmon et al. 2003); b) Sediment mass fluxes and reservoir geometry (as described in, and based on Figure 2 of, Lauer & Willenbring 2010). Mass fluxes include upstream and lateral inputs ($M_{Upstream}$ & $M_{Lateral}$, respectively), downstream outputs ($M_{Downstream}$), aggradation via overbank deposition and sediment burial (M_{Agg}), and channel-floodplain exchanges (M_{Ex}); while reservoir geometry consists of depth, width, valley length (V_{Length}) and channel length (C_{Length}). The model was designed to trace storage and transport patterns of isotopically tagged sediments in floodplains, which is defined as the space subject to lateral reworking via the channel. Sediment residence time is affected by the size, geometry and aggradation rate of the floodplain (see Lauer & Willenbring 2010).

Key limitations of this approach highlighted in Malmon et al.'s (2002, 2005) Los Alamos papers, include assuming steady-state conditions, neglect of particle size sorting and selective transport, and ignoring the effects of potential extrinsic forcing mechanisms such as major hydroclimatic changes (Malmon et al. 2002, 2005). Many of these studies utilise a single time-invariant sediment flux rate. As this review has shown, residence time length can be highly sensitive to rates of reservoir turnover, and recognising this,

some report a range of residence time values arising from varying sediment flux rates (Blöthe & Korup 2013; Hoffmann 2015). In subsequent work, some attempts were made to address Malmon et al.'s highlighted limitations. For example, recognising the issue of differing rates of sand and gravel mobility (e.g. Kleinhans & van Rijn 2002), Lauer & Willenbring (2010) incorporated grain size distribution effects on down-channel radioactive tracer profiles into their model.

Another important limitation is the use of a probability density function of storage times to determine how long sediment will remain stored. As this review has demonstrated, there is no one-size-fits-all function that can be applied universally across sediment-routing systems. While most of the literature suggests either an exponential function (e.g. Everitt 1968; Martin & Church 2004) or a power law function (e.g. Lancaster et al. 2010; Bradley & Tucker 2013) best describes the distribution of sediment storage times, the nature of this distribution still merits further testing (Pizzuto et al. 2017). Given the diversity of storage time distributions across different fluvial systems, as well as the propensity for these distributions to change form in response to environmental conditions (Moody 2017), a more complex two-parameter model, such as a Weibull or lognormal function, will likely be necessary to accommodate dynamic responses in sediment storage behaviour to environmental conditions. Therefore, further work should be undertaken using the techniques described in sections 3.2.2 and 3.2.3 to improve future stochastic modelling of particles in sediment-routing systems.

2.4. Synthesis

2.4.1. The importance of storage in sediment routing systems

Residence time has been described as a useful summary of the storage and removal of sediments from terrestrial systems (Skalak & Pizzuto 2010), and can be determined throughout the fluvial system at a range of scales. This review has shown that a combination of inter-connected physiographic factors, including slope, sediment supply, hydrology and vegetation, and process rates influence residence time length and the distributions of ages and storage

times. While there is still much to advance in terms of our understanding of controls and environmental management implications, as well as developing quantification methods, it is hoped this review will catalyse further interest in quantifying the timescales of sediment storage and delivery.

Several potential future research areas are categorised here (Table 2.2) under three broad themes, but the list is not exhaustive nor are all the questions new. Indeed, preliminary attempts to answer some of these questions are evident in the literature, and the scope for future research could be broadened further by linkage beyond fluvial geomorphology.

Table 2.2: Three thematic groupings of example future research questions: A. Controls on sediment delivery times and distributions of sediment ages and storage times, B. Biogeochemical, ecological and water quality issues, and C. Methods and techniques.

A.	***Controls on residence time length and sediment storage behaviour:***
1.	How do sediment storage and delivery times vary between catchments or reaches of varied sizes and geometries, but similar climates, lithology and land-use histories?
2.	What are the impacts of vegetation cover and in-stream wood on the distributions of sediment ages and storage times in river floodplains, and the delivery times through valley floor corridors?
3.	To what extent do increases in the frequency, magnitude and duration of hydrological extremes influence sediment storage and delivery times?
4.	To what extent do different channel planform types and valley geometries control floodplain sediment age and storage time distributions?
5.	How do sediment residence times in temperate catchments and stores compare with those in dryland, tropical or arctic environments?
6.	How much do storage and delivery times vary across different sediment grain sizes?
7.	How do channel hydraulics and interactions with bed topography and grain sorting affect sediment storage times?
B.	***Biogeochemical, ecological and water quality issues:***
1.	Can the distribution of sediment storage times of a pollutant-rich system, such as microplastic-laden rivers, be used to predict how long a catchment or reach-scale valley floor corridor will remain contaminated for?
2.	How do sediment storage time distributions influence the natural cycling of carbon and other macronutrients in fluvial landforms?
3.	Which factor most limits organic carbon storage in floodplain and riparian ecosystems: residence time of floodplain sediment or microbial metabolism (see Sutfin et al. 2016:54)?

4. How does channel bed fine sediment storage affect exchanges between flow and the hyporheic zone?
5. How will sediment and organic matter residence time regulate riparian vegetation establishment and *vice versa*?

C. Methods and techniques:

1. To what extent can planimetrically resolved ages of floodplain deposits from channel change mapping be used to construct reach scale storage time distributions?
2. Can storage time distributions be reconstructed from past environmental changes, and predicted based on likely future scenarios?
3. Can landscape evolution models (LEMs) be evaluated with observations, such as the mapped or dated alluvial record, to constrain sediment storage time distributions?
4. How can sediment storage time distributions be used to quantify catchment response to environmental change and disturbance in different sediment-routing systems?
5. What potential do developments in real-time particle tracking techniques pose for quantifying timescales of storage and transit at short time scales?
6. How accurate are storage time distributions inferred from age populations when evaluated against directly recorded storage time data?

2.4.2. Controls on sediment storage dynamics

Residence times and distributions of ages and storage times have been shown to vary widely between different fluvial system reservoirs. For channel beds, residence times range from minutes to decades, whereas for surrounding terrestrial stores including floodplains, these are many orders of magnitude larger (centuries to millennia). Attempts to quantify sediment storage and delivery times have often focussed on a specific catchment management issue, such as the diffusion of contaminants through river networks. Many of these studies have also quantified the effects of different controls on storage timescales (Figure 2.14). Miller & Friedman (2009) attributed power-law storage time distributions to declining frequency of high magnitude flow events, while Moody (2017) was able to correlate changes in the shapes of age and storage time distributions with the timing of phases of geomorphic activity such as aggradation and incision.

To assist interpretation of sediment storage behaviour for the reviewed techniques (Table 2.3) a conceptual model is presented (Figure 2.14) that is applicable across spatio-temporal scales and illustrates the inter-connections between these key environmental controls. While it has been demonstrated in

earlier research that a change in one control can directly affect residence time length, e.g. increased residence times behind log jams (Fisher et al. 2010), in other cases, this is not as predictable. For example, increased sediment supply to a valley floor reach may theoretically increase residence times by increasing the size of floodplains and immobilising more of their sediments through burial. On the other hand, it may metamorphose a stable, meandering channel with low rates of turnover into an unstable, braided planform with higher rates of erosion (see Macklin & Lewin 1989 and Miller 1997). Furthermore, these different components interact and respond over space and time, often with a high degree of complexity and unpredictability. For instance, vegetation cover, sediment supply, hydrology, channel planform and slope will exert feedbacks on each other and co-evolve over time (Collins et al. 2012). These impelling and resisting force elements, as well as blockages (buffers, barriers and blankets), may also vary in position, configuration and scale over space and time (Fryirs et al. 2007). Indeed, a pulsed disturbance such as a landslide or flood may destroy former blockages and other resisting elements and create new ones of a different scale and in a new location (see Fryirs 2013, 2017 and references within).

Table 2.3: Controls on fluvial sediment storage and delivery timescales with reference to published examples.

Control	**Examples**	**Summary of effects**
Large woody debris (LWD)	Skalak & Pizzuto (2010); Fisher et al. (2010)	LWD accumulations impede flows and promote deposition. Combination of LWD presence, valley slope and sediment supply act to store sediments in the channel over several days to decades.
Vegetation cover	Nanson & Beech (1977); Gottesfeld & Johnson Gottesfeld (1990); O' Connor et al. (2003); Konrad (2012)	The probability an area of floodplain abandoned within the past decade will be re-occupied by the channel is an order of magnitude higher than areas that were abandoned 30 years ago. Increased stability of floodplain patches by vegetation is one controlling factor.
Flow magnitude	Bonniwell et al. (1999); Miller & Friedman (2009); Moody (2017)	Larger flow magnitudes increase particle transport distances and reduce delivery times through river networks. Lateral

		migration rates decline with flow magnitude, increasing storage times in floodplains. Successive floods cause aggradation and subsequent incision of sediment slugs formed after catchment disturbance.
Sediment supply	Hoffmann (2015); Croissant et al. (2017)	Shifts from transport- to supply-limited conditions via self-organisation dramatically reduce delivery times.
Sediment calibre	Malmon et al. (2005)	Reach-scale bedload delivery times between channel reservoirs may be much shorter than fine fluxes between floodplain reservoirs.
Process type	Lancaster & Casebeer (2007); Lancaster et al. (2010)	Debris-flow processes may rework sediments faster than fluvial processes, decreasing residence times.
Reservoir geometry	Blöthe & Korup (2013); Kuo & Brierley (2013)	High volume valley fills store sediments for 10^5-year scales. Confined valleys limit storage capacity.
(Dis)connectivity, coupling, blockages and boosters	Fryirs et al. (2007); Fryirs (2013, 2017); Hoffmann (2015)	The degree of (dis)connectivity characterises how (in)efficiently sediment will flux through the fluvial system. The distributions of blockages (buffers, barriers and blankets) and boosters impede and facilitate sediment flux, respectively.

Enhancing our understanding of controls on sediment storage and delivery times remains a major research gap and is important to address if we are to predict how sediment may be (re)mobilised in response to future environmental change. Virtual velocity experiments have attempted to elucidate sediment storage and transport controls. For example, in Allt Dubhaig, Scotland, analyses of tracer pebble (16-256 mm in diameter) movements revealed that mean transport distances declined with increasing grain size and as channel slope and shear stress decreased with increasing distance downstream (Ferguson & Wathen 1998). Using a 160-metre long flume, Parsons et al. (2018) measured the virtual velocity of sand particles (0.5-2 mm in diameter). They found that, contrary to expectations, virtual velocity was lowest for the smallest particle sizes, suggesting that increasing susceptibility to trapping along a rough bed surface with decreasing grain size was a primary explanation (Parsons et al. 2018).

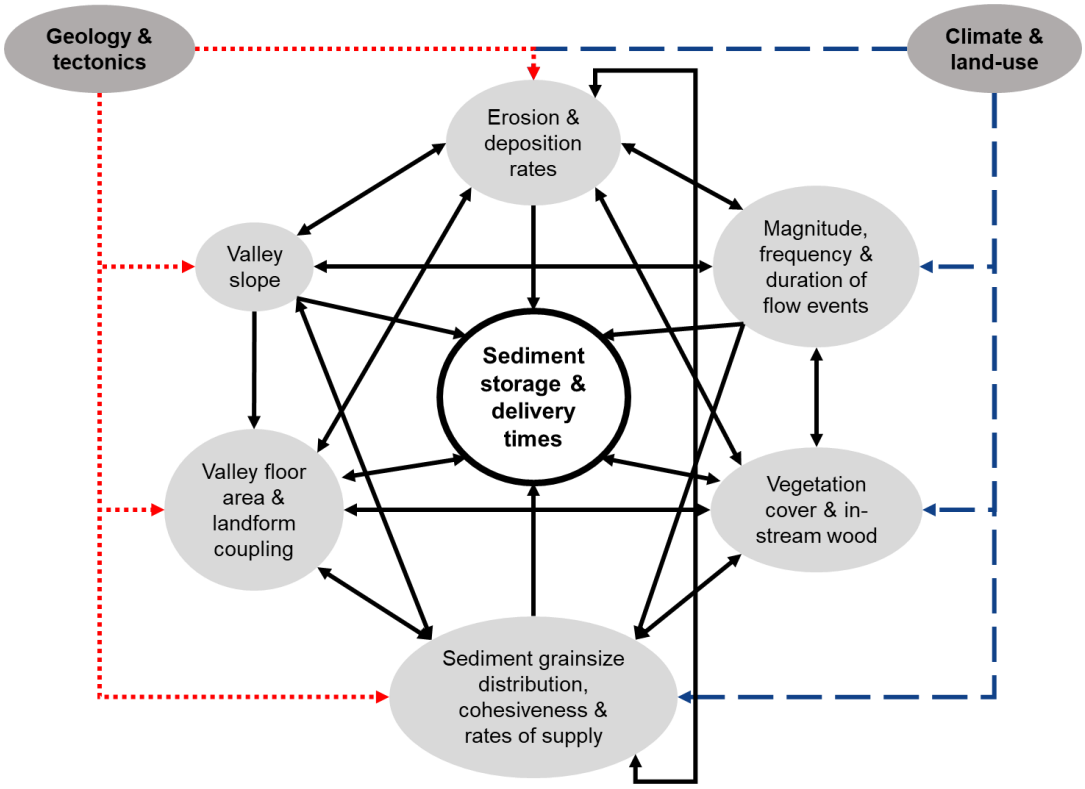

Figure 2.14: Major controls on sediment storage and delivery times in fluvial systems. How storage and delivery time respond to reservoir morphology, hydrology, vegetation and sediment supply will also depend upon how these factors interact. Turnover processes include degradation and aggradation, and the featured climatic and geological controls will govern whether the system is under transient (aggrading or degrading) or steady-state conditions, and will likely affect the shapes of sediment age and storage time distributions.

2.4.3. Non-linear behaviour in LEMs and self-organised criticality

The impacts of environmental change on river systems are non-linear by nature (Phillips 2003). Non-linearity is exhibited by the processes of landscape evolution such as sediment transport (e.g. Singh et al. 2009; Van De Wiel & Coulthard 2010) and by the external forcing conditions acting upon the river system – principally, climate and land-use (Van De Wiel et al. 2011). Previous work using numerical models has shown that non-linearity occurs as a result of feedbacks between morphological processes and landscape, the existence of intrinsic thresholds within the fluvial system, and by a sensitivity to the initial conditions (Phillips 2003; Coulthard & Van De Wiel 2007; Van De Wiel et al.

2011). For example, Coulthard and Van De Wiel (2007) undertook over 20 simulations to understand the relative importance of different controls (storm event magnitudes and variability, sediment heterogeneity, sources of sediment supply, and catchment morphology) as possible drivers of non-linearity in sediment flux behaviour. They found that the manner in which catchments process the variable rainfall (i.e. through spatial and temporal variations in drainage network connectivity), as opposed to just the rainfall variability itself, was responsible for producing the non-linearity of sediment yields (Coulthard & Van De Wiel 2007).

River meandering has been characterised as a 'chaotic' process – that is, deterministically non-linear (see Phillips 2006 and references therein). In other words, it is possible to simulate river meandering from the same initial point in space and time repeatedly and get the same result at the end of a single timeframe. However, because of this non-linearity, the ranges of possible configurations of channel position and morphology expand over time to such an extent that precise predictions (e.g. down to individual bends or to the resolution of a few tens of metres of channel length) are impossible to make beyond a few decades into the future. Furthermore, chaotic systems are highly sensitive to initial conditions such that, for instance, a simulated river channel might be located in a different part of the valley floor and exhibit large differences in morphology, such as sinuosity and meander wavelength, compared with another simulated channel as a result of small differences in initial conditions including topography (Van De Wiel et al. 2011). The scale of these differences in morphological change may be exacerbated by various non-linear process mechanisms (see Phillips 2003 for a detailed list).

Self-organised criticality (SOC) is one type of non-linear process mechanism operating in natural systems such as river catchments, and since the emergence of this concept from initial studies of sand piles (Bak et al. 1987), has been suggested as an explanation for river meandering (e.g. Stolum 1996; Hooke 2004), high levels of scatter in the response of bedload yields to identical floods (e.g. Van De Wiel & Coulthard 2010), and the frequency-magnitude distribution of riverbank failures at catchment-scale (Fonstad & Marcus 2003). While there is not a sufficient list of conditions to diagnose

beyond doubt SOC in a system, the following are necessary conditions: 1) nonlinear dynamics in the occurrence of disturbance events within the system over time; 2) an inverse power-law relationship between the frequency and magnitude of events; 3) a critical state of the system to which readjustment occurs following a disturbance; and 4) a cascading process mechanism that leads to the possibility of low and high-magnitude events occurring in response to the same process (Phillips 2003).

SOC-systems, as examples cited in the previous paragraph highlight, organise themselves around a dynamic equilibrium between order and chaos so that identical external disturbances can cause internal system responses that are highly variable in magnitude (Van De Wiel et al. 2011). This makes it impossible to predict the exact geomorphic response that will occur at a particular point in space and time as a result of a change in environmental forcing conditions (Van De Wiel et al. 2011). Taking an alluvial valley floor with a dynamic, meandering river channel as an example, it would be impossible to make any trustworthy predictions of the timings of erosion and deposition processes for a given square metre of floodplain over timescales spanning beyond multiple decades. By extension, this would render it impossible to make any predictions of the residence time of the floodplain deposit and its constituent sediment particles. However, as Van De Wiel and Coulthard (2010) highlight, it may still be possible to detect the effects of environmental change in the distribution of the magnitudes of sediment yield. Furthermore, it is also possible to relate differences in the slope of the magnitude-frequency function of riverbank failures to different environmental conditions – e.g. lower function slopes occur for low-gradient alluvial reaches, indicating these reaches are more susceptible to high-magnitude riverbank failures (Fonstad & Marcus 2003). In the context of sediment storage times, this emphasises two important points: 1) the need to derive a full distribution of sediment storage times for a larger area than a specific point on the floodplain (e.g. a reach of valley floor or entire catchment); and 2) by comparing distributions of sediment storage times, it may be possible to detect a change in the overall dynamics of storage behaviour in response to a change in environmental forcing conditions.

2.4.4. Implications and future research

2.4.4.1. Contaminant fluxes

In catchment systems, reservoirs including floodplain soils and riverbed sediments may be enriched in pollutants, such as heavy metals and pesticides. Thus, the modelling of fine sediment storage and delivery times is crucial for predicting the occurrence and longevity of contamination hotspots. Several prediction attempts have already been made. For heavy metals, these attempts include using estimated storage and export rates from published contaminated sediment budgets (Walling & Owens 2003) in the Swale catchment (Dennis et al. 2009), and applying a natural decay model with various restoration scenarios in the Clark Fork River catchment (Moore & Langner 2012). For ^{137}Cs-enriched soils, quantification has involved stochastic modelling of contaminated particle delivery times in the Los Alamos Canyon (Malmon et al. 2002, 2005). Yet some of these past attempts rely on assumptions that might not hold. For example, the estimates of Dennis et al. (2009) assume that any removed contaminated sediments are replaced by equivalent quantities of uncontaminated particles. Modelling by Malmon et al. (2002, 2003) fails to account for any changes in long-term sediment flux rates – an important limitation given the potential effects of future climate change on sediment supply and exchange processes.

Recently, attention has turned towards coupling sediment storage timescale measurements to better understand riverine carbon flux dynamics. Organic carbon storage in riparian ecosystems is controlled by decomposition rates and the residence times of floodplain sediment and organic matter (Sutfin et al. 2016). Sutfin et al. (2016) distinguish between “labile” (readily metabolised soil organic carbon by micro-organisms) from “recalcitrant” forms, which may remain stored in floodplain sediments for several 10^2-10^5 years, depending on local valley floor characteristics (geometry, hydraulics, sedimentology and vegetation cover) and ecoregion (temperate, tropical, arid or boreal). A key question they posit is: “Which factor most limits OC [organic carbon] storage in floodplains, residence time of floodplain sediment or rate of microbial metabolism?” (Sutfin et al. 2016:54). Some recent work has attempted to address this question. Model predictions of floodplain evolution and organic

carbon cycling by Torres et al. (2017) demonstrate that sedimentary storage is highly important in regulating the age of riverine dissolved organic carbon. Younger deposits are shown to be preferentially eroded, which for a well-mixed reservoir at steady-state, requires that older deposits are stored for longer than exponential distributions predict (Torres et al. 2017). Most global exports of riverine dissolved organic carbon are currently dominated by younger, less microbially processed forms via shallow flow paths (Barnes et al. 2018). However, intensification of the hydrological cycle and increased soil disturbance, e.g. via floodplain reworking, is increasing export rates of older dissolved organic carbon from deeper soils associated with longer residence times in the contiguous U.S. and Arctic (Barnes et al. 2018).

Another emerging issue is the diffusion of plastics to the marine environment – mainly microplastics (<5 mm in diameter) – which are exported via terrestrial and freshwater pathways. Freshwaters, including river networks, receive microplastics from the surrounding land, produce additional microplastics via break-up of larger forms and store significant quantities within sedimentary landforms such as floodplains and channel beds (Horton & Dixon 2018). Within European terrestrial and freshwater environments, an estimated 473,000 to 910,000 metric tons of plastic is stored annually (Horton et al. 2017). Within riverbed sediments in the Mersey catchment, UK, Hurley et al. (2018) calculated a maximum concentration of 517,000 particles m^{-2}. River networks have also been shown to efficiently export microplastics. After severe flooding in 2015/16, approximately 70% of microplastics stored within Mersey catchment riverbed sediments (equivalent to 0.85 ± 0.27 tonnes or 43 ± 14 billion particles) was exported, resulting in complete decontamination altogether at seven sites (Hurley et al. 2018). This is perhaps unsurprising considering the very short delivery times of river network sediments found elsewhere in the UK (e.g. Smith et al. 2014) and large transport lengths for fine sediments during storm events (e.g. Bonniwell et al. 1999).

More work is needed to elucidate the role of sediment residence times in biogeochemical cycling and the potential ramifications. For example, to what extent does fine sediment accumulation on the channel bed affect hyporheic nutrient exchange (Boano et al. 2014)? How will sediment and organic matter

residence time regulate riparian vegetation establishment and *vice versa* (Collins et al. 2012)?

In the case of microplastics, more work is required to understand storage and transport processes. Horton & Dixon (2018) provide a preliminary attempt at this, conceptualising microplastic pollution as a “Plastic Cycle”. Their review suggests that the processes and controls that affect sediment transport and storage broadly apply to microplastics as well (Horton & Dixon 2018). Thus, sediment residence times potentially reflect microplastic residence times and *vice versa*. Key questions that arise from this include: can the distribution of sediment storage times of a microplastic-laden river be used to predict how long a catchment or reach-scale valley floor corridor will remain contaminated?

2.4.4.2. Landscape evolution and interpreting stratigraphic records

This review has focussed heavily on reach-scale systems in the context of quantifying sediment storage behaviour. However, in order to discuss the wider implications of sediment storage behaviour on landscape evolution and the reconstruction of palaeoenvironments from the stratigraphic record, it is important to consider the entire catchment system.

A key challenge to the interpretation of stratigraphic records is the phenomenon of ‘shredding’ of environmental signals by sediment transport through river networks (Jerolmack & Paola 2010). It has been commonly assumed that when external processes such as climate and sea level change operate at similar timescales to internally-generated (autogenic) processes, the external signal can still be recorded, albeit partially (Jerolmack & Paola 2010). However, being non-linear by nature, sediment transport acts as a filter that shreds (destroys) environmental signals (unless their time and amplitude scales are large enough to overcome this filter) before they can appear within the stratigraphic record (Jerolmack & Paola 2010). While this shredding is impossible to avoid in most systems, quantifying the distributions of storage and delivery times of sediment particles in river catchments may provide useful insight into which environmental signals are likely to appear in the stratigraphic record.

Over $10^{3\text{-}6}$ year timescales, uranium-series (U-series) isotopes may serve as chronometers for determining rates of catchment denudation processes such as hillslope weathering, and sediment residence times (e.g. Dosseto et al. 2006, 2008a, 2008b). Quantifying these parameters has been fundamental to understanding catchment-scale relationships between climate change, tectonics and landscape evolution over the Quaternary period (Handley et al. 2013a). For example, Dosseto et al. (2010) observed that over the last 100 kyr in the Murrumbidgee catchment, Australia, climate indirectly controlled rates of sediment weathering (and hence ages and residence times of palaeochannel sediments) by influencing the types and distributions of stabilising vegetation ecosystems.

Using comminution age data to calculate residence times spans roughly two decades of research. Comminution age refers to the weathering and deposition lifecycle of a particle, from initial bedrock or parent material weathering, transport through the river network to a zone of final deposition, and the time since final deposition (see DePaolo et al. 2006). Assuming depositional ages of sediment can be independently constrained, the residence time of sediment in a reservoir, T_{res}, can be computed from:

$$T_{res} = T_{com} - T_{dep} \qquad (7)$$

where T_{com} and T_{dep} are comminution age and deposition age, respectively.

Figure 2.15 shows published residence time values from several catchments where the main basis of these studies has been the determination of the "comminution age" of sediments. Values range over multiple orders of magnitude, from ~1 x 10^3 to ~1.7 x 10^6 years, reflecting factors such as catchment size and coupling/connectivity. Residence times also vary dramatically by grainsize. In the Ganges catchment, fine sediments were exported from the catchment within <20-25 kyr, whereas bedload remained stored for >100 kyr (Granet et al. 2010). Conversely, in the Nunnock catchment, suspended sediment is stored for up to an order of magnitude longer than bedload (Dosseto et al. 2014).

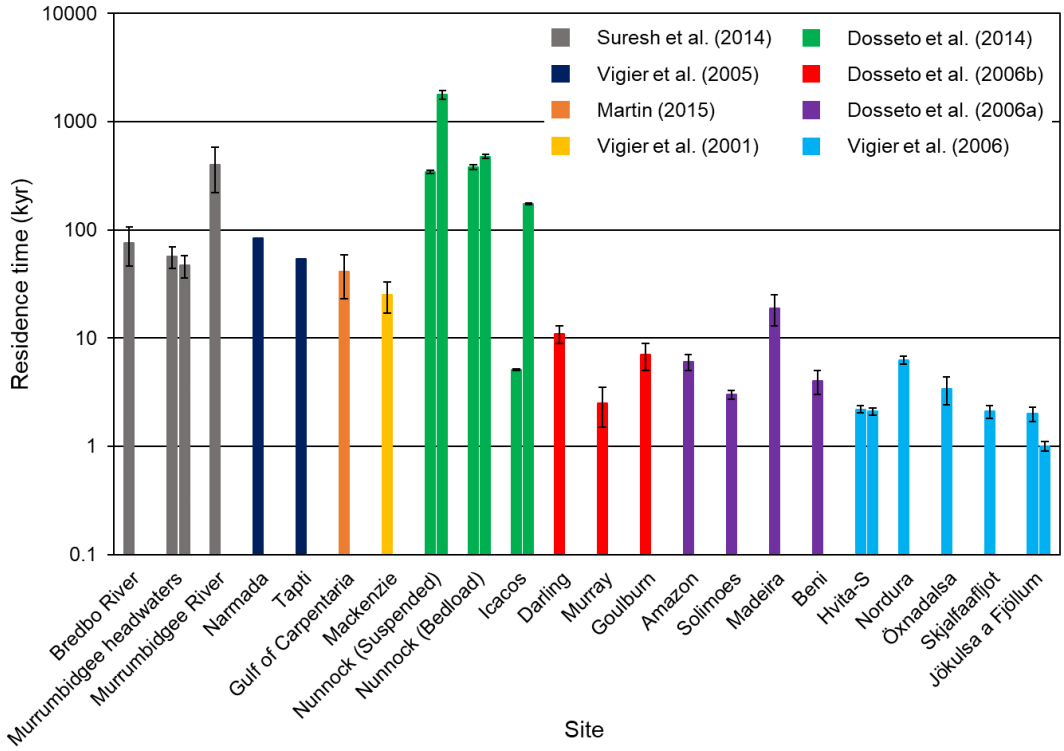

Figure 2.15: Published residence times calculated for catchments in Australia (Dosseto et al. 2006b, 2014; Suresh et al. 2014; Martin 2015), the Ganges (Vigier et al. 2005), the Amazon (Dosseto et al. 2006a), Canada (Vigier et al. 2001) and Iceland (Vigier et al. 2006) using the comminution age determination method (see also Li et al. 2015 for another synthesis).

These catchment-scale residence time estimates integrate the cumulative sum of all individual sediment storage and transport episodes. Thus, interpreting these data requires the determination of spatio-temporal changes of environmental controls within the system. Dosseto et al. (2010) for example, found that in the Murrumbidgee catchment, residence times were an order of magnitude higher during interglacials (3.2-4.8 x 10^5 years than during glacials (minimum of 2.8 x 10^4 years). They attributed this to sediment connectivity changes with land cover and climatic change over the last 100 kyr (Dosseto et al. 2010). In British Columbian rivers, Canada, specific sediment yield increases with increasing catchment area (up to 3 x 10^4 km^2) because of secondary remobilisation of Quaternary sediments (Church & Slaymaker 1989). This reflects a pattern of lengthy landscape relaxation times (≥ 10 kyr) of many formerly glaciated basins (Church & Ryder 1972). Ballantyne (2002)

proposed a model of paraglacial sediment exhaustion. Under steady-state conditions, the residence time of paraglacial sediment may be calculated by relating sediment yield (as a proxy of reworking rates) with the amount of remaining available sediment (Ballantyne 2002). The distribution of storage times is best fit by an exponential decay model, which suggests all the paraglacial sediment will eventually leave the system after a maximum time duration. However, base level fluctuations and slope instability, induced by extreme rainstorms, may cause episodic pulses of paraglacial sediment flux (Ballantyne 2002), resulting in lower residence times than exponential models would predict.

The delivery times of many sediment particles to catchment outlets (particularly in large sediment-routing systems of $\geq 10^3$ km in length) is on the order of geological timescales – i.e. several millions of years (Pizzuto et al. 2017). Thus, any major fluctuations in sediment residence times, in response to an environmental change (e.g. a glacial-interglacial transition), will likely generate poor estimates of delivery times in sediment-routing models to catchment outlets, and hence, the stratigraphic record. This is problematic if the goal is to reconstruct precisely the timing, scale and specific types of past landscape evolutionary processes, and indeed, future processes for the forecasting of natural hazards.

Residence times estimated from U-series disequilibria offer major potential for the parameterisation and evaluation of sediment-routing models over geological timescales. However, as Kelsey et al. (1987) stress, it is the distribution of sediments amongst the short- and long-term reservoirs within the fluvial system that drive patterns of landscape evolution. This is because if sediment storage is concentrated primarily within long-term reservoirs, then it will be the most infrequent and highest magnitude geomorphic events that will drive landscape evolution in the system (Kelsey et al. 1987; Martin & Church 2004) and register within stratigraphic records. For example, when sinusoidal input signals, with periods of 10 and 10^4 years, were filtered through their 1000 km delivery time distribution model, Pizzuto et al. (2017) found that the lower frequency (10^4-year period) signals were transmitted through the river network with higher fidelity and were most likely to appear in the

stratigraphic record of downstream depocentres. Therefore, it is important to constrain distributions of sediment storage times correctly to parameterise sediment-routing models.

2.4.5. Conclusions

The sediment-routing system entails an interconnected series of trajectories each with a unique delivery timescale. The larger the sediment-routing system, the more likely it is that these trajectories will be punctuated with multiple episodes of sediment storage that act to lag, attenuate or phase-shift incoming erosion signals (i.e. catchment buffering of disturbance) and increase sediment delivery times. Quantifying the duration of sediment storage in various landforms – be it estimating turnover times, constraining the ages of deposits, or recording storage time directly at the point erosion occurs – is essential to unpacking the "sediment delivery problem" (*sensu* Walling 1983). This will help to guide interpretation of the stratigraphic record (e.g. for the occurrence of high-magnitude catchment-scale disturbances) and monitoring of contaminant fluxes in polluted basins.

Much of the existing literature concerns quantifying sediment storage times (or a proxy of this such as age or turnover time) within reach-scale channel-floodplain systems. One-dimensional mass-balance modelling offers a simple means of estimating the mean storage time (the residence time) by taking the total mass of a defined reservoir (e.g. total floodplain area) and dividing by a representative long-term flux rate (e.g. mean annual lateral erosion rate). However, this approach assumes that all of the mass contained in the reservoir will be completely recycled and that the cumulative mass to undergo turnover increases as either a linear or exponential function (see Konrad 2012). As the sediment storage dynamics in many channel-floodplain systems do not conform to these assumptions, it is necessary to constrain the full distribution of storage times, which can be either inferred from an age distribution, or modelled directly from the timings of sediment erosion. Simulations of the stochastic fluxes and delivery times of sediment particles require a probability density function of storage times for model parameterisation.

To date, much work has been completed to constrain the distribution of sediment storage times and predict the distribution of delivery times through sediment-routing systems. However, further research is required to elucidate the range of controls on sediment storage behaviour such as climate, vegetation and the occurrence of blockages in the system over space and time. Other challenges include how to parameterise catchment-scale sediment-routing models over geological timescales using data collected at reach-scale over multi-decadal to millennial timescales, and how techniques reviewed here may be applied to the monitoring of pollutants such as micro-plastics.

CHAPTER 3:

Modelling the decadal dynamics of reach-scale river channel evolution and floodplain turnover in CAESAR-Lisflood*

***Published, with some slight differences in the text, in:** Feeney, C.J. et al., 2020. Modelling the decadal dynamics of reach-scale river channel evolution and floodplain turnover in CAESAR-Lisflood. *Earth Surface Processes and Landforms*, **45**(5), 1273–1291.

Summary and linkages to other thesis chapters

The previous chapter reviewed several approaches to quantifying sediment storage times in alluvial floodplains. Landscape evolution modelling is an attractive approach as it captures the timings and spatial extents of erosion and deposition processes (key to calculating sediment storage times), data collection over greater spatial and temporal scales than monitoring methods will permit, and accommodates careful control over experimental conditions, such as the inclusion of various environmental controls (e.g. vegetation cover, sedimentology and stream discharge) and the temporal frequency of recorded data points. However, before landscape evolution modelling can be used, the model in question requires calibration to justify parameter choices.

This chapter aims to address Research Question 2: “To what extent can a landscape evolution model accurately reconstruct recent historical planimetric channel dynamics of reach-scale valley floor systems?” Here, the model chosen to complete this thesis, CAESAR-Lisflood, was calibrated by comparing simulated river channel changes with a time-series of historical changes, that were digitised from the historical map record, along ten 1 km-long reaches of rivers in northern England. This region is replete with laterally dynamic fluvial systems (see Hooke & Redmond 1989; Gregory 1997), with a rich record of historical daily flows from National River Flow Archive gauge sites that overlaps with historical maps and aerial images. Parameters governing rates of erosion and lateral channel change were calibrated for five reaches by determining which simulation out of a wider ensemble is the most accurate, based on a set of assessment criteria. Calibrated parameter combinations were then applied to the other five reaches as part of a split sample test to evaluate the potential transferability of calibrated parameters. Floodplain turnover times were estimated by extrapolating erosion rates to assess the suitability of calibrated parameters over longer timescales. The results of this chapter were used to justify the methodological designs of Chapters 4 and 5.

3.1. Introduction

Sedimentary units preserved in depositional basins provide useful evidence of environmental change, including records of sediment fluxes driven by tectonic, climatic and anthropogenic disturbances (Whittaker et al. 2010). In catchments, sediments are mobilised from upland sources, pass through transfer zones, and ultimately deposited in long-term or permanent storage (Schumm 1977). However, signals of sediment flux of catchment disturbances are typically lagged by temporary storage in landforms (e.g. Castelltort & Van Den Driessche 2003; Blöthe & Korup 2013) and in some cases, the signal is completely destroyed by "shredding" (Jerolmack & Paola 2010). Additionally, multiple drivers can operate in parallel to initiate erosion, complicating interpretation of sedimentary records (Coulthard & Van De Wiel 2013).

Floodplains are significant reservoirs of sediment in fluvial systems, covering $8 \times 10^5 – 2 \times 10^6$ km^2 of the Earth's land surface (Leopold et al. 1964; Tockner & Stanford 2002; Mitsch & Gosselink 2015). A combination of vertical and lateral accretion processes, limited only by sediment supply, allows floodplains to accumulate rapidly large volumes of sediments over a short period of time (decades to centuries) (Trimble 2010). However, sediment removal from the floodplain is largely restricted to lateral channel erosion, hence, sediments may remain stored for a prolonged period of time – potentially many thousands of years (Trimble 2010). It is this 'fast in, slow out' principle (*sensu* Trimble 2010) that contributes to storage processes lagging sediment signals generated upstream.

Floodplain turnover, defined here as the set of processes of sediment removal from the floodplain, provides a useful measure for the longevity of sediment in storage (Bolin & Rodhe 1973). Aalto et al. (2008) calculated turnover times of ~1000 years for floodplain sediments along 300 km of the Strickland River, Papua New Guinea, by dividing floodplain area by long-term average lateral erosion rates. Beechie et al. (2006) and Konrad (2012) quantified rates of (re)occupation of floodplain areas by river channels for several valley floors in North America.

Sediment storage within floodplains is also important in terrestrial geochemical cycling. Sutfin et al. (2015) estimate that soil organic carbon stored in floodplains accounts for 12-80 Pg C worldwide. Simulations, combining channel-floodplain evolution with biosphere-atmosphere carbon exchanges, show that the residence time (the mean amount of time a mass of particles resides in storage) of organic carbon is strongly controlled by sediment residence times (Torres et al. 2017). River catchments with a legacy of metal mining feature floodplains enriched with potentially harmful contaminants (e.g. Lewin & Macklin 1987; Macklin & Dowsett 1989; Bird et al. 2009). Modelling rates of floodplain turnover can help to constrain the timescale for decontamination of polluted catchments. For example, approximately 123,000 tonnes of Pb is stored within the main channel belt of the River Swale, UK, and under present rates of floodplain erosion, will take >5000 years to be removed from the catchment (Dennis et al. 2009).

River channel morphology and processes governing changes over time and space, such as riverbank erosion, are important controls on floodplain sediment storage (Hooke 1980). As derivatives of their channel systems, any significant environmental change should lead to a transformation of floodplain forms and processes (Nanson & Croke 1992). In their analysis of different floodplain environments in the US Pacific Northwest, Beechie et al. (2006) determined that the mean ages (defined here as the time since deposition) of floodplain sediments decreased from 85 to 63, 41 and 12 years for straight, meandering, island-braided and braided reaches, respectively. Miller and Friedman (2009) identified a strong positive correlation ($r = 0.95$) between the magnitude of the peak instantaneous flow event and rates of floodplain erosion that occurred in a given measurement interval. Separating out the multiple potential independent variables that control channel changes and the persistence of sediment storage in floodplains remains an important challenge (O'Connor et al. 2003). Therefore, methods that allow for careful control of potentially important variables, such as numerical modelling, need to be employed.

Landscape evolution models (LEMs) are used to simulate the redistribution of sediments in the landscape, and can operate over a range of spatial and

temporal scales and environmental conditions (Tucker & Hancock 2010). CAESAR-Lisflood is a coupled hydrodynamic LEM capable of simulating channel change and floodplain evolution at catchment and reach spatial scales (Coulthard et al. 2013), and has been used to quantify the effects of environmental change on sediment storage and fluxes. Applications of CAESAR-Lisflood include modelling the effects of vegetation cover on catchment-scale sediment delivery (Coulthard & Van De Wiel 2017), impacts of tectonic uplift and rainfall-regime variability on sediment fluxes (Coulthard & Van De Wiel 2013) and quantifying the role of self-organised criticality in governing bedload yields (Van De Wiel & Coulthard 2010). At reach-scale, Ziliani and Surian (2012) related phases of channel change along the Tagliamento River, Italy to changes in unit stream power, riverbank protection and a legacy of sediment mining. These studies highlight the importance of sediment storage at both catchment and reach-scales and demonstrate the potential for modelling river channel changes and sediment residence times with CAESAR-Lisflood.

Here, the effectiveness of CAESAR-Lisflood in reproducing historical river channel changes and modelling processes of floodplain turnover is tested. To achieve this, several objectives are addressed. First, recent historical channel changes were reconstructed for a range of floodplain reaches across northern England. Second, model performance was evaluated by assessing how accurately the simulations replicated 2D planimetric historical channel changes using the annual surface areal erosion and deposition rates of floodplains and lateral migration rates of channels as performance criteria. Further evaluation of model performance included quantifying the spatial match between modelled and mapped patterns of channels and floodplain. From the modelling ensemble, the lowest overall error across these criteria identified the best-fit simulations and hence, the parameterisation of variables governing erosion rates and channel morphology. A split-sample testing approach was adopted, whereby calibration focussed on half of the selected reaches, with the other half reserved for further testing of model parameter accuracy. The most accurate simulation provided the erosion rates to model the areal extents of floodplain occupation by the river channel, which were

compared with results derived from historical observations. Finally, the implications of the findings are discussed, including suggestions for future research into modelling channel-floodplain evolution processes.

3.2. Methods

3.2.1. Overview and model description

CAESAR-Lisflood is a coupled hydrodynamic LEM capable of simulating channel change and floodplain evolution at reach scale (Coulthard et al. 2013). The model routes water and sediments across a regular grid of cells, including divergent and convergent flows. This allows both single and multi-thread channel patterns to be modelled, meaning a wide range of floodplain evolution processes can be captured (Coulthard et al. 2002). During simulations, each cell records the elevation, sediment grain size distribution, flow depth, vegetation conditions, and net erosion and deposition since the start of the simulation, updating these with each timestep (Coulthard et al. 2002). CAESAR-Lisflood operates using a digital elevation model (DEM) of a real-world system or an artificially generated system. The model can be used for hind- or fore-casting purposes and to test experimental 'what-if?' scenarios (Coulthard & Macklin 2001, 2003; Coulthard et al. 2002, 2005; Coulthard & Van De Wiel 2007, 2013, 2017).

The scope of this study is two-fold. The first stage is determining how realistically CAESAR-Lisflood can model river channel changes. The selected reaches have multi-decadal overlapping records of river flows and channel patterns. These reaches provide a test for the effectiveness of CAESAR-Lisflood at modelling channel changes through comparison of mapped historical and hind-cast modelled channel changes. Parameter values representing vegetation cover, sediment erosion and transport, and hydrology were derived from the existing literature and are described further in Section 2.4. An ensemble of runs, testing different combinations of values for parameters governing erosion rates and channel morphology, were tested to calibrate the model. A key part of the model evaluation was determining the range and variation in selected parameter values between similar reaches.

The second stage involved applying simulated geomorphic changes to determine the total area of occupation of floodplain by the river channel. These results are compared with geomorphic changes derived from mapped datasets to evaluate further how effectively CAESAR-Lisflood could be used to model floodplain turnover processes over longer timescales.

It is worth explaining here why an “evaluation” approach was adopted over “validation”. As it is difficult, or even impossible, to account for all uncertainty that exists in nature and quantitative models, validation is argued by some to be impossible to achieve theoretically (Oreskes 1998). Equifinality for instance, means multiple models can produce acceptable fits to empirical data, making it challenging to validate a single set of parameter values successfully (Beven 2006). Previous application of CAESAR-Lisflood to a reach of the River Pellice, Italy demonstrated that validation was inhibited by incomplete understanding of natural phenomena, input data uncertainties, and the inability of a reduced-complexity model to replicate nature completely (Pasculli & Audisio 2015). Thus, some, including previous users of CAESAR-Lisflood (e.g. Meadows 2014), have argued for the evaluation rather than validation of models. Another advantage of evaluation is that both positive and negative results are possible outcomes of a model assessment and may facilitate improving the model and observed data (Oreskes 1998).

3.2.2. Study sites and model data inputs

Ten 1 km-length valley floor reaches were chosen from across northern England (Figure 3.1) and modelled using CAESAR-Lisflood version 1.9b. Historical maps show that the selected reaches incorporate a gradient in the rates of geomorphic change. These reaches also exhibit a variety of channel planform characteristics (e.g. sinuosity, meander wavelength, occurrence of multiple channels), and differences in floodplain morphology (e.g. valley width, number of terraces). Nearby flow gauges provide the multi-decadal time series of discharges required to run CAESAR-Lisflood, and these overlap with a rich historical record of channel changes discerned from maps and aerial imagery (Table 3.1).

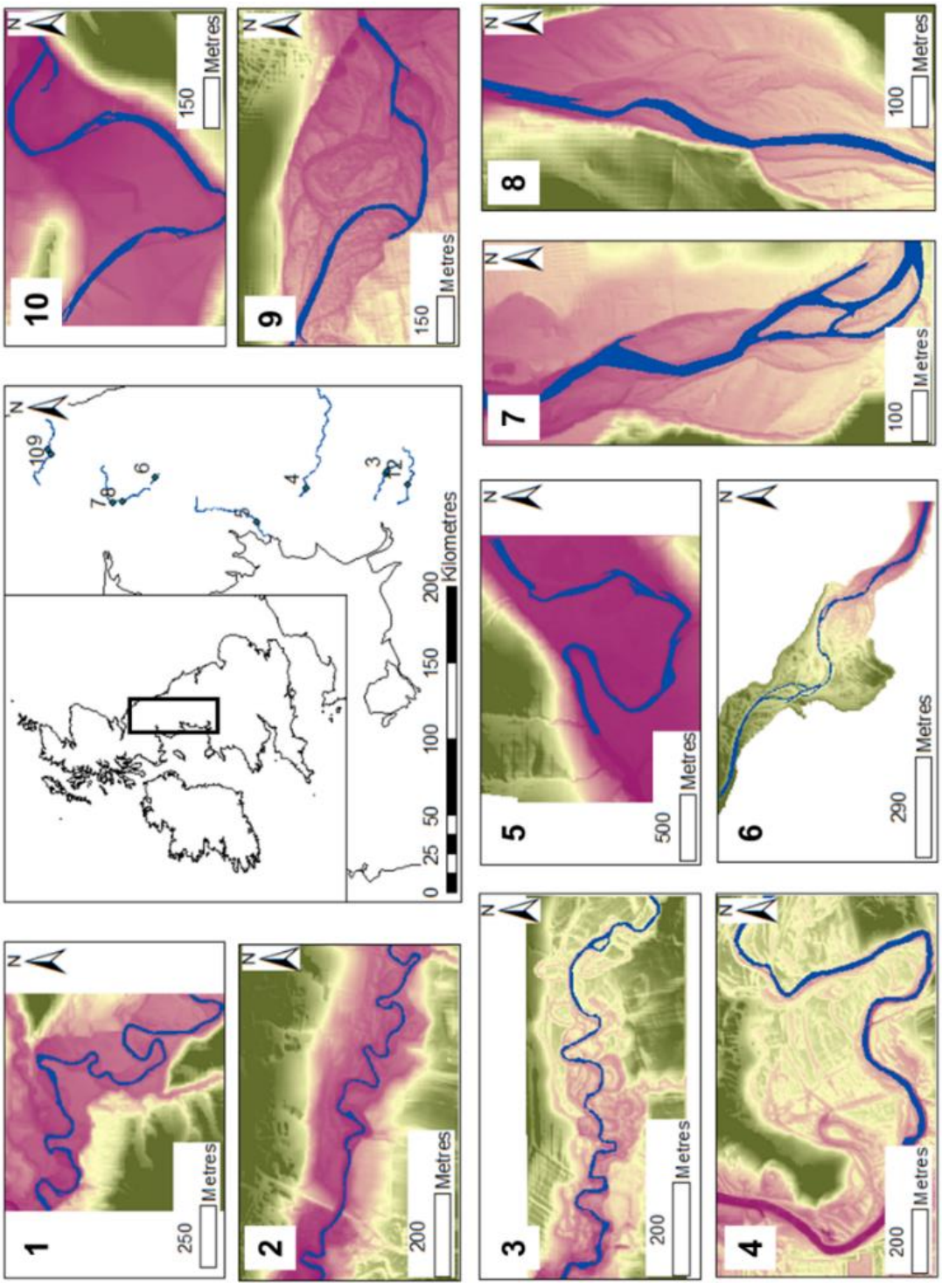

Figure 3.1: Environment Agency LiDAR 2m and Ordnance Survey Terrain 5m elevation models for the study reaches: 1. Dane, 2. Bollin1, 3. Bollin2, 4. Calder, 5. Lune, 6. Harwood Beck, 7. South Tyne1, 8. South Tyne2, 9. Coquet1 and 10. Coquet2. © Crown copyright and database rights 2019 Environment Agency and Ordnance Survey.

DEMs obtained from sources listed in Table 3.1 were clipped to reach boundaries, each encompassing 1 km of valley length and were resampled to a coarser grid resolution to expedite simulations (Table 3.2). The contemporary channel was smoothed out using elevation interpolation tools in RasterEdit software (available at https://sourceforge.net/projects/caesar-lisflood/files/) and the historical channel from the start of the simulation period was burned in using the Raster Calculator tool in ArcGIS (Table 3.2).

Table 3.1: Datasets used in channel change reconstruction and model set up.

Dataset	Description & purpose	Source
DEMs	DEMs of sites are required inputs for CAESAR-Lisflood. 5 to 15 m resolution depending on channel width and model run times.	Environment Agency (2 m LiDAR); OS Terrain 5 DTM (EDINA Digimap)
Daily flow records	A flow series is required to run CAESAR-Lisflood in reach mode. Daily historical discharge data from the nearest available flow gauge.	National River Flow Archive
Historical maps	1:10 000 scale maps. Contemporary OS map and historical map from approximately the start of the daily flow record selected for each site. Where possible, a map from the middle of the flow record period was also acquired.	Ordnance Survey (EDINA Digimap)
Aerial imagery	Aerial imagery from the early 2000s chosen to digitise channel morphology from the middle of the available flow record in cases where historical maps were unavailable. 25 cm resolution	Google Earth

Nine sediment grain size classes (mm) in the downloaded model were taken originally from the Swale catchment (see Table 3.1 in Coulthard & Van De Wiel 2017), and used as the basis for establishing individual separate grain size distributions for channel and floodplain cells (Figure 3.2) using the grainfilemaker tool (available at https://sourceforge.net/projects/caesar-lisflood/files/). The proportions of each grain size class (see "Default" in Figure 3.2) were rearranged for the nine grain sizes to match closely to published data on channel bed and floodplain grain size distributions. This was to

account for floodplains and terraces tending to consist of finer sized sediments and channel beds consisting of coarser material due to bed armouring.

Table 3.2: Combined overlapping flow and map/aerial image records for each site, and inputs used to run the model.

Site	Flow record used to run the model	Map/image years	DEM resolution (m)
Bollin1	Wilmslow, 01/01/1987 – 30/09/2014	1987, 2003, 2015	5
Bollin2	Wilmslow, 01/01/1976 – 30/09/2014	1976, 2003, 2015	5
Calder	Whalley Weir, 01/01/1988 – 30/09/2015	1988, 2003, 2015	10
Coquet1	Rothbury, 01/01/1976 – 30/09/2015	1978, 2002, 2015	10
Coquet2	Rothbury, 01/01/1976 – 30/09/2015	1979, 2002, 2015	10
Dane	Rudheath, 01/01/1969 – 30/09/2015	1969, 1992, 2015	10
Harwood Beck	Harwood, 01/01/1977 – 30/09/2015	1977, 2001, 2015	5
Lune	Caton, 01/01/1979 – 30/09/2015	1974, 2000, 2015	15
South Tyne1	Featherstone, 01/01/1982 – 30/09/2015	1982, 2003, 2015	15
South Tyne2	Featherstone, 01/01/1982 – 30/09/2015	1982, 2003, 2015	10

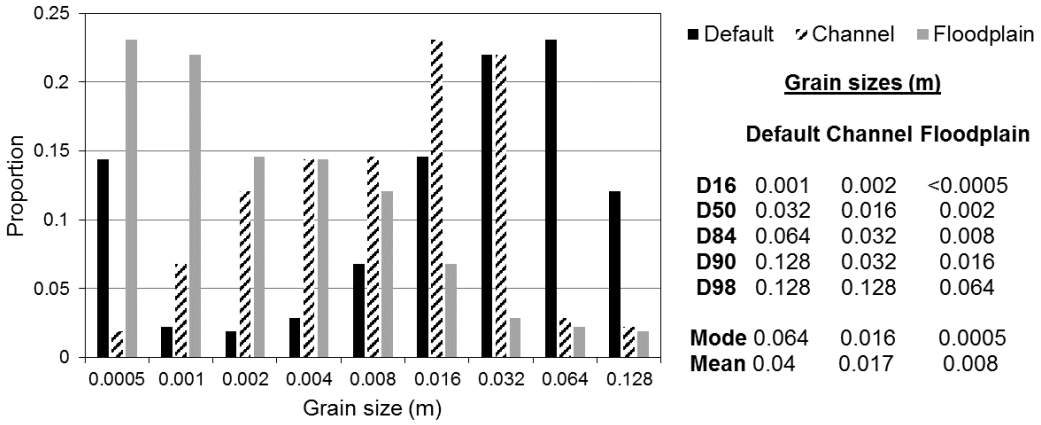

Figure 3.2: Grain size distributions for our simulations. The order of size proportions in the Swale catchment distribution was rearranged such that floodplains consisted predominantly of fine sediments (<2 mm) and channels consisted mainly of coarse sands and gravels. If erosion exceeds the combined depth of the surface layer and 10 sub-surface strata, the unaltered 'default' grain size distribution of the Swale characterises the new surface.

Setting the same grain size distribution for all reaches was intended to provide greater control over drivers of geomorphic changes, facilitating the testing of calibrated parameter values on uncalibrated reaches. Published data for reaches of the Coquet, Lune and South Tyne near our chosen sites show comparable grain sizes to each other and to our input grain size distributions (see Fuller et al. 2002; Graham et al. 2005; Wittenberg & Newson 2005). While descriptions of channel bed and bar grain sizes for the River Dane reflect our channel bed grain size distribution (Hooke 2003), local floodplain and terrace material consist mainly of sediments that are finer than the smallest grain size (0.0005 m) in our floodplain grain size distribution (Hooke et al. 1990). This may affect the values selected for parameters governing erosion rates and limit the application of calibrated parameters to experimental modelling.

CAESAR-Lisflood requires time to "spin-up" – a process characterised by the winnowing of fine sediments from the channel bed and an exaggerated rate of geomorphic change and sediment output at the beginning of simulations. To determine the duration of model spin-up, a separate set of simulations for each reach was run using a synthetic hydrograph. Synthetic hydrographs were generated by starting with the maximum discharge in the historic flow-series, lowering to the minimum recorded discharge after 182 days, and increasing to the maximum value again at day 365 (see Batz 2010). This 365-day flow series was repeated to generate a 20-year synthetic flow-series with one large flood event per year (Figure 3.3a). This approach was chosen to ensure that inter-annual variability in sediment yields could not result from any inter-annual variations in discharge. Assessment of inter-annual variability in sediment yields over 20 years (Figure 3.3b) suggest initially exaggerated rates of sediment flux stabilised within 10 years. This is comparable with results from the Tagliamento (Batz 2010) and Toutle-Cowlitz (Meadows 2014) systems. Simulations were therefore run for the full 25-45 years of flow data in Table 3.2, with evaluation of calibrated model parameters conducted using the latter of the two time-intervals, from the 1990's/2000's to present day (see Table 3.2), to ensure model spin-up effects had ceased and were not a component of the results.

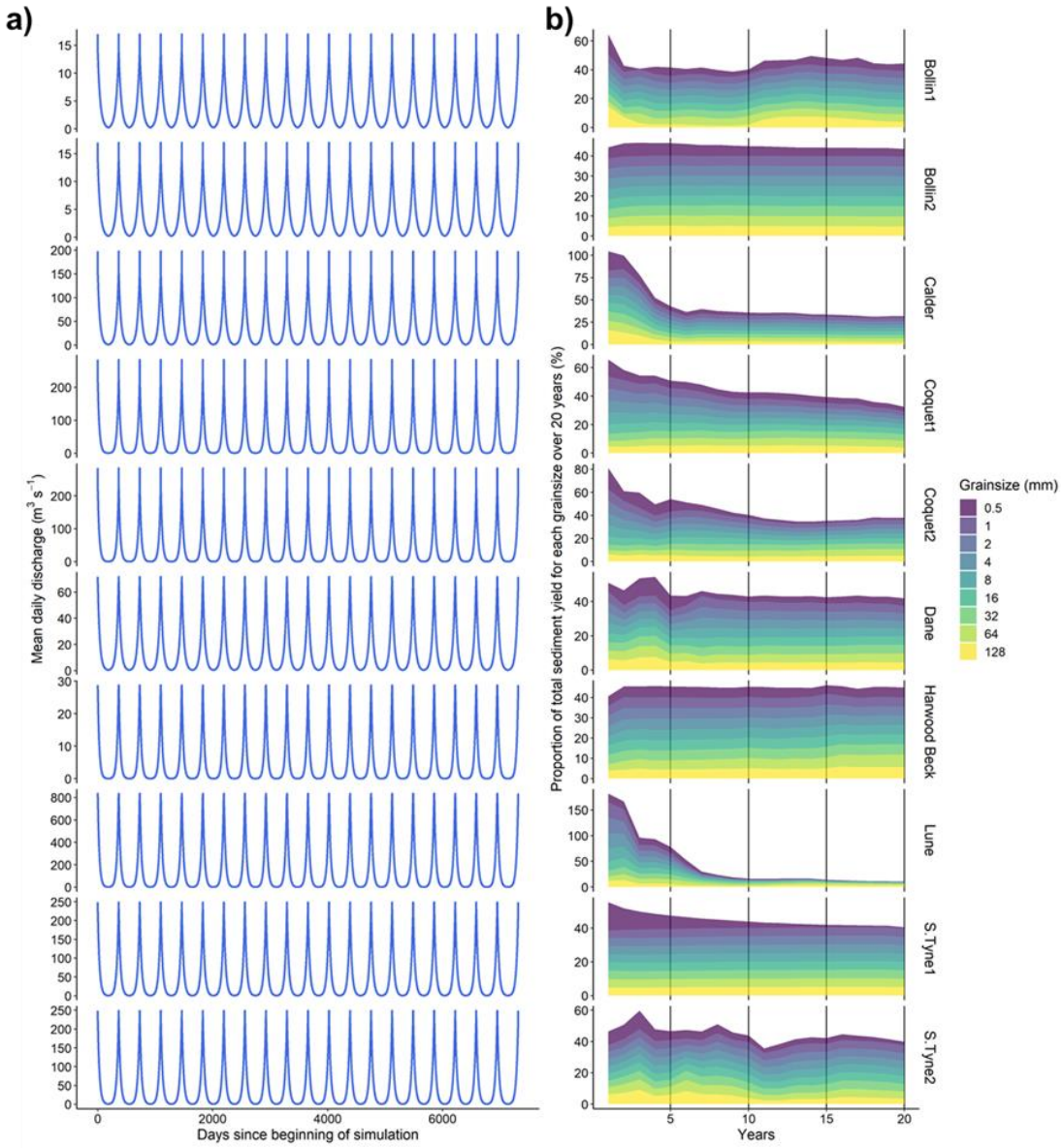

Figure 3.3: a) Synthetic hydrographs developed for model spin-up simulations (Note: these are separate to the calibration simulations); b) Modelled annual sediment yields from reaches and for each grain size from simulations designed to identify the model 'spin up' time. Annual sediment yields were normalised by the cumulative total sediment yield over 20 years and expressed as percentages. When inter-annual variability in sediment yields stabilises, spin-up is deemed to have completed (Note: plots for each of the grain sizes are stacked, hence the large upper limits along the y axis).

Historical daily flow records for the periods listed in Table 3.2 were used to drive simulations. Missing data were estimated by linear interpolation between recorded measurements. For the Dane flow series, a gap of more than 8 months (01/06/1978 – 12/02/1979) was filled using a linear regression between data from both the nearby Ashbrook gauge (River Weaver) and Rudheath gauge (Dane). No historical record of sediment transport data for the daily flow data taken from the streamflow gauges was available. Therefore, over the course of each simulation, the sediment output recorded at the reach outlet for each model iteration was recirculated into the top of the reach for subsequent iterations to provide upstream sediment fluxes.

3.2.3. Reconstructing historical channel changes

The main river channel within the selected reaches was digitised from the modern Ordnance Survey (OS) map, a historical map dating to the start of the combined map and flow record, and aerial imagery from the middle of the combined record (Table 3.2). Prior to digitising, aerial imagery were georeferenced to the modern base map. Typically, between 15 and 25 ground control points per image were used, concentrated close to the river channel, and wherever possible, located at 'hard edge' features (*sensu* Hughes et al. 2006), such as the corners of field boundary walls. Photos were georeferenced to the OSGB36 coordinate system using 2nd order polynomial transformation to reduce overall error associated with image distortions and then resampled using the nearest neighbour method. On average, total root mean square error (RMSE) for rectified images was 2.84 m (standard deviation = 1.15 m). For the Dane, a second historical map (1992) was used *in lieu* of aerial imagery as the midpoint record (see Appendix 1A for further details).

For the CAESAR-Lisflood simulations, DEMs, water depths, grain size information (including daily sediment fluxes and surface D_{50} maps) and animation image files were saved annually. For each of the corresponding historical map and aerial image years, DEM and water depth files were first converted from ASCII to raster format. Water depths were subsequently

converted to shapefiles and edited to the dimensions of the channel area, based on visual assessment of the DEMs and animation images.

Digitised channels were overlaid to calculate areas of erosion and deposition between years. Areas abandoned by the channel were classified as “deposition”, and areas newly occupied by the channel as “erosion”. Areas that indicated a combination of erosion and deposition, (e.g. floodplain areas between a former and a more recent channel position) were classified as “erosion and deposition” (Figure 3.4a). Total eroded and deposited areas (m^2) were converted to rates ($m^2\ yr^{-1}$) by dividing by the number of years in the interval between the modern and historic channel.

Channel centrelines from each year were extracted from channel polygons and lateral migration rates were calculated from measured migration distances, which were taken along equally-spaced transects created perpendicular to the mapped historical migration area centreline (Figure 3.4b; see also Appendix 1B) using the Channel Migration Toolbox in ArcGIS (Legg et al. 2014). For each transect that recorded a lateral migration distance (m), values were converted to rates ($m\ yr^{-1}$) in the same way as for erosion and deposition. For all sites, the mean annual lateral migration rate was calculated using data recorded along each transect.

Floodplains and digitised channels from the mid-point and end-years of the record were rasterised to the same DEM grid resolution used in our simulations. For each of the map and model channel-floodplain raster grids, cells were assigned a value depending on whether they were part of the floodplain (2) or channel (1), and these were subtracted from each other in Raster Calculator. Cells with a value of 0 following subtraction indicated a match between mapped and modelled landforms (Figure 3.4c). The number of successful matches of channel and floodplain cells between the model and mapped datasets was divided by reach area and expressed as a percentage.

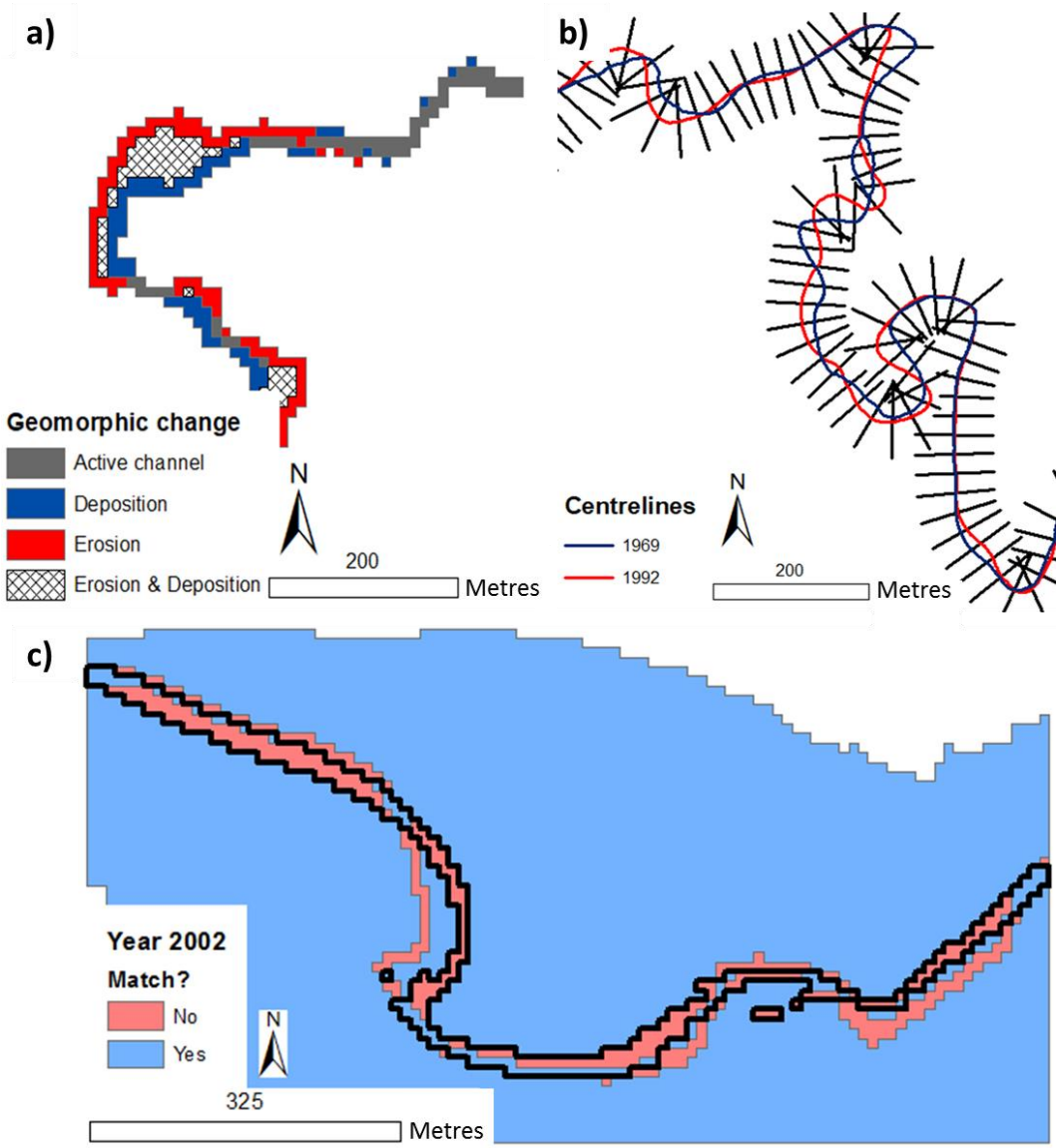

Figure 3.4: a) Channel and floodplain geomorphic change classification (example: simulation of Coquet2); b) Channel centrelines and lateral migration transects (example: 2 centrelines extracted from historical channels of the River Dane); c) Map-model raster overlay indicating successful landform cell matches between model and map datasets, with mapped channel boundary highlighted in black (example: Coquet1 reach from 2002).

3.2.4. Model calibration, performance and evaluation

3.2.4.1. Calibration

The procedure for model calibration, error quantification and selection of parameter values largely follows the framework outlined in a previous

CAESAR-Lisflood modelling study by Meadows (2014). Model calibration consisted of two key stages. First, values were selected for the parameters listed in Table 3.3.

Secondly, different combinations of values were trialled for two equations that make up the lateral erosion algorithm in CAESAR-Lisflood (Coulthard & Van De Wiel 2006; Van De Wiel et al. 2007). The parameters for these two equations are lateral erosion (θ) and in-channel erosion rate (λ):

$$E_{lat} = \frac{1}{R_{ca}} \theta \tau T \qquad (1)$$

where E_{lat} is the rate at which bank cells are lowered (m timestep^{-1}), R_{ca} is radius of curvature (m), θ is a user specified (through calibration) lateral erosion parameter (dimensionless), τ is the critical shear stress of the cell next to the channel bank (N m^{-2}) and T is time (s);

$$\Delta Z_{n-1} = V_{n-1} \lambda \frac{(Z_n - Z_{n-1})}{Dx} \qquad (2)$$

where ΔZ is the change in cell elevation (m), V is volume of eroded sediment (m^3), Dx is grid cell size (m), λ is a user-specified in-channel erosion rate (dimensionless), and n and n-1 are the donor and recipient cells, respectively, in the context of sediment transfer.

The first equation governs the rate at which the channel laterally migrates. Local radius of bend curvature is determined for each cell by identifying channel edge cells (Coulthard & Van De Wiel 2006) and determining whether these cells reside along the inside or outside of the meander bend, based on the number of surrounding wet and dry cells (Coulthard et al. 2007). Radius of curvature is then input into equation 1 each iteration of the simulation to determine lateral erosion rate. As the accuracy of radius of curvature depends on the number of passes the edge smoothing filter makes (Van De Wiel et al. 2007), modelled lateral erosion rates will depend on the choice of values for N_{smooth} and N_{shift} (Table 3.3) as well as θ.

Equation 2 controls channel hydraulic radius and allows sediment to move laterally within the channel, independently of the effects of channel sinuosity resulting from equation 1 (Coulthard et al. 2013). Higher values of λ allow

greater volumes of sediment to transfer between the donor and recipient cells. Effectively, equation 2 represents sediment cohesion, with lower values of λ indicating boundary materials are more cohesive, limiting lateral sediment redistribution, and *vice versa* for higher values of λ (Coulthard et al. 2013).

Some systems exhibit significant mid-channel deposition. A user-defined parameter, ΔC_{max} (Table 3.3) sets the maximum size difference between radius of curvature values for outer bank cells and values for inner bank cells between consecutive smoothing iterations (Van De Wiel et al. 2007). This affects the volume of sediment transferred across the cross-channel radius of curvature gradient over successive model iterations, with higher values facilitating mid-channel deposition and formation of mid-channel bars (Van De Wiel et al. 2007).

During calibration, most sites were run with grass cover, which includes grass, forb and herbaceous plants that are <2 m in height (Lyons et al. 2000), based on observations from aerial imagery. Although the Dane reach consists of a mix of both grass and forest cover, it was judged that forest cover, encompassing trees and shrubs that are ≥2 m in height (Lyons et al. 2000), was more appropriate. Much of the river banks were lined with trees and, based on historical analysis of a 5 km long river corridor just upstream (Hooke & Chen 2016), tree cover is shown to be increasing in this area.

Table 3.3 describes the three vegetation model parameters and choice of values for forest and grass cover. The highest threshold shear stress values listed in Table 2 of Fischenich (2001) for "long native grasses" (~80 N m^{-2}) and "hardwood trees" (~120 N m^{-2}) were chosen for grass and forest, respectively. Literature on the relationship between vegetation maturity and rates of sediment erosion is scant. Some sources state a threshold of about 20 years to distinguish between mature and immature forest (e.g. Trimble 2004; Fryirs & Brierley 2013). Given the typical life cycles of herbaceous plants (Lack & Evans 2001), it is assumed that grass reaches full maturity within a year. Thus, maturity times of 1 and 20 years were set for grass and forest, respectively. By default, CAESAR-Lisflood sets the proportion of erosion allowed to occur at full maturity to 0.1. Assuming this parameter is adjustable by increments of

0.1 and mature forest provides the greatest protection from erosion, but allows some erosion to occur, a value of 0.1 was set for forest cover. Based on a relationship of unit riparian biomass to net geomorphic work along river channels (see Figure 3.9 in Trimble 2004), grass cover was judged to also protect sediments from erosion by a significant amount, but not quite as much as fully mature, steady-state forest cover. Thus, a value of 0.2 was set here. Manning's *n* coefficient was adjusted (based on Chow 1959) to reflect impacts of different vegetation cover types on floodplain hydraulic roughness. Values of 0.035-0.05 and 0.06-0.08 were used for grass and forest, respectively.

No cross-parameterisation took place between simulations during calibration – i.e. one parameter at a time was altered, while the others were used as handles. For each reach, a range of values for θ, λ, N_{smooth}, N_{shift} and ΔC_{max} was identified for testing, based on recommendations in the literature (see Table 3.3).

Table 3.3: The sediment, vegetation and flow model parameters (modified from Tables 4.3, 4.5 and 4.9 in Meadows 2014). Guidance for parameter selection is from the model website: (https://sourceforge.net/p/caesar-lisflood/wiki/Home/ last accessed: 15/02/19). Details on operation of sediment model parameters are found in (Coulthard & Van De Wiel 2006; Van De Wiel et al. 2007) and for the flow model (Bates et al. 2010; Coulthard et al. 2013).

Parameter (units)	Operation	Impact & sensitivity	Parameter value selection
Sediment entrainment, transport & redistribution			
Sediment transport equation	Calculates volume of sediment eroded from a cell in a single iteration	Transport rates can vary significantly between the 2 formulae: Einstein (1950) and Wilcock & Crowe (2003).	Wilcock & Crowe (2003)
v_f (m s^{-1})	Suspended sediment settling velocity	Lower values increase suspended sediment deposition.	Estimated using Stokes' law.
ΔZ_{max} (m)	Maximum allowable elevation change per cell per iteration	Lower values restrict time step and enhance model stability.	Default = 0.02 used; can be lower for fine resolution DEMs (10m).
L_h (m)	Stratum thickness within the active layer system	Low values could affect transport rates through detachment-limitation.	Must be at least four times ΔZ_{max}. 0.2 used.

N_{smooth}	Number of passes made by edge smoothing filter that is used to calculate radius of curvature	Low values may cause irregular lateral development; high values may lead to over-smoothed channels.	Low values for high sinuosity meandering or braided systems; higher for low sinuosity systems. Must be an integer. Estimated using meander wavelength (in grid cells).
N_{shift}	Determines number of cells the cross-channel gradient shifts downstream to model downstream bend migration	May lead to unrealistic evolution of meander bends if set incorrectly.	One tenth of N_{smooth} and must be an integer.
ΔC_{max}	Calculates cross-channel gradient from radius of curvature which is used to control lateral transfer of eroded sediment from the outer to inner banks	Lower values ensure distribution across the entire channel width, but increase model run time. Higher values encourage mid-channel deposition.	Default = 0.0001 used; can be increased or decreased by an order of magnitude depending on channel width or if modelling mid-channel deposition.
Vegetation			
τ_{crveg} (N m^{-2})	Threshold bed shear stress for vegetation removal by flows	Higher values relate to greater resistance to removal.	Estimated from vegetative strength data†. For grass cover: 80 For forest cover: 120
T_{veg} (years)	Time required for vegetation to reach full maturity	Higher values negate the role of this over short time scales.	Estimated from known vegetation growth rates. For grass cover: 1 For forest cover: 20
Proportion of erosion allowable at full maturity	Determines how vegetation maturity affects erosion	0-1 scale: 1 means vegetation has no impact on erosion; 0 means no erosion occurs at full maturity.	0 – 1 (default = 0.1); Estimated by known effects of vegetation on erosion. For grass cover: 0.2 For forest cover: 0.1
Hydrology & flow routing			
Q_{min} (m^3 s^{-1})	Run time optimisation. Minimum discharge in a cell necessary for depth to be calculated	Higher values reduce run times but may restrict flow and erosion in peripheral cells if too high.	One tenth of DEM grid resolution (m).
d_{min} (m)	Run time optimisation. Minimum water depth in a cell necessary for erosion to be calculated	Higher values reduce run times but may restrict flow and erosion in peripheral cells if too high.	Default = 0.01 used. Can be lowered for grid cells <5m or increased for cells >50m.
Q_{diff} (m^3 s^{-1})	Run time optimisation. Difference between the input and expected output discharge that can allow the model to shift to steady state mode.	Higher values reduce run times, but if too high can cause too many discharge events to be missed and lead to numerical instabilities.	Can be approximated by catchment mean annual flow. User judgement also necessary regarding acceptable difference between input and output discharge and

			speed of model operation.
h_{flow} threshold (m)	Run time optimisation. Depth through which water can flow between two cells	Higher values reduce run times but may limit flow when gradient between neighbouring cells is low.	Default = 0.00001 used.
Courant number	Controls model time step and affects stability	Higher values increase time step but increase risk of instabilities such as chequerboarding (rapid flow reversals between cells).	Must be 0.3 – 0.7. 0.3 chosen as this is recommended for 10 m cells or finer; coarser grids can use larger values.
Froude number	Controls model stability and flow rate between cells	Low values reduce speed of flood waves and erosion. High values may induce chequer-boarding.	Default = 0.8 used. Lower values could be used for very deep, slow flows.
Manning's *n*	Calculation of flow depth and velocity	High values increase flow depths, reduce flow velocities, and reduce erosion.	Estimated from reach / catchment attributes and relevant literature. Values chosen from reference table (Chow 1959).
Slope for edge cells	Calculates flow out of the model at the down-stream boundary	High values can cause excessive bed scour and upstream propagating knickpoints; low values can cause excessive deposition at the outlet.	Mean bed slope of the channel near the DEM outlet.

†Note: This refers to critical shear stress values of "long native grasses" and "hardwood trees" presented in Table 2 of Fischenich (2001). These values are recommended permissible thresholds for stream restoration materials and are based on data for natural vegetation.

3.2.4.2. Selection of parameter values

Assessment of model accuracy focussed on four key characteristics: surface areal erosion rates, surface areal deposition rates, lateral migration rates, and successful matches between modelled and mapped landforms. Erosion and deposition were judged jointly most important, followed by lateral migration, with successful landform matches least important. Surface areal erosion and deposition directly quantify the extents of floodplain destruction and creation in 2D, respectively. Lateral migration is judged to be the primary control on erosion and deposition. Successful landform matches between modelled and mapped datasets assess how accurately the model reproduces spatial

patterns of planform channel change, including active channel width/area. When values for the four criteria for assessing accuracy were calculated for each simulation, they were compared with the corresponding mapped data to calculate absolute relative error values. Absolute error measures ensure both positive (over-estimation) and negative (under-estimation) observations contribute to the overall error and do not cancel each other out (Bennett et al. 2013). For each criterion, error values were compared across calibration runs for a reach and were ranked from 1 to n (smallest to largest error).

In order to determine the most accurate model run overall, the Analytic Hierarchy Process (AHP) was used (following Meadows 2014). AHP is a decision-making framework whereby multiple criteria of differing importance, derived from user judgement, are compared in a pairwise manner in order to select the best outcome from a range of competing alternatives (Saaty 1990; Vargas 1990). A goal (i.e. selecting the most accurate simulation from a wider ensemble of calibration runs) and the criteria (see previous paragraph) to meet the goal are defined. A matrix records the judgements in which each criterion is compared with all other criteria. Judgements represent the relative importance of a criterion in the far-left column of the matrix over a criterion in the top row (see example in Appendix 1C) using a 1 to 9 scale (Table 3.4). All seven possible combinations of 1 to 9 judgement ranks were used whereby erosion and deposition were always judged to be jointly most important, matching landforms least important, and lateral migration only slightly less important (i.e. 1 rank lower) than erosion and deposition. Assuming this order of importance stays the same; the full range of possible judgement values is considered, eliminating one potential area of user bias.

After all combinations of judgement values were trialled, the resulting weights meant that erosion and deposition each contributed 35.1-39.2%, lateral migration 16.2-18.9% and landforms matched 5.5-10.9% to the final model score. For each criterion, simulations were ranked 1-n (1 = lowest and n = highest degree of error). The calculated weights were multiplied by the ranks of the corresponding accuracy criteria and summed. The simulation with the smallest cumulative value was ranked best (a rank of 1) in terms of overall model accuracy. The simulation ranked best the most times out of all 7

combinations was selected (see Appendix 1C for more details of how the AHP method works, including a step-by-step guide using data from the Dane as an example).

Table 3.4: The 1-9 scale of importance for pairwise comparison between selection criteria (modified from Saaty 1986, 2008).

Rank of importance	Definition	Explanation
1	Equal	Equal contribution of criteria to the objective
2	Weak or slight	-
3	Moderate	Slightly favouring one criterion over another
4	Moderate plus	-
5	Strong	Strongly favouring one criterion over another
6	Strong plus	-
7	Very strong	Very strongly favouring a criterion
8	Very, very strong	-
9	Extreme	Evidence favouring a criterion is of the highest degree of importance over another
Reciprocals of above	If criterion *a* has one of the above rank values assigned to it when compared with criterion *b*, then *b* has the reciprocal value when compared with *a*	-

3.2.4.3. Evaluating the accuracy of calibrated parameter value ranges

A split-sample testing approach was conducted here. Five of the ten reaches were reserved for calibration, while the other five reaches were reserved to test the robustness of calibrated parameters more comprehensively. Each of the five reaches reserved for calibration were parameterised individually, regardless of whether some reaches were from the same river system. To evaluate the selection of parameter values more thoroughly, the calibrated lateral erosion rate (θ) and in-channel erosion rate (λ) parameter values from each of the five calibration reaches were tested on the remaining five uncalibrated reaches. Rates of erosion, deposition and lateral migration and successful landform matches between map and model datasets were calculated to assess which of the five calibrated parameter combinations was

the most accurate, and to what extent, by comparison with the mapped reconstructions.

3.2.5. Modelling floodplain turnover processes

Floodplain turnover can be quantified using a number of measured variables, including the turnover time (the total area of floodplain that has been eroded over a time interval) and the area of the floodplain that has been occupied by the river channel at least once over time (Figure 3.5). Quantified erosion rates should be strong predictors of floodplain occupation rates by the channel. However, the ten sites range widely in a number of physical characteristics, including area (0.14 – 1.67 km^2), sinuosity (1.04 – 2.48) and slope (0.002 – 0.008). Therefore, in order to compare erosion rates and areal extents of floodplain occupation by the channel across sites and between mapped and modelled datasets, values for these two variables were divided by the total area of each reach. After normalising by reach area, values derived from mapped reconstructions for these two processes were arranged by decreasing order of size across the ten reaches to establish gradients. The values derived from modelled reconstructions were subsequently plotted adjacent to these to evaluate how accurately mapped values were reproduced. Relationships between erosion rates and total floodplain area occupied by the channel over time were determined. These relationships were then used to estimate the length of time required for all areas of the floodplain to become occupied by the channel (i.e. the floodplain turnover time) for all the reaches.

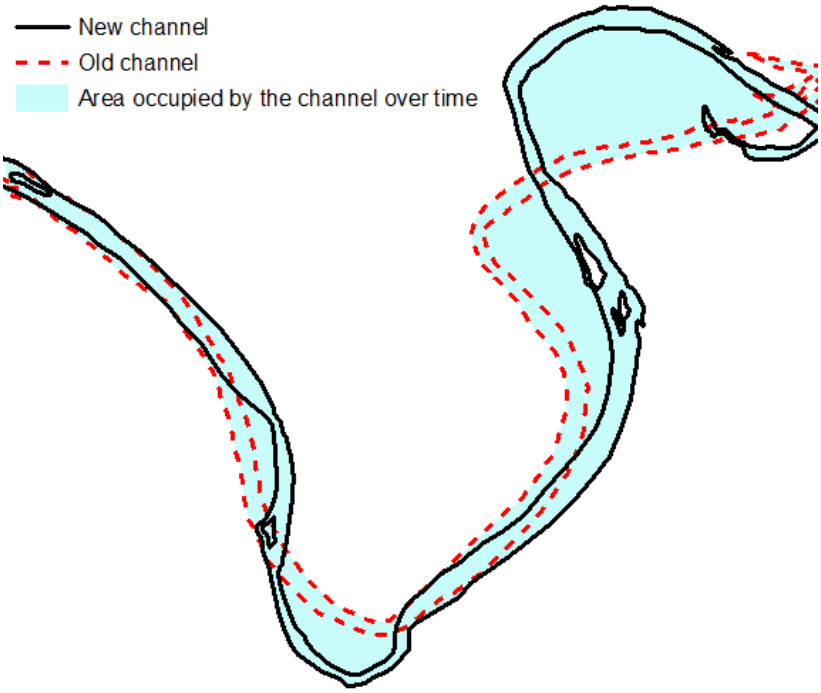

Figure 3.5: Example of the area occupied by the channel at least once over time. The shaded polygon includes the areas of floodplain occupied by both the old and new channel positions and the area of floodplain that was eroded as the channel migrated from its old to its new position.

3.3. Results

3.3.1. Model calibration and performance

On average, 30 simulations were run for each of the five sites reserved for model calibration (total of 154 runs). These included initial test runs to determine the upper and lower bounds for the lateral erosion rate parameter, which for most sites ranged over a single order of magnitude (10^{-5}-10^{-6}). Table 3.5 lists selected parameter values for each site from the most accurate simulations. For single channel meandering systems, values of 15-20 for in-channel erosion rate (λ) were found to be most accurate based on comparison with mapped channel changes. As the Harwood Beck reach was relatively wide in places (despite being one of the narrowest rivers on average of the ten sites) and showed evidence of braiding and mid-channel sediment deposition, $\lambda = 23$ was used here.

Table 3.5: Summary of calibrated values for the two erosion rate parameters, number of passes for edge smoothing filter and number of cells the cross-channel gradient shifts downstream for the selected model run (lowest overall error). Test ranges and increments are given for the two erosion parameters.

Site		Lateral erosion rate, θ (x10^{-5})	In-channel erosion rate (λ)	No. of passes by edge smoothing filter (N_{smooth})	No. of cells cross-channel gradient shifts downstream (N_{shift})
Coquet1	Calibrated:	0.1	19	80	8
	Test range:	0.1-1	15-20		
	Increments:	0.1	1		
Coquet2	Calibrated:	0.3	15	80	8
	Test range:	0.05-0.35	15-20		
	Increments:	0.05	1		
Dane	Calibrated:	0.1	14	10	1
	Test range:	0.1-0.12	10-20		
	Increments:	0.01	1		
Harwood Beck	Calibrated:	0.1	23	100	10
	Test range:	-	15-25		
	Increments:	-	1		
Lune	Calibrated:	2	15	30	3
	Test range:	1-5	15-20		
	Increments:	1	1		

Results for the four evaluation criteria – erosion rate, deposition rate, lateral migration rate and percentage of matching landforms – demonstrate that simulations replicated historical changes accurately. Erosion rates derived from mapped reconstructions were matched closely by modelled erosion rates across all five sites. Reconstruction accuracy ranged from an over-prediction of 6% along the Lune to an under-prediction of 36% for Coquet2 (Figure 3.6). Deposition rates along both of the Coquet reaches were reconstructed accurately by the model. However, deposition rates were under-estimated along the Dane and the Lune by as much as 70% and 79%, respectively, and over-estimated for the Harwood Beck by more than 800% (Figure 3.6). Lateral migration rates were reconstructed accurately overall. Again, the most accurate reconstructions were for the Coquet reaches (over-estimated by 3% for Coquet1 and under-estimated by 11% for Coquet2). The least accurate result was for the Harwood Beck where mean lateral migration rates were over-estimated by 80% (Figure 3.6). Successful matches between modelled and mapped landforms were ≥85% on average for all sites (Figure 3.6).

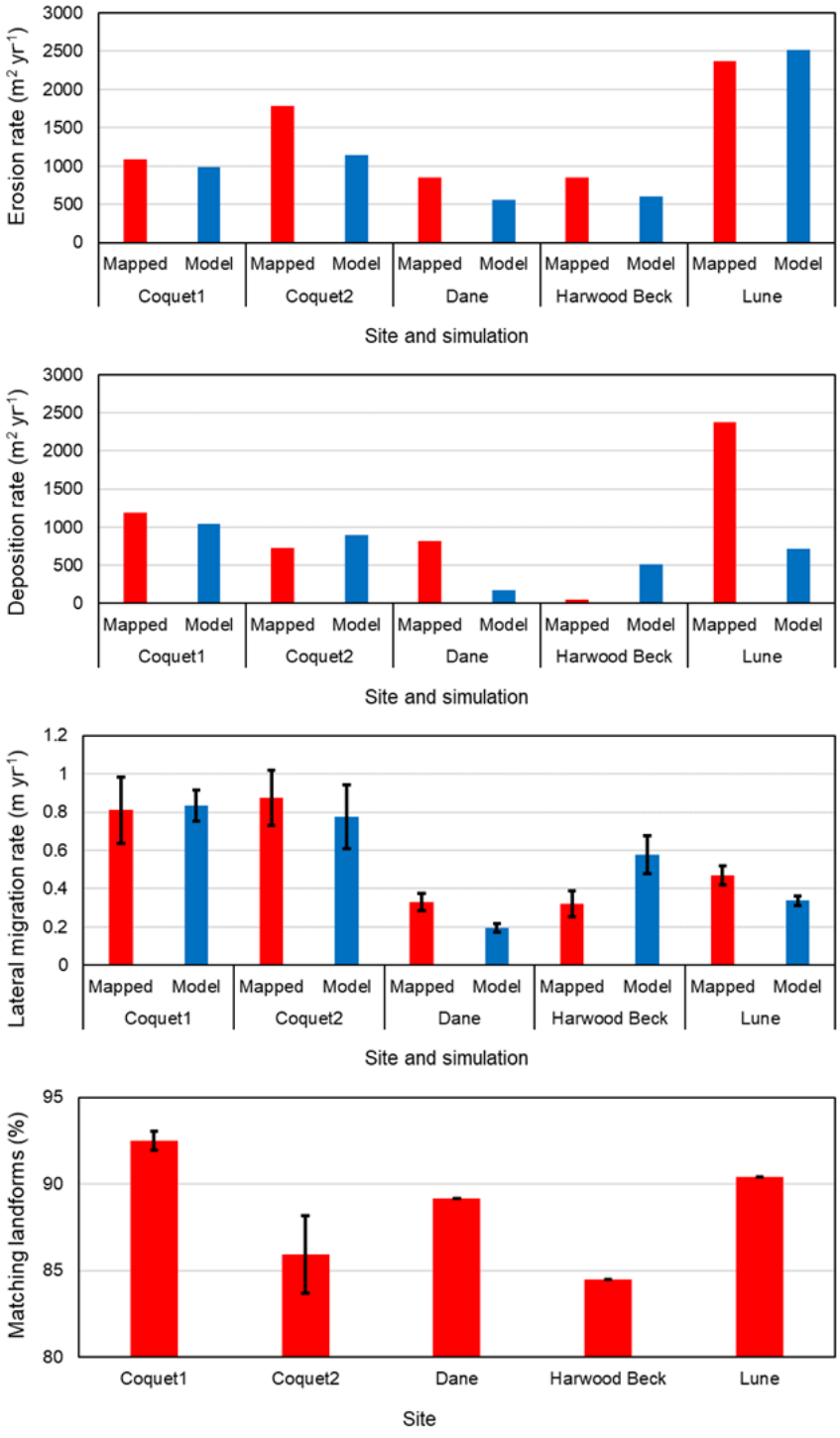

Figure 3.6: Results of the single most accurate model run for each site compared to data from mapped historical reconstructions for the four evaluation criteria: erosion rate, deposition rate, lateral migration rate and successful landform matches between mapped and modelled datasets. Mean lateral migration rates are calculated from all measurement transects. For matching landforms, the mean is calculated from successful matches at the midpoint and endpoint years. Error bars equal one standard error of the mean.

3.3.2. Evaluation of model parameterisation

The five calibrated reaches vary widely in physical characteristics, including reach and channel area, valley slope, number of peak over threshold events per year (POT/yr), and mean channel sinuosity and thalweg lengths. Reaches reserved for evaluating calibrated parameter value ranges show a similar variability in physical characteristics to the calibrated reaches. Hence, the five reserved reaches should provide an appropriate basis to evaluate the transferability of calibrated parameter values (Table 3.6).

Table 3.6: Physical characteristics of the calibrated and reserved reaches. Values relate to mapped datasets. Mean channel area, sinuosity and thalweg length values are calculated for the three mapped channel years listed in Table 3.2. POT stands for peak over threshold events and the mean is calculated based on the number of individual days with a discharge higher than the specified POT flow for the stream gauges listed in Table 3.2).

	Reach area (10^3 m^2)	Mean channel area (10^3 m^2)	Valley slope	Mean channel sinuosity	Mean no. POT events/yr	Mean thalweg length (m)
Calibrated reaches						
Coquet1	724.9	258.825	0.002	1.33	3	1367.4
Coquet2	423.8	369.65	0.004	1.77	3	1744.4
Dane	474.5	382.591	0.004	2.48	5	2604.8
Harwood Beck	138.65	145.978	0.003	1.15	3	1188.2
Lune	1667.475	2071.74	0.002	2.47	5	4169.6
Reserved reaches						
Bollin1	140.2	120.038	0.002	1.52	1	1507.4
Bollin2	155.775	153.646	0.005	1.84	1	1654.1
Calder	448.2	352.528	0.004	2.01	7	1800
S. Tyne1	440.325	461.276	0.008	1.25	3	1209.1
S. Tyne2	262.9	286.757	0.008	1.04	3	1017

Figure 3.7 shows the simulated rates of erosion, deposition, lateral migration and the degree of successful reconstruction of mapped landforms for each of the tested calibrated parameter value combinations when applied to the reserved reaches. Erosion rates of the most accurate simulations (highlighted in red) were over-predicted by ~11% for Bollin2 and were under-predicted for the other reaches by ~22-46% (Figure 3.7). Deposition rates were under-predicted by ~21% and ~23% for the Calder and Bollin1 reaches, respectively.

Elsewhere, rates were over-predicted by as much as ~200% (Figure 3.7). Lateral migration rates were underpredicted by between ~9 and 21% for four reaches and overpredicted by 36% for Bollin2. Mapped landforms were reconstructed to a similar level of accuracy to the calibrated reaches, with successful reconstruction ranging from ~86 to ~93%.

Parameter values calibrated for the two Coquet reaches were found to produce the most accurate simulations for four of the reserved reaches. This would suggest a high potential of transferability in the choice of parameter values for the Coquet reaches. However, the failure to reconstruct mapped data for untested cases using parameter combinations from other calibrated reaches would suggest the need to calibrate reaches individually. This also applies if the reaches in question come from the same river system.

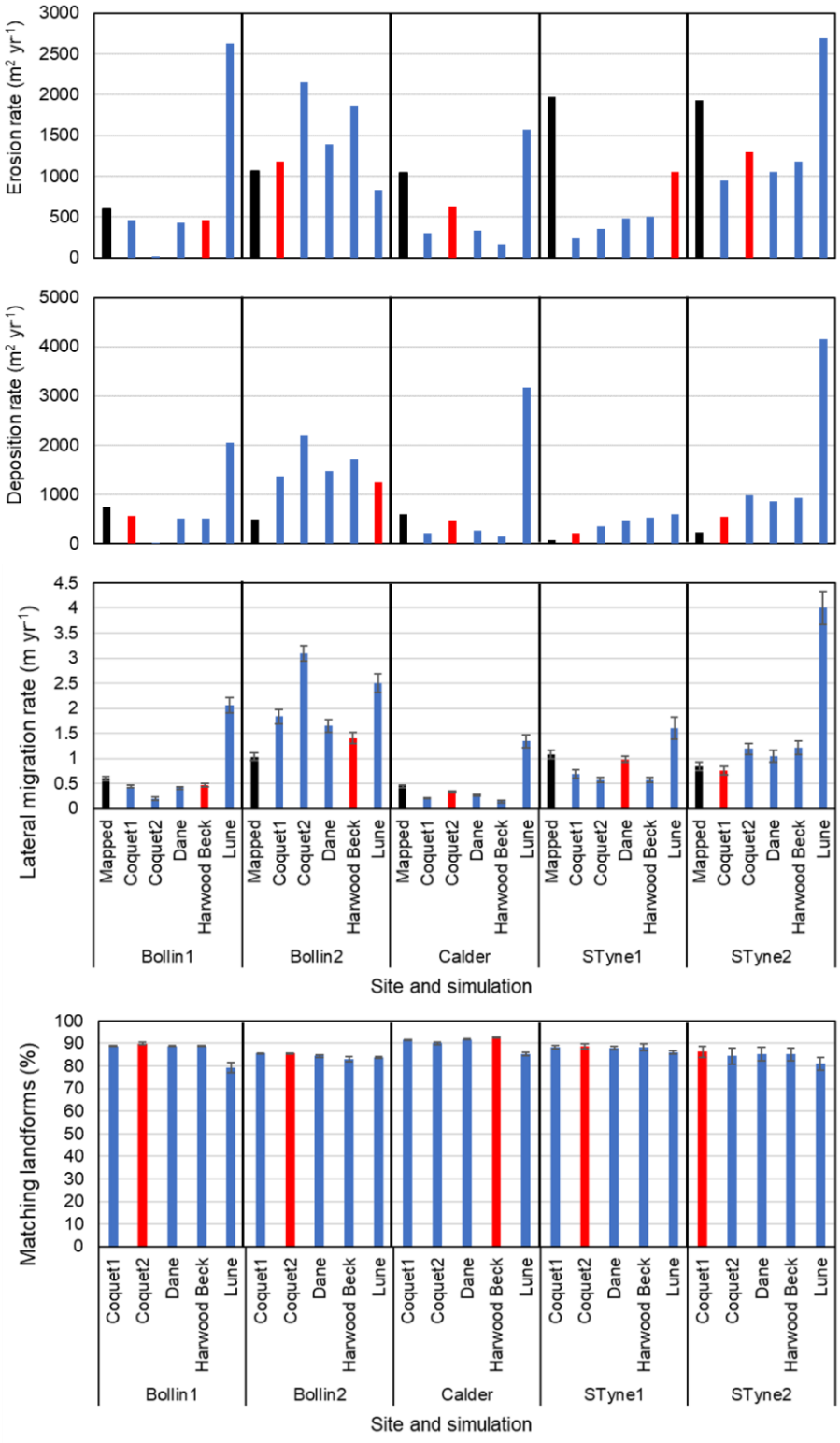

Figure 3.7: Results of split-sample test, running the five reserved reaches (Bollin1, Bollin2, Calder, S. Tyne1 and S. Tyne2) with parameter values from the calibrated sites (Coquet1, Coquet2, Dane, Harwood Beck and Lune). The most accurate result is highlighted in red. Error bars equal one standard error of the mean.

Table 3.7: The most accurate combination of calibrated parameter values for each of the reserved reaches.

Reserved reach	Reach with the most accurate calibrated parameters overall when applied to the reserved reach	Lateral erosion rate, θ (x10^{-6})	In-channel erosion rate, λ
Bollin1	Harwood Beck	1	23
Bollin2	Coquet1	1	19
Calder	Coquet2	3	15
South Tyne1	Coquet1	1	19
South Tyne2	Coquet1	1	19
	Coquet2	3	15

3.3.3. Floodplain turnover processes

When mapped floodplain erosion rates were normalised by reach area, the upper reaches of the South Tyne (South Tyne2) and Bollin (Bollin2) were shown to be the most actively changing systems over time, with erosion rates of 7.2 and 6.8% of floodplain area per year respectively (Figure 3.8). The Dane, Coquet1 and Lune reaches were the least active, with normalised erosion rates ~4 times lower (Figure 3.8). Modelled erosion rates followed a similar gradient overall, with Bollin2 recording the highest erosion rates and the Dane, Coquet1 and South Tyne1 reaches the lowest rates (Figure 3.8). Areal extents of floodplain occupation by the channel produced a similar gradient to erosion rates for the mapped dataset. Harwood Beck, and the upper reaches of the South Tyne and Bollin had the highest values (>15 %), while the Coquet1 reach had the lowest value of <6 % (Figure 3.8). Simulations produced similar results to mapped data, including a similar overall gradient.

Normalised erosion rates were found to correlate positively with the extent of channel occupation of the floodplain for both the mapped and modelled datasets (R = 0.76 and 0.74, respectively) (Figure 3.9a). Results of linear regression indicate that the extent of channel floodplain occupation could be predicted from erosion rates. Linear models could be fitted to both the map and model datasets, with similar gradients and intercepts (Figure 3.9b).

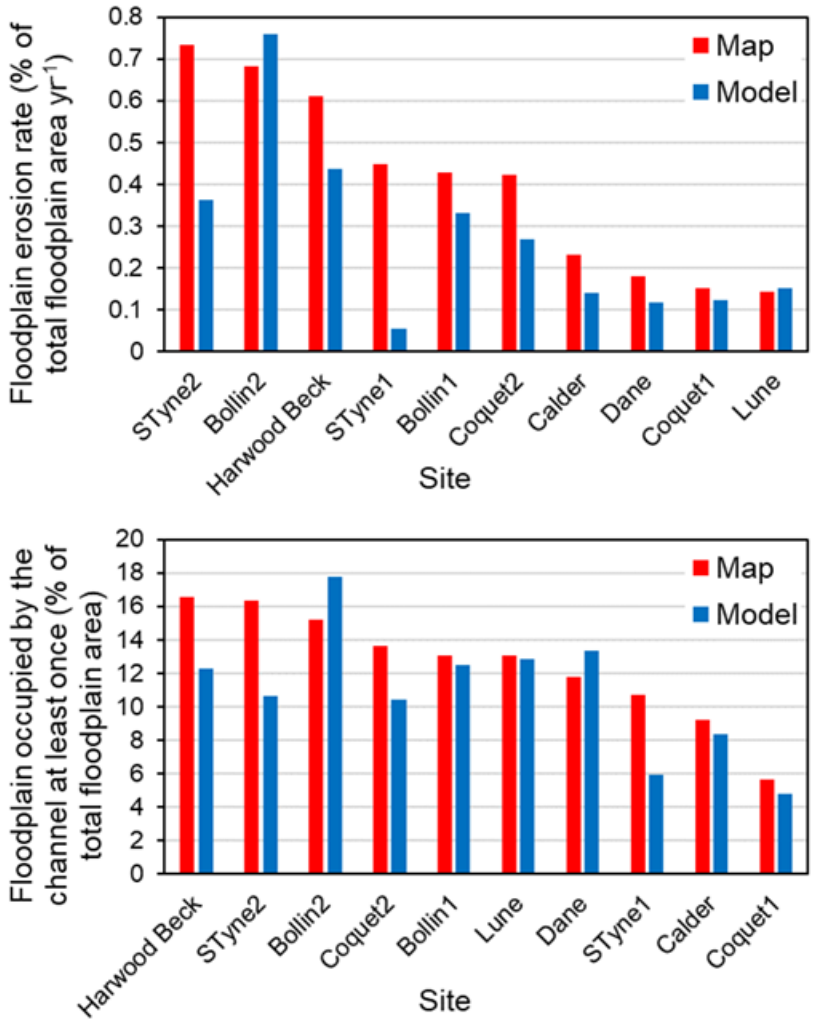

Figure 3.8: Erosion rates and estimated areal extents of floodplain occupation derived from mapped mean erosion rates. Data for these two dependent variables are normalised by floodplain area. Data in each plot are ordered from largest to smallest based on mapped data (red) to establish a gradient across the ten reaches, with modelled data (blue) adjacent for comparison.

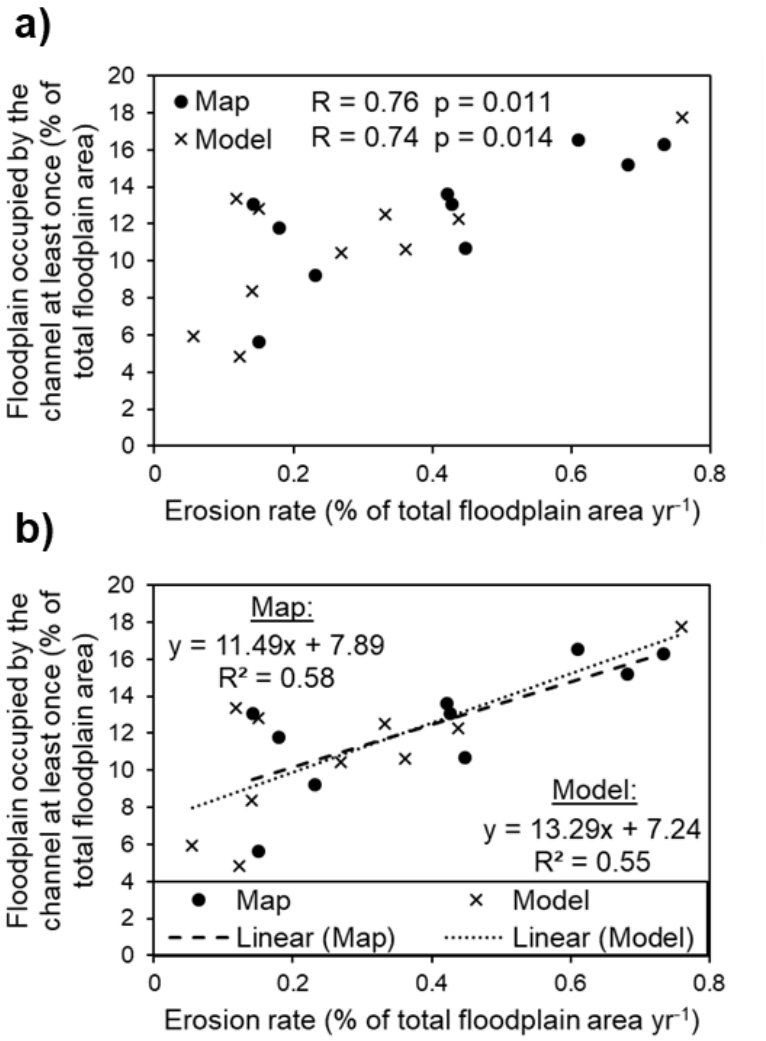

Figure 3.9: a) Pearson's correlations for mapped and modelled data between erosion rate and floodplain occupation by the channel (after both of these variables have been normalised by reach area); b) Linear regression results to predict floodplain (re)occupation extents by the channel from erosion rates.

Assuming that the extent of channel floodplain occupation increases linearly with erosion rates up to 100 % floodplain occupation (or turnover), the linear models in Figure 3.9b could be used to estimate floodplain turnover times (as defined by Bolin & Rodhe 1973). First, normalised erosion rates (x) are estimated when floodplain occupation by the channel over time is 100 % (y = 100). The estimated normalised erosion rates when y = 100 are then divided by the normalised erosion rates for each site in Figure 3.8. These values are then multiplied by the measurement interval (years) for the channel change at

each reach (e.g. the measurement interval for the Dane – 1992-2015 = 23 years). Estimated floodplain turnover times ranged widely, between 137 and 1095 years for mapped erosion rates and between 72 and 1080 years for modelled erosion rates. Estimated turnover times were replicated by the model accurately overall. Turnover times for half of the sites were over- or under-predicted by <20 % and under-predicted for four others by <50 % (Figure 3.10). Turnover time for South Tyne1 was over-predicted by the model by nearly 400% (Figure 3.10). This is unsurprising as modelled erosion rates, using the Coquet1 parameter values (Table 3.7) were 8 times lower than rates measured from mapped reconstructions along this reach (see Figure 3.8). This suggests that despite being the most accurate overall, the Coquet1 reach's calibrated parameters are still a poor fit for South Tyne1, emphasising further the necessity to calibrate on a reach-specific basis. These results also show how errors in predicted erosion rates by the model can propagate when extrapolated to predict floodplain erosion dynamics over longer timeframes.

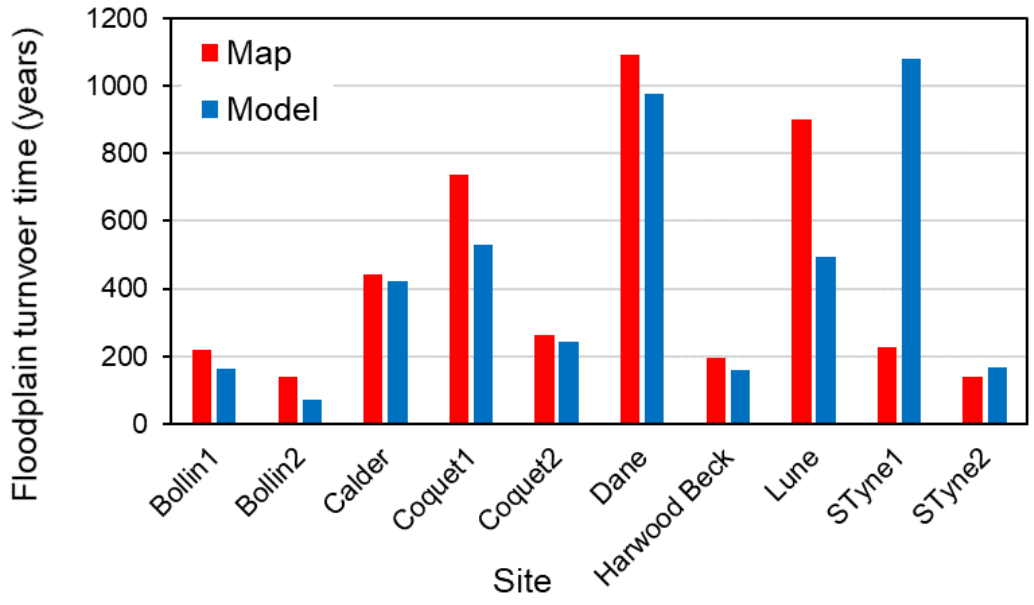

Figure 3.10: Estimated times to complete floodplain occupation (turnover). Turnover times for the map and model datasets are estimated by solving the linear equations from Figure 3.9b when y =100 (complete floodplain erosion), dividing by the normalised floodplain erosion rates presented in Figure 3.8, and multiplying by the number of years in the channel change measurement interval for each site.

3.4. Discussion

3.4.1. Model calibration and reconstruction of geomorphic processes

Generally, modelled channel morphology seemed to replicate mapped reconstructions accurately. In some cases, there was a tendency for the size of meander bends to be over-estimated. This is especially true for reaches where channel cut-offs occurred during the studied record. For example, in both Bollin reaches, modelled cut-offs occurred either later than they should have, failed to occur at all along some bends or occurred in the wrong places. However, given the stochastic and self-ordering nature of channel cut-off behaviour (Hooke 2004; Camporeale et al. 2008), simulated channel cut-offs may be unlikely to occur in exactly the same places and/or at exactly the same time. Hence, it may be satisfactory to settle for similar numbers of cut-offs occurring over the course of the simulation to the compared mapped record. Nevertheless, issues with simulating channel cut-offs have been identified previously for simulations of a reach of the River Teifi (Coulthard & Van De Wiel 2006). Conversely, for the Coquet2 and Dane reaches, cut-offs formed too easily during calibration trials, limiting the sizes of λ and θ values that could be tested.

In most cases, modelled lateral migration rates were within the error bounds of mapped data. However, there was a pattern of under-estimated modelled mean values for these three rates. Modelled lateral migration distances, recorded along regularly spaced transects, tend to lie within a smaller range of values and are skewed towards lower values (Figure 3.11). The use of single λ value and θ values may restrict the range of lateral migration distances along transects. In particular, the choice of low values for systems prone to forming cut-offs during simulations, e.g. Coquet2 and Dane (Figure 3.11e & 11f), would very likely skew this range towards lower lateral migration rates. It is possible for our simulations that a relatively coarse grid cell resolution (e.g. 10 m) means that a relatively high threshold lateral migration distance (>5 m) is necessary for a floodplain cell to become a channel cell and *vice versa*. DEM scaling effects have been shown to influence erosion and deposition rates in previous CAESAR-Lisflood applications. For example, soil erosion plot simulations from the Hühnerwasser catchment, Germany revealed a decrease

in rill network density with increased grid cell size, as incisions with cross-sections smaller than the cell size could not be initiated (Schneider 2013). Elsewhere, running simulations using a higher DEM resolution than 2 m was suggested as a way to improve the accuracy of modelled reconstructions of ephemeral gully geometry and spatial dynamics (Hoober et al. 2017).

Channel changes simulated along four out of five of the reaches reserved for evaluating calibrated parameters were reconstructed most accurately using parameters calibrated for the two Coquet reaches. This demonstrates some potential transferability in calibrated parameters from one reach to an untested reach. However, the wide range in calibrated values for parameters listed in Table 3.5, and the results displayed in Figure 3.7 and Table 3.7 demonstrate that reach-specific parameterisation is necessary with CAESAR-Lisflood. As an example, the Lune required a value for the lateral erosion rate coefficient, θ, that was 20 times larger than the value set for the Dane (Table 3.5), a reach with similar average sinuosity and number of POT/yr (Table 3.6) as well as similar channel change behaviour (gradual lateral migration with no avulsions). However, because the Lune had a channel that was ~1.5 times longer and ~5.5 times larger in area than the Dane, a much higher values for the lateral erosion rate parameter were needed to generate similar rates in mapped lateral migration.

Channel changes in both Coquet reaches consisted purely of lateral erosion and growth of meander bends. Larger values for the lateral erosion rate parameter for Coquet2 were likely due to a higher mapped annual erosion rate than recorded in Coquet1 (Figure 3.6). The lower λ setting reflected a balance between maximising the size of θ to drive higher lateral migration rates, while preventing an avulsion across the neck of the large central meander loop in Coquet2.

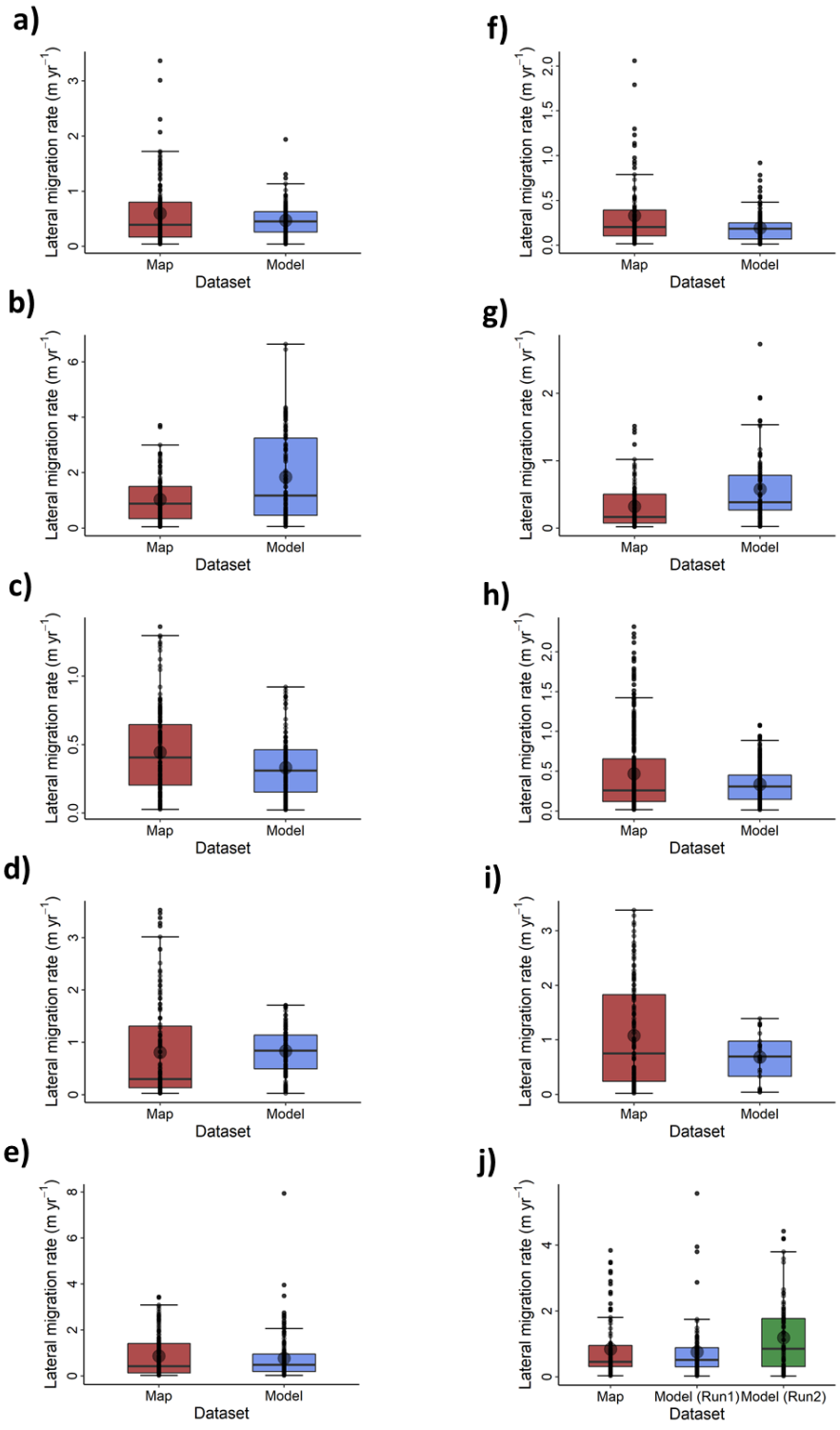

Figure 3.11: Annual lateral migration rates calculated for map and model channel changes along equally spaced transects. Boxplots for both time intervals (big circles represent mean values) for all measured lateral migration rates from top left to bottom right: a) Bollin1, b) Bollin2, c) Calder, d) Coquet1, e) Coquet2, f) Dane, g) Harwood Beck, h) Lune, i) South Tyne1 and j) South Tyne2. Note, two simulations were jointly most accurate for South Tyne2.

As sediment is transferred between channels and their adjoining floodplain, there is the potential for uneven sediment exchange to occur. For instance, relatively coarse sediment transported as bedload that is deposited along the channel margins could be replaced by relatively finer material from the floodplain, causing incision to occur (Lauer & Parker 2008). If this is the case, it may compromise the accuracy of simulated channel changes and call into question the calibration results. CAESAR-Lisflood is designed to conserve the mass of sediment in each size class (Coulthard et al. 2013), meaning the risk of uneven sediment exchanges between the channel and floodplain should be low. To test this independently, the saved output discharge and sediment flux file from the end of the original Coquet1, Coquet2, Dane and Lune calibration simulations were used as inputs to drive new simulations (with sediment recirculation switched off). Grain size distributions for the input and output sediment transport files were compared for selected days throughout the simulations. In general, output sediment fluxes showed similar distributions to input sediment fluxes, indicating that uneven sediment exchange was unlikely to have occurred during model calibration (see Appendix 1D for further details).

3.4.2. Floodplain turnover processes

The simulations captured reach-specific turnover times accurately and variability across reaches for the most part. Modelled estimates of floodplain turnover time corresponded well with mapped estimates, with values ranging over an order magnitude (from ~100 to ~1000 years). Turnover times for each site, estimated from mapped erosion rates and using the linear relationship of these fitted in Figure 3.9b, were reproduced accurately (ranging from ≤20 % over- or under-estimation to <50 % under-estimation by the model compared to estimates by mapped erosion rates) in most cases by the modelled erosion rates and the resultant linear model of these data. On average, the margin of error between turnover times estimated from mapped erosion rates and from modelled erosion rates was between ~15 and ~20 %. However, under-predicted erosion rates of ~85 % resulted in modelled turnover times

exceeding mapped turnover times by ~400 % along the South Tyne1 reach. These results demonstrate that for the most part, erosion rates predicted from calibrated parameter values over decadal timescales can be extrapolated to simulate longer-term floodplain evolution (over centennial to millennial timescales) accurately. This increases confidence in the choice of parameter values for most of the ten reaches.

The estimation of the extent of channel floodplain occupation is predicated on two assumptions: i) all areas of the floodplain will be eroded; ii) rates of geomorphic change will remain constant through time. The distribution of floodplain ages has been shown to decay exponentially in some valley floor systems (e.g. Everitt 1968), supporting the assumptions of stable erosion rates through time and eventual complete turnover of the floodplain. This is also supported by more recent analysis along the Queets and Quinault River systems in Washington (O'Connor et al. 2003). However, O'Connor et al. (2003) show that some recently abandoned locations on the floodplain will be reoccupied sooner than expected as channels move back and forth. Due to the limited timeframe of the simulations here (only one channel change measurement interval per reach), the reoccupation of abandoned channels by back-and-forth channel movements is not recorded at all.

If parts of the floodplain were to remain uneroded for longer than the mass balance equation of floodplain turnover time: M_0/Q_0 (Bolin & Rodhe 1973) predicts, we would expect to see a decrease in the proportion of new floodplain eroded with each successive timestep (O'Connor et al. 2003). If this is the case and floodplain turnover time was to be calculated as M_0/Q_0, there would be an under-estimation for areas of the floodplain infrequently occupied by the channel, and an over-estimation in areas where repeated rapid cycling of erosion and deposition occurs (Miller & Friedman 2009). Floodplain vegetation age reconstructions along the Morice River, Canada revealed that re-occupation of abandoned channels occurred much more frequently than the creation of new channels (Gottesfeld & Johnson Gottesfeld 1990). Analysis of several valley floor systems from North America indicate that the probability of a floodplain area becoming (re)occupied by the river channel can be predicted from floodplain age using a power law relationship (Konrad 2012). This is also

corroborated by reconstructions of channel-floodplain dynamics in both field (Phillips et al. 2007; Miller & Friedman 2009) and numerical modelling (Bradley & Tucker 2013) contexts. Therefore, one would likely need to employ methods that accounted for repeated rapid reworking of floodplain patches.

Bradley & Tucker (2013) and Torres et al. (2017) demonstrated using a grid of nodes to record the timing of channel occupation, that simulating several thousands of years of river channel changes, resulted in some parts of the floodplain being reworked many times while the channel would abandon other parts, leaving them unoccupied indefinitely. This is unsurprising for some systems given the presence of alluvial terraces that may be thousands of years or more in age – including along some of the tested reaches here (e.g. the Dane and the South Tyne). Floodplain ages in these studies were recorded as time since abandonment by the river channel, and storage times as the age at the time of re-occupation by the river channel (Bradley & Tucker 2013; Torres et al. 2017). As part of the assessment of CAESAR-Lisflood's accuracy in reconstructing historical channel changes, channel polygons were overlain to determine total areas of floodplain erosion and deposition. This could be expanded to calculate age and storage time (the length of time until sediment is released from storage) values for every floodplain cell and timestep. In fact, CAESAR-Lisflood would offer significant advantages over earlier studies. For instance, it would be possible to model sediment storage behaviour arising from multi-thread channel patterns.

3.4.3. Implications and suggestions for future research

Trimble (2010) characterised sediment storage in alluvial floodplains as 'fast in, slow out', whereby sediments accumulate rapidly (decades to centuries) via vertical and lateral accretion, and sediments are removed via lateral erosion processes over much longer timeframes (centuries to millennia). Based on this, floodplains store significant quantities of sediment, and often for extensive periods of time, delaying their delivery to catchment outlets, and introducing lags between erosion signals upstream and their appearance in the stratigraphic record – if appearance in stratigraphy occurs at all (Hoffmann

2015). Floodplains, as significant buffers of upstream erosion signals, are diverse in terms of their processes and forms and are liable to change as environmental conditions (e.g. streamflow and vegetation cover) change (Nanson & Croke 1992). The findings presented here have demonstrated that floodplain turnover, including erosion rates and areal extents of floodplain occupation by river channels, can vary widely across different sites, encompassing differences in morphology (e.g. area, valley slope, channel pattern). Reach-scale floodplain sediment storage is critical for models of particle trajectories and travel times through valley floor systems (Pizzuto et al. 2017). Modellers simulating sediment transit through valley floor corridors must incorporate the high variability of floodplain sediment storage dynamics into their models. This is particularly important considering some sediments will become incorporated into chronic storage, and may be subsequently liberated from storage as environmental conditions change (Hoffmann 2015).

The model calibration and performance assessment presented here demonstrate the accuracy of parameterised erosion rate equations in driving "realistic" dynamics of channel changes in CAESAR-Lisflood. These calibrated parameters can be applied using a DEM, grain size distribution and flow-series to drive channel changes over much longer timeframes (10^2 – 10^4 years). Taking this longer perspective could form a series of modelling experiments exploring how different river systems rework their floodplains, e.g. the development of alluvial terraces, and assessing the impacts of environmental changes such as variations in the vegetation cover and flood magnitudes on channel-floodplain systems.

3.5. Conclusion

CAESAR-Lisflood was used here to reconstruct river channel changes, including key geomorphic processes of erosion, deposition, lateral migration and landform reconstruction. The robustness of ranges of calibrated parameter values were demonstrated through successful application of calibrated parameter values to untested reaches via a split-sample testing approach to reconstruct geomorphic changes accurately. CAESAR-Lisflood

was used to predict the extent of channel floodplain occupation from erosion rates, with simulations producing a similar relationship between these two variables to that derived from mapped reconstructions. Key conclusions include:

1) CAESAR-Lisflood has been used to reconstruct geomorphic changes, including channel planform, and erosion, deposition and lateral migration rates, of ten alluvial reaches from across the north of England. This application demonstrates both the feasibility and convenience in parameterising the model to specific real-world sites, and the utility of such sites and calibrated parameters as templates for virtual flume laboratory settings where experimental modelling can be undertaken. Although the analysis reveals that parameters calibrated for one reach can be applied to model channel changes along a similar reach accurately, the lack of transferability of parameter values from most of the calibrated reaches shows that reach-specific calibration is needed to produce accurate simulations.
2) Normalised erosion rates show a positive correlation with the extent of channel floodplain occupation. Floodplain turnover times, estimated using linear models derived from the relationship between erosion rates and floodplain occupation extents, are reconstructed accurately by the model for most sites.
3) The results here demonstrate that CAESAR-Lisflood has utility in both simulating 2D planimetric river channel changes accurately (based on comparison with mapped historical changes) and quantifying longer-term dynamics such as the role of floodplains in lagging signals of sediment supply downstream. The calibrated parameter values provide a basis for further simulation of channel change and floodplain turnover over much longer time periods. It is suggested that further research should focus on quantifying sediment storage timescales by modelling the timing, location and spatial extent of channel occupation, with emphasis on quantifying the effects of environmental change on the longevity of sediment storage.

CHAPTER 4:

Modelling the distribution and behaviour of sediment storage times in alluvial floodplains

Summary and linkages to other thesis chapters

In Chapter 2, landscape evolution modelling was presented as a potential tool with which to quantify storage times of floodplain sediment and controls on these. Chapter 3 presented an evaluation of the accuracy of river channel changes simulated at reach-scale in CAESAR-Lisflood (based on comparison with mapped historical changes). Results of this showed that there was a close match between modelled and mapped geomorphic changes over multi-decadal timescales for most of the ten tested reaches. The close match up between mapped and modelled datasets also held when erosion rates were extrapolated to predict floodplain turnover times (total time for the channel to erode all areas of the floodplain), increasing confidence the calibrated parameters would be applicable over much longer timescales.

This chapter aims to address Research Question 3: “How can a LEM be applied to quantify the distributions of sediment ages and storage times?” and Research Question 4: “How sensitive are reach-scale channel-floodplain systems to various environmental conditions in terms of sediment storage duration?” Here, three of the ten reaches tested in Chapter 3 were used as virtual laboratories to model sediment storage time distributions in floodplains. A methodology was developed, building on existing approaches to floodplain age modelling, whereby the storage time of a mass of sediment was calculated from the timing and surface areal extents of erosion and deposition processes. Simulations were run for 1000 years under different vegetation scenarios, and with model outputs saved at four different time-steps (10, 20, 50 and 100 years), to test a series of hypotheses: i) floodplain sediment storage is dependent upon floodplain age, ii) sediment storage behaviour will vary between the different reaches and vegetation conditions, and iii) a function can be determined that best describes sediment storage behaviour for these tested reaches for application to analogous systems. Insights gained from this chapter should improve further modelling efforts of phenomena such as contaminant dispersal and erosion signal shredding within river catchments.

4.1. Introduction

Erosion signals, induced by climatic, anthropogenic and tectonic disturbances, pass through catchments from a zone of erosion to one of deposition (Schumm 1977). Between these zones, sediment can become sequestered temporarily within floodplains or channels. Consequently, depocentres, such as lakes and deltas, at catchment outlets may receive significantly lower sediment inputs than the volumes initially generated by erosion – a phenomenon referred to as the "buffering" of erosion signals of catchment disturbance (Castelltort & Van Den Driessche 2003; Allen 2008). This complicates the interpretation of stratigraphic records of environmental change obtained from lake beds and alluvial terraces.

Alluvial floodplains are some of the largest terrestrial reservoirs of sediments, encompassing $8 \times 10^5 – 2 \times 10^6$ km^2 of the Earth's surface (Leopold et al. 1964; Mitsch & Gosselink 2015; Tockner & Stanford 2002). Their spatial extent, combined with relatively rapid rates of sediment accumulation (decades to centuries) versus rates of sediment removal (centuries to millennia) result in the storage of large volumes of sediment over protracted periods of time (Trimble 2010). Quantifying the longevity of sediment storage in floodplains is key to illuminating the "sediment delivery problem" of fluvial systems (Walling 1983) and by extension, the buffering of erosion signals.

Here, the aim is to simulate patterns of sediment ages, storage times and erosion hazard, by running an ensemble of channel change simulations using the landscape evolution of model (LEM) CAESAR-Lisflood (Coulthard et al. 2013). This ensemble includes nine simulations each spanning 1000 years, applied using three reaches using parameters and inputs from model runs calibrated previously, and three hypothetical scenarios for vegetation cover. The three reaches describe a range of different channel planform morphologies, erosion and floodplain turnover rates, and potential variations in system responses to different environmental conditions. CAESAR-Lisflood is a LEM that can capture both single-thread and multi-thread channel dynamics. Several hypotheses are tested using the ensemble of simulations:

- First, floodplain sediment erosion is dependent upon floodplain age.

- Second, sediment storage time behaviour will vary between the different reaches and vegetation conditions.
- Third, a sediment storage time distribution function can be determined for these tested reaches, with parameters that can be estimated to create a storage time distribution for other reaches.

Non-linear regression was used to determine the best-fit models, based on a suite of goodness of fit criteria, to the simulated storage time distributions. To determine whether erosion rates decrease with increasing age, the age-dependent probabilities of erosion (erosion hazard) of sediments were calculated, and the mean ages were compared with the simulated mean storage times through time. In attempting to test the hypotheses, experimental conditions, such as sampling frequency, may influence results. For example, increasing the sampling frequency of stream water isotopes from weekly time intervals produced a 50 % lower recorded residence time value of stream water particles in a monitored catchment in Germany (Stockinger et al. 2016). Therefore, sediment ages and storage times were calculated from simulated river channel changes at four different time-intervals (10-, 20-, 50-, and 100-year frequencies) to assess their influence on the distributions of ages and storage times.

4.2. Review and context

4.2.1. Sediment storage times

Several measures of sediment storage duration, including sediment age, storage time, residence time, and erosion hazard, can be used to quantify sediment storage behaviour. Age is a measure of the length of time since the original sediment deposition at a point in space. Storage time is the amount of time sediment remained in storage before erosion, with the residence time equalling the mean of the storage time distribution of a population of sediment particles in a floodplain under steady-state conditions (Bolin & Rodhe 1973). Erosion hazard refers to the probability that sediment of a particular age will be eroded (Bradley & Tucker 2013).

An ongoing debate in the literature centres on whether the distributions of sediment ages and storage times are exponential (e.g. Martin & Church 2004; Lauer 2012) or best described by a 'heavy-tailed' model such as a power law function (e.g. Miller & Friedman 2009; Skalak et al. 2015). Exponential decay implies that sediment ages are 'well mixed' (i.e. each part of the reservoir contains particles that have resided for a range of different lengths of time) within floodplains and that the storage times of sediments could be estimated using a simple mass balance approach whereby the total mass in storage is divided by rates of removal (Bolin & Rodhe 1973). Examples of this include the confined meandering rivers of the Canadian prairies, where meanders migrate downstream as a coherent waveform (see Nicoll & Hickin 2010 and Figure 4.1). In these systems, the channel will erode deposits of a wide range of ages with similar fidelity. A heavy-tailed model by contrast, arises when sediments are not well mixed and deposits of younger ages are more susceptible to erosion than older material (e.g. Miller & Friedman 2009; Skalak & Pizzuto 2010; Bradley & Tucker 2013). Arguably, this is the more typical behaviour of channel-floodplain environments, given the youngest deposits are typically closest to the channel and the oldest deposits are located in the floodplain periphery. Further, as these areas will be the least protected by vegetation in forested reaches, the channel will erode the closest/youngest deposits preferentially over areas with older ages (Konrad 2012). This distinction between the two distributions is important, because if the sediment storage time distribution was heavy-tailed, and a mass balance approach was applied to model an exponential distribution instead, storage times of younger deposits would be over-estimated and storage times of older deposits would be under-estimated – by multiple orders of magnitude potentially (Miller & Friedman 2009; Bradley & Tucker 2013). If a catchment is heavily polluted due to a legacy of metal mining for example, any contaminants will also mobilise at differing rates depending on their position within the sedimentary reservoir (Skalak & Pizzuto 2010; Skalak et al. 2015). Models of sediment delivery timescales (the time required for particles to travel from initial entrainment into the channel network to a zone of permanent deposition) rely on accurate models of sediment storage time distributions to generate predictions (Malmon et al. 2002, 2003, 2005; Pizzuto et al. 2017).

Example 1: Beaver River, Alberta, Canada

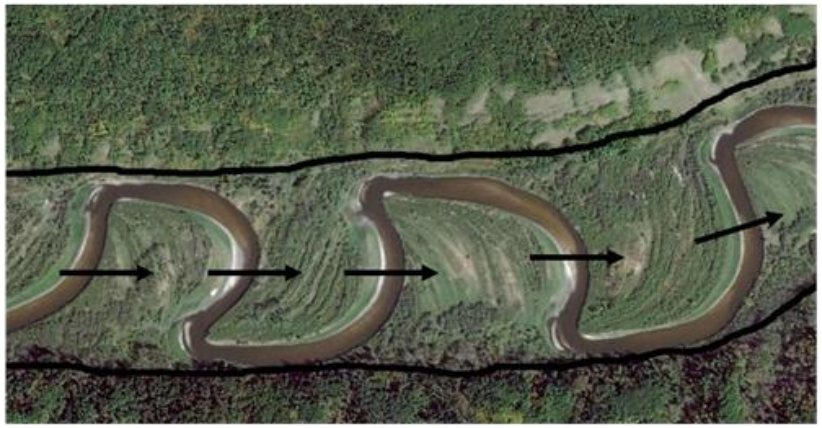

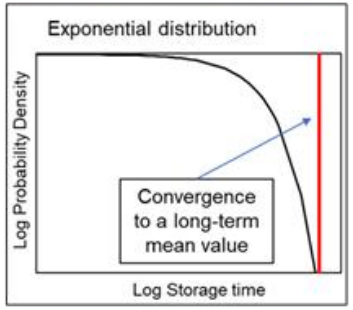

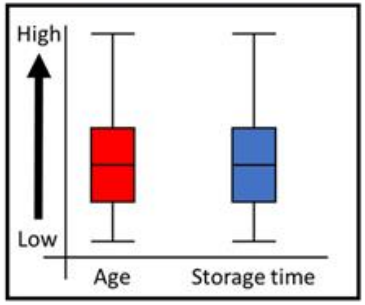

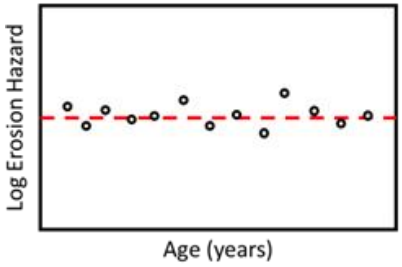

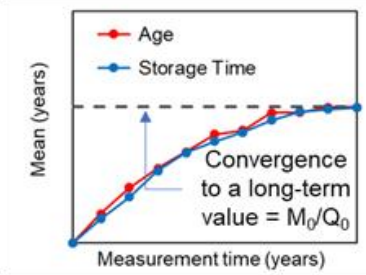

Example 2: River Bollin, Cheshire, UK

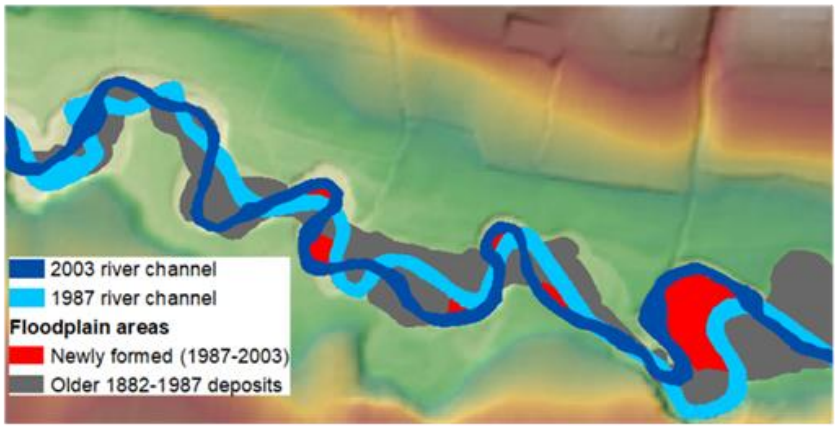

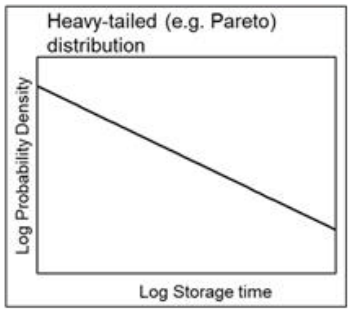

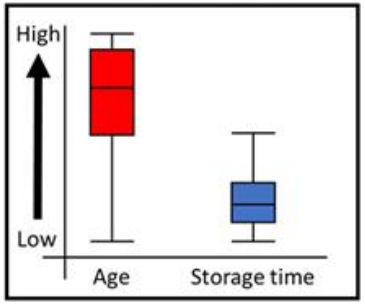

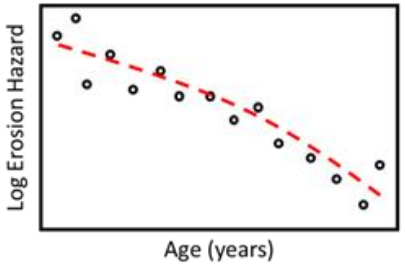

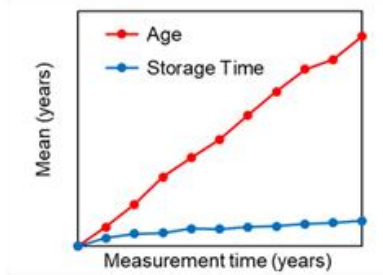

Figure 4.1: Examples of two reach-scale channel planforms (the Beaver River in Canada and the River Bollin in the UK) with contrasting floodplain evolution behaviour. Characteristics of different floodplain behaviour for the two rivers are displayed in each of the four graphs (note: each of these is a schematic illustration of likely age, storage time and erosion hazard distributions for the example river systems and are not generated from collected data). Clockwise from top left graph: the storage time probability density function (logarithmic x and y-axes); age and storage time distributions presented as boxplots for visual comparison; trends in mean age and mean storage time over measurement time; the distribution of erosion hazard values for different floodplain surface ages. In Example 1, the channel migrates in one direction (downstream) as a coherent waveform, maintaining its sawtooth, truncated-meandering form (see Nicoll & Hickin 2010). As a result, the entirety of the floodplain is eroded over time with equal probability for surfaces of different ages. This produces an exponentially distributed probability distribution of storage times and ages, a uniform erosion hazard distribution, and trends in mean ages and storage times that track closely to each other over time. By contrast, in Example 2, the Bollin channel is confined to a central axis in the valley floor for most of the time. Thus, the deposits that are nearest to the channel (and the youngest in age) are reworked preferentially while more distal floodplain patch areas are left preserved. As a result, the storage time distribution is even more strongly right-skewed (and not well-fitted by an exponential function), while the age distribution may be left-skewed. The gap between the mean age and mean storage time widens over time also, and the erosion hazard probability distribution decays with increasing age.

Several studies have contributed to this ongoing debate. For example, Miller and Friedman (2009) found a strong correlation between reductions in peak flow magnitudes through the 20th Century with increasing rates of erosion of younger floodplain surfaces along the Little Missouri River, USA. This contradicts earlier work by Everitt (1968) who derived an exponential distribution of vegetation ages on the floodplain of the same reach, as this would imply that younger floodplain surfaces were no more susceptible to

erosion than floodplain surfaces of older ages. Elsewhere, the youngest sediment deposits have been shown to be the most susceptible to erosion in the valley floors of the Waipaoa River, New Zealand (Phillips et al. 2007), of the Saru River, Japan (Nakamura & Kikuchi 1996), and in the headwater valleys of the Oregon Coast Range, USA (Lancaster et al. 2010). Bradley and Tucker (2013) demonstrated, using a 100,000-year simulation of river channel changes, that erosion favoured very young sediments (<600 years old) over every other age class. By contrast, employing a similar model to Bradley and Tucker, it was found that after 5,700 years of simulation along a reach of the Strickland River, Papua New Guinea, the resulting floodplain age distribution decayed exponentially (Lauer 2012). The discovery of an exponential storage time distribution of a valley fill in one reach and a power law distribution in a valley fill upstream in the Bear Creek basin, USA (Lancaster & Casebeer 2007) demonstrates that both forms of storage time behaviour can occur within the same river system.

Floodplain forms and processes, including controls on sediment storage and removal, are derivatives of their channel systems (Nanson & Croke 1992), yet few studies have attempted to link channel patterns and dynamics to sediment storage duration. Lauer (2012) and Bradley and Tucker (2013) focus on single-tread meandering river channel dynamics, which capture only a limited number of floodplain development processes. Estimated floodplain ages have been related to channel patterns for forested mountain river systems in the Pacific Northwest, USA. Surveys of vegetation patch ages in different reaches revealed a range of floodplain mean ages from 63 to 85 years for laterally stable straight and sinuous channel planforms to 12 years for laterally unstable braiding channel planforms (Beechie et al. 2006). Major challenges associated with linking channel dynamics to sediment storage behaviour include lengthy gaps between successive recorded channels (often successive historical maps are separated by multiple decades, leading to potential underestimation of floodplain turnover rates) and quantifying the effects of separate independent variables (e.g. stream discharge, sedimentology and vegetation) on channel and floodplain morphology (Miller & Friedman 2009; O'Connor et al. 2003).

4.2.2. Reservoir theory and erosion hazard

Floodplains exchange sediments with their adjoining channel systems via processes of erosion, entrainment, transport and deposition. The accumulation of sediments on floodplains and their removal at various points in time results in a spatially distributed mosaic of deposits of differing ages (Phillips et al. 2007). This distribution of sediment ages can be modelled by a function, M(τ), which denotes the total mass of sediment with age ≤ τ (Bradley & Tucker 2013). The cumulative distribution function (CDF) – the age distribution of sediment in storage – is G(τ) = M(τ)/M_0, and the derivative probability density function (PDF) of this, g(τ) is:

$$g(\tau) = \frac{1}{M_0}\frac{d}{d\tau}M(\tau) \quad (1)$$

where M_0 is the total mass of sediment on the floodplain (Bradley & Tucker 2013). The distribution of ages of sediments that leave the floodplain via channel erosion can be modelled by the function, Q(τ), which denotes the total mass of sediment of age ≤ τ leaving storage (Bradley & Tucker 2013). The CDF of ages leaving storage – the storage time distribution – is F(τ) = Q(τ)/Q_0, with the corresponding PDF:

$$f(\tau) = \frac{1}{Q_0}\frac{d}{d\tau}Q(\tau) \quad (2)$$

where Q_0 is the erosive flux (Bradley & Tucker 2013).

The storage time distribution described here has been termed elsewhere as the ‘transit time distribution’ (e.g. Bolin & Rodhe 1973; Malmon et al. 2003) and as the ‘waiting time distribution’ (e.g. Pizzuto et al. 2017). The term, ‘storage time’ is used here because, as sediment grains will likely enter and exit storage multiple times during transit through alluvial valley floors, a distinction between the timescale of storage for individual storage episodes (storage time) and the total timescale, aggregated over all episodes (transit time), has previously been made (see Torres et al. 2017). It has been demonstrated that over relatively short river valley lengths (25 km), few particles enter storage, and even fewer enter into multiple episodes of storage

before reaching the valley outlet (Pizzuto et al. 2017). Given the even shorter lengths of valley floor reaches investigated here (~1 km each), it is assumed that all sediments undergo only one episode of storage and thus, sediment is regarded to have transported out of the reach upon erosion.

Under steady-state conditions, the mass of sediments stored in floodplains, the erosive flux rate, and the shapes of the age and storage time distributions are constant (Bolin & Rodhe 1973). To satisfy the assumptions of steady-state conditions, the mass of sediment in flux that is older than τ, needs to be balanced by sediments in latent storage reaching age τ:

$$Q_0 - Q(\tau) = \frac{d}{d\tau} M(\tau) \quad (3)$$

that is, the age and storage time distributions must be equal (Bolin & Rodhe 1973; Bradley & Tucker 2013).

The forms of the age and storage time distributions are set by h(τ), the 'erosion hazard function', defined as the probability of erosion of available material in each age (Bradley & Tucker 2013). This is calculated by dividing the storage time PDF by the age PDF:

$$h(\tau) = \frac{Q_0}{M_0} \frac{f(\tau)}{g(\tau)} \quad (4)$$

Should the age and storage time distributions be equal, one would expect the erosion hazard to be uniform across all ages and be equivalent to the ratio of the total flux to the total mass (Bradley & Tucker 2013). In cases where younger material is more susceptible to erosion (e.g. Nakamura & Kikuchi 1996; Miller & Friedman 2009), the erosion hazard decreases with increasing age (see Figure 1 in Bradley & Tucker 2013). Analysis of floodplain reoccupation rates demonstrate that typically, floodplains abandoned within the preceding decade were 10 times as likely to be re-occupied by the channel than an area abandoned 30 years ago, as a result of short-term fluctuations in channel area from floods and progressive lateral movement within narrow meander belts in the valley floor (Konrad 2012). While studies like this reveal useful information on floodplain reoccupation dynamics, the full set of controls remain unclear. For example, given that floodplain vegetation age

communities vary between different channel pattern types (e.g. Beechie et al. 2006), does the probability of floodplain reoccupation also vary between channel patterns? If different floodplain reoccupation processes can operate over different timescales (e.g. channel area fluctuations in response to flood events over ≤10^0-year timescales versus progressive lateral migration over 10^1 – 10^2-year timescales), how might recording reoccupation rates over different temporal resolutions affect results? To investigate these ideas further, a landscape evolution modelling approach is applied.

4.3. Data and methods

4.3.1. The CAESAR-Lisflood model and simulations

Landscape evolution models (LEMs) simulate sediment fluxes and geomorphic changes under the action of water (Tucker & Hancock 2010). CAESAR-Lisflood is an example of a coupled 2D-hydrodynamic model and LEM that can simulate geomorphic changes at catchment and reach spatial scales (Coulthard et al. 2013). CAESAR-Lisflood routes water and sediments across a cellular grid, which allows both single-channel and multi-channel patterns to be simulated (Coulthard et al. 2002). This is a key advantage over planimetric centreline models like the IPS model (Ikeda et al. 1981) as this allows a wider range of floodplain environments (see Nanson & Croke 1992) to be simulated. Like the IPS model used by Lauer (2012) and the CHILD model used by Bradley & Tucker (2013), CAESAR-Lisflood is a reduced-complexity model, using a few simplifying equations to represent real-world phenomena (Coulthard et al. 2002). This facilitates model parameterisation by restricting the number of variables that require calibration, compared to computational fluid dynamics models (Coulthard & Van De Wiel 2006). Advantages of numerical modelling over field studies include easier control over inputs and boundary conditions, and hypothetical scenarios can be simulated. This overcomes issues such as monitoring time constraints and irregular sampling frequencies. Modelling also permits investigation into the effects of different environmental conditions on channel changes and the resulting sediment storage behaviour. CAESAR-Lisflood has been applied in several experimental modelling contexts to quantify sediment storage

behaviour under different conditions, including simulations of the effects of vegetation cover and land-use change, tectonics and changes to the rainfall-regime on sediment fluxes and channel morphodynamics (e.g. Coulthard & Macklin 2001; Coulthard & Van De Wiel 2013, 2017; Van De Wiel & Coulthard 2010).

Data collection consists of two main stages. First, channel changes for three reaches and three vegetation cover scenarios are simulated over the course of 1000 years. The chosen study sites are 1 km long valley reaches from the Dane and Coquet river catchments in northern England (Figure 4.2). While floodplain evolution spans timescales beyond 1000 years, this length of time is used for two reasons: 1) to keep simulation times tractable (in some cases, it took over a month to complete a single simulation); and 2) when the total floodplain area was divided by a mean erosion rate (determined from historical channel change reconstructions), estimated floodplain turnover times were 1095, 737 and 263 years for the Dane, Coquet1 and Coquet2 reaches, respectively (see Chapter 3 – Figure 3.10). This shows that not only should the floodplains be completely reworked within ~1000 years (assuming the channel occupies every part of the valley floor at least once), but that these sites encompass a clear gradient in sediment storage duration, which raises the likelihood that sediment storage times may differ significantly between these reaches. Age and storage time data are recorded based on the timings of channel abandonment (floodplain deposition) and (re)occupation (floodplain erosion). Second, distribution functions are fitted to the resulting empirical storage time distributions using non-linear regression, and the results are compared across each of the scenarios, reaches and sampling frequencies.

The reach-scale application of CAESAR-Lisflood requires parameterisation of several variables governing sediment dynamics, hydrological processes and vegetation cover. Most parameter settings depend on the characteristics of the DEM, sediment grainsize distribution and stream flow input files, and are parameterised based on recommendations from the existing literature. Parameters governing erosion rates and channel morphology require calibration. Calibration of key parameter values (Table 4.1) for the three reaches is presented in Chapter 3 (Feeney et al. 2020), where historical

mapped channel changes were compared with channel planforms from a series of simulations driven using the historical daily flow record in CAESAR-Lisflood.

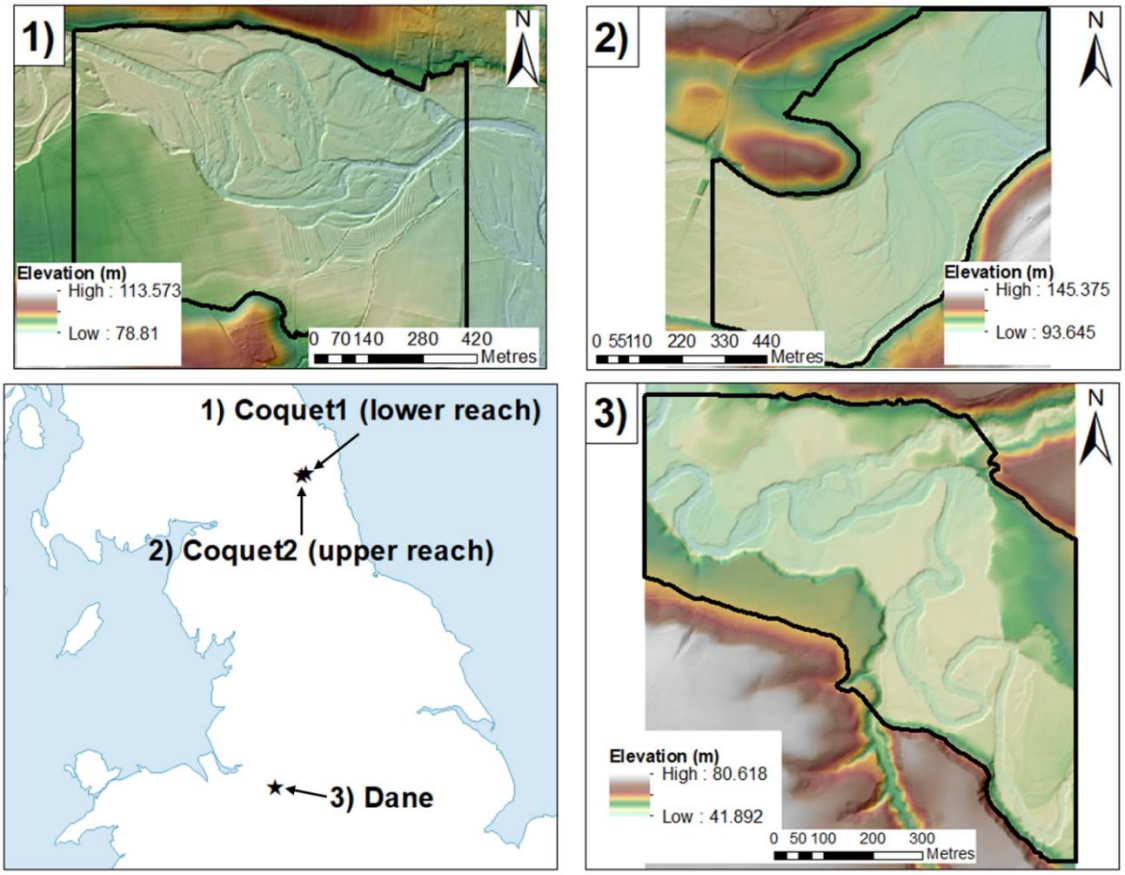

Figure 4.2: Location and geomorphology of each of the tested reaches in northern England: 1) Coquet1 (lower reach), 2) Coquet2 (upper reach), and 3) Dane. DEMs created from 2m LiDAR data and are superimposed on hillshade surfaces (© Environment Agency). Black outline indicates the reach boundary.

Table 4.1: Calibrated values for key parameters for each of the three reaches.

	Site		
Parameter	Coquet1	Coquet2	Dane
Lateral erosion rate, θ	0.000001	0.000003	0.000001
In-channel erosion, λ	20	15	14
Number of passes for edge smoothing filter	80	80	10
Number of cells to shift lateral erosion downstream	8	8	1
Sediment transport formula	Wilcock & Crowe	Wilcock & Crowe	Wilcock & Crowe
Manning's n:			
Forest	0.055	0.055	0.055

Grass	0.035	0.035	0.035
Unvegetated	0.025	0.025	0.025
Critical shear stress threshold ($N\ m^{-2}$):			
Forest	120	120	120
Grass	80	80	80
Unvegetated	0	0	0
Vegetation maturity time (years):	20	20	20
Forest	1	1	1
Grass	1000	1000	1000
Unvegetated			
Proportion of erosion that can occur at full maturity:			
Forest	0.1	0.1	0.1
Grass	0.2	0.2	0.2
Unvegetated	1	1	1

The final output DEM (10 m horizontal resolution) and grainsize distribution from calibrated model runs were used as initial boundary conditions for the simulations. To drive the model, a 25-year historical daily flow record (01/01/1988 – 31/12/2012), obtained from gauges close to the reaches, was repeated 40 times to make up a 1000-year long input file. For the Dane and Coquet1, no input sediments were supplied with the input flow series. An option to recirculate sediments was applied so that while there would be no sediment inputs into the reach initially, subsequent timesteps would include bedload and suspended sediment fluxes. For Coquet2, initial 1000-year runs revealed progressively decreasing sediment outputs with time – until virtually no sediments at all were being transported for some simulations. As this is unrealistic, a 25-year period of recorded sediment fluxes (between 50 and 75 years after the start of the simulation) from the initial forest, grass and unvegetated runs was repeated 40 times and included with the input flow series to drive the analysed simulations. When the analysed simulations were run, linear regressions to the difference between input and output sediment fluxes have slopes and y-intercept values that are not significantly different from zero (based on one-sample t-test results) (see Appendix 2A).

CAESAR-Lisflood represents vegetation cover with three parameters: vegetation maturity rate, a threshold critical shear stress before removal of vegetation, and proportion of erosion allowed to occur at full vegetation maturity. In addition, the Manning's n coefficient is adjusted to account for

differences in hydraulic roughness for different types of vegetation cover (Chow 1959). The focus here is on three different scenarios for vegetation cover: mature-forest cover, long-grass cover and unvegetated. Maturity rates of 20 and 1 years were set for forest and grass cover, respectively, to reflect typical maturity rates for trees and grasses (Lack & Evans 2001). For the unvegetated scenario, the choice of value was set arbitrarily to 1000 years, although the choice of value for this scenario is meaningless as the proportion of erosion allowed to occur was set to 1, removing the impact vegetation cover has on erosion rates under this scenario. Settings for the critical shear stress threshold and Manning's n coefficient parameters under the different scenarios were chosen (Table 4.1) from reference tables in Fischenich (2001) and Chow (1959). It is assumed that while mature forest cover provides the maximum amount of protection from erosion possible for floodplain sediments, lateral erosion does still occur (see Trimble 2004). Therefore, the proportion of allowable erosion at full maturity is set to 0.1 for forest cover. Grass cover was also judged to provide significant but lesser protection from erosion, with a value of 0.2. Unvegetated cover provided zero protection. For all forest and grass cover simulations, vegetation was set to full maturity at the start.

4.3.2. Modelling ages, storage times and erosion hazard

Simulations were run using version 1.9b of the CAESAR-Lisflood model. Figure 4.3 summarises the procedure for simulating river channel changes and quantifying the resultant sediment storage behaviour in floodplains. DEM and water depth spatial grids were saved every ten years. Water depths captured generally the position and morphology of channels. The channels were vectorised and, where applicable, edited to the extents of channel positions based on visual assessment of the DEMs.

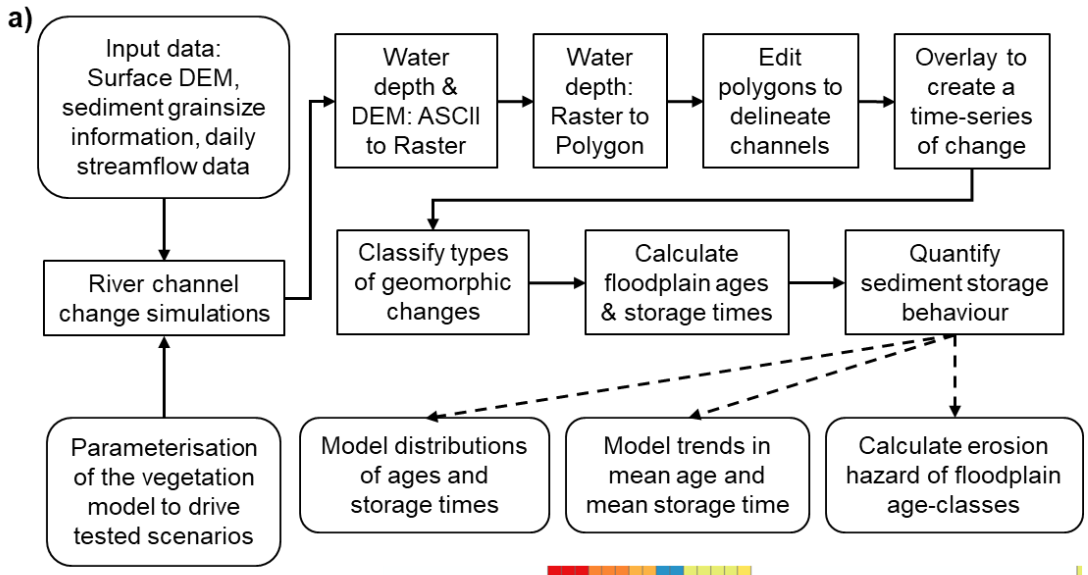

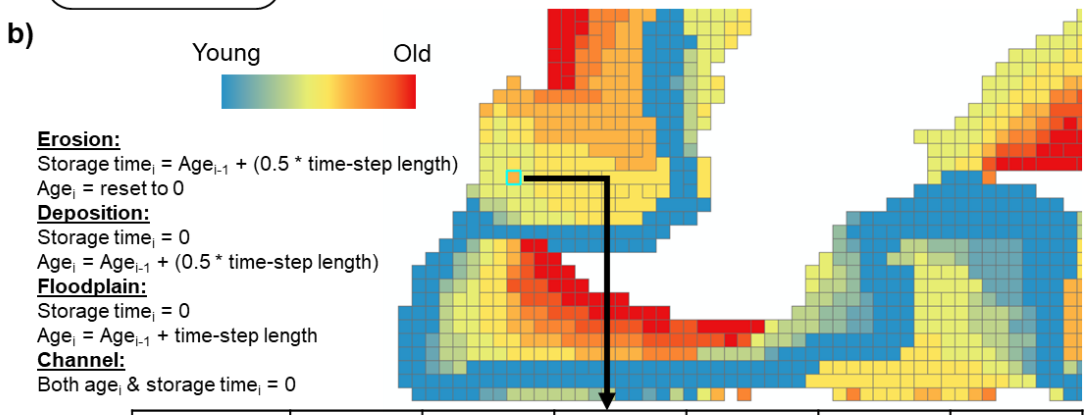

Time interval (years)	60-70	70-80	80-90	90-100	100-110	110-120
Area classification	Floodplain	Floodplain	Erosion	Deposition	Floodplain	Floodplain
Age (years)	45	55	0	5	15	25
Storage time (years)	0	0	60	0	0	0

Figure 4.3: Summary of the procedure of sediment storage behaviour quantification. a) Schematic workflow of the main steps involved with simulating river channel changes in CAESAR-Lisflood and producing the data to analyse sediment storage behaviour in floodplains; b) A snapshot of recorded geomorphic changes and resultant floodplain sediment age and storage time data from one 'cell' in the polygon mosaic of channel changes after 1000 years.

The channel polygons were overlain to calculate surface areal extents of erosion and deposition. For a given interval, any unchanged 'wet' and 'dry'

cells were classed as ‘channel’ and ‘floodplain’ areas, respectively. New ‘wet’ cells indicated ‘erosion’ and new ‘dry’ cells indicated ‘deposition’. For time step, i, the age was calculated as the time since deposition as:

$$Age_i = 0.5t + nt \quad (5)$$

where t is the time step in units of either 10, 20, 50 or 100 years and n is the number of time steps until that part of the floodplain is eroded by the channel.

Storage times were recorded whenever erosion occurred at specific points in the valley floor. These were calculated as:

$$Storage\ time_i = Age_{i-1} + 0.5t \quad (6)$$

Age_i is reset to 0 and begins to accumulate once the channel abandons that area of the floodplain. At the end of each simulation, the result is a mosaic of individual polygons, each containing a unique time-series of geomorphic changes and ages (Figure 4.3). The process of quantifying areal extents of erosion and deposition, and calculating the age and the storage time within each polygon is repeated for each of the four tested time steps.

Empirical CDFs and empirical PDFs of the ages and storage times are computed for every simulation. The shape of the age PDFs is useful for discerning whether predominantly young or old sediments are stored, while the shape of storage time PDFs indicates if younger or older sediments dominate erosion fluxes. CDFs are useful for visualising the steepness of the decay function, including statistics such as the median age and storage time. Using the ‘fitdistrplus’ package in R (Delignette-Muller et al. 2019), non-linear regression models were fitted to the empirical storage time distributions. Best-fit models were selected based on comparing the results of five statistical tests: Anderson-Darling, Kolmogorov-Smirnov, Cramer-Von Mises, Akaike’s Information Criterion and the Bayesian Information Criterion. Apart from the exponential model, all tested models were two-parameter functions and include Pareto (power law), Weibull, gamma and lognormal functions.

To investigate further the relationship between age and erosion, the erosion hazard was computed by aggregating data into 100-year bins and dividing the

storage times by the ages. In addition, the mean age and the mean storage time were recorded every 100 years and compared. If the mean age and the mean storage time recorded at each time step match closely to one another, then the probability of erosion is likely equal for all the age classes. If the mean age exceeds the mean storage time, this indicates that younger sediments are preferentially eroded by the channel (Bolin & Rodhe 1973; Dietrich et al. 1982).

4.4. Results

4.4.1. Coquet1

Rates and processes of channel changes differed between the three vegetation cover types. Little lateral migration occurred under forest cover and the channel maintained its single-thread sinuous form (Figure 4.4a). Significantly more erosion occurred under grass cover, with channel-floodplain evolution driven by scroll meandering and truncated bends developing where the channel has eroded terraces (Figure 4.4a). Under unvegetated conditions, channel planform switched from meandering to braided morphology (Figure 3d). Mean rates of erosion and deposition through time were highest for unvegetated conditions (1898.2 m^2 yr^{-1} and 1873.9 m^2 yr^{-1}, respectively), followed by grass (475.3 m^2 yr^{-1} and 456 m^2 yr^{-1}, respectively) and forest (107.7 m^2 yr^{-1} and 88.6 m^2 yr^{-1}, respectively) (Figure 4.4b).

For all combinations of scenario and time step, younger ages were most susceptible to erosion. Visually, the age and storage time distributions do not match closely with each other (Figure 4.4c). This is confirmed by Wilcoxon-rank sum analysis, which indicates significant differences between the age and the storage time distributions for all twelve datasets ($p << 0.05$). The left-skewed age distributions and the right-skewed storage time distributions, which are better fit by lognormal than exponential models, demonstrates the dominance of older ages in storage and younger ages in the erosion fluxes.

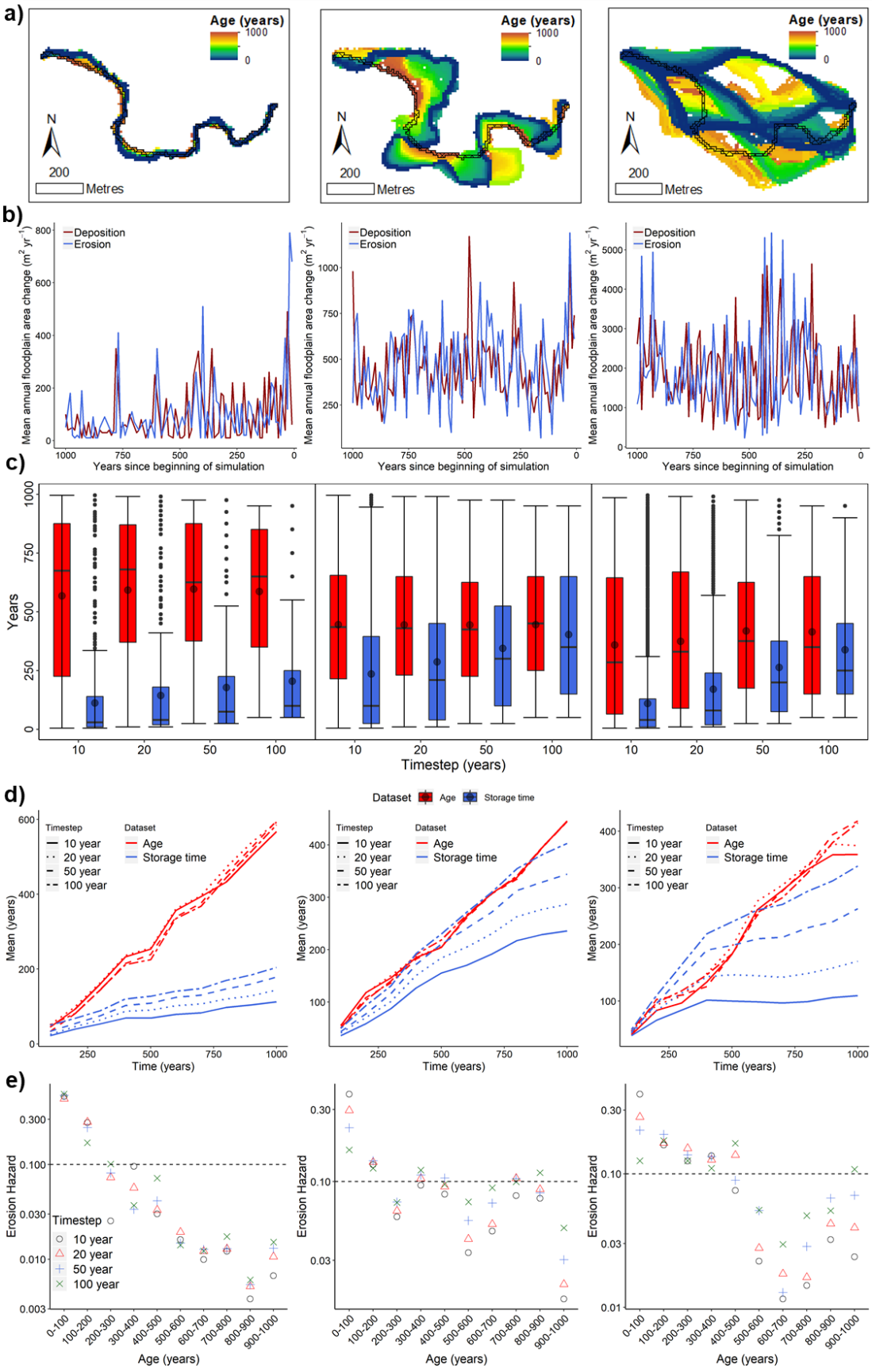

Figure 4.4: Sediment storage behaviour quantified for Coquet1 under forest (left), grass (middle) and unvegetated (right) conditions. a) floodplain surface

ages after 1000 years of simulation recorded every 10 years (initial channel position shown in cross-hatched polygon), b) time-series of mean erosion and deposition rates, c) age (red) and storage time (blue) distributions, d) mean age and mean storage time trends, and e) erosion hazard distributions.

Mean ages exceed consistently the mean storage times for forested conditions, and the gap between these values increases with time (Figure 4.4d). Similar behaviour is evident for the other vegetation scenarios, though the divergence between the mean age and the mean storage time begins around ~500 years for the unvegetated scenario and at various points in time after 500 years for the grass cover scenario (depending on the analysis time step) (Figure 4.4d). These delays in the timing of the mean age diverging from the mean storage time may indicate that a shift in behaviour (from uniform to non-uniform erosion hazard) has occurred. For the 50- and 100-year time steps of the unvegetated simulation, the mean storage time consistently exceeded the mean age for the first 500 years, indicating that during this period, older sediments dominated erosion fluxes (Figure 4.4d).

Erosion hazard decays with increasing age, reflecting the tendency of the channel to occupy recently abandoned locations more frequently than areas that had seldom or never been visited before (Figure 4.4e). There is a degree of noise in erosion hazards for ages >500 years for unvegetated data, which may reflect the sporadic erosion of older aged sediment by the formation of multiple channels during flood events.

4.4.2. Coquet2

Total eroded floodplain area was again smallest for forest cover (Figure 4.5a). Like Coquet1, the mean annual erosion and deposition rates increased from forest (147.5 m^2 yr^{-1} and 159.2 m^2 yr^{-1}, respectively) to grass (797.6 m^2 yr^{-1} and 802.1 m^2 yr^{-1}, respectively) to unvegetated (2308.8 m^2 yr^{-1} and 2299.5 m^2 yr^{-1}, respectively) conditions (Figure 4.5b). A large cut-off across the neck of the central meander bend occurred within the first 20 years of the forest cover simulation, where after the channel remained laterally stable for the most part

(Figure 4.5a). Under grass cover, floodplain evolution was driven by meander scrolling. However, the channel migrated back and forth across the full width of the valley floor and avulsed more frequently (Figure 4.5a). Like Coquet1, under unvegetated conditions, the channel switched from a meandering to a braided planform, whereafter the channel was able to rework sediments of nearly all ages with similar fidelity (Figure 4.5a).

Younger sediment dominates the erosion fluxes for the most part. Like Coquet1, the age and storage time distributions do not match closely to each other for forested and grass cover datasets (Figure 4.5c). However, for the 10- and 20-year time step of the unvegetated scenario, the age and storage time distributions appeared to correspond closely (Figure 4.5c). A Wilcoxon-rank sum test confirmed that the distributions of the 10-year time step were not significantly different ($p = 0.06$).

Under forest cover, the mean age exceeded the mean storage time throughout (Figure 4.5d). Similar to Coquet1, mean ages and mean storage times track closely to each other for the 10- and 20-year time steps initially, and begin to diverge after 500 years; for the 50- and 100-year time steps, this divergence occurs after 750 years (Figure 4.5d). For unvegetated datasets, the mean age and mean storage time trends tracked closely overall. However, while these means appeared to converge after 900 years for the 10- and 20-year time steps, the reverse occurred at approximately 750 years for the 50- and 100-year time steps (Figure 4.5d). Like Coquet1, the mean storage time exceeded the mean age for the first 500 years of the unvegetated: 50-and 100-year time step datasets (Figure 4.5d), indicating erosion of older ages here.

Erosion hazard decreased with age overall for the forest and grass datasets, albeit with some noise for sediment older than 700 years in the case of the latter (Figure 4.5e). Most of the calculated erosion hazards appeared to lie close to the uniform erosion hazard line for the unvegetated scenario (Figure 4.5e).

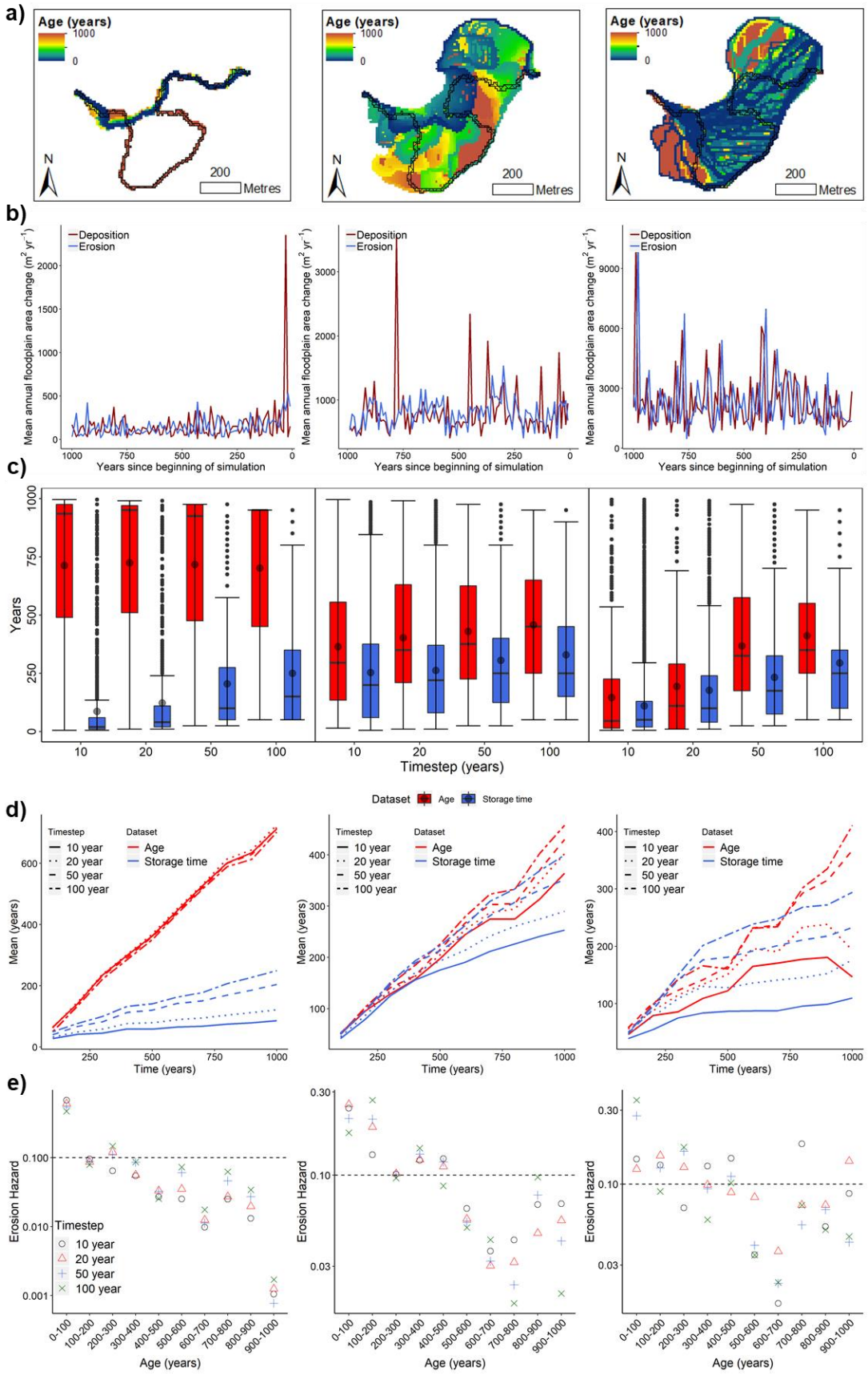

Figure 4.5: *Sediment storage behaviour quantified for Coquet2 under forest (left), grass (middle) and unvegetated (right) conditions. a) floodplain surface*

ages after 1000 years of simulation recorded every 10 years (initial channel position shown in cross-hatched polygon), b) time-series of mean erosion and deposition rates, c) age (red) and storage time (blue) distributions, d) mean age and mean storage time trends, and e) erosion hazard distributions.

4.4.3. Dane

Similar to the Coquet reaches, the least amount of erosion occurred under forest cover, but the channel evolved from a meandering to a braided planform under unvegetated conditions (Figure 4.6a). The mean annual erosion and deposition rates for forest cover (282.7 m^2 yr^{-1} and 300.1 m^2 yr^{-1}, respectively) were slightly lower than for grass cover (457.6 m^2 yr^{-1} and 478.4 m^2 yr^{-1}, respectively), and were highest for unvegetated cover (3203.3 m^2 yr^{-1} and 3197.2 m^2 yr^{-1}, respectively) (Figure 4.6b). As with Coquet2, the channel under forest cover, developed cut-offs and remained laterally stable for the remainder of the simulation. Under grass cover, the channel avulsed several times, but unlike Coquet2, the channel did not traverse the full width of its floodplain within 1000 years (Figure 4.6a). Channel braiding under unvegetated conditions resulted in the reworking of nearly all the floodplain area (Figure 4.6a).

As with Coquet2, younger ages dominated erosion fluxes for the forest and grass cover scenarios, whereas under unvegetated conditions, this bias is much weaker overall. Age and storage time distributions differ significantly for all twelve combinations of scenario and time step (Figure 4.6c). Like the other reaches, the largest differences between the age and storage time distributions occur under forest cover. While the age and storage time distributions of each of the four unvegetated datasets appear to match visually (Figure 4.6c), each pair of distributions was found to be significantly different (Wilcoxon-rank sum test; $p << 0.05$).

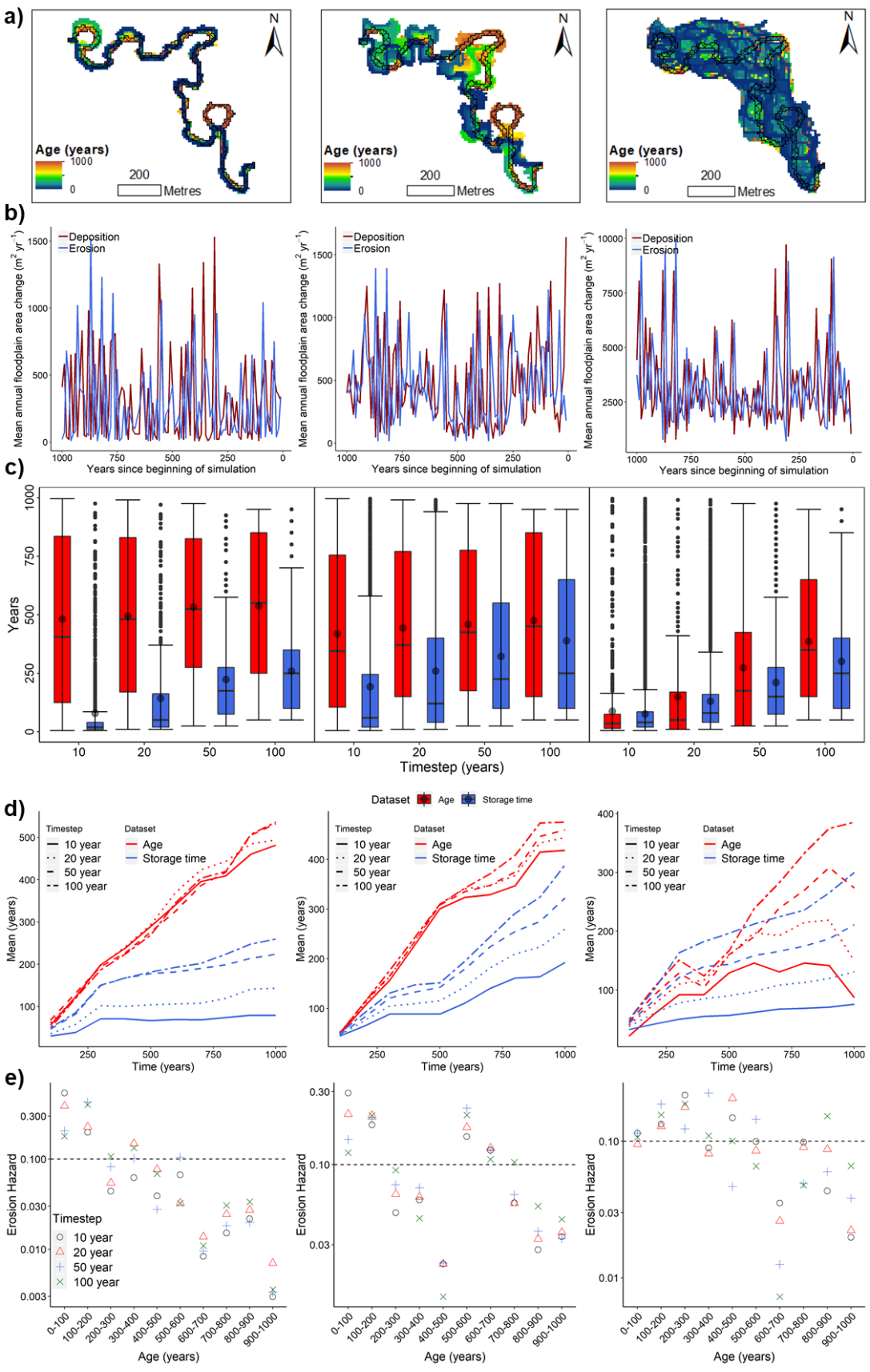

Figure 4.6: *Sediment storage behaviour quantified for the Dane under forest (left), grass (middle) and unvegetated (right) conditions. a) floodplain surface*

ages after 1000 years of simulation recorded every 10 years (initial channel position shown in cross-hatched polygon), b) time-series of mean erosion and deposition rates, c) age (red) and storage time (blue) distributions, d) mean age and mean storage time trends, and e) erosion hazard distributions.

The mean age and mean storage time trends across most of the datasets indicate younger ages constitute predominantly erosion fluxes (Figure 4.6d). Mean ages exceed mean storage times under forest cover, and the gap between these means increases through time (Figure 4.6d). A similar pattern occurs under grass cover, albeit with some convergence after 500 years. Data for the 10- and 20-year time steps for the unvegetated scenario correspond with the same datasets of Coquet2: the mean ages and mean storage times track closely to one another before converging after 900 years (Figure 4.6d). In addition, the mean storage time exceeds the mean age between 250 and 500 years for the 50- and 100-year datasets (Figure 4.6d).

Like Coquet2, the erosion hazard decays with age under forest cover and lies close to the uniform erosion hazard line for most of the age classes under unvegetated conditions (Figure 4.6e). Under grass cover, the erosion hazard decays sharply with age up to 500 years. However, the erosion hazard appears to 'reset' such that sediments aged 500-600 years have a similar probability of removal to sediments aged 0-100 years. A second declining trend in the erosion hazards emerges for sediments aged between 500 and 1000 years (Figure 4.6e). A possible explanation for this is that when avulsions occur, in some places the channel begins to migrate in a different direction into areas of the floodplain unvisited previously by the channel during the simulation. As it does this, older material is eroded just as readily as younger material is eroding in other parts of the valley floor where the channel is migrating back to its former position. Given the greater number of bends along this reach, this phenomenon would be likelier to occur here than along either of the other two reaches.

4.4.4. Distributions of sediment storage time

Five different functions were fitted to the storage time distributions using non-linear regression (exponential, Pareto, gamma, Weibull and lognormal). Almost half of the distributions (16 out of 36) were best modelled by a lognormal function (Table 4.2; see also Appendix 2B). This indicated that the youngest deposits were eroded more easily than older deposits in the floodplain, concurring with results presented in Figure 4.4-4.6. Hence, the lognormal function was particularly good at describing the distribution of storage times under forest cover, where erosion was concentrated along the closest deposits to the channel, and unvegetated conditions, where high rates of lateral erosion maintained a very young floodplain surface and a ready supply of young ages in erosion fluxes (Table 4.2). The empirical CDFs of most storage time distributions showed steeper rates of increase than the best fitting exponential model could capture. Only one distribution (Dane reach, grass scenario, 50-year time step) was best fitted by an exponential function (Table 4.2).

Considering that more storage time distributions were fitted more accurately by a lognormal function than with any other function (based on the goodness of fit criteria outlined earlier), we try to formulate a general equation of sediment storage times on this model. The PDF of this distribution, f(τ) is expressed as:

$$f(\tau) = \frac{1}{\sigma\tau\sqrt{2\pi}} e^{\frac{-(\ln(\tau)-\mu)^2}{2\sigma^2}}, \tau > 0 \quad (7)$$

where τ is the storage time, and μ and σ are the mean and standard deviation of the lognormal distribution, respectively. The corresponding CDF, F(τ) is:

$$F(\tau) = \Phi\left(\frac{\ln(\tau)-\mu}{\sigma}\right), \tau > 0 \quad (8)$$

where ϕ is the CDF of the standard normal distribution.

To evaluate the accuracy of this general storage time model, equations 9 and 10 were used to estimate the values of μ and σ for all thirty-six combinations of site, scenario and measurement time step. These were used to generate lognormal distribution curves, which were then fitted to the recorded storage time observations. In order to properly calibrate and evaluate the accuracy of

the model, leave one out cross-validation was undertaken. Here, all data for one vegetation cover scenario were reserved for validation while the rest of the data were used to calibrate the model. This process was repeated, until data for each vegetation dataset had been reserved for validation. The same process was then carried out using sites as validation datasets. The range of R^2 coefficient of determination values were computed and compared across the six validation datasets to obtain the best possible model fits.

Table 4.2: Best-fit models to each storage time dataset determined using non-linear regression. Best-fitting models are determined by comparison of five goodness of fit tests (Cramer-von-Mises, Anderson-Darling, Kolmogorov-Smirnov, Akaike's Information Criterion and Bayesian Information Criterion) across five different non-linear models (gamma, exponential, Weibull, Pareto and lognormal) using the R 'fitdistrplus' library (Delignette-Muller et al. 2019).

Site	Scenario	Timestep (years)	Model	Parameters
Coquet1	Forest	10	Pareto	Shape = 1.24; scale = 50.01
		20	Pareto	Shape = 1.38; scale = 83.2
		50	Lognormal	Meanlog = 4.5; sdlog = 1.17
		100	Lognormal	Meanlog = 4.8; sdlog = 0.97
	Grass	10	Weibull	Shape = 0.77; scale = 203.96
		20	Gamma	Shape = 0.89; rate = 0.003
		50	Weibull	Shape = 1.21; scale = 365.83
		100	Weibull	Shape = 1.47; scale = 444.37
	Unvegetated	10	Lognormal	Meanlog = 3.79; sdlog = 1.33
		20	Pareto	Shape = 3.47; scale = 432.71
		50	Weibull	Shape = 1.19; scale = 280.24
		100	Gamma	Shape = 1.98; rate = 0.006
Coquet2	Forest	10	Lognormal	Meanlog = 3.4; sdlog = 1.28
		20	Pareto	Shape = 1.56; scale = 83.11
		50	Lognormal	Meanlog = 4.7; sdlog = 1.12
		100	Lognormal	Meanlog = 5.03; sdlog = 0.98
	Grass	10	Gamma	Shape = 0.98; rate = 0.004
		20	Weibull	Shape = 1.14; scale = 275.63
		50	Gamma	Shape = 1.73; rate = 0.006
		100	Gamma	Shape = 1.89; rate = 0.006
	Unvegetated	10	Lognormal	Meanlog = 3.98; sdlog = 1.21
		20	Lognormal	Meanlog = 4.61; sdlog = 1.09
		50	Weibull	Shape = 1.21; scale = 248.73
		100	Gamma	Shape = 1.89; rate = 0.006
Dane	Forest	10	Lognormal	Meanlog = 3.38; sdlog = 1.24
		20	Lognormal	Meanlog = 4.16; sdlog = 1.23
		50	Gamma	Shape = 1.36; rate = 0.006
		100	Weibull	Shape = 1.26; scale = 280.42
	Grass	10	Lognormal	Meanlog = 4.25; sdlog = 1.5
		20	Lognormal	Meanlog = 4.84; sdlog = 1.3

		50	Exponential	Rate = 0.003
		100	Weibull	Shape = 1.21; scale = 8.82
	Unvegetated	10	Lognormal	Meanlog = 3.68; sdlog = 1.09
		20	Lognormal	Meanlog = 4.32; sdlog = 1.04
		50	Lognormal	Meanlog = 4.98; sdlog = 0.89
		100	Lognormal	Meanlog = 5.43; sdlog = 0.78

Reserving unvegetated data for model validation produced the strongest model fits (Figure 4.7). The R^2 coefficient of determination for each of the fitted models ranged from ~0.92 to ~0.96 for the PDFs and from ~0.98 to ~1 for the CDFs (Figure 4.7).

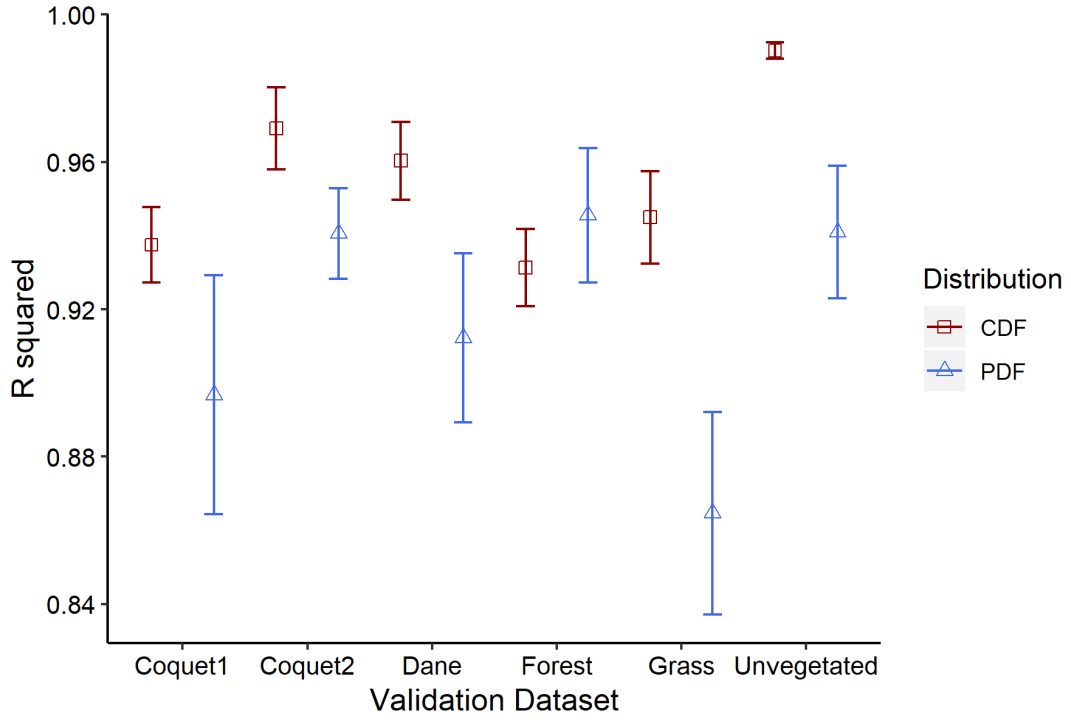

Figure 4.7: Mean R^2 values (±1 standard error) for PDF and CDF model fits when each site and scenario is reserved for validation.

When unvegetated data were reserved for model validation, the values of the two lognormal parameters, μ and σ, can be predicted using the median storage time, T_{50} (years) and measurement time step, t (years) as follows:

$$\mu = 0.7827\, ln(\tau_{50}) + 1.0792 \quad (9)$$

$$\sigma = -0.202\, ln(t) + 1.8501 \quad (10)$$

Lognormal PDF and CDF curves for all unvegetated datasets are displayed in Figure 4.8. Tests for equal distributions (Kolmogorov-Smirnov, Anderson-Darling and Epps-Singleton) indicated that there was no statistically significant difference between any of the observed and modelled distributions (p values > 0.05 for all pairs of empirical and modelled distributions).

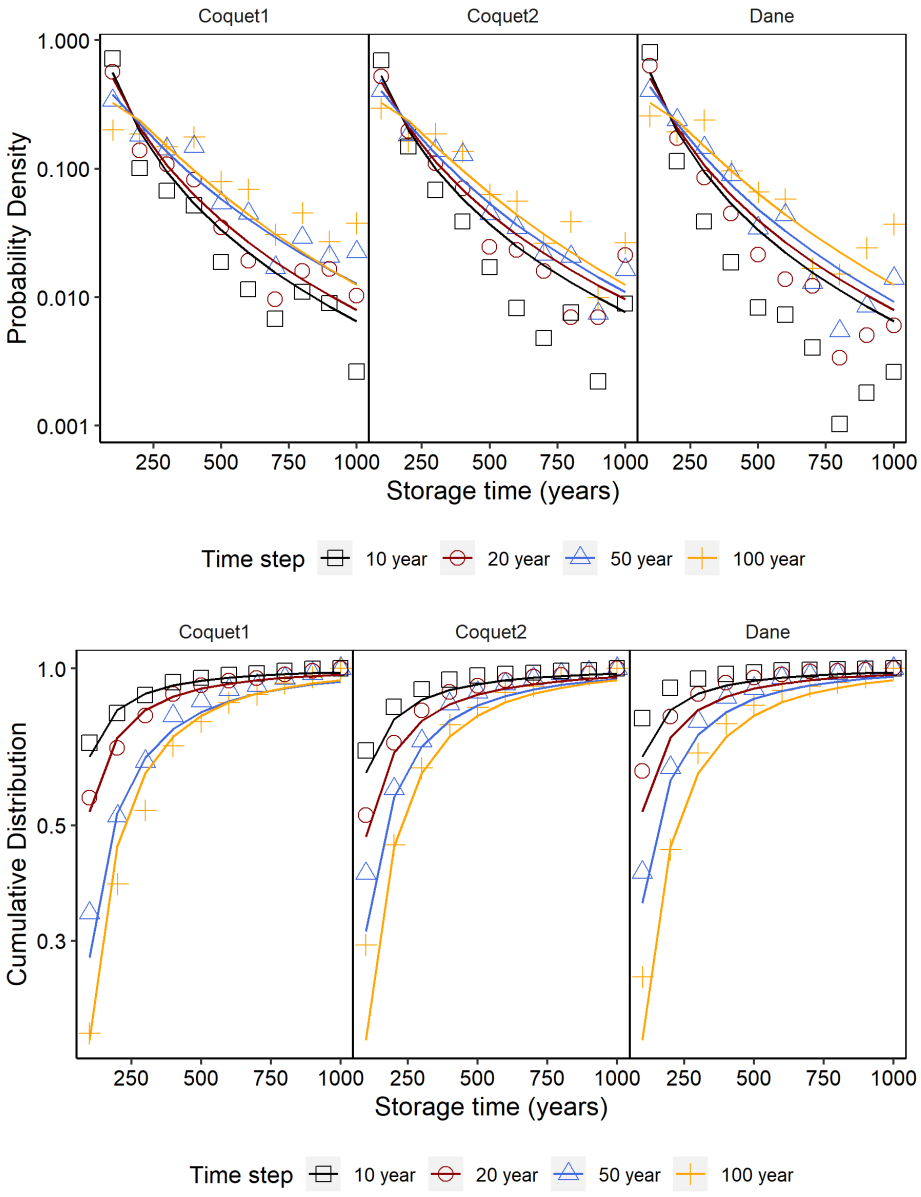

Figure 4.8: Fitted lognormal functions to storage time distributions of each validation (in this case, unvegetated) dataset. TOP: Empirical PDFs with fitted lognormal curves (note the logarithmic scale along the y axis); BOTTOM: Empirical CDFs with fitted lognormal curves.

4.5. Discussion

4.5.1. Sediment storage time dynamics under different environmental conditions

Across all three reaches, erosion rates and the total floodplain area that had been occupied by the channel at least once increased from forest to grass to unvegetated cover. This is expected, given previous findings on the relationships between types of vegetation cover and rates of geomorphic change (e.g. Micheli & Kirchner 2002; Trimble 2004), and the role of vegetation in processes such as the biostabilisation of river banks and the construction and consolidation of depositional features including channel bars (see Corenblit et al. 2007; Church & Ferguson 2015). Further, the erosion hazard of nearly all the floodplain storage time datasets presented in Figures 4.4-4.6 decayed with increasing age, with the gradient of these decay relationships declining in steepness from forest to grass to unvegetated conditions. In part, this reflects the variability in erodibility controls for floodplain surfaces of different ages within CAESAR-Lisflood (i.e. the elevation of floodplain surface areas, the distance of deposits from the channel and the age of any protective vegetation cover on the floodplain surface). It is also a function of floodplain reoccupation rates by the channel based on age. Modelled reoccupation probabilities decayed as power law functions with age under forest cover for all four time-steps of analysis and under unvegetated cover for 10-year measurement time-steps (see Appendix 2C for results and details on calculation). Under forest cover, fully grown trees reduced the erodibility of the floodplain areas they occupied to the extent that reoccupation by the channel was restricted to areas where tree growth had yet to reach full maturity. Konrad (2012) identified similar patterns of floodplain reoccupation probability that were linked to persistent stands of late seral stage riparian forest. When no vegetation cover was present, floodplain erosion occurred via high rates of lateral migration and frequent avulsions – both, processes that were captured most effectively at 10-year time-steps. Elsewhere, the decay was exponential, reflecting comparably higher rates of erosion of a wide range of ages under grass cover and when measured at coarser time-steps.

Another factor that needs to be considered is the role of sediment supply. In order to create a time-series of sediment supply for the reaches, simulations were run with a sediment recirculation utility activated. This had the effect of simulating (at least in the form of sediment flux rates) the same vegetation conditions at catchment scale. Thus, if a reach was simulated with forest cover, the sediment supply fed into the reach would reflect a catchment covered entirely with forest. This is important because sediment supply is an important control on channel morphodynamics (Church & Ferguson 2015). For example, river bank erosion rates have been shown to correlate positively with sediment supply (Constantine et al. 2014). In the Amazon Basin, reaches with lower rates of sediment supply were found to have constructed smaller point bars on average and had lower lateral migration rates along bends, compared with reaches with higher rates of sediment supply (Ahmed et al. 2019).

The combination of low rates of sediment supply and floodplain surfaces that are highly resistant to erosion under forest cover leads to a laterally stable single-thread meandering channel system. Under unvegetated conditions, high rates of sediment supply and an easily erodible floodplain sediments are enough to initiate a switch from a meandering to a braided channel planform (Nanson & Croke 1992; Church & Ferguson 2015). Median sediment storage times of forested and unvegetated conditions are similar, but arrived at by completely different mechanics. Under forest cover, the youngest sediments are removed preferentially due to their relative proximity to the channel and because these sediments are least likely to be protected by fully mature vegetation (Miller & Friedman 2009). Under unvegetated conditions, the channel reworks enough of the valley floor so frequently that relatively few areas of the floodplain achieve old age. Therefore, under both end member states when sediments are eroded, most of them are relatively young.

Few studies to date have attempted to relate channel pattern and lateral (in)stability with sediment storage behaviour. Miller and Friedman (2009) identified a reduction in erosion rates of the Little Missouri River floodplain over the 20th Century that was non-uniform – i.e. younger surfaces were eroded at higher rates than older surfaces. In the Saru River Basin, Japan, areas of floodplain deposits decreased with increasing age, regardless of the channel

pattern (Nakamura & Kikuchi 1996). Beechie et al. (2006) identified three distinct age distributions related to channel planform: floodplains dominated by older ages for straight channel reaches; floodplain area decreasing with increasing age for braided channel reaches; and floodplains dominated by intermediate ages for meandering and island-braided reaches (Figure 4.9). All the unvegetated simulations here produced a similar floodplain age distribution to the braided channel systems, whereas forested age distributions tended to resemble the straight channel systems (Figure 4.9). Grass cover simulations were somewhat mixed, with the Coquet1 and Dane reaches producing similar age distributions to meandering and anabranching systems (Figure 4.9) while the Coquet2 reach showed a decay in floodplain area with increased age similar to the Nunobe River (Nakamura & Kikuchi 1996).

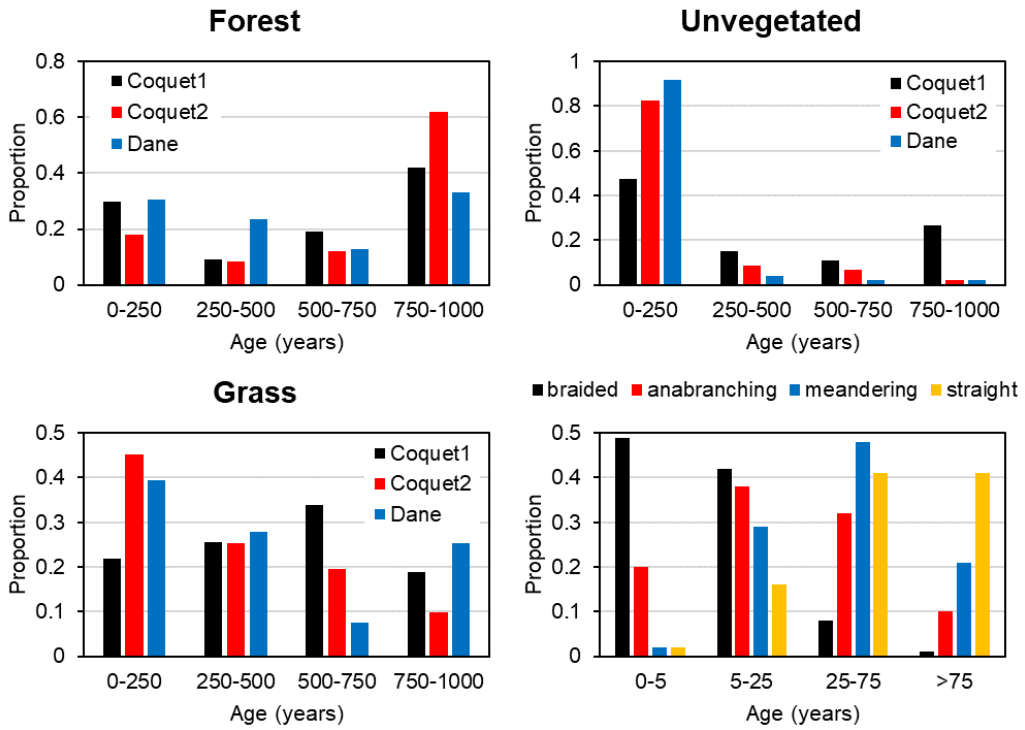

Figure 4.9: Distributions of the mean ages of four age classes (0-250, 250-500, 500-750 and 750-1000 years) for each site and vegetation cover scenario for the 10-year measurement time step. Bottom right: data for four channel planforms (braided, anabranching, meandering and straight) of forested mountain valleys in the Pacific Coastal Forest of North America (adapted from Beechie et al. 2006).

Trends between pairing of 1) age and storage time distributions and 2) mean age versus mean storage time vary significantly across the different measurement time steps – particularly for the unvegetated simulations (Figures 4.4-4.6). Braided channel planforms develop for all unvegetated simulations. Under these conditions, floodplain surfaces are reworked by a combination of high rates of lateral channel migration and by channel avulsion. The reason why older surfaces appear to be eroded proportionally more often under coarse time steps (50- and 100-year) than under finer time steps (10- and 20-year) is two-fold: First, lateral migration processes are captured more completely at finer time steps. This is because there will be areas of temporary floodplain occupation that are missed out of the analysis when channel positions are recorded less frequently. Over the course of 1000 years, these missing areas accumulate (Figure 4.10), and because younger sediment ages tend to be located closest to the channel, the erosion of young sediments will be under-estimated proportionately more. Second, avulsions will erode a mix of younger and older sediments as erosion along old and newly formed channels occurs, particularly during large flood events. Similar to lateral migration, a more complete time-series of avulsions is captured when channel changes are recorded at a finer temporal resolution, a fact reflected by the differences in the number of cells reworked by the channel between different time steps (Figure 4.10). Consequently, erosion of relatively young sediments from the floodplain may be under-estimated in the simulations.

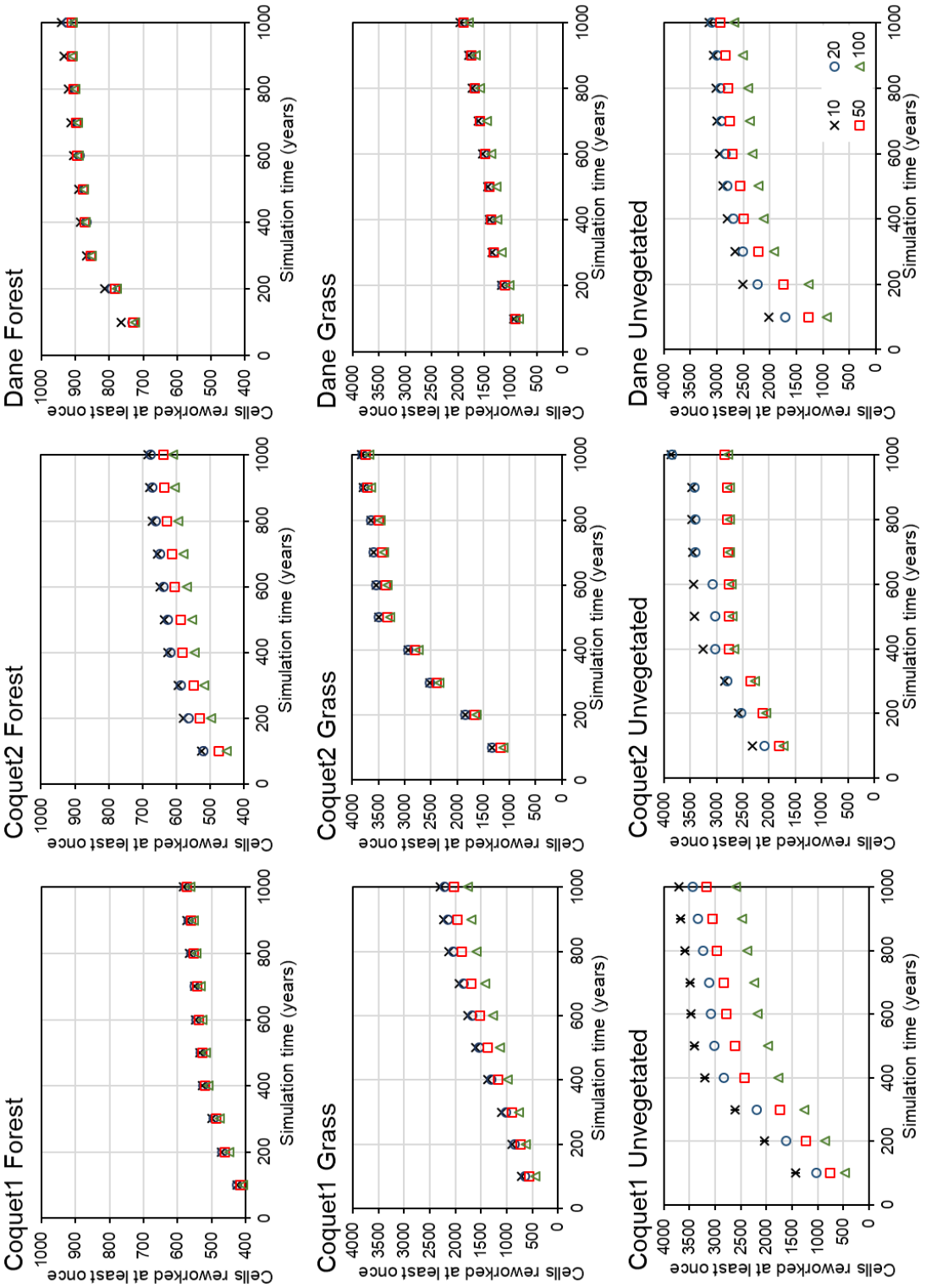

Figure 4.10: Number of valley floor cells that were occupied by the channel at least once during the simulation for all sites, scenarios and time steps.

4.5.2. Representing sediment storage time behaviour

Distributions of sediment storage times were generally found to be best described by lognormal functions, which indicate the youngest deposits were more susceptible to erosion than older parts. Even in cases where another model was found to be the best fit (Table 4.2), the lognormal function was found to represent sediment storage time behaviour accurately (based on a visual assessment of the goodness of fit of the function to storage time PDFs and CDFs – see Appendix 2B).

This is not the first time that a two-parameter function has been used to model the distribution of storage times. Moody (2017), found that the age and storage time distributions of sediment of a superslug deposit in Colorado were best modelled by two-parameter Weibull functions. Here, the shape parameter increased linearly with time since the extreme flood event that first formed the superslug and the scale parameter approximated the median values of recorded ages and storage times (Moody 2017). The strong relationship between the median storage time and the parameter, μ of the lognormal distribution is important because of the skewed nature of the storage time distributions. As it is less sensitive to outliers than the mean, which is sensitive to all values in the distribution, the median is a more reliable indicator of the average sediment storage behaviour. If younger ages dominate fluxes, as seems to be the case frequently (see Bradley & Tucker 2013; Moody 2017; and Pizzuto et al. 2017 for syntheses), then assuming there is no deviation from this behaviour, it is possible that the median storage time will converge to a stable value in the long-term, whereas the mean will continue to increase with the range of storage time values. It would follow that using equation 9 to estimate μ, and equation 10 to estimate σ for a given time-step of analysis, the distribution of storage times for a longer time period than considered here (e.g. 10,000 years) could be modelled. However, given the run time constraints of CAESAR-Lisflood, it would be difficult to validate this with this LEM.

The successful fitting of lognormal distribution curves to datasets encompassing a range of environmental conditions is significant for several reasons. First, if the assumptions described earlier hold, predictions of sediment storage times could be extended over much greater time scales than this study has focussed on. This is important given the length of time many

sediment particles will reside in some floodplain systems far exceeds 1000 years (e.g. Phillips et al. 2007). Considering that delivery timescales, from initial entrainment to eventual final deposition at catchment outlets, also span geological timeframes well in excess of 1000 years (see Pizzuto et al. 2017), this could be useful for interpretation of the stratigraphic record. Second, given this model seems to apply universally across the tested sites and scenarios, it may be justifiable to assume that it could be applied to an untested analogous valley floor reach. The reach in question may be heavily contaminated as a result of historical metal mining activity for example, and so the general storage time formula developed here could be used to constrain the timescale of decontamination (Dennis et al. 2009; Moody 2017). Finally, the relationship between time step and the parameter, σ demonstrates how recorded measurement frequency affects the shape of the storage time distribution function. This is useful as it offers a way of comparing datasets that cover decadal time intervals (e.g. planimetric channel change mapping) with data generated over centennial intervals (e.g. a set of radiocarbon dates from a sediment core) to produce sediment storage time distributions more easily.

Age distributions by contrast, are more complex and varied, and cannot be modelled by a single general equation for all sites, scenarios and time steps. However, it is possible to identify some common patterns. Under forest cover, the age distributions tend to consist of two peaks: one for the very youngest ages (up to 300 years old) and one for the very oldest ages (800-1000 years old). A similar pattern emerges for the Dane grass cover and Coquet1 unvegetated cover simulations (Figure 4.11). This bimodal age distribution is expected in cases where younger sediments dominate fluxes. A large peak will be present for the very youngest sediments which will have had less exposure to erosion than any of the other age classes, while another peak for much older ages will reflect preserved sedimentary deposits, usually located further from the channel (Miller & Friedman 2009). It has been argued that the age distribution of a typical single-channel meandering system is bimodal, reflecting the rapid transit of some sediment through a valley floor and the prolonged storage of other sediment in the floodplain (Belmont et al. 2014).

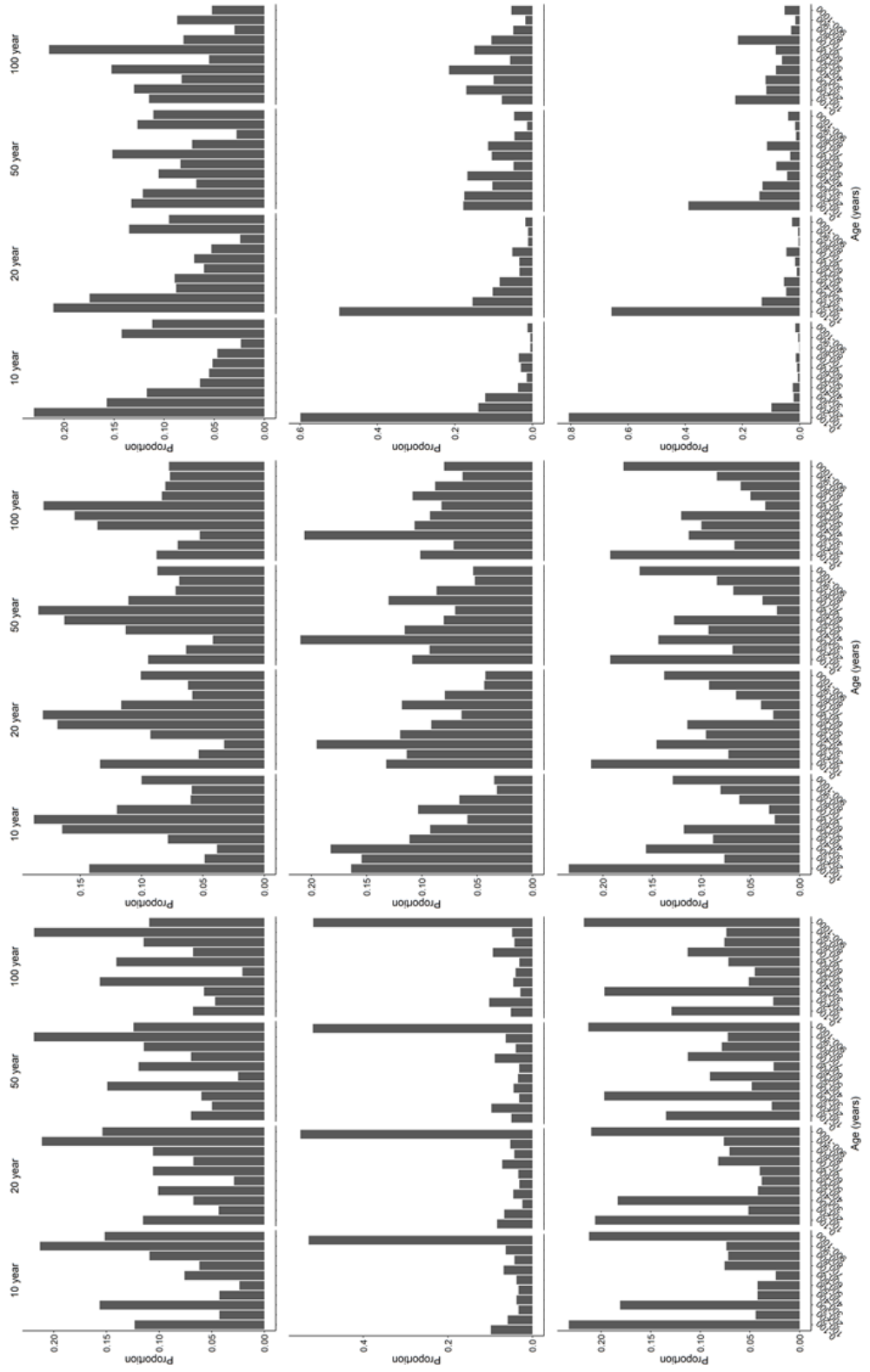

Figure 4.11: Age histograms for all 36 combinations of site, scenario and time step. From left to right: forest, grass and unvegetated cover scenarios; from top to bottom: Coquet1, Coquet2 and Dane reaches. For easier comparability across time steps, all ages are grouped into 100-year bins.

In other cases, including some of the grass cover and most of the unvegetated cover datasets, the proportion of sediment in storage decays with increasing age. This type of result is expected for systems where erosion hazard is uniform and the population of sediments could be characterised as being 'well-mixed' (Bolin & Rodhe 1973). Based on the evidence presented in Figures 4.4, 4.5 and 4.6, the datasets that show the weakest age bias for erosion seem to correspond closely with the age distributions in Figure 4.11 that show a decrease in the proportion of stored sediment with increasing age.

A third pattern shows the dominance of intermediate ages (between ~300 and ~700 years old). This is shown most clearly in the Coquet1 grass cover datasets and for the unvegetated age distributions constructed from the coarsest time steps (50 and 100-year time steps) (Figure 4.11). As described previously, the age distributions for these datasets closely resemble the age distributions of meandering and island-braided channel patterns of forested mountain valley reaches in Northwest America (Figure 4.9).

4.5.3. Limitations

This study is the first attempt to simulate and compare the distribution and behaviour of sediment storage times under different environmental and experimental conditions. It is the first study to apply a LEM capable of simulating multi-thread as well as single-channel meander scrolling dynamics to generate a floodplain age and storage time distribution from a time-series of river channel change. Despite the novelty of this approach, there are several limitations that need to be clarified.

First, given the size of many river valley floor corridors and that sediment delivery from initial source to ultimate sink occurs over geological timescales, it would have been ideal to simulate channel changes over much longer than 1000 years and for much larger reaches. The issue of keeping simulation times tractable and the focus on very laterally mobile river systems to mitigate the restrictions of this time constraint have been discussed. However, restricted to 1000 years, the scope for environmental disturbances to occur is limited, as well as any observable channel responses to these. One of the primary

objectives of this study was to observe variations in sediment storage behaviour under different conditions. Despite the small spatial and temporal scales here, it was possible to observe clear variations in channel evolution and floodplain sediment storage times.

Simulations were run using nine specified grainsizes, with spatial distributions in these established during earlier calibration runs (see Chapter 3 – Figure 3.2). While the data presented here refer to floodplain deposits, there are no data for variables such as the virtual velocity or delivery times of individual grainsize fractions. Storage and transit timescales will vary across different grainsizes (Lauer & Willenbring 2010), and it may be important to measure these variables for a specific size fraction (e.g. fine sediments <2 mm in diameter for contaminant flux modelling). Although this limitation is important, even if particles of a certain size could be tracked in a model, such as CAESAR applications of the TRACER sub-model (e.g. Gamarra et al. 2014), empirical sediment storage and delivery time data of sufficient temporal scale (multiple decades) to calibrate such a model would be challenging to acquire.

Another issue is the possibility that the grainsize distribution of sediment supplied at the top of the reach is not equal to the distribution at the reach outlet. For example, if the channel deposits significant amounts of coarse sediment and entrains fine sediment from the floodplain, the channel will likely incise (Lauer & Parker 2008). This means that despite simulating channel changes under constant vegetation and flow conditions, the system may (at least temporarily) not be operating under steady-state conditions. Given that transient state conditions violate one of the assumptions underpinning reservoir theory (Bolin & Rodhe 1973), the likelihood of all floodplain deposits possessing an equal and constant probability of being reworked at a point in time will be much lower, biasing results towards non-uniform erosion hazard behaviour. As these simulations were set up to recirculate sediments, it is difficult to test here whether the output sediment grainsize distribution matched the input distribution. However, CAESAR-Lisflood is designed to conserve mass in each grainsize fraction (Coulthard et al. 2013) and separate testing during model calibration confirmed that the grainsize distribution of supplied sediment matches that of outputs for all tested simulations (see Chapter 3).

4.6. Conclusions

A method of quantifying sediment storage time, based on LEM simulations of river channel changes that captures both multi- and single-channel patterns, was developed and tested successfully on three valley floor alluvial reaches. Despite the relatively short timescale of 1000 years tested here, there was considerable variability in sediment storage time dynamics under different environmental conditions. Storage time distributions were also sensitive to the time-step of analysis, with the proportion of younger sediments leaving storage increasing with time-step resolution from 100 to 10 years. This sensitivity arose from how effectively erosional processes operating over short timescales, such as the expansion and contraction of channel widths in response to changing stream flow stage, were captured at particular time-steps. Decadal and bidecadal time-steps are often used to analyse floodplain (re)occupation processes and the resulting effects on the age structure of riparian vegetation, whereas coarser time-steps are associated with radiocarbon-dating of valley-fill deposits. Considering the apparent sensitivity of storage time models to the time-step of analysis, it is important to consider not just the total mass of particles in storage and rates of removal as part of the reservoir theory framework for calculating sediment storage times (Bolin & Rodhe 1973), but also the specific processes of sediment removal themselves.

Turning to the three hypotheses outlined in the introduction, the evidence presented in Figures 4.4-4.6 indicated overwhelmingly that sediment storage times are dependent upon the age of floodplain deposits. In most cases, age and storage time distributions failed to match and erosion hazard distributions decayed with increasing age. This was particularly evident in the forest cover simulations and when analysed at the finest time-steps.

Differences in vegetation cover exerted the strongest influence on rates and patterns of channel changes, which were driven primarily by interactions between sediment supply and floodplain erodibility. The approach produced differences in the distributions of sediment ages and storage times that were replicated across the differing reaches. For example, all age distributions were

left-skewed and storage time distributions were right-skewed under forested conditions, indicating that younger-aged floodplain sediments dominated erosion fluxes. Erosion hazard plots confirmed this and indicated that similar behaviour occurred under grass covered conditions. Changes in the mean age and mean storage time values through time showed that sediment storage behaviour seemed to alternate between decaying and uniform erosion hazard under grass and unvegetated conditions. This dynamic was particularly clear when channel changes were recorded at coarser time steps of 50 and 100 years, with older sediments appearing to dominate erosion fluxes at some stage for the unvegetated simulations.

Distributions of sediment storage times were found to be best fit by a lognormal function. The parameters, μ (the mean of the lognormal distribution) and σ (the standard deviation of the lognormal distribution) could be estimated from power law relationships with the median storage time and the size of the measurement time step, respectively. When μ and σ values were estimated, the resultant lognormal PDFs and CDFs were found to fit all the empirical storage time distributions well (Figure 4.8). Further, assuming the sediment storage behaviour does not change significantly over time, these lognormal curves could be extended to estimate storage times over much longer timescales than the 1000 years simulated here. This provides significant potential for modelling the delivery times of eroded sediments to depositional basins such as lakes and alluvial terraces, with direct implications for interpreting the sedimentary archives of environmental change preserved in the stratigraphy of these deposits, as well as for monitoring contaminant fluxes in polluted catchments.

CHAPTER 5:

The impact of gradual and sudden-onset environmental changes on the longevity of sediment storage in alluvial floodplains

Summary and linkages to other thesis chapters

Chapter 4 introduced a method of calculating the age and storage times of floodplain sediment deposits from reach-scale river channel change simulated in CAESAR-Lisflood. An ensemble of 36 storage time distributions in that chapter, incorporating varying experimental and environmental conditions, demonstrated that sediment storage is highly sensitive to vegetation cover and the temporal frequency which storage times are recorded over. In general, storage time distributions were best-fit by a lognormal decay function. This reflected the tendency for sediments to mobilise from storage at differing rates depending on when they were first deposited on the floodplain (i.e. their ages). As a result, more than 50 % of sediments would remobilise after a few decades – faster than alternative models relying on dividing the total floodplain area by an erosion rate would have been able to predict – while much of the remaining material would have resided in storage for orders of magnitude longer. The scenarios tested in Chapter 4 did not however, incorporate a change in conditions during the simulations. This is problematic as storage time distributions can change shape in response to catchment disturbance.

This chapter seeks to address Research Question 4 (“How sensitive are reach-scale channel-floodplain systems to various environmental conditions in terms of sediment storage duration?”) in further detail to the previous chapter. Here, the same approach of using 1000-year simulations of channel changes is applied to a new ensemble of scenarios, each incorporating either a gradual or sudden-onset change in environmental conditions. Gradual changes include steady increases or decreases in daily flow magnitudes during the simulation. Sudden-onset changes include instantaneous shifts in vegetation cover after 500 years from unvegetated to grass, grass to forest and forest to grass. The lognormal function derived in Chapter 4 is applied to the storage time datasets generated here to evaluate its robustness as a predictor of sediment storage times under transient-state environmental conditions.

5.1. Introduction

River channels have been described as “nature’s gutters” (Church & Ferguson 2015: 1883), serving as conduits delivering water and sediment to catchment outlets. Natural river systems are self-formed in that the active boundary of the channel, including width, depth, slope, planform pattern and bed sediment characteristics adjust via erosion and deposition of the labile sediment over which rivers flow (Church & Ferguson 2015) to accommodate the dynamic hydrologic and sediment regimes of the catchments they drain (Wohl et al. 2015). As channel systems adjust, their adjoining floodplains are constructed and reworked via deposition and erosion (Bridge 2003). As derivatives of their parent channel systems (Nanson & Croke 1992), floodplain forms and processes, including morphology, the volume of sediment they store and the length of time sediment particles reside in storage, depend directly on channel morphodynamics – defined as the interaction between channel morphology and sediment erosion, transport and deposition (Church & Ferguson 2015).

After decades of research, several different controls on channel morphodynamics have been identified, including sediment supply (e.g. Constantine et al. 2014; Ahmed et al. 2019), riparian vegetation (e.g. Trimble 2004; Corenblit et al. 2007), in-stream wood (e.g. Collins et al. 2012; Wohl 2013), stream hydrology, including floods (e.g. Hooke & Mant 2000; Hooke 2016) and flow manipulation from dams (e.g. Provansal et al. 2014), and autogenic factors such as self-organised criticality (e.g. Hooke 2004). Through adjustment to these different controls and forms of disturbance, river systems transmit erosion signals downstream (Brunsden & Thornes 1979). These signals often become lagged before reaching the catchment outlet by long-term storage in floodplains (Fryirs 2013), complicating our ability to reconstruct past environmental change from sedimentary archives.

Constraining the longevity of sediment storage in floodplains is key to unpacking this signal shredding problem, as the distribution of sediment storage times is important for estimating the long-term virtual velocity of sediment particles (Martin & Church 2004) and is necessary to parameterise stochastic sediment transport models that are based on sediment budgets

(Kelsey et al. 1987; Malmon et al. 2003; Pizzuto et al. 2017). In addition, storage time quantification can enhance our understanding of chemical weathering of grains in storage, which allows sandstone composition to be used as a palaeo-environmental indicator (Johnson & Meade 1990), and to model the cycling of carbon (Sutfin et al. 2016; Torres et al. 2017) and contaminated sediments (Skalak & Pizzuto 2010).

Several attempts have been made to quantify sediment storage times in fluvial systems. These have often employed reservoir theory (Bolin & Rodhe 1973), a set of equations that calculate the distribution of ages of a mass residing in storage (the age distribution) and the distribution of ages of a mass exiting storage (the transit or storage time distribution). Under steady-state conditions, and assuming that all particles are equally susceptible to removal from storage, 1) the distribution of ages and storage times should be equal and 2) both distributions should decay exponentially (Bolin & Rodhe 1973). Data for several channel-floodplain systems confirm this (see Table 5.1). However, as channels will preferentially erode their nearest deposits, and because these deposits will most likely be younger than other parts of the floodplain, younger sediment will tend to make up a disproportionately large fraction of eroded sediment fluxes, and hence, exponentially decaying ages is unlikely to be the norm (Konrad 2012). For example, Konrad (2012) found that a typical river is 10 times more likely to reoccupy a part of the floodplain that was abandoned within the past decade than an area abandoned 30 years ago. Bradley and Tucker (2013) computed an ‘erosion hazard’ function, defined as the age-dependent probability of erosion, for a simulated channel-floodplain system. They found that the erosion hazard distribution of a simulated floodplain age population decayed with age, indicating that the youngest ages were at significantly greater risk of removal from storage (Bradley & Tucker 2013). Several other studies have found that the distribution of storage times is heavy-tailed and best fitted by a power law function, reflecting the dominance of younger ages in sediment fluxes (Table 5.1).

Table 5.1: Examples of fluvial sedimentary systems where erosion hazard is uniform across all ages and where erosion hazard decays with age.

Erosion hazard is not correlated with age		**Erosion hazard decays with age**	
Example	Reference	Example	Reference
Little Missouri River. Vegetation patch areas decayed exponentially with increasing age.	Everitt (1968)	**Little Missouri River.** The annual percentage of floodplain area eroded during measured photo intervals is consistently the highest for the very youngest age classes. Floodplain area is positively correlated with floodplain age, implying older surfaces are left uneroded by the channel more than younger surfaces.	Miller & Friedman (2009)
Nunobe River. Ages of different floodplain areas, quantified from vegetation and aerial image analyses, decayed exponentially.	Nakamura (1986); Nakamura et al. (1987)	**Saru River.** Large flood in 1992 eroded a larger fraction of younger ages than predicted by the exponential function.	Nakamura & Kikuchi (1996)
Bella Coola, Fraser, Saru and Grand Rivers. The age distribution of floodplain deposits for studied reaches of these rivers is approximately exponential (Methods of age quantification not described).	Martin & Church (2004)	**South River.** Fine-grained channel margin deposits and floodplain sediments have age distributions that decay as a power law function, implying younger ages are eroded disproportionately more than older ages.	Skalak & Pizzuto (2010); Skalak et al. (2015)
Oregon Coast Range: lower reach. ^{14}C-dated sediment ages are used to infer an exponential storage time distribution, indicating uniform probability of erosion across all ages.	Lancaster & Casebeer (2007)	**Oregon Coast Range: upper reach; Golden Ridge Creek and Cedar Creek.** Storage time distributions inferred from ^{14}C-dated sediments are right-skewed and heavy-tailed, implying younger ages erode preferentially.	Lancaster & Casebeer (2007); Lancaster et al. (2010)
Strickland River. Several thousand-year simulation of channel changes created a floodplain age distribution that decayed exponentially.	Lauer (2012)	**Channel change model.** Erosion hazards, calculated by dividing storage times by ages, found to be negatively correlated with age over 100,000 years.	Bradley & Tucker (2013)
		Channel change model. Older floodplain deposits are stored for longer than predicted for a well-mixed sedimentary reservoir with storage time distributions best fit by an exponentially tempered power law model over 100,000 years.	Torres et al. (2017)

The examples listed in Table 5.1 demonstrate that both forms of sediment storage behaviour can occur under steady-state conditions. However, because fluvial systems are susceptible to regular episodes of environmental disturbance, steady-state conditions are uncommon (Hoffmann 2015). A number of studies have shown that sediment storage time distributions are sensitive to these disturbance events. For example, the overall shapes of age and storage time distributions of a sediment superslug deposit in Colorado were found to change in response to whether incision or aggradation processes were prevalent at a point in time (Moody 2017). In fact, because of this complexity, it was not possible to fit one-parameter exponential or power law functions to these distributions (Moody 2017). Voepel et al. (2013) modelled time-series of bed elevation fluctuations to compute a storage time distribution of tracers seeded on the surface of a flume bed. They observed initial power law storage time functions over a timescale (seconds to minutes) set by the thickness of the channel bed and elevation fluctuation statistics, before the longer-term distribution became exponential in form as bed elevation stabilised (Voepel et al. 2013).

Here, the aim is to quantify sediment time behaviour under various environmental disturbances, by running an ensemble of channel change simulations spanning 1000 years. This ensemble includes fifteen simulations, encompassing three reaches and five hypothetical environmental disturbance scenarios. Simulations were run using a landscape evolution model (LEM) that captures both single-thread and multi-thread channel dynamics. Previously, an analysis of 36 storage time distributions, covering three vegetation cover scenarios, three tested reaches and four tested measurement time-steps, revealed that the erosion of sediment from floodplains depended strongly on the age of the floodplain deposit (Chapter 4). Vegetation cover was applied homogenously (i.e. one type covering the entire reach for the full duration of each model run). While the study presented in Chapter 4 is novel (i.e. the first time that floodplain storage times have been quantified under carefully controlled changes in environmental and experimental conditions), the lack of testing of how other variables, such as daily flow magnitudes, affect sediment storage times, and the impact of changes in such variables over time, means

the hypothesis that erosion hazard decays with age merits further testing. Storage time distributions were found to be best fit by lognormal functions. The two parameters of the lognormal function could be estimated from median storage time values and the measurement frequency of recorded channel changes. However, it is unclear if the lognormal function can be fitted accurately to a storage time distribution of a disturbed floodplain system (based on visually assessing the fit of the model curve to the empirical storage time distribution). This chapter addresses the following key questions: First, does the overall behaviour of sediment removal from storage depend on the age of floodplain deposits and environmental conditions? Second, does the distribution of sediment storage times change in response to simulated disturbances? Third, does the lognormal function, using the equations to predict the two parameters derived in Chapter 4, fit the storage time distributions of disturbed channel-floodplain systems accurately? These results are discussed in relation to findings presented in earlier studies, and the potential implications for sediment dynamics and environmental management are explained.

5.2. Methods

5.2.1. CAESAR-Lisflood and study sites

CAESAR-Lisflood, a coupled 2D-hydrodynamic model and LEM applicable at catchment and reach spatial scales (Coulthard et al. 2013) is used to simulate channel-floodplain evolution of three reaches taken from the River Dane and River Coquet in northern England (Figure 5.1). Simulations cover 1000 years of channel changes, with each reach spanning 1 km in length and with a horizontal DEM resolution of 10 m. Ideally, channel-floodplain evolution modelling should encompass larger spatial and longer temporal extents than applied here. However, because of the lengthy run times of CAESAR-Lisflood (in some cases, it took over a month to complete a single simulation), the spatial and temporal extents were set to keep simulation times tractable. Initial conditions (including grid cell elevations and grainsize distributions) were established during earlier calibration runs (Chapter 3; Feeney et al. 2020).

Parameter values, governing sediment erosion rates and vegetation characteristics were set for each site according to Table 5.2.

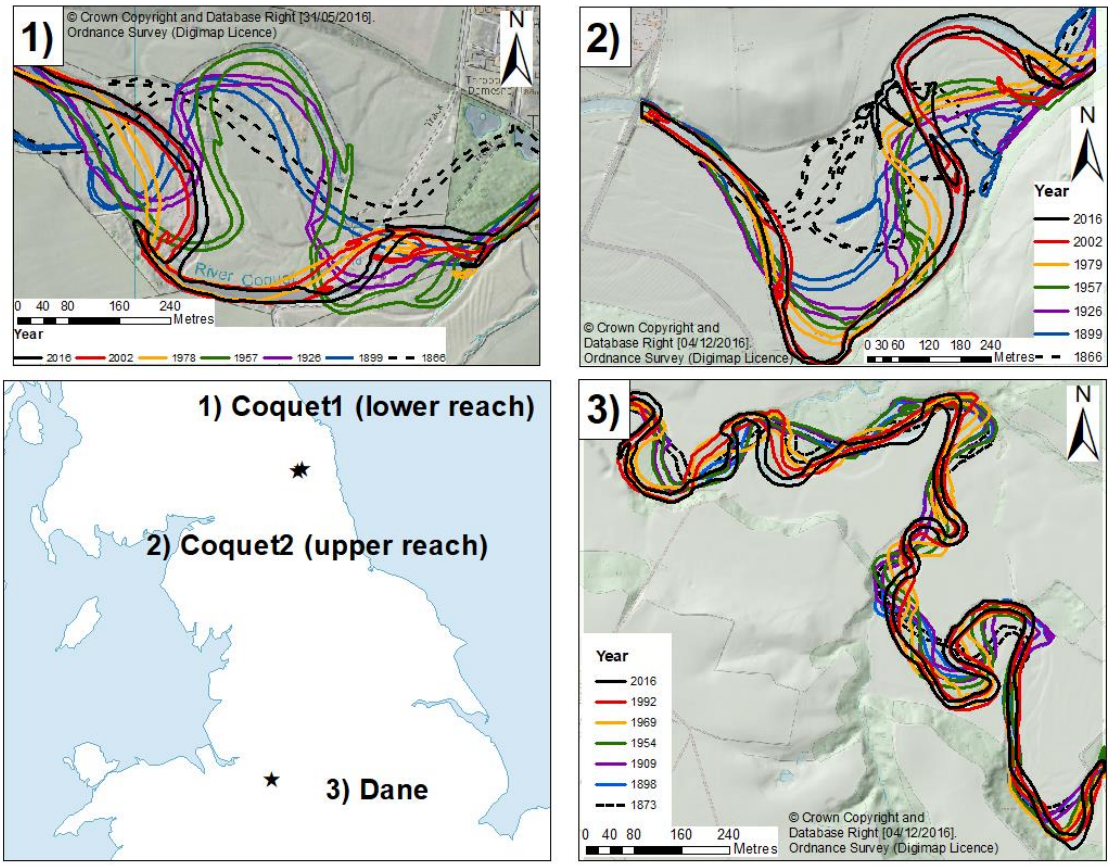

Figure 5.1: Locations of each of the tested reaches in northern England: 1) Coquet1 (lower reach), 2) Coquet2 (upper reach), and 3) Dane. Ordnance Survey base maps from 2016 are superimposed on hillshade surfaces created from 2 m LiDAR data DEMs (© Environment Agency). River channels from various years were digitised from historic maps and aerial imagery and display the variety of rates of channel changes through time and between the reaches.

The three reaches were chosen for three reasons. First, all three contain laterally mobile channels with complex variations in planform morphology over time (Figure 5.1). Second, there is variation in local geomorphology between the reaches, including valley width, channel sinuosity, number and size of bends, and presence of terraces. Finally, the same reaches were used to simulate 1000 years of channel changes previously, where it was

demonstrated that sediment storage behaviour varied both between reaches and under different vegetation cover scenarios (Chapter 4).

Table 5.2: Parameters for the three sites and vegetation change scenarios.

	Site					
Parameter	Coquet1		Coquet2		Dane	
Lateral erosion rate, θ	0.000001		0.000003		0.000001	
In-channel erosion, λ	20		15		14	
Number of passes for edge smoothing filter	80		80		10	
Number of cells to shift lateral erosion downstream	8		8		1	
Sediment transport formula	Wilcock & Crowe		Wilcock & Crowe		Wilcock & Crowe	
Vegetation cover change scenarios:						
500-year period of simulation	1st	2nd	1st	2nd	1st	2nd
Manning's n:						
Forest to Grass	0.055	0.035	0.055	0.035	0.055	0.035
Grass to Forest	0.035	0.055	0.035	0.055	0.035	0.055
Unvegetated to Grass	0.025	0.035	0.025	0.035	0.025	0.035
Critical shear stress threshold (N m^{-2}):						
Forest to Grass	120	80	120	80	120	80
Grass to Forest	80	120	80	120	80	120
Unvegetated to Grass	0	80	0	80	0	80
Vegetation maturity time (years):						
Forest to Grass	20	1	20	1	20	1
Grass to Forest	1	20	1	20	1	20
Unvegetated to Grass	1000	1	1000	1	1000	1
Proportion of erosion that can occur at full maturity:						
Forest to Grass	0.1	0.2	0.1	0.2	0.1	0.2
Grass to Forest	0.2	0.1	0.2	0.1	0.2	0.1
Unvegetated to Grass	1	0.2	1	0.2	1	0.2

Despite the limitation of lengthy simulation run times, CAESAR-Lisflood was chosen because it is one of the few models that allows both single- and multi-channel patterns to be simulated (Coulthard & Van De Wiel 2006). This allows a more complete range of floodplain evolution processes to be captured, which given that lateral instability and the formation of braided planforms can result from an environmental disturbance, such as a large pulse of sediment (see Miller 1997 for examples), this is a significant advantage over models like

CHILD that have been used for earlier storage time modelling studies (e.g. Bradley & Tucker 2013). CAESAR-Lisflood has been applied in numerous experimental modelling contexts (e.g. Coulthard & Van De Wiel 2007, 2013, 2017), with several studies (e.g. Pasculli & Audisio 2015; Ziliani & Surian 2012; Ziliani et al. 2013), as well as results from Chapter 3, demonstrating that the model can replicate reach-scale morphodynamics with reasonable accuracy.

5.2.2. Gradual and sudden-onset environmental change scenarios

Channel changes are controlled by a multitude of interacting factors. Although our understanding of these controls and interactions is incomplete, the form and evolution of floodplains is essentially shaped by stream power and sedimentology including sediment supply and erodibility of the floodplain sediment (Nanson & Croke 1992). Against this background, five scenarios, encompassing changes in stream discharge and floodplain vegetation, were simulated for each of the study reaches (making a total of fifteen simulations). These scenarios are illustrated in Figure 5.2 and described in more detail in Table 5.3, but include a scenario where flow magnitudes gradually increase over time partway through the simulation, a decreasing flow magnitudes scenario where the flow series of the first scenario is run in reverse, and three scenarios where the vegetation cover changes instantaneously after 500 simulated years. These latter three scenarios include a switch from grass to forest cover, unvegetated to grass cover and forest to grass cover. For the three vegetation change scenarios, simulations were run for 500 years with one set of parameters, then restarted with a new set of parameters to reflect the altered vegetation conditions (see Tables 5.2 & 5.3). Although gradual changes in vegetation cover would have been more realistic, without changes to the CAESAR-Lisflood code, this was not possible. However, pollen data from across the British Isles do show evidence of abrupt shifts in vegetation cover having occurred over the Holocene (Fyfe et al. 2013). Given the short length of the simulations here, introducing instantaneous vegetation cover changes may act as a useful analogue for the changes reported by Fyfe et al. (2013) over 10,000 years.

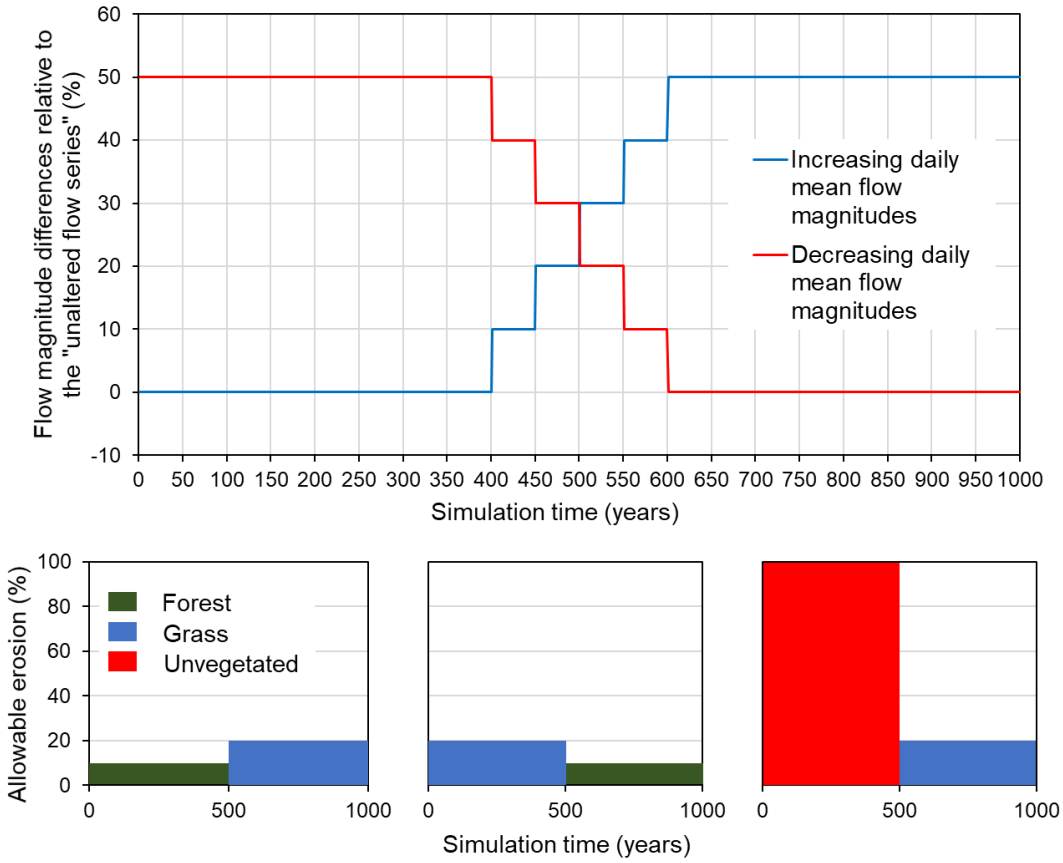

Figure 5.2: Illustrations of the five environmental change scenarios tested in this chapter. For the flow magnitude scenarios, daily mean discharges are increased/decreased immediately by 10 % after 400 years. These stepped changes are repeated every 50 years until 600 years into the simulation, when the flow magnitudes are increased/decreased by 50 % relative to the first 400 years of the simulation. Vegetation cover changes are introduced instantaneously at 500 simulation years (see Table 5.3 for further details). This changes the level of protection of sediment from erosion – allowable erosion (%) – within CAESAR-Lisflood by the amounts shown in the bottom three plots.

Table 5.3: Environmental disturbance scenarios and how these are implemented in CAESAR-Lisflood.

Scenario	Description
Increasing flow magnitudes	Simulation is split into 3 main parts. 0-400 years: Flow series is unaltered. 400-600 years: Daily flow magnitudes increase by 10% increments every 50 years until year 600 when flow magnitudes are 50% higher than at the beginning of the simulation. 600-1000 years: No further changes to daily flow magnitudes.

Decreasing flow magnitudes	Flow series for 'Increasing flow magnitudes' scenario is run in reverse. By running the flow series in reverse, the total cumulative discharge through time for both changing flow magnitudes is the same. This will allow us to observe the channel changes and floodplain sediment ages and storage times that occur purely as a result of the effects of decreasing flow magnitudes through time.
Grass to forest	Simulation is run with the same undisturbed flow series as the first 400 years of the 'Increasing flow magnitudes' scenario throughout all 1000 years. Grass cover parameter settings are set for the first 500 years, after this time the simulation is stopped. The simulation resumes with new setting for forest cover.
Forest to grass	Simulation is run with the same undisturbed flow series as the first 400 years of the 'Increasing flow magnitudes' scenario throughout all 1000 years. Forest cover parameter settings are set for the first 500 years, after this time the simulation is stopped. The simulation resumes with new setting for grass cover.
Unvegetated to grass	Simulation is run with the same undisturbed flow series as the first 400 years of the 'Increasing flow magnitudes' scenario throughout all 1000 years. Unvegetated cover parameter settings are set for the first 500 years, after this time the simulation is stopped. The simulation resumes with new setting for grass cover.

5.2.3. Age and storage time modelling

For each simulation, DEM and water depth files were saved every ten years. Water depths generally captured the position and morphology of channels, and so were vectorised and edited to the extents of channel positions based on visual assessment of the DEMs. All 100 channel polygons were overlaid in sequence to create a time-series of river channel changes and calculate surface areal extents and timings of floodplain occupation and abandonment by the channel. The timings of floodplain abandonment by the channel (deposition) and floodplain (re)occupation (erosion) are used to calculate ages and storage times as follows:

$$Age_i = 0.5t + nt \quad (1)$$

$$Storage\ time_i = Age_{i-1} + 0.5t \quad (2)$$

where t is the time step in units of 10 years and n is the number of time steps until that part of the floodplain is eroded by the channel. When a floodplain

surface becomes (re)occupied by the channel, Age_i is reset to 0 and age begins to accumulate again once the channel abandons that area of the floodplain. The result after 1000 years is a single shapefile, consisting of a mosaic of polygons with their own unique history of geomorphic changes and recorded age and storage time values. These age and storage time values are subsequently used to construct age and storage time distributions, plot trends in mean age and mean storage time values through time and constrain erosion hazard distributions.

Inverse cumulative distribution functions (CDFs) of ages and storage times are plotted for each simulation. According to Moody (2017), the primary shapes of the distribution curves provide useful information on the nature of sediment storage behaviour. For example, for a floodplain where younger ages are more susceptible to erosion than older ages, the age distribution will be convex in shape, reflecting the prevalence of older deposits in storage. Conversely, the storage time distribution will be steeply concave, reflecting both the prevalence of younger ages in erosion fluxes and the heavy-tailed nature of the storage time distribution model. If an increase in erosion rates leads to proportionately higher volumes of older sediment leaving storage over a given period of time, this will be reflected by a change in the form of the storage time distribution from concave to convex curvature (Moody 2017). Thus, the inverse CDFs should indicate the nature of sediment storage behaviour, any changes in behaviour in response to environmental disturbance, and the timing and duration of any changes.

Trends in mean age and mean storage time through time can indicate whether erosion hazard is uniform or correlated with age, and the timing and duration of any changes in sediment storage behaviour. If mean age equals mean storage time, it is likely that erosion hazard is approximately the same across all deposit ages; if mean age exceeds mean storage time, then the age distribution is dominated by relatively much older ages than the storage time distribution; if mean storage time exceeds mean age, the reverse is true. By comparing the trends in these two means, it may be possible to detect whether erosion hazard switches from uncorrelated to correlated with age (or *vice*

versa) in response to environmental disturbance, or if disturbance exacerbates an existing form of behaviour.

In chapter 4, lognormal distribution curves were found to best describe the distribution of sediment storage times in floodplains across all 36 tested combinations of site, scenario and measurement time step. The PDF and CDF respectively take the forms:

$$f(\tau) = \frac{1}{\sigma\tau\sqrt{2\pi}} e^{\frac{-(\ln(\tau)-\mu)^2}{2\sigma^2}}, \tau > 0 \quad (3)$$

$$F(\tau) = \Phi\left(\frac{\ln(\tau)-\mu}{\sigma}\right), \tau > 0 \quad (4)$$

where τ is the storage time, μ and σ are the mean and standard deviation of the lognormal distribution, respectively, and ϕ is the CDF of the standard normal distribution.

The two parameters, μ and σ, were found to be predicted using the following equations:

$$\mu = 0.7827\, ln(\tau_{50}) + 1.0792 \quad (5)$$

$$\sigma = -0.202\, ln(t) + 1.8501 \quad (6)$$

where τ_{50} and t are the median storage time (years) and time-step (years), respectively.

For each of the 15 simulations modelled here, lognormal curves are fitted to the empirical data to evaluate the accuracy of this distribution function under disturbed environmental conditions. Values of μ and σ are predicted by inputting median storage time values after 1000 years, and a time-step of 10 years into equations 5 and 6, respectively, to generate the lognormal curves.

5.3. Results

5.3.1. Channel changes, floodplain ages and net geomorphic changes

Simulated river channel changes varied widely across the different scenarios. Under the increasing flow magnitudes scenario, the channel continuously

erodes previously unvisited floodplain throughout the simulation, with total floodplain turnover increasing from 17.5 to 38.4% for Coquet1 (Figure 5.3), 29.7 to 62% for Coquet2 (Figure 5.4) and from 23.5 to 50.8% for the Dane reach (Figure 5.5). Net erosion and deposition fluctuations varied between reaches, with large peaks in both processes occurring throughout the Coquet1 simulation (Figure 5.6). High net deposition peaks between 350 and 700 years occurred along Coquet2, reflecting the high number and large size of abandoned channels following avulsions during this period (Figure 5.6). Similarly, the Dane exhibited high net deposition peaks, reflecting the large number of avulsions that occurred in the latter half of the simulation, in addition to high net erosion peaks which are indicative of accelerated lateral migration rates (Figure 5.6).

Floodplain turnover rates under the decreasing flow magnitudes scenario are higher than under the increasing flow magnitudes scenario for the first 750 years. During the first 750 years under decreasing flow magnitudes, total floodplain turnover increases from 22.7 to 42.9% along Coquet1 (Figure 5.3), 44.7 to 68.3% along Coquet2 (Figure 5.4) and from 29.1 to 50.2% along the Dane (Figure 5.5). Turnover rates slowed subsequently, increasing to 46.5, 72.7 and 54.9% by 1000 years for the Coquet1, Coquet2 and Dane reaches, respectively. Net erosion peaks were highest during the first 400 years along both Coquet reaches, reflecting the relatively high lateral migration rates during this period (Figure 5.6). Unexpectedly, the highest net erosion peaks along the Dane occurred during the last 400 years of the simulation, after flow magnitudes stopped decreasing (Figure 5.6). Between 750 and 1000 years, a large number of cut-offs occurred and it appears that the channel has rapidly reworked its most recently deposited point bar surfaces via lateral migration (Figure 5.5). This was probably the channel adjusting rapidly to its original form after cut-offs reduced its earlier higher sinuosity (Hooke 2004).

When vegetation cover switched from grass to forest, all reaches responded in a similar way. During the first 500 years, channels were laterally mobile, with floodplain turnover reaching 22.2, 64 and 30.1% for the Coquet1, Coquet2 and Dane, respectively. After this time, channels stabilised, reworking between 0.5 and 2% of unvisited floodplain during the latter 500 years. When vegetation

cover switched in the opposite direction, from forest to grass, the response in lateral migration rates (in this case, from stable to laterally mobile) was also concurrent across all reaches.

Reaches responded differently to each other however, when vegetation cover switched from unvegetated to grass. During the first 500 years when no vegetation cover was present, the channel planform was braided, with high floodplain turnover extents (46.9, 67.4 and 60.9% of all previously unvisited floodplain reworked after 500 years for the Coquet1, Coquet2 and Dane, respectively). When grass cover was introduced, the Coquet1 main channel remained laterally stable, with regular avulsions through old secondary channels during flood events generating net erosion peaks in the last 250 years of the simulation (Figure 5.6). By contrast, the Coquet2 system evolved from a braided to a highly active scrolling meandering channel, reworking a further 11.9% of the previously unvisited floodplain during the last 500 years of the simulation (Figure 5.4). Rates of geomorphic change along the Dane lay somewhere in between the other reaches. Like Coquet2, the system transformed into a laterally migrating single channel, albeit with lower rates of floodplain turnover – reworking 6.1% of unvisited floodplain during the final 500 years (Figure 5.5).

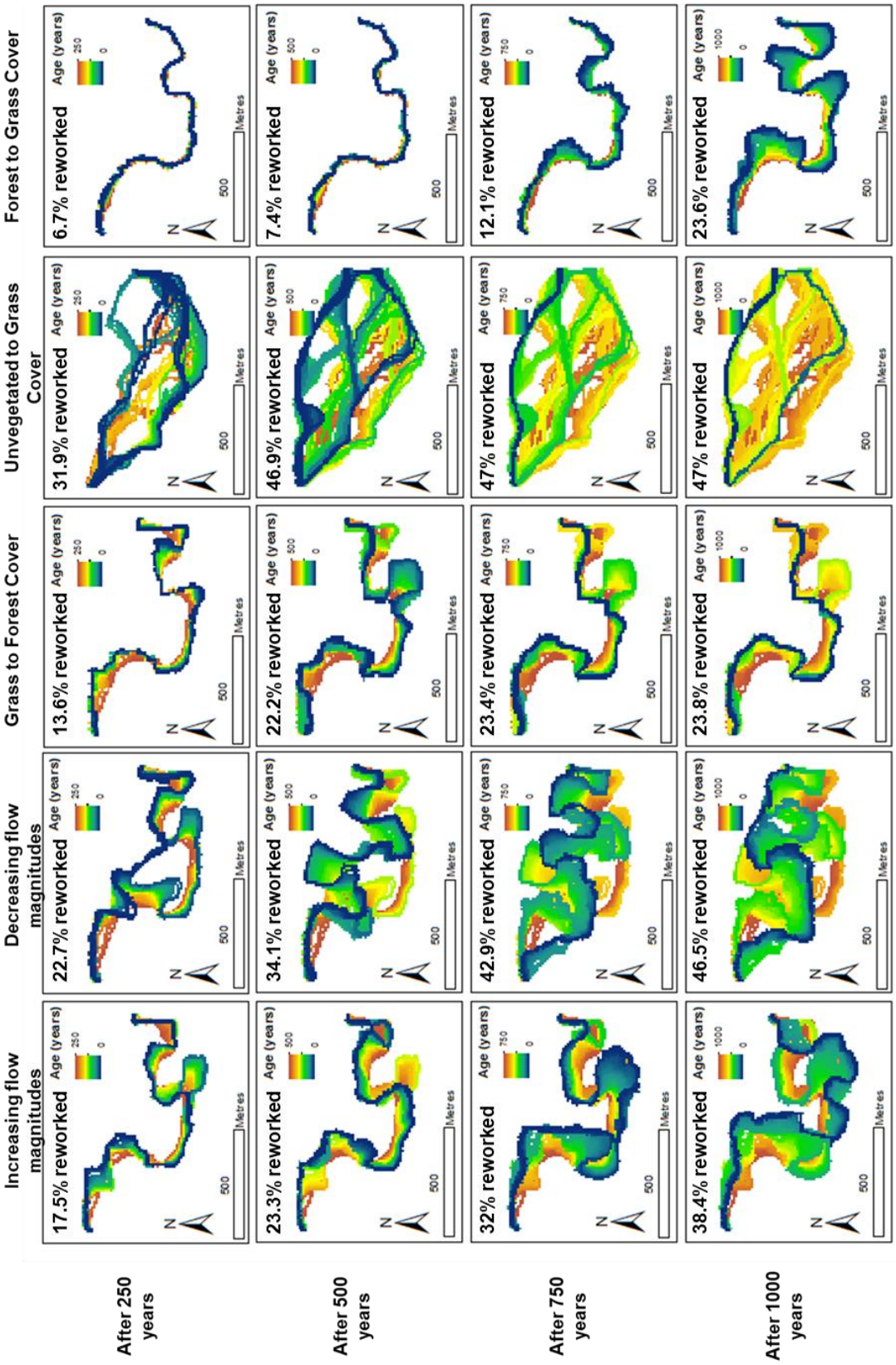

Figure 5.3: Floodplain surface ages of Coquet1 after 250, 500, 750 and 1000 years of simulated channel changes for each scenario. Percentages indicate the fraction of the floodplain area that has been eroded during the simulation.

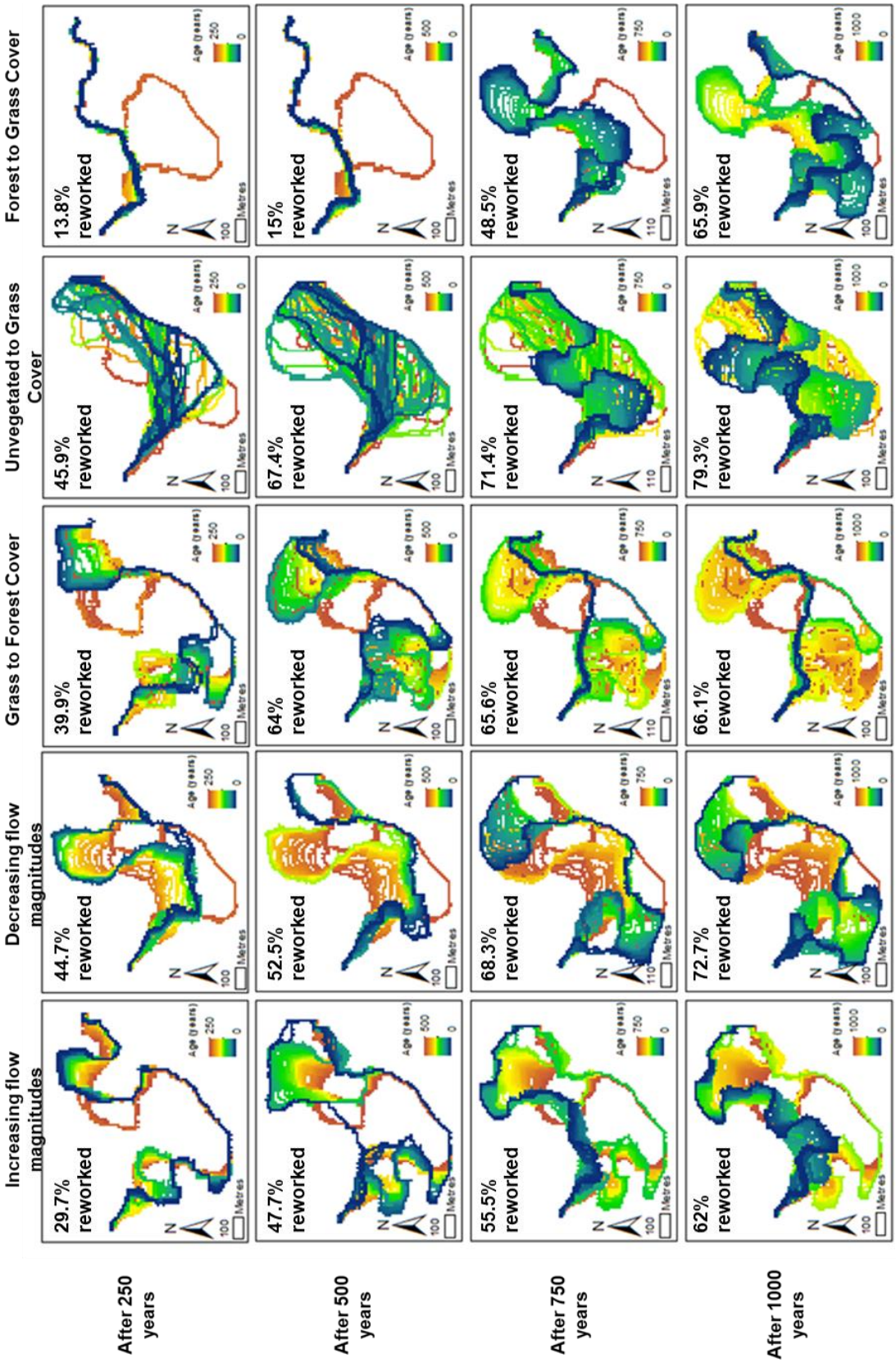

Figure 5.4: Floodplain surface ages of Coquet2 after 250, 500, 750 and 1000 years of simulated channel changes for each scenario. Percentages indicate the fraction of the floodplain area that has been eroded during the simulation.

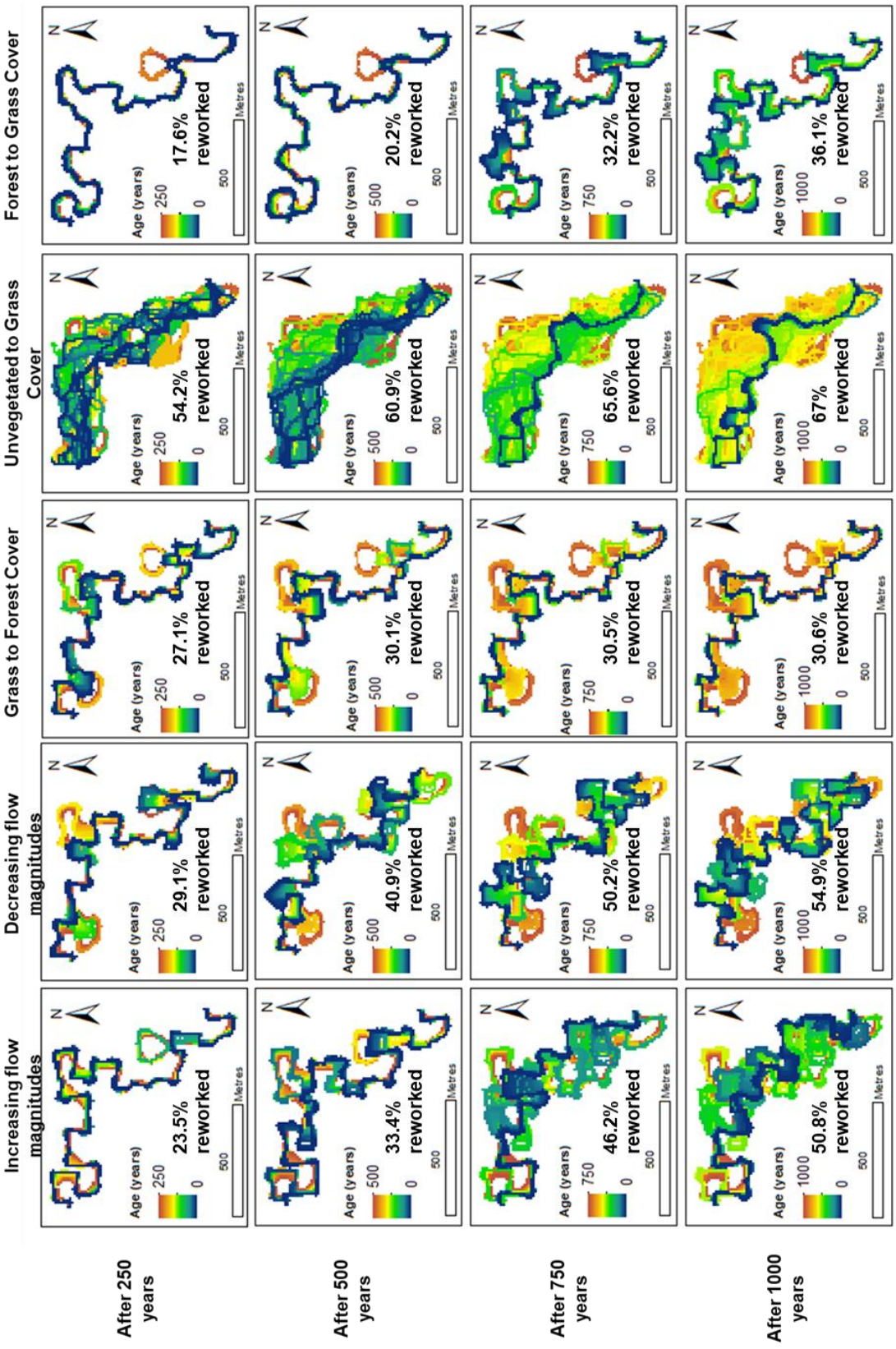

Figure 5.5: Floodplain surface ages of the Dane after 250, 500, 750 and 1000 years of simulated channel changes for each scenario. Percentages indicate the fraction of the floodplain area that has been eroded during the simulation.

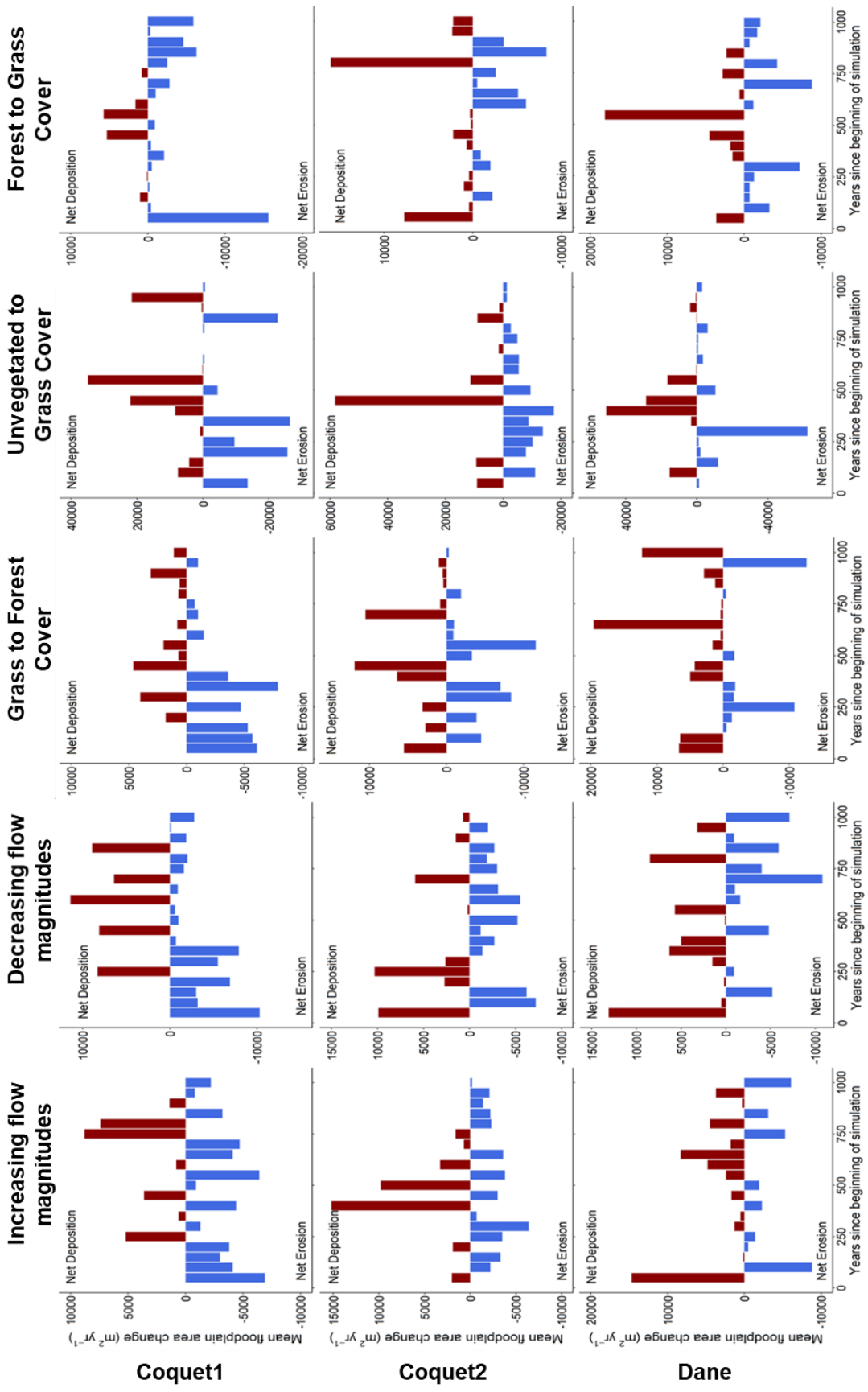
Increasing flow magnitudes
Decreasing flow magnitudes
Grass to Forest Cover
Unvegetated to Grass Cover
Forest to Grass Cover
Coquet1
Coquet2
Dane
Net Deposition
Net Erosion
Mean floodplain area change (m² yr⁻¹)
Years since beginning of simulation

Figure 5.6: Net geomorphic changes over 1000 years of simulated channel changes for the Coquet1 (top row), Coquet2 (middle row) and Dane (bottom row) reaches under the five environmental change scenarios. From left to right: Increasing flow magnitudes, decreasing flow magnitudes, grass to forest, unvegetated to grass and forest to grass. Data are grouped into 50-year bins.

5.3.2. Age and storage time distribution curvature

Age and storage time distributions varied across the different sites and scenarios (Figure 5.7). Age distributions under the grass to forest simulations displayed convex curvature, reflecting the dominance of older ages retained in storage. Storage time distributions were concave, indicating erosion fluxes consisted mostly of younger aged material. Similar behaviour emerged for the unvegetated to grass scenario. However, unlike the other reaches, the Coquet2 channel migrated freely across the full width of its floodplain (Figure 5.4). In the process, the channel eroded sediment from deposits with a range of different ages, producing concave curvature for both the age and storage time distributions (Figure 5.7b & e). Forest to grass scenarios saw an increase in net erosion rates during the latter 500 years of the simulations (Figure 5.6). This had the effect of inducing a temporary switch in the storage time distribution curvature from concave to convex after 500 years (Figure 5.7), reflecting the period of time when the channel began to rework older ages much more frequently than during the first 500 years of the simulation. The duration of this switch in curvature varied across the reaches, lasting from ~500-900 years for Coquet1 (Figure 5.7d), ~500-600 years for Coquet2 (Figure 5.7e) and ~500-700 years for the Dane (Figure 5.7f). Age and storage time distributions were also saved after 250, 500 and 750 years, and plotted with the distributions after 1000 years (see Appendix 3A). Displaying the distributions over these time periods shows when changes in sediment storage behaviour occurred, how long these changes in behaviour persisted for, and changes in the median age and median storage time values (where the curves intersect the horizontal dotted line on the plots) over time (Appendix 3A).

Age and storage time distribution curves under the two changing flow magnitudes scenarios were broadly similar to each other and across all reaches (Figure 5.7). For the Dane however, the curvature of the increasing flow magnitudes storage time distribution does switch from concave to convex at ~300 years, though this is temporary and not as pronounced as the forest to grass curvature changes (again, see Appendix 3A for further details of timings and durations of these curvature changes).

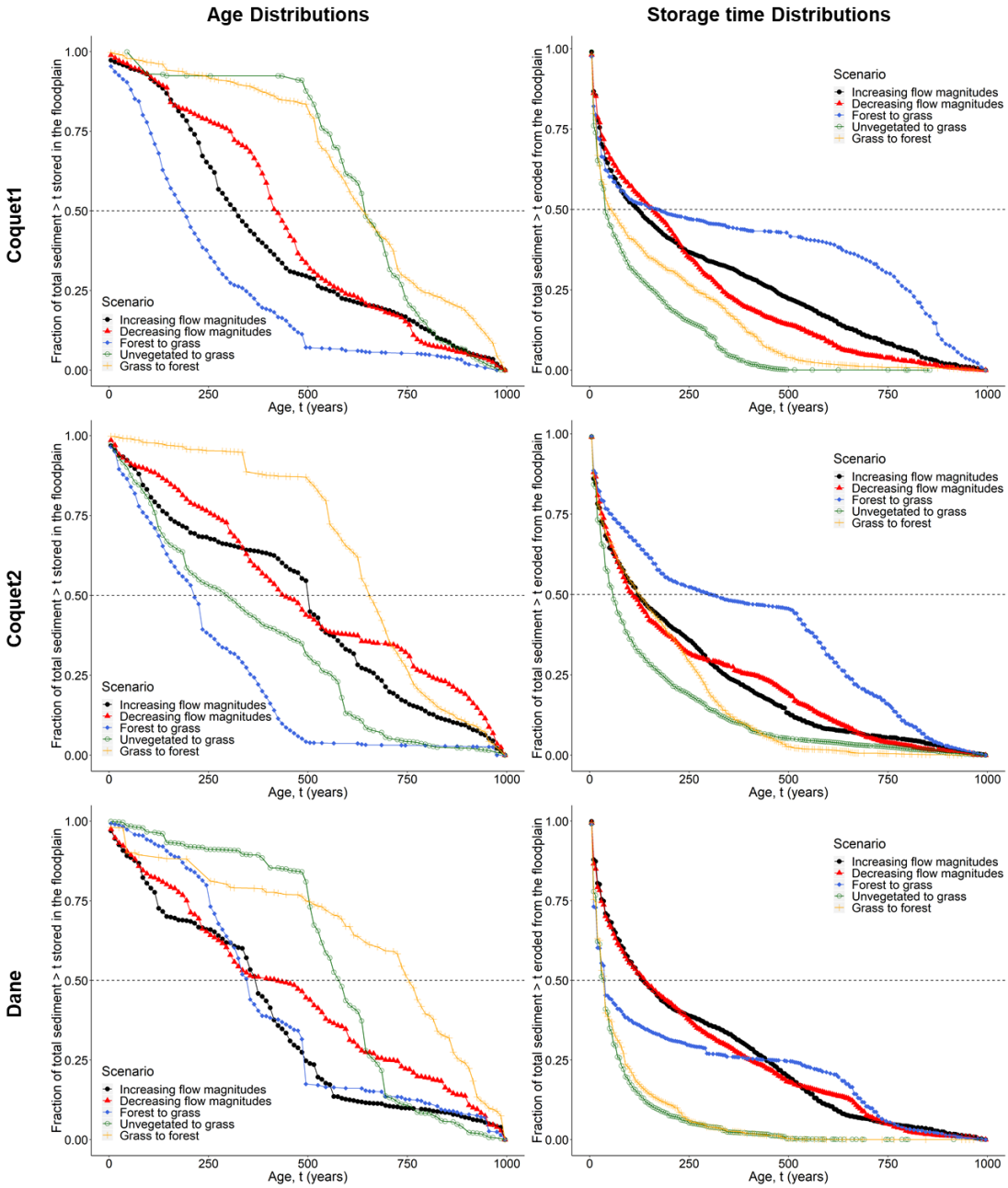

Figure 5.7: LEFT - Inverse cumulative distribution functions of ages for the three sites: Coquet1, Coquet2 and Dane under the five scenarios. RIGHT -

Inverse cumulative distribution functions of storage times for the three sites: under the five scenarios. Dashed line indicates the median age and storage time for each of the fifteen simulations. Changes in the primary shape of the distribution (i.e. concave or convex curvature), can indicate changes in storage behaviour. If curvature is concave, younger ages dominate the distribution; if convex, older ages dominate. The median equals where the curves intersect with the dotted line.

5.3.3. Erosion hazard

Erosion hazard decayed with age when vegetation changed to more resistant conditions (from grass to forest and from unvegetated to grass cover). Under the forest to grass scenario, erosion hazard decayed with age for the youngest 500 years (Figure 5.8). However, erosion hazards for the oldest ages (500-1000 years) lie close to the expected uniform erosion hazard value of 0.05 for the most part (albeit, a second negative correlation with age can be seen for the Dane) (Figure 5.8). Under the two changing flow magnitudes scenarios, erosion hazard values for most ages fluctuated close to the uniform erosion hazard value. Overall, there is a weak negative correlation between erosion hazard and age for each of the increasing and decreasing flow magnitudes simulations.

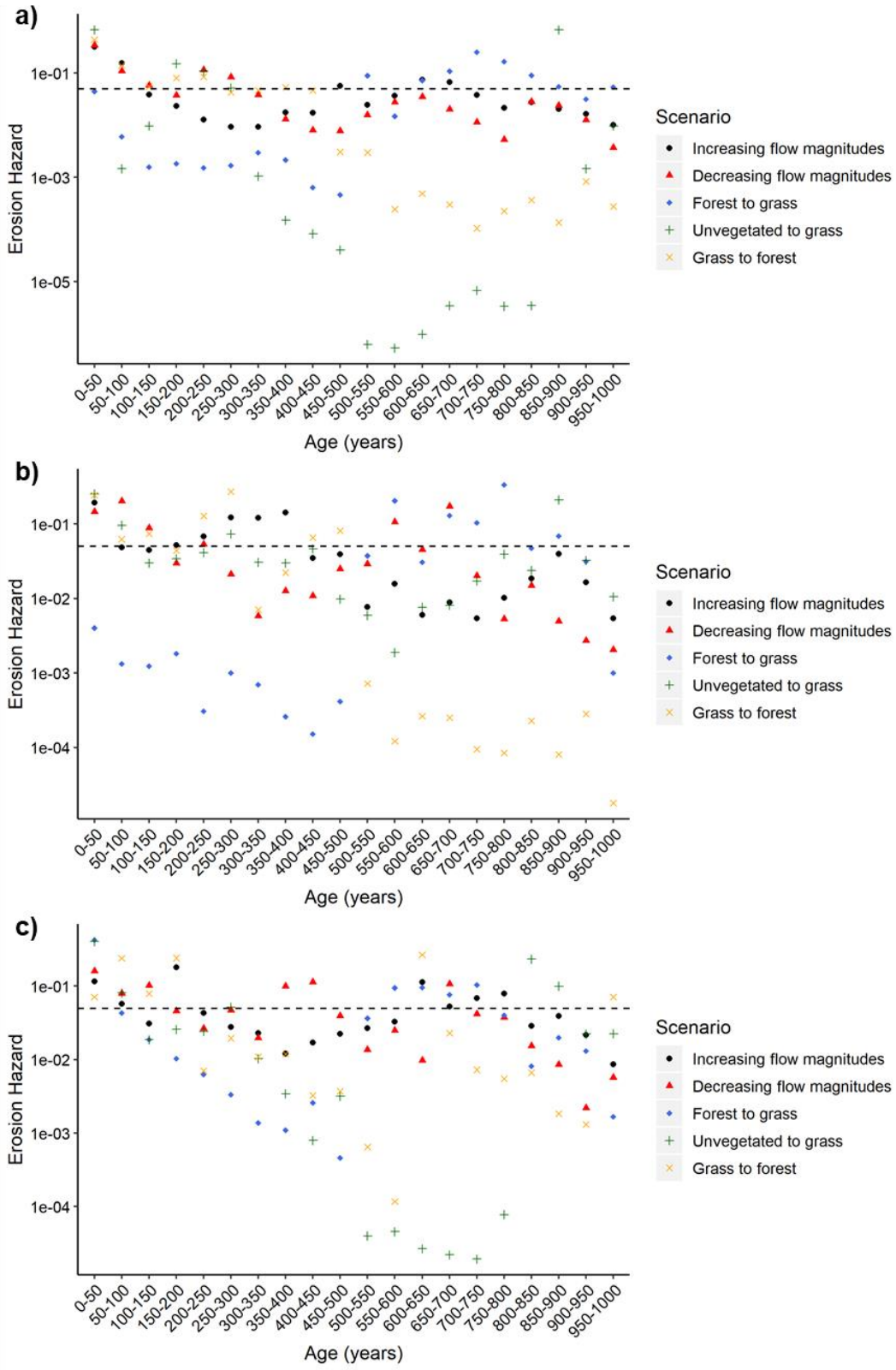

Figure 5.8: Erosion hazards for each of the three sites: Coquet1 (a), Coquet2 (b) and Dane (c) under the five scenarios. Dashed line indicates the uniform erosion hazard value if all sediments of all ages were eroded with equal probability.

5.3.4. Trends in mean ages and mean storage times

Trends in mean ages and mean storage times through time varied between different scenarios and reaches (Figure 5.9). Under the scenarios that induced a reduction in erosion rates (decreasing flow magnitudes, grass to forest and unvegetated to grass), the gap between mean age and mean storage time widened at increasing rates throughout the latter half of the simulations (Figure 5.9). This is further evidence that older sediment ages, tending to be located further away from the channel, are more likely to remain in long-term or permanent storage, while younger sediment, proximal to the channel, will have the highest chance of erosion. Also, it supports that this is particularly the case when erosion rates decline over time and the channel is less able to rework the majority of its adjoining floodplain.

Under increasing flow magnitudes, mean ages and mean storage times for the Coquet1 reach began to converge after ~650 simulation years (Figure 5.9). However, these two trends began to diverge from each other after ~800 years. For the other reaches, mean storage times converged with mean ages around ~500 simulation years, and like Coquet1, began to diverge from each other again after flow magnitudes stopped increasing (Figure 5.9).

Mean ages began to converge with mean storage times immediately after 500 years when forest cover switched to grass cover (Figure 5.9). For both Coquet reaches, the mean storage time values increased enough to exceed mean age for most of the final 500 simulation years. Mean age and mean storage time for the Dane just about converged at ~750 years, after which, these values began to diverge again.

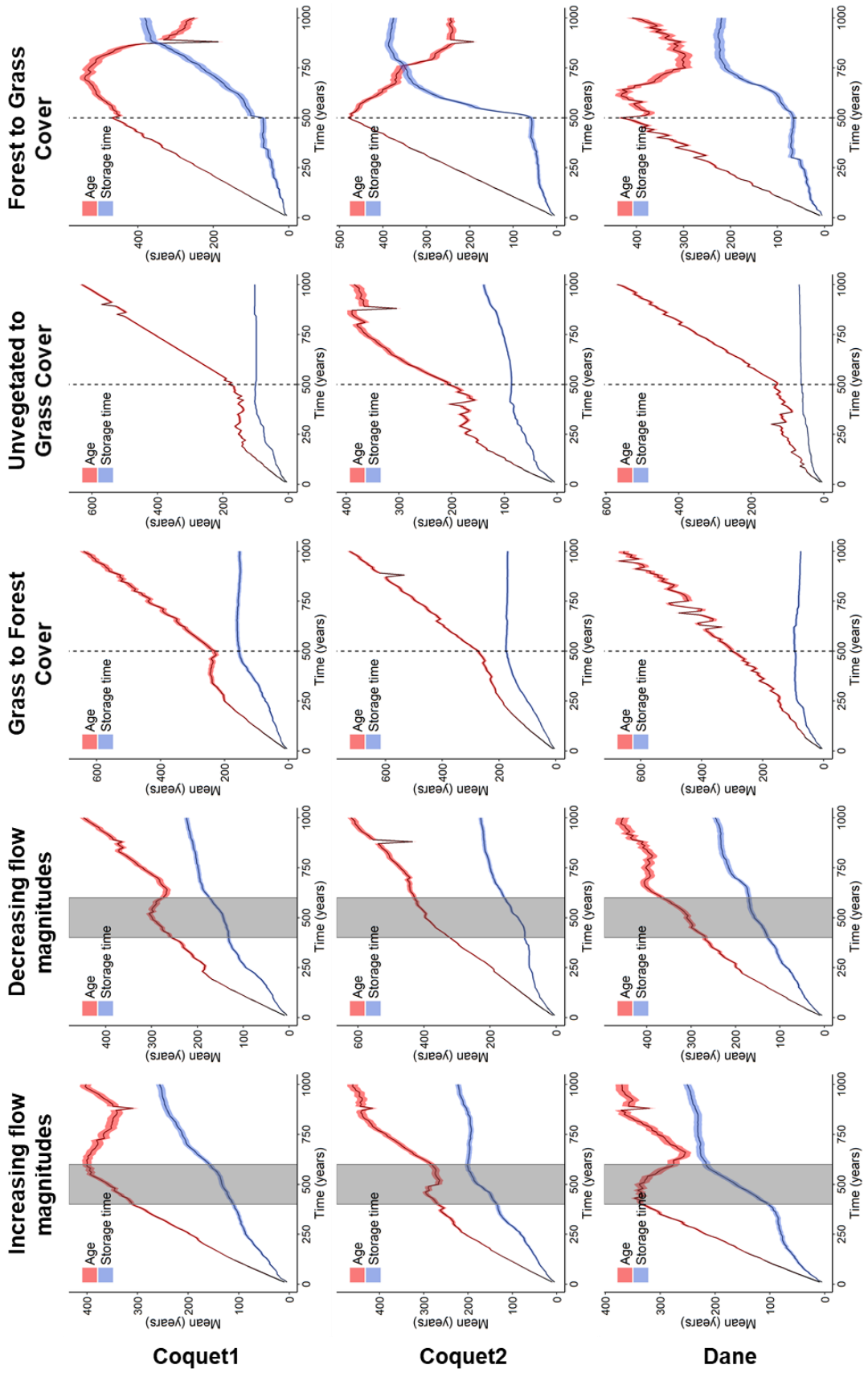

Figure 5.9: Changes in the mean age and the mean storage time (recorded every 10 years) for the three reaches: Coquet1 (top row), Coquet2 (middle

row) and Dane (bottom row) under the five environmental change scenarios. When mean age is equal to mean storage time, it likely indicates equal probability of erosion of sediments of all ages. When mean age exceeds mean storage time, this likely indicates that the probability of erosion decays with age, and vice versa for when mean storage time exceeds mean age. The grey bars indicate the period when changes in flow magnitudes occurred and the vertical dashed lines indicate the timings of vegetation changes. The shaded areas of the trendlines equal the mean ± 2 × the standard error of the mean.

5.3.5. Evaluating the lognormal model fit to storage time distributions

Figure 5.10 compares the best fitting lognormal functions with the empirical storage time data produced during each simulation. For the two changing flow magnitudes scenarios, the model seems to fit well overall for all reaches (Figure 5.10). However, the model is not a good fit for most of the vegetation change scenarios. Storage time values for the grass to forest and unvegetated to grass scenarios displayed steeper decay than the lognormal model could capture. Data for forest to grass simulations were noisy and, based on a visual comparison of the lognormal function curve with the empirical storage time distribution, could not be fitted accurately at all by the lognormal decay model. The Coquet2 unvegetated to grass simulation was the only vegetation change scenario where the empirical storage time distribution could be modelled accurately by the lognormal function (Figure 5.10).

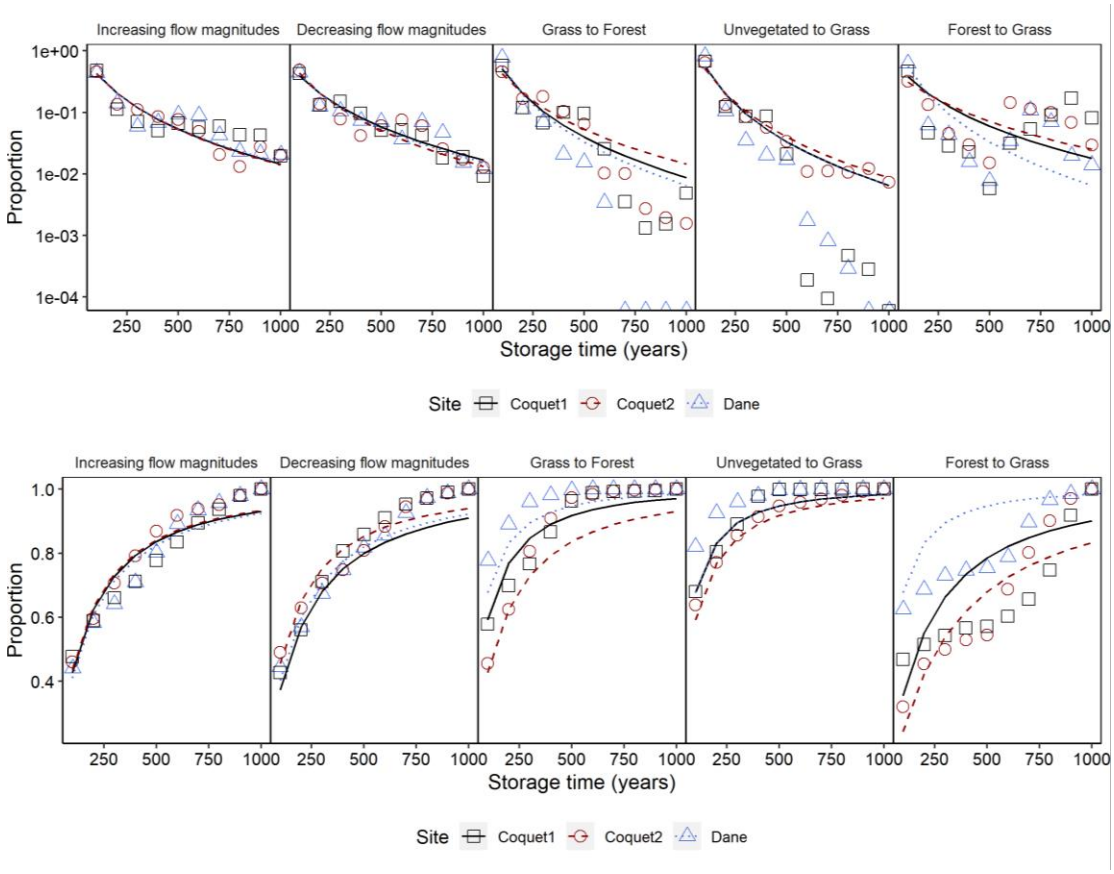

Figure 5.10: TOP – storage time PDFs for each of the scenarios; BOTTOM – storage time CDFs for each of the five scenarios. Lines represent the lognormal distribution curves fitted using the PDF and CDF functions outlined in the methods. Each panel represents data for individual reaches.

5.4. Discussion

This study aimed to address the following questions: 1) Does the removal of sediment from storage depend on the age of floodplain deposits and environmental conditions (in this case, under different scenarios and between different sites)? 2) Does the distribution of sediment storage times change in response to the introduction of an environmental disturbance? 3) Can an existing model of sediment storage behaviour capture the distribution of storage times of disturbed channel-floodplain systems?

5.4.1. Do erosion rates vary across deposit ages and what effect do environmental conditions have on storage behaviour?

Turning to the first two of the above questions, in Figure 5.7, where the age distribution of a simulation is convex and its corresponding storage time distribution is concave, it follows that the erosion fluxes from that floodplain system must be dominated by younger ages, while predominantly older deposits reside in storage (Moody 2017). This is the case for most vegetation change simulations, with the possible exception of the Coquet2 unvegetated to grass cover simulation which shows concave curvature for both the age and storage time distributions (Figure 5.7). Curvature of the age and storage time distributions appear to resemble each other closely for both changing flow magnitudes scenarios. However, the age and storage time distributions are significantly different (Kolmogorov-Smirnov test, $p << 0.05$), and the erosion hazard decays with age (albeit weakly) (Figure 5.8). Comparisons between the mean age and mean storage time over the course of the simulations (Figure 5.9) demonstrate how storage behaviour varies across different vegetation cover types. Under the first 500 years of the unvegetated to grass simulations, mean age and mean storage time values match closely to each other. This suggests that, for an initial 500 years, erosion hazard may not have been correlated with floodplain age. Apart from the Dane simulation, this appears to be the case for the grass to forest cover simulations too. These patterns accord with data from the previous chapter, that if the channel is more laterally mobile, it is more likely to erode sediment containing a broader mix of ages than a channel that is comparatively stable and reworks only the youngest most proximal deposits (Chapter 4).

5.4.2. Does the storage time distribution change in response to a disturbance?

Storage time distributions displayed a concave shape overall, with no noticeable change in their primary shape in most cases (Figure 5.7). The exception was the shift from forest to grass cover scenario, which was significant enough to initiate a change in the shape of the storage time

distributions from concave to convex curvature. Moody (2017) found that several age distributions, quantified from cross-sections of a sediment superslug deposit, exhibited an inflection point, where the curvature of the distributions changed from concave to convex. This evolution occurred as geomorphic activity switched from an early aggradation phase during a flood-rich period to channel incision and stabilisation, increasing the relative proportion of older deposits residing in storage through time. The shift from concave to convex curvature in the forest to grass storage time distributions indicates that as forest is replaced with grass cover, deposits of older ages are eroded with greater fidelity than before. The switch back to concave curvature however, demonstrates that this phase of increased erosion rates of older material is only temporary. Moreover, the difference in the timings of this switch back to concave curvature between the three sites illustrates the variation in sensitivity amongst different reaches.

Apart from the decreasing flow magnitudes scenario, the introduction of a disturbance did appear to affect changes to the mean age and mean storage time through time (Figure 5.9). When vegetation cover switched to more resistant conditions, mean age diverged from mean storage time at an accelerated rate compared to the first 500 years of the simulation. This indicates that as time progressed, the system evolved into one where the youngest ages became the most susceptible to erosion – a fact also supported by the erosion hazard distributions of the grass to forest and unvegetated to grass simulations (Figure 5.8). Increased susceptibility of younger floodplain areas to erosion has been linked to declining erosion rates along the Little Missouri River, USA (Miller & Friedman 2009). The most laterally stable channel systems in the Pacific Coastal Forest region of North America have also been shown to have higher mean floodplain deposit ages than any reaches with laterally dynamic channels (Beechie et al. 2006).

When environmental changes resulted in an increase in erosion rates (such as the increasing flow magnitudes and the forest to grass cover scenarios), reduction in mean age and increases in mean storage time occurred along all reaches (Figure 5.9). This led to a brief period where erosion fluxes consisted of either sediment eroded from a mix of deposit ages or from predominantly

older ages. This compares with data for unvegetated cover simulations from Chapter 4. One theory is that under high erosion rates, the channel (at least temporarily) erodes proportionally more unvisited floodplain deposits than areas of any age that had been visited before. The sharp increase in total floodplain turnover area through time (between 500 and 750 years) for the forest to grass cover simulations supports this theory (Figure 5.11).

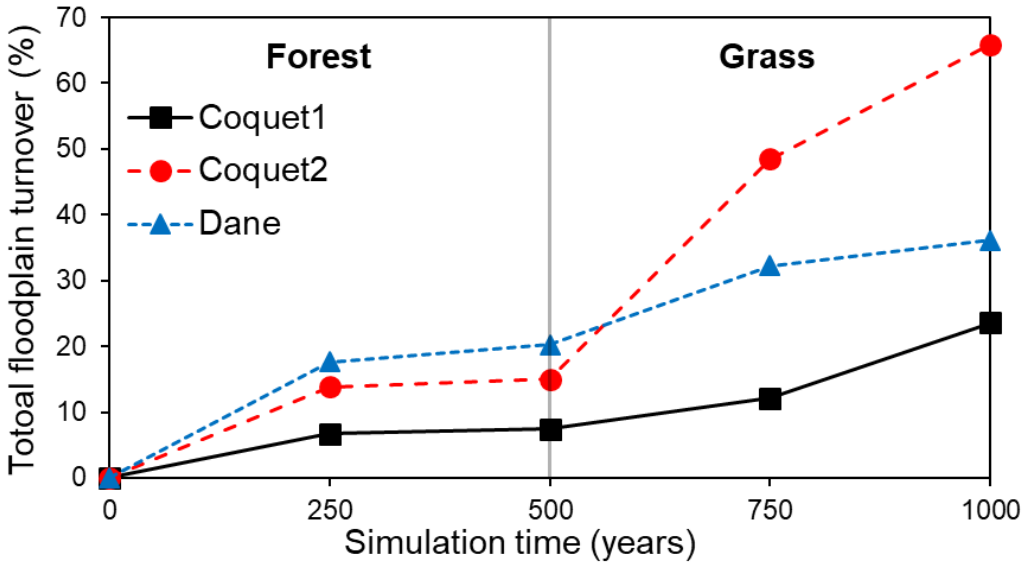

Figure 5.11: Total floodplain turnover area (defined as the area of floodplain to have been reworked by the river channel at least once) for the forest to grass cover simulations.

5.4.3. Can a lognormal function be fitted accurately to describe the storage time distributions of floodplains in disturbed reaches?

Changes in the shapes of the storage time distributions (i.e. between concave and convex curvature) make it difficult, if not impossible, to fit either an exponential or a one-parameter power law function to the datasets produced in this chapter. Moody (2017) for instance, found that two-parameter Weibull functions were necessary to model the distributions of ages and storage times, including changes between concave and convex curvature, of deposits in a sediment superslug. In Chapter 4, comparisons between several two-parameter non-linear functions revealed that in general, storage time distributions were best described by a lognormal function. It was also

suggested that if environmental conditions did not change too much (or at least, were not significant enough to affect overall sediment storage time behaviour), the lognormal function could be extrapolated to predict the distribution of storage times over much longer timescales (Chapter 4).

Application of the lognormal function here produced mixed results across the 15 storage time distributions (Figure 5.10). Scenarios that included gradual changes to flow magnitudes through time were fitted accurately, based on a visual comparison of the lognormal function curve with the empirical storage time distribution by the lognormal function. This suggests that gradual changes in flow magnitudes were not significant enough to alter sediment storage behaviour radically over the course of the simulation. The Coquet2 unvegetated to grass simulation was also modelled accurately using the lognormal function. This may be because, compared to other vegetation change simulations, floodplain erosion rates remained relatively high and the channel continued to erode sediment of a mix of ages.

By contrast, instantaneous changes in vegetation cover were significant enough to alter storage behaviour to the point where the distribution of sediment storage times could not be modelled by a single function. This may have been expected for the forest to grass cover scenario results where the switch from concave to convex storage time distribution curvature (Figure 5.7) and the changes in mean age and mean storage time trends (Figure 5.9) were most pronounced. Despite inducing little change in the overall shape of the storage time distributions (Figure 5.7), the switch from unvegetated to grass (along the Coquet1 and Dane reaches) and from grass to forest did reduce channel lateral migration rates dramatically. As a result, the youngest deposit ages became even more susceptible to erosion, relative to older ages, causing the storage time distributions to decay much more steeply in the latter 500 years than during the first 500 years (Figure 5.10).

Similar to Chapter 4, lognormal functions were not good fits to the age distributions. Instead, Gaussian and Weibull functions were found to be better fits to the age distributions than any of the other tested functions (Exponential, Pareto, lognormal and Gamma) when using the “fitdistrplus” library in R

(Delignette-Muller et al. 2019). This was likely due to the complex shapes of the age distributions which developed as fluctuations in erosion and deposition rates led to alternations between concave and convex curvature – similar to findings from Moody (2017) (see Appendix 3B).

Although it is highly unlikely that the types of vegetation cover changes presented here would occur instantaneously, other sudden onset events such as the deposition of a large superslug following wildfire (Moody 2017) or an instantaneous fault uplift from an earthquake (Coulthard & Van De Wiel 2013) could occur, altering sediment dynamics dramatically. However, these results raise some important questions in relation to how sediment storage times can be modelled in the event of a disturbance occurring within a river system. For instance, is it appropriate to model sediment storage time distributions with more complex models (three or more parameters) or does this risk 'over-fitting' models to datasets? Should sediment storage time distributions only be modelled between disturbance events, and if so, how might this become incorporated into stochastic models of particle trajectories over much longer timescales? These issues will be discussed further in Chapter 6.

5.5. Conclusions

Channel changes for three 1 km-long river valley reaches under an ensemble of gradual and sudden-onset disturbance scenarios were modelled in CAESAR-Lisflood. Channel-floodplain evolution varied widely across different simulations, with instantaneous changes in vegetation inducing the most abrupt and significant changes in channel morphodynamics. River channels stabilised laterally as soon as grass cover switched to forest cover, and became highly active when vegetation cover changed in the opposite direction. Responses to disturbance events also varied between reaches, highlighting the importance of site-specific controls on floodplain erosion dynamics and sediment storage behaviour. For example, a switch from unvegetated to grass cover transformed one reach from an avulsing and braided system into a laterally stable single channel, while in another reach,

the main channel continued to rework its floodplain as a rapidly migrating meandering system.

The shapes of age and storage time inverse CDFs were generally concave and convex, respectively. This, along with erosion hazard distributions and timeseries of mean age and mean storage time trends, indicated that predominantly older sediment was retained in storage while erosion fluxes mainly consisted of younger ages. Distributions of sediment ages and storage times were also shown to change in shape in response to some disturbances, particularly when erosion rates increased significantly. For instance, a change from forest to grass cover after 500 years of simulation time caused the storage time distribution to change from concave to convex curvature, as floodplain deposits of older ages began to be eroded proportionally more as the channel became more laterally mobile.

Lognormal functions were fitted to the storage time distributions in an attempt to best describe the sediment storage behaviour of each of the simulations. The lognormal function was found to be a good fit for each of the changing flow series scenarios, suggesting that overall sediment storage behaviour was insensitive to gradual increases or decreases in streamflow magnitudes. However, with the exception of one simulation, instantaneous changes in vegetation cover had a significant enough impact that a single lognormal function could not model accurately, based on a visual comparison of the lognormal function curve with the empirical storage time distribution, the full distribution of sediment storage times. This raises important issues about how best to model sediment storage behaviour in channel-floodplain systems, particularly over geological timescales and in systems that may be sensitive to rapid-onset large-scale disturbance events. Questions such as whether to use more complex non-linear functions (e.g. three or four-parameter models) to represent storage time behaviour, or whether to incorporate multiple storage time distribution functions into stochastic models of particle trajectories, will need to be addressed if we are to improve predictions of sediment travel times through valley floor corridors.

CHAPTER 6:

Synthesis

6.1. Extended Discussion

Storage time defines the length of time sediments will reside in storage in a landform such as a floodplain. Better understanding of sediment storage times in floodplains is necessary to calculate the storage and fluxes of organic carbon in river systems (Sutfin et al. 2016; Torres et al. 2017), model the dispersal of contaminated particles through river networks and valley corridors (e.g. Malmon et al. 2003; Pizzuto et al. 2014), and to gain insight into the chemical weathering of stored grains, which may contribute to the downstream fining of fluvially transported sediments (Johnson & Meade 1990). Simulations of channel changes over 1000 years run using the CAESAR-Lisflood landscape evolution model (LEM) were developed to explore the distributions of storage times for floodplain sediments across a variety of environmental conditions and gradients of environmental change. The findings presented in Chapters 4 and 5 provide new insights into how channel-floodplain systems may evolve under changing and different conditions and how these relate to the storage and release of sediments. Applying CAESAR-Lisflood to hindcast recent channel changes over multi-annual to multi-decadal timescales demonstrates the model can reproduce changes quantified from historical maps and aerial imagery with some accuracy. Further, the dynamics of floodplain sediment turnover calculated from mapped process rates were replicated closely overall in the simulated process rates. From this, one gains confidence that the channel changes simulated over longer timescales are realistic and these findings provided the foundation for further investigation of sediment storage behaviour in floodplains.

The three reaches used to quantify sediment storage time behaviour revealed complex and varied responses to differing experimental and environmental conditions, including the model set-up (i.e. how frequently channel changes and storage times were recorded), the types and scales of vegetation cover, and the environmental disturbance scenarios used in simulations. These responses were captured in the shapes of the storage time distributions of floodplain sediment after 1000 years. Storage time distributions are modelled – rather than just a single average value – because sediment will enter and leave storage at different times. Further, there is no guarantee that rates of

sediment accumulation and removal are constant. Indeed, the shape of the storage time distribution can show whether erosion rates are in fact constant, with exponential decay model fits confirming this, and heavy-tailed, strongly right-skewed model fits refuting this. While it was possible to fit a single non-linear function to most storage time distributions (a two-parameter lognormal function, which indicates erosion rates vary with floodplain deposit age), some disturbances were significant enough to "reset" the distribution and invalidate the model fits in these cases. Nevertheless, the modelling undertaken in this thesis represents perhaps the most comprehensive investigation of sediment storage time dynamics in fluvial systems to date. Here, the extent to which the four key research questions (Chapter 1) have been addressed, the limitations of this research, and the wider implications extending beyond the scope of the papers developed in this thesis, is assessed.

Research Question 1) Identifying an approach to quantifying the timescales of sediment storage in floodplains and the effects of varying environmental controls

Approaches that aim to quantify sediment storage and delivery timescales in fluvial systems have been ongoing for decades (see Dietrich & Dunne 1978; Dietrich et al. 1982 for early examples), and this research has contributed important sediment flux data to models of particle trajectories and contaminant dispersal (e.g. Malmon et al. 2002, 2005; Pizzuto et al. 2017). Quantification techniques have become more sophisticated over time, evolving from simple one-dimensional mass balance approaches based on sediment budgets (e.g. Dietrich & Dunne 1978; Dietrich et al. 1982; Kelsey et al. 1987) to methods that either infer a storage time distribution from a population of ages (e.g. Lancaster & Casebeer 2007; Lancaster et al. 2010; Skalak & Pizzuto 2010) or calculate storage times directly from timings of erosion processes at specific points in space (e.g. Bradley & Tucker 2013; Moody 2017; Torres et al. 2017). As methods have developed and attempts to quantify sediment storage time dynamics have proliferated, several important questions have emerged including:

i. Does the probability density function of storage times decay as an exponential or a heavy-tailed power law (or similar) distribution?
ii. Is the probability of sediment removal from storage uniform with age or does it increase as a linear function or decrease as a power law?
iii. To what extent do environmental controls (e.g. sediment supply and grain size distribution, discharge, vegetation cover and presence of in-stream wood) affect distributions of storage times?
iv. How do significant changes in environmental conditions during a monitoring or modelling period affect the shape of the storage time probability density functions?
v. How might the above four questions affect models of stochastic particle trajectories and delivery times?

The paucity of attempts to review or synthesise storage time literature was the primary motivation for the literature review (Chapter 2). The review of sediment storage time quantification literature shows that both exponential and power law distributed storage times are possible. Exponential distributions imply that floodplain erosion rates are constant over time. Effectively, this treats the longevity of sediment storage as analogous to a radionuclide with a “half-life”, which can be extrapolated to predict when complete sediment exchange between the channel and floodplain occurs (turnover time). Power law fits on the other hand, suggest erosion rates vary across the floodplain surface, with erosion rates declining with increasing floodplain deposit age. When the balance between impelling and resisting forces (*sensu* Fryirs & Brierley 2013) is tilted towards increased resistance, river channels are more likely to (re)occupy and erode areas of the floodplain that were abandoned most recently, increasing the proportion of younger material leaving storage relative to older material, thus producing a strongly right-skewed distribution (e.g. Miller & Friedman 2009; Konrad 2012). Conversely, when erosion rates increase (e.g. when rates of sediment supply to a reach fall, leading to “hungry water”) an increasing proportion of older ages become susceptible to erosion, skewing the distribution of storage times in the opposite direction to when erosion rates are lower (e.g. under more resistant land cover) (Moody 2017).

Building on the findings presented in the previous paragraph, a conceptual model was devised to illustrate the various impelling and resisting force controls (and their interactions) on storage times, and to guide future research that could quantify their effects (Figure 2.13). This conceptual model was used to support the rationale for modelling channel-floodplain evolution, study site selection and the scenario design used to explore Research Questions 3 and 4. LEMs were discussed in Chapter 2 as tools which could be used to quantify storage times of floodplain sediments and their controls. Advantages of a landscape evolution modelling-based approach include: i) overcoming data limitations and restrictions on temporal scale and resolution of other available techniques (see Chapter 2), ii) applicable over a range of spatial scales, from whole river basins to field plots, and iii) the ability to simulate, and control for, the effects of environmental drivers, including vegetation cover, flow magnitude variability and changing sediment supply rates, on channel-floodplain evolution.

The three test reaches, taken from the Coquet and Dane river systems exhibit a range of estimated floodplain turnover times (Chapter 3). They also demonstrate an apparent sensitivity in storage time dynamics to environmental conditions, including commonalities in their responses to different vegetation cover settings (discussed further in Research Question 3) as well as under different disturbance scenarios (see Research Question 4). However, subtle differences between these reaches in their sensitivity to environmental conditions were also identified.

Research Question 2) Exploring the drivers and conditioning of historical channel dynamics for reach-scale alluvial floodplains using a landscape evolution model

The ability of the CAESAR-Lisflood model to simulate reach-scale fluvial geomorphic processes was first established more than a decade ago (Coulthard & Van De Wiel 2006; Van De Wiel et al. 2007). However, despite its pedigree of reach-scale applications (e.g. Ziliani & Surian 2012; Ziliani et al. 2013; Howard et al. 2016), CAESAR-Lisflood has not been subject to the same level of rigorous testing at reach-scale as it has at catchment-scale. In

particular, this includes evaluating the accuracy of modelled process rates against multiple assessment criteria of varying importance and the possibility that parameters calibrated for one reach can be applied to an untested reach to simulate geomorphic changes. Results across the ten sites tested in this thesis support the calibration of CAESAR-Lisflood model parameters in replicating accurately known patterns of river channel changes. Further, in some circumstances, the calibrated values for parameters governing lateral channel erosion rates for a tested reach could be applied directly to an untested reach with similar characteristics. In these cases, modelled geomorphic changes, including erosion, deposition and lateral migration rates were similar to rates derived from mapped historical reconstructions. However, because very large errors occur for some of the sites between the mapped data and the most accurate simulation, site-specific parameterisation of CAESAR-Lisflood is recommended.

Reach erosion rates were normalised by dividing by the total area and correlated against the percentage of the simulated total floodplain occupied by the channel at least once. Here, relationships between erosion rates and the extent of channel occupation of the floodplain were identified, with similar linear functions derived for both the mapped and modelled datasets (Figure 3.9). When these linear functions were extrapolated to estimate floodplain turnover times, values ranged from ~100 to ~1000 years across the ten sites, providing a preliminary indicator of how the variability in reach-scale geomorphology influences sediment storage behaviour. Not only are these predictions within the range of reported values in Chapter 2; Figure 2.5 – further affirming the simulations reflect real-world sediment storage dynamics, they provide partial justification for simulating channel changes over 1000 years in Chapters 4 and 5. Additionally, estimated turnover times illustrated the degree to which errors associated with poorly predicted erosion rates could propagate. For example, using parameter values calibrated for the Coquet1 reach, modelled erosion rates along the South Tyne1 reach were under-predicted by ~85 %, while the estimated floodplain turnover time was over-predicted by ~400 %. This reinforces the importance of undertaking a thorough calibration process on a site-specific basis if “realistic” river channel dynamics

are to be simulated. Thus, attempts to simulate geomorphic processes across multiple sites should account for the need to parameterise on a site-specific basis when planning the timing and delivery of modelling projects.

Research Question 3) Quantifying the distributions of sediment ages and storage times from landscape evolution model simulations

There are several examples of using numerical models to simulate river channel changes and then derive distributions of floodplain ages and sediment storage times (Chapter 2). These have tended to utilise a planimetric centreline evolution (1-D planform) model of some form, such as the Ikeda, Parker & Sawai model (Ikeda et al. 1981), that simulates the lateral migration of single-thread meandering channel systems. As the general composition of lateral storage reservoirs in fluvial systems and associated lateral fluxes control changes to the floodplain age distribution, and because the occurrence of cut-offs is designed to stabilise the long-term average river geometry around a statistically steady-state (Camporeale et al. 2008), 1-D planform models have been the favoured approaches to derive floodplain age distributions and explore their controls (Lauer 2012). However, because floodplains develop via channels braiding and avulsing, as well as scroll meandering (Nanson & Croke 1992), and not simply along point bars as channels migrate laterally (see Wolman & Leopold 1957), this limits the amount that 1-D planform modelling can tell us about sediment storage times.

Chapters 4 and 5 represent probably the first attempt to model the age and storage time distributions of floodplain sediments using a LEM that simulates both multi- and single-thread channel dynamics. A total of 36 storage time distributions for an ensemble of model conditions, combining differences in site, vegetation cover, river flow (climate) and frequencies (or time-steps) over which channel changes were recorded, revealed important insights into the nature and controls over the sediment storage behaviour of floodplains (Chapter 4). First, the vast majority of storage time distributions were right-skewed and heavy-tailed, and could not be fitted by an exponential function, indicating that younger ages were more likely to dominate storage time distributions. This confirms the findings of much of the floodplain sediment

storage time quantification literature (e.g. Miller & Friedman 2009; Konrad 2012; Skalak et al. 2015) including some approaches that utilised river channel change modelling (Bradley & Tucker 2013; Torres et al. 2017). Second, although exponential models were poor fits to the storage time distributions, it was found that lower resistance conditions (i.e. grass and unvegetated cover) were more likely to indicate that the probability of a floodplain area eroding would not be dependent upon age (see Research Question 4 for further discussion). This was also the case when channel changes were recorded less frequently (e.g. every 100 years vs every 10 years). When channel changes were recorded less frequently, there were greater areal extents of floodplain erosion and deposition that were likely to be unquantified than if channel changes were recorded more frequently. If the floodplain in question was characterised by a strongly right-skewed storage time distribution, then the proportion of younger ages that were unrecorded would exceed the proportion of older ages that were unrecorded. This is important, because shorter-term dynamics (e.g. erosion and deposition via fluctuations in channel width) would be missed, under-quantifying short storage times associated with these processes. Similar phenomena have been highlighted in measurements of stream water transit times. Isotope measurements sampled at higher resolutions than the typical weekly intervals developed more strongly right-skewed transit time distributions, with lower mean values of 5 years vs 9.5 years (Stockinger et al. 2016).

To predict the distribution of storage times for untested locations and over longer timescales than 1000 years, a lognormal function was proposed as an accurate model of sediment storage times. Testing of environmental variables revealed that the standard deviation of the lognormal function (the parameter, σ) could be predicted from the time-step of recorded channel changes. As both age-dependent and age-independent erosion rates and storage time dynamics are possible, it is more appropriate to use the median than the mean (which is more sensitive to skew in the distribution) as a potential predictor of the mean log (μ) parameter of the lognormal function. Assuming steady-state conditions in sediment flux rates, the median should converge to a stable value throughout time, regardless of whether floodplain erosion is age-dependent.

The long-term stability of these two parameter values could mean that a lognormal curve that has been fitted to a 1000-year dataset might be extrapolated to predict the storage times of floodplain sediment over longer time periods (e.g. 10,000 years) – though this is an idea that requires further testing. If geomorphic changes were reconstructed (e.g. using LEM simulations), a lognormal function that was representative of sediment storage times over thousands of years could facilitate the quantification of sediment storage dynamics in reach-scale valley floor systems over the Holocene. This would enhance our understanding of how environmental change impacts on the transmission of sediment signals (e.g. superslugs) in river catchments. Lognormal curves, generated using μ and σ parameters estimated from two logarithmic relationships (see Chapter 4: equations 9 and 10) were found to fit accurately to datasets from Chapter 4. Thus, there appears to be scope to apply the lognormal function derived here to untested analogous sites. If a stochastic sediment transport model was parameterised using this lognormal function and process rates, such as the velocity of sediment particles in transport, the delivery times of any contaminated sediments could be predicted (see Pizzuto et al. 2017). This would have useful environmental management implications including designing remediation strategies of polluted soils and water courses.

Research Question 4) The sensitivity of storage time dynamics in floodplains to different environmental conditions

Several studies have quantified the effects of one or more variables on floodplain sediment storage time dynamics. Miller and Friedman (2009) for example, described the effect of declining flow magnitudes on mean annual erosion rates, and how this increased the susceptibility of the youngest-aged deposits to erosion. Similar patterns emerged from the CAESAR-Lisflood simulations run under uniform environmental conditions. Under forest cover, mean annual erosion rates were at their lowest for all reaches, restricting the total floodplain area the channel eroded over time. This had the effect of restricting erosion to the youngest floodplain deposits which lay closest to the channel and were least likely to be covered with fully mature trees – according with results from other forested floodplain systems (Gottesfeld & Johnson

Gottesfeld 1990; Nakamura & Kikuchi 1996; Konrad 2012). In contrast, grass and unvegetated conditions permitted greater lateral mobility of the channel, allowing a higher proportion of older sediment deposits to be eroded (Chapter 4). Chapter 4 represents the first attempt to compare the effects of different environmental conditions on storage times within the same set of reaches.

Fluvial systems are subject to a variety of sudden-onset disturbance events and gradual fluctuations in environmental conditions, with the responses ranging from the transmission of sediment superslugs through valley floors (Moody 2017) to changes in long-term average erosion rates over 10^3-10^4-year timescales in response to land-use changes (Hoffmann 2015). These all have implications for the longevity of sediment storage in floodplains. Determining the impacts of environmental change on sediment storage times is therefore an important, but, largely unexplored step in storage time distribution modelling.

The 15 simulations undertaken in Chapter 5 reveal interesting patterns in the response of tested reaches to different environmental changes. Although gradual increases and decreases in daily flow magnitudes were significant enough to influence floodplain erosion rates (Figures 5.2-5.5), storage time distributions could still be modelled accurately with a lognormal function, using the same methods of parameter estimation as outlined in Chapter 4. By contrast, an instantaneous shift in vegetation cover after 500 years was powerful enough to not only impact erosion rates, but changed the shape of the storage time distribution to the extent that the lognormal function was no longer an appropriate model. A further complication was the difference in response of reaches to some scenarios. For example, when conditions switched from unvegetated to grass cover, the Coquet1 and Dane reaches metamorphosed from braiding and avulsing channels to laterally stable channel systems (Figure 5.2 and 5.4). By contrast, the Coquet2 exhibited an interesting equifinality in sediment storage behaviour between the two phases of vegetation cover. While the channel also metamorphosed as soon as grass cover was introduced, erosion rates remained high as the channel continued to laterally migrate. As a result, the shape of the storage time distribution under unvegetated conditions was preserved throughout the 500 years of grass

cover, and the entire distribution over 1000 years was well-fitted by the lognormal function.

Overall, this thesis demonstrates that there are sufficient commonalities across floodplain conditions to fit the same type of function (a lognormal model) to the distribution of storage times in most cases, using a sub-set of easily obtainable data (such as the median storage time and the frequency of storage time measurements). However, the apparent sensitivity of some storage time distributions to sudden-onset disturbance events raises some important issues. Sediment delivery – particularly in large sediment-routing systems (≥1000 km long) – occurs over geological timescales (Pizzuto et al. 2017), far beyond the timescales simulated in this thesis. Given that significant environmental changes, including multiple large disturbance events can occur over geological timeframes, accounting for the evolution of storage time distributions over time will be important for future stochastic modelling of sediment delivery.

6.2. Limitations and Further Work

A novel method of quantifying sediment storage time distributions has been established and tested successfully on multiple floodplains under different environmental conditions. However, a number of limitations related to the choice of LEM, calculation of deposit ages and storage times, and experimental design, including scenarios and model boundary conditions need to be addressed:

i. The evaluation of CAESAR-Lisflood in this thesis has contributed important information on the ability of this model to simulate historical reach-scale channel changes over multi-decadal timescales. However, because of the relatively short time span of overlapping map and daily flow records and a paucity of historical maps and aerial images to quantify channel changes during this period for most sites, only one time-interval per reach was used for evaluation. Assessing model accuracy against several time-intervals of channel changes would

increase confidence in the choice of erosion rate parameter settings. Further, it would allow a more thorough assessment of floodplain turnover dynamics, such as channel reoccupation rates (Konrad 2012) or surface age reconstruction (Miller & Friedman 2009) to be undertaken. Acquiring additional time-intervals could have been achieved by focussing only on sites with long overlapping map and daily flow records (as well as sites with several map and aerial images over this period) or by running CAESAR-Lisflood in catchment mode first to extend the daily flow record by several more decades. The problem with both approaches is they increase data demands to such an extent that it would be difficult to cover as many as ten reaches. Another issue with the latter approach is that daily flows generated by catchment-scale simulations will be offset from "real-world" values by a degree of error which could propagate through subsequent reach-scale simulations, potentially calling the calibration of lateral erosion rate parameters into question.

ii. Daily mean flow data were used to drive CAESAR-Lisflood simulations throughout this thesis. In part, this was due to the ready availability of daily mean flow data from the National River Flow Archive website, and in part to keep run times for CAESAR-Lisflood tractable – particularly the 1000-year simulations where some of them would take ~1 month to complete with daily timesteps. However, as daily flow data provide only a mean value for each day, and nothing about the distribution or range of flows that might have occurred within that particular day. This is an important issue for the Dane and Coquet at least, as even a cursory observation of the annual hydrographs of the gauges at these reaches (Rudheath for the Dane and Rothbury for the Coquet) shows that the stream discharge can often vary over multiple orders of magnitude in a single day (e.g. from <1 to ≥100 $m^3 s^{-1}$) (UKCEH 2020). This does not necessarily call the results of Chapter 3 into question, as calibration was carried out using daily flow data, although it may contribute towards explaining the issue of under-estimated erosion and lateral migration rates by the model. However, it may have a significant impact on the results of the 1000-year simulations, including the timing/frequency of

meander bend cut-offs forming and the rates of lateral erosion that are detectable at 10-year sampling frequencies. The effect this might have on the resulting floodplain surface age and storage time distributions is something that would merit investigation, as it may be a limitation that needs to be stressed in future long-term landscape evolution modelling studies.

iii. Due to a lack of available sediment transport data for the tested river systems in this thesis, CAESAR-Lisflood simulations were run with the sediment recirculation utility switched on in order to maintain some kind of sediment transport time-series that could be fed into the reach at the beginning of every time step. Two issues occur with this approach, however. First, it is assumed that recirculating sediment from the end of timestep, n to the start of timestep, $n+1$ is an accurate substitute for the sediment transport that actually occurred (or would have occurred) at that time. Obviously, if a time-series of historical sediment transport data existed for the tested reaches, with which the time-series of sediment transport generated by the recirculation utility could be compared against, there would have been no need to recirculate sediment transport in the first place. However, even if it could be concluded that the sediment transport time-series generated by recirculating sediment over successive model iterations was accurate, in general, the second issue concerns a potential positive feedback mechanism. For example, if there is a large amount of lateral erosion by the channel towards the outlet of the reach, a large pulse of sediment will be generated and recorded at the end of timestep, n. Subsequently, the sediment flux that is fed into the inlet of the reach at the beginning of timestep, $n+1$ will be elevated as a result of the high erosion rates of the previous timestep. This in turn might drive higher lateral erosion rates, producing elevated sediment flux rates at the reach outlet that are recirculated again. Over 1000 years, this will drive lateral erosion rates that may be much higher than they should be for the reach in question. Consequently, this may influence the form of the age and storage time distribution (e.g. producing an exponential decay curve as

a result of more even floodplain turnover across different ages, when a power law or lognormal function may occur otherwise). One solution to this may be to run a simulation with a sub-set of the total flow series (e.g. the first 10% of the total flow series) with the sediment recirculation utility switched on. Then, use the sediment flux data generated from this initial run to create a time-series of sediment fluxes for a full 1000 years to drive the 1000-year simulation without the sediment recirculation utility switched on.

iv. Estimated floodplain turnover times for the ten reaches suggest that all sediments will be exchanged with the channel within 100 to 1000 years (Chapter 3; Figure 3.10), and this was used to justify the 1000-year timeframe of channel change simulations in Chapters 4 and 5. However, this assumes that erosion rates will remain constant over time and the cumulative area of floodplain occupation by the channel will increase linearly. Rivers tend to reoccupy parts of the floodplain that have just been abandoned by the channel (O'Connor et al. 2003), meaning that even if all areas of the floodplain are eroded by the channel, floodplain turnover times will likely exceed the 100-1000 year timeframe estimated in Chapter 3. Simulations of the Coquet1, Coquet2 and Dane reaches revealed that the whole floodplain was not reworked by the channel over 1000 years. While Figure 4.10 shows that the cumulative area of floodplain occupation by the channel plateaus within 1000 years, extending analysis beyond this timeframe could have allowed further testing of effects of environmental changes on sediment storage times. The literature is replete with examples of reconstructions of valley floor evolution and associated drivers, extending right the way through the Holocene (including for the Dane - see Hooke et al. 1990), which could provide the basis for additional experimental scenario testing. It should be noted though, that another justification for simulating over 1000 years was the lengthy run times of CAESAR-Lisflood. In some cases, it took a month to complete a single simulation.

v. Floodplain sediment age and storage time calculations were derived from planimetric river channel changes and did not account for vertical processes of sediment exchange (overbank deposition and incision).

This is problematic given the formation and eventual reworking of alluvial terraces are a natural component of sediment exchanges within valley floors over multi-centennial (and longer) timescales. Addressing this is not a simple task, however. Depositional and erosional changes were measured over pairs of sequential planform channel positions, spaced apart by a specified time-interval (e.g. 10 years). Initially, age and storage time calculations are very simple, with erosion during the first time-interval producing a storage time value equal to half the time-interval length and deposition producing an age also equal to half the time-interval length. Any undisturbed floodplain increases in age by the length of the time-interval. However, as time goes on, deposits of a range of ages will be eroded, and the deposition of new floodplain surfaces will widen this range further. As the number of time-intervals increases, this creates an increasingly complex accounting problem, which becomes even more intractable when vertical geometric changes are incorporated too – an issue identified in earlier storage time literature (see Moody 2017). Accounting for this problem in 2-D planform perspective was achieved by using similar approaches to track floodplain ages to those in existing literature (see Greco et al. 2007 and Bradley & Tucker 2013 for examples). One solution may be to modify the CAESAR-Lisflood code to calculate age and storage times as a result of vertical erosion and deposition processes. However, even if this were to be undertaken, evaluating geomorphic changes and the resulting effects on floodplain ages in 3-D would be hampered by a lack of long-term measurement data with which to parameterise and compare simulations.

vi. Sediment storage time dynamics varied with environmental conditions including vegetation cover and stream discharge, with tested reaches exhibiting some key similarities and differences in their behaviour. The tested scenarios do not represent the total range of environmental controls, nor do the three reaches encapsulate the entire taxonomy of floodplain environments (Nanson & Croke 1992). Further work could include quantifying the effects of varying sediment supply, different grain size distributions, valley confinement effects (e.g. Howard 1992),

tectonic uplift scenarios (e.g. Coulthard & Van De Wiel 2013) and the effects of heterogeneous erosion surfaces conditioned by geology and vegetation cover (*sensu* Larsen et al. 2006). If lengthy run times of the CAESAR-Lisflood model could be mitigated, larger reaches than 1 km in length could also be simulated to see if the storage time dynamics are replicated. Further, recent analysis of 40 years of satellite imagery has revealed that river confluences are much more laterally dynamic than thought previously (Dixon et al. 2018). Given their importance in controlling downstream routing of sediments (Dixon et al. 2018), river confluences could be an important environment in which to quantify sediment storage times – especially for large river basins like the Ganges or the Amazon.

6.3. Concluding Remarks

Sediment storage time dynamics, including controls, implications for the wider environment, and methods of quantification and analysis have been comprehensively reviewed. Here, the strengths and limitations of different approaches, and the identification of key research gaps – particularly the effects of environmental drivers such as streamflow and vegetation cover – helped to formulate the four key research questions and overall aim and objectives of this thesis.

A landscape evolution modelling approach, using CAESAR-Lisflood to simulate river channel changes over long timescales, was adopted to constrain the distributions of sediment storage times in alluvial floodplains. Reconstructed river channel changes using historical maps and aerial photos provided a useful set of metrics (planform morphology, lateral migration rate, erosion rate and deposition rate) with which to calibrate CAESAR-Lisflood and to evaluate the accuracy of simulated channel-floodplain evolution. In general, simulated river channel changes corresponded closely with mapped datasets, and there was some possible transferability of calibrated parameter values from one reach to an untested reach, though it is recommended that model calibration should be undertaken on a reach-by-reach basis. Although the

period over which calibration/evaluation was conducted was relatively brief (~15-25 years), both mapped and modelled datasets produced similar relationships in terms of estimated long-term floodplain turnover dynamics, increasing confidence in the model parameterisation.

Estimated floodplain turnover times ranged between ~100 and ~1000 years across the ten tested reaches. Three of these reaches – incorporating both ends and a mid-point of this turnover time range – were the focus of storage time distribution modelling. Channel changes were simulated over 1000 years, considering the estimated turnover time range, with floodplain deposit ages and storage times calculated from planimetric geomorphic changes. Sediment storage time distributions were sensitive to model time step (i.e. the frequency of recorded channel changes), highlighting potential issues in comparing storage time behaviour across different studies. A lognormal function, using model time-step and median storage time to predict the two parameters of this equation, was found to fit the storage time data well overall. In terms of potential applications, this lognormal function could be applied to an untested, heavily polluted reach to predict the time it would take sediment removal from a floodplain to decontaminate a valley floor.

Storage time behaviour varied widely under different vegetation cover types. Highest erosional resistance conditions under forest cover restricted erosion rates to the very youngest deposits, creating a strongly right-skewed and heavy-tailed storage time distribution. Under weaker erosional resistance conditions (grass and unvegetated cover), a wider range of floodplain ages were eroded and storage time distributions were more likely fitted by an exponential decay function (though other non-linear models remained better fits). Storage time distributions changed shape in response to instantaneous vegetation cover changes. Vegetation cover appeared to be a much greater influence on the lateral dynamics of river channels, hence a switch from unvegetated to grass cover metamorphosed channel patterns from braided to meandering. This invalidated fitted lognormal functions, though with one exception where high lateral migration rates under grass cover continued to rework a wide range of deposit ages with similar fidelity to the braided channel when no vegetation cover was present.

Sediment-routing models predict the distribution of sediment delivery times to catchment outlets, with significant implications for stratigraphic sequences in depocentres (e.g. floodplains, lakes and deltas) and the throughputs of contaminants in river networks. As these types of model are stochastic by design, they require an accurate probability density function of storage times to generate robust predictions of sediment delivery from source to sink. This thesis contributes important advancements towards this goal. This includes simulating multi-thread channel changes in addition to the single-thread dynamics of earlier storage time studies, as well as the investigation of different experimental set-ups (frequency of recorded channel changes and comparison of multiple reaches) and testing a wide ensemble of environmental change simulations. Further work is needed to quantify the effects of other environmental controls, over longer timeframes and covering a wider range of floodplain systems. In addition, efforts should be made to incorporate geomorphic changes in 3D to obtain a more holistic picture of the temporal dynamics of sediment storage. Such improvements in our understanding of storage times in fluvial landforms, such as floodplains, will bring important new insights into the effects of environmental change on landscape evolution. Indeed, results from U-series dating techniques have already demonstrated the impacts of climate and vegetation cover shifts on sediment delivery through river catchments worldwide (see Figure 2.15 and references from which the figure was derived). Interest in modelling the cycling of carbon in the terrestrial biosphere is likely to intensify in the face of climate change, and the presence of microplastics in waterways is likely to continue to attract attention. As carbon cycling and microplastics in waterways have been linked to sedimentary environments and processes in river systems, it is imperative to gain better understanding of sediment storage times in order to enhance our ability to monitor and manage these two emerging issues more effectively.

References

Aalto, R., Lauer, J.W. & Dietrich, W.E., 2008. Spatial and temporal dynamics of sediment accumulation and exchange along Strickland River floodplains (Papua New Guinea) over decadal-to-centennial timescales. *Journal of Geophysical Research: Earth Surface*, **113**(1), 1–22.

Ahmed, J., Constantine, J.A. & Dunne, T., 2019. The role of sediment supply in the adjustment of channel sinuosity across the Amazon Basin. *Geology*, **47**(9), 1–4.

Allen, P.A., 2008. From landscapes into geological history. *Nature*, **451**(7176), 274–276.

Almond, P., Roering, J. & Hales, T.C., 2007. Using soil residence time to delineate spatial and temporal patterns of transient landscape response. *Journal of Geophysical Research*, **112**(F3), F03S17.

Armitage, J.J. et al., 2015. Sediment Transport Model For the Eocene Escanilla Sediment-Routing System: Implications For the Uniqueness of Sequence Stratigraphic Architectures. *Journal of Sedimentary Research*, **85**(12), 1510–1524.

Armitage, J.J. et al., 2013. Temporal buffering of climate-driven sediment flux cycles by transient catchment response. *Earth and Planetary Science Letters*, **369**–**370**, 200–210.

Armitage, J.J. et al., 2011. Transformation of tectonic and climatic signals from source to sedimentary archive. *Nature Geoscience*, **4**(4), 231–235.

Aufdenkampe, A.K. et al., 2011. Riverine coupling of biogeochemical cycles between land , oceans , and atmosphere. *Frontiers in Ecology and the Environment*, **9**, 53–60.

Bak, P., Tang, C. & Wiesnfeld, K., 1987. Self-Organized Criticality: An Explanation of 1/f Noise. *Physical Review Letters*, **59**(4), 381–384.

Ballantyne, C.K., 2002. Paraglacial Geomorphology. *Quaternary Science Reviews*, **21**(18–19), 1935–2017.

Barker, R., Dixon, L. & Hooke, J., 1997. Use of terrestrial photogrammetry for monitoring and measuring bank erosion. *Earth Surface Processes and Landforms*, **22**(13), 1217–1227.

Barnes, R.T. et al., 2018. Riverine Export of Aged Carbon Driven by Flow Path Depth and Residence Time. *Environmental Science and Technology*, **52**(3), 1028–1035.

Batz, N., 2010. *Predicting Ecological Diversity of Floodplains Using a Hydromorphic Model (CAESAR)*. Wageningen University.

Beechie, T.J. et al., 2006. Channel pattern and river-floodplain dynamics in forested mountain river systems. *Geomorphology*, **78**(1–2), 124–141.

Begin, Z.B., 1986. Curvature Ratio and Rate of River Bend Migration—Update. *Journal of Hydraulic Engineering*, **112**(10), 904–908.

Belmont, P. et al., 2014. Toward generalizable sediment fingerprinting with tracers that are conservative and nonconservative over sediment routing timescales. *Journal of Soils and Sediments*, **14**(8), 1479–1492.

Bennett, G. et al., 2014. A probabilistic sediment cascade model of sediment transfer in the Illgraben. *Water Resources Research*, **50**, 1225–1244.

Bennett, N.D. et al., 2013. Characterising performance of environmental models. *Environmental Modelling and Software*, **40**, 1–20.

Beven, K., 2006. A manifesto for the equifinality thesis. *Journal of Hydrology*, **320**(1–2), 18–36.

Bird, G. et al., 2009. Dispersal of Contaminant Metals in the Mining-Affected Danube and Maritsa Drainage Basins, Bulgaria, Eastern Europe. *Water, Air, and Soil Pollution*, **206**(1–4), 105–127.

Blöthe, J.H. & Korup, O., 2013. Millennial lag times in the Himalayan sediment routing system. *Earth and Planetary Science Letters*, **382**, 38–46.

Boano, F. et al., 2014. Hyophreic flow and transport processes. *Reviews of Geophysics*, **52**(4), 603–679.

Bolin, B. & Rodhe, H., 1973. A note on the concepts of age distribution and transit time in natural reservoirs. *Tellus A*, **25**(1), 58–62.

Bonniwell, E.C., Matisoff, G. & Whiting, P.J., 1999. Determining the times and distances of particle transit in a mountain stream using fallout radionuclides. *Geomorphology*, **27**, 75–92.

Boyle, J., Chiverrell, R.C. & Schillereff, D.N., 2015. Lacustrine Archives of Metals from Mining and Other Industrial Activities—A Geochemical Approach. In Blais, J., Rosen, M., & Smol, J., eds. *Environmental Contaminants. Developments in Paleoenvironmental Research*. Dordrecht: Springer, pp. 121–159.

Bradley, D.N. & Tucker, G.E., 2013. The storage time, age, and erosion hazard of laterally accreted sediment on the floodplain of a simulated meandering river. *Journal of Geophysical Research: Earth Surface*, **118**(3), 1308–1319.

Brewer, P.A. & Taylor, M.P., 1997. The spatial distribution of heavy metal contaminated sediment across terraced floodplains. *Catena*, **30**(2–3), 229–249.

Bridge, J.S., 2003. *Rivers and Floodplains Forms, Processes and Sedimentary Record*, Oxford: Blackwell Science Ltd.

Bronk Ramsey, C., 2008. Radiocarbon dating: Revolutions in understanding. *Archaeometry*, **50**(2), 249–275.

Brunsden, D. & Thornes, J.B., 1979. Landscape Sensitivity and Change. *Transactions of the Institute of British Geographers*, **4**(4), 463–484.

Camporeale, C., Perucca, E. & Ridolfi, L., 2008. Significance of cutoff in meandering river dynamics. *Journal of Geophysical Research: Earth Surface*, **113**, F01001.

Castelltort, S. & Van Den Driessche, J., 2003. How plausible are high-frequency sediment supply-driven cycles in the stratigraphic record?

Sedimentary Geology, **157**(1–2), 3–13.

Centre for Ecology and Hydrology, 2015. Future Flows and Groundwater Levels. Available at: https://www.ceh.ac.uk/our-science/projects/future-flows-and-groundwater-levels [Accessed October 24, 2019].

Chesapeake Bay Program, 2014. Chesapeake Bay Watershed Agreement.

Chiverrell, R.C., Foster, G.C., Marshall, P., et al., 2009. Coupling relationships: Hillslope-fluvial linkages in the Hodder catchment, NW England. *Geomorphology*, **109**(3–4), 222–235.

Chiverrell, R.C., Foster, G.C., Thomas, G.S.P., et al., 2009. Sediment transmission and storage: the implications for reconstructing landform development. *Earth Surface Processes and Landforms*, **35**(1), 4–15.

Chow, V.T., 1959. *Open channel hydraulics*, New York: McGraw-Hill.

Church, M. & Ferguson, R.I., 2015. Morphodynamics: Rivers beyond steady state. *Water Resources Research*, **51**(4), 1883–1897.

Church, M. & Ryder, J.M., 1972. Paraglacial sedimentation: A consideration of fluvial processes conditioned by glaciation. *Bulletin of the Geological Society of America*, **83**(10), 3059–3072.

Church, M. & Slaymaker, O., 1989. Disequilibrium of Holocene sediment yield in glaciated British Columbia. *Nature*, **337**(6206), 452–454.

Clevis, Q. et al., 2006. A simple algorithm for the mapping of TIN data onto a static grid: Applied to the stratigraphic simulation of river meander deposits. *Computers and Geosciences*, **32**(6), 749–766.

Collins, B.D. et al., 2012. The floodplain large-wood cycle hypothesis: A mechanism for the physical and biotic structuring of temperate forested alluvial valleys in the North Pacific coastal ecoregion. *Geomorphology*, **139**–**140**, 460–470.

Constantine, J.A. et al., 2014. Sediment supply as a driver of river meandering and floodplain evolution in the Amazon Basin. *Nature Geoscience*, **7**(12), 899.

Corenblit, D. et al., 2007. Reciprocal interactions and adjustments between fluvial landforms and vegetation dynamics in river corridors: A review of complementary approaches. *Earth-Science Reviews*, **84**(1–2), 56–86.

Coulthard, T.J. et al., 2013. Integrating the LISFLOOD-FP 2D hydrodynamic model with the CAESAR model: implications for modelling landscape evolution. *Earth Surface Processes and Landforms*, **38**(15), 1897–1906.

Coulthard, T.J., 2001. Landscape evolution models: a software review. *Hydrological Processes*, **173**, 165–173.

Coulthard, T.J., Hicks, D.M. & Van De Wiel, M.J., 2007. Cellular modelling of river catchments and reaches: Advantages, limitations and prospects. *Geomorphology*, **90**(3–4), 192–207.

Coulthard, T.J., Lewin, J. & Macklin, M.G., 2005. Modelling differential catchment response to environmental change. *Geomorphology*, **69**(1–4), 222–241.

Coulthard, T.J. & Macklin, M.G., 2001. How sensitive are river systems to climate and land-use changes? A model-based evaluation. *Journal of Quaternary Science*, **16**(4), 347–351.

Coulthard, T.J. & Macklin, M.G., 2003. Modeling long-term contamination in river systems from historical metal mining. *Geology*, **31**(5), 451–454.

Coulthard, T.J., Macklin, M.G. & Kirkby, M.J., 2002. A cellular model of Holocene upland river basin and alluvial fan evolution. *Earth Surface Processes and Landforms*, **27**(3), 269–288.

Coulthard, T.J. & Van De Wiel, M.J., 2006. A cellular model of river meandering. *Earth Surface Processes and Landforms*, **31**(1), 123–132.

Coulthard, T.J. & Van De Wiel, M.J., 2013. Climate, tectonics or morphology: What signals can we see in drainage basin sediment yields? *Earth Surface Dynamics*, **1**(1), 13–27.

Coulthard, T.J. & Van De Wiel, M.J., 2017. Modelling long term basin scale sediment connectivity, driven by spatial land use changes. *Geomorphology*, **277**, 265–281.

Coulthard, T.J. & Van De Wiel, M.J., 2007. Quantifying fluvial non linearity and finding self organized criticality? Insights from simulations of river basin evolution. *Geomorphology*, **91**(3–4), 216–235.

Croissant, T. et al., 2017. Rapid post-seismic landslide evacuation boosted by dynamic river width. *Nature Geoscience*, (AUGUST).

Čufar, K., 2007. Dendrochronology and Past Human Activity—A Review of Advances Since 2000. *Tree-Ring Research*, **63**(1), 47–60.

Delignette-Muller, M.-L. et al., 2019. Package 'fitdistrplus'. , 87.

Dennis, I.A. et al., 2009. The role of floodplains in attenuating contaminated sediment fluxes in formerly mined drainage basins. *Earth Surface Processes and Landforms*, **34**, 453–466.

DePaolo, D.J. et al., 2006. Sediment transport time measured with U-series isotopes: Results from ODP North Atlantic drift site 984. *Earth and Planetary Science Letters*, **248**(1–2), 379–395.

Déry, S.J. et al., 2009. Observational evidence of an intensifying hydrological cycle in northern Canada. *Geophysical Research Letters*, **36**(13), L13402.

Dietrich, W.E. et al., 1982. Construction of sediment budgets for drainage basins. *Sediment Budgets and Routing in Forested Drainage Basins: Proceedings of the Symposium*, **1**, 5–23.

Dietrich, W.E. & Dunne, T., 1978. Sediment budget for a small catchment in mountainous terrain. *Zeitschrift für Geomorphologie*, **29**, 191–206.

Dixon, S.J. et al., 2018. The planform mobility of river channel confluences: Insights from analysis of remotely sensed imagery. *Earth-Science Reviews*, **176**(August 2017), 1–18.

Donovan, M. et al., 2015. Sediment contributions from floodplains and legacy sediments to Piedmont streams of Baltimore County, Maryland. *Geomorphology*, **235**, 88–105.

Dosseto, A. et al., 2010. Climatic and vegetation control on sediment

dynamics during the last glacial cycle. *Geology*, **38**(5), 395–398.

Dosseto, A. et al., 2006. Time scale and conditions of weathering under tropical climate: Study of the Amazon basin with U-series. *Geochimica et Cosmochimica Acta*, **70**(1), 71–89.

Dosseto, Anthony, Bourdon, B. & Turner, S.P., 2008. Uranium-series isotopes in river materials: Insights into the timescales of erosion and sediment transport. *Earth and Planetary Science Letters*, **265**(1–2), 1–17.

Dosseto, A., Buss, H.L. & Chabaux, F., 2014. Age and weathering rate of sediments in small catchments: The role of hillslope erosion. *Geochimica et Cosmochimica Acta*, **132**, 238–258.

Dosseto, Anthony, Turner, S. & Douglas, G., 2006. Uranium-series isotopes in colloids and suspended sediments: Timescale for sediment production and transport in the Murray–Darling River system. *Earth and Planetary Science Letters*, **246**(3–4), 418–431.

Dosseto, A., Turner, S.P. & Chappell, J., 2008. The evolution of weathering profiles through time: New insights from uranium-series isotopes. *Earth and Planetary Science Letters*, **274**(3–4), 359–371.

Einstein, H.A., 1950. *The bed-load function of sediment transportation in open flows*, Washington D.C.: U.S. Department of Agriculture.

Eriksson, E., 1971. Compartment models and reservoir theory. *Annual Review of Ecology and Systematics*, **2**, 67–84.

Eriksson, E., 1961. Natural reservoirs and their characteristics. *Geofisica International*, **1**(2), 27–43.

Everitt, B.L., 1968. Use of the cottonwood in an investigation of the recent history of a flood plain. *American Journal of Science*, **266**(6), 417–439.

Feeney, C.J. et al., 2020. Modelling the decadal dynamics of reach-scale river channel evolution and floodplain turnover in CAESAR-Lisflood. *Earth Surface Processes and Landforms*, **45**(5), 1273–1291.

Ferguson, R.I., 1981. Channel forms and channel changes. In Lewin, J., ed. *British Rivers*. London: Allen and Unwin, pp. 90–125.

Ferguson, R.I. & Wathen, S.J., 1998. Tracer-pebble movement along a concave river profile: Virtual velocity in relation to grain size and shear stress. *Water Resour. Res.*, **34**(8), 2031–2038.

Fischenich, C., 2001. *Stability thresholds for stream restoration*, Engineer Research and Development Center Vicksburg MS Environmental Lab.

Fisher, G.B. et al., 2010. Constraining the timescales of sediment sequestration associated with large woody debris using cosmogenic7Be. *Journal of Geophysical Research: Earth Surface*, **115**(1), 1–20.

Florsheim, J.L. et al., 2011. From deposition to erosion: Spatial and temporal variability of sediment sources, storage, and transport in a small agricultural watershed. *Geomorphology*, **132**(3–4), 272–286.

Fonstad, M. & Marcus, W.A., 2003. Self-organized criticality in riverbank systems. *Annals of the Association of American Geographers*, **93**(2), 281–296.

Foster, G.C. et al., 2009. Fluvial development and the sediment regime of the lower Calder, Ribble catchment, northwest England. *Catena*, **77**(2), 81–95.

Fryirs, K., 2013. (Dis)Connectivity in catchment sediment cascades: A fresh look at the sediment delivery problem. *Earth Surface Processes and Landforms*, **38**(1), 30–46.

Fryirs, K. & Brierley, G.J., 2001. Variability in sediment delivery and storage along river courses in Bega catchment, NSW, Australia: Implications for geomorphic river recovery. *Geomorphology*, **38**(3–4), 237–265.

Fryirs, K.A. et al., 2007. Buffers, barriers and blankets: The (dis)connectivity of catchment-scale sediment cascades. *Catena*, **70**(1), 49–67.

Fryirs, K.A. & Brierley, G.J., 2013. *Geomorphic Analysis of River Systems An Approach to Reading the Landscape*, Chichester: John Wiley & Sons Ltd.

Fuchs, M. et al., 2011. The temporal and spatial quantification of Holocene sediment dynamics in a meso-scale catchment in northern Bavaria , Germany. *The Holocene*, **21**(7), 1093–1104.

Fuller, I.C. et al., 2002. Annual sediment budgets in an unstable gravel-bed river: the River Coquet , northern England. *Geological Society, London, Special Publications*, **191**(1), 115–131.

Fyfe, R.M. et al., 2013. The Holocene vegetation cover of Britain and Ireland: overcoming problems of scale and discerning patterns of openness. *Quaternary Science Reviews*, **73**, 132–148.

Gamarra, J.G.P. et al., 2014. Modelling remediation scenarios in historical mining catchments. *Environmental Science and Pollution Research*, **21**(11), 6952–6963.

Gloor, M. et al., 2013. Intensification of the Amazon hydrological cycle over the last two decades. *Geophysical Research Letters*, **40**(9), 1729–1733.

Glur, C., 2018. Package 'ahp'. Available at: https://cran.r-project.org/web/packages/ahp/ahp.pdf [Accessed January 30, 2019].

Gottesfeld, A.S. & Johnson Gottesfeld, L.M., 1990. Floodplain dynamics of a wandering river, dendrochronology of the Morice River, British Columbia, Canada. *Geomorphology*, **3**(2), 159–179.

Graham, D.J., Rice, S.P. & Reid, I., 2005. A transferable method for the automated grain sizing of river gravels. *Water Resources Research*, **41**(7), W07020.

Granet, M. et al., 2010. U-series disequilibria in suspended river sediments and implication for sediment transfer time in alluvial plains: The case of the Himalayan rivers. *Geochimica et Cosmochimica Acta*, **74**(10), 2851–2865.

Greco, S.E. et al., 2007. A tool for tracking floodplain age land surface patterns on a large meandering river with applications for ecological planning and restoration design. *Landscape and Urban Planning*, **81**(4), 354–373.

Gregory, K.J., 1997. *Fluvial Geomorphology of Great Britain*, London: Chapman & Hall.

Grotzinger, J. & Jordan, T., 2010. *Understanding Earth* 6th ed., New York: W.H. Freeman & Co Ltd.

Hancock, G.R., Lowry, J.B.C. & Coulthard, T.J., 2015. Catchment reconstruction — erosional stability at millennial time scales using landscape evolution models. *Geomorphology*, **231**, 15–27.

Handley, H.K. et al., 2013. Sediment residence times constrained by uranium-series isotopes: A critical appraisal of the comminution approach. *Geochimica et Cosmochimica Acta*, **103**, 245–262.

Harvey, A.M., 2002. Effective timescales of coupling within fluvial systems. *Geomorphology*, **44**, 175–201.

Haschenburger, J.K. & Church, M., 1998. Bed material transport estimated from the virtual velocity of sediment. *Earth Surface Processes and Landforms*, **23**(9), 791–808.

Hickin, E.J. & Nanson, G.C., 1975. The Character of Channel Migration on the Beatton River, Northeast British Columbia, Canada. *Geological Society of America Bulletin Bulletin*, **86**(4), 487–494.

Hoffmann, T. et al., 2007. Holocene floodplain sediment storage and hillslope erosion within the Rhine catchment. *The Holocene*, **17**(1), 105–118.

Hoffmann, T., 2015. Sediment residence time and connectivity in non-equilibrium and transient geomorphic systems. *Earth-Science Reviews*, **150**, 609–627.

Hoffmann, T. et al., 2009. Trends and controls of Holocene floodplain sedimentation in the Rhine catchment. *Catena*, **77**(2), 96–106.

Hoober, D., Svoray, T. & Cohen, S., 2017. Using a landform evolution model to study ephemeral gullying in agricultural fields: the effects of rainfall patterns on ephemeral gully dynamics. *Earth Surface Processes and Landforms*, **42**(8), 1213–1226.

Hooke, J., 2003. Coarse sediment connectivity in river channel systems: A conceptual framework and methodology. *Geomorphology*, **56**(1–2), 79–94.

Hooke, J. & Chen, H., 2016. Evidence of increase in woody vegetation in a river corridor, Northwest England, 1984–2007. *Journal of Maps*, **12**(3), 484–491.

Hooke, J.M., 2004. Cutoffs galore!: Occurrence and causes of multiple cutoffs on a meandering river. *Geomorphology*, **61**(3–4), 225–238.

Hooke, J.M., 1980. Magnitude and distribution of rates of river bank erosion. *Earth Surface Processes*, **5**(2), 143–157.

Hooke, J.M., 2016. Morphological impacts of flow events of varying magnitude on ephemeral channels in a semiarid region. *Geomorphology*, **252**, 128–143.

Hooke, J.M. et al., 1990. The chronology and stratigraphy of the alluvial terraces of the River Dane Valley, Cheshire, NW England. *Earth Surface Processes and Landforms*, **15**(8), 717–737.

Hooke, J.M. & Harvey, A.M., 1983. Meander changes in relation to bend morphology and secondary flows. In Collinson, J. D. & Lewin, J., eds. *Modern and Ancient Fluvial Systems*. Oxford: Blackwell Scientific Publications, pp. 121–132.

Hooke, J.M. & Mant, J.M., 2000. Geomorphological impacts of a flood event on ephemeral channels in SE Spain. *Geomorphology*, **34**, 163–180.

Hooke, J.M. & Redmond, C.E., 1989. River-Channel Changes in England and Wales. *Water and Environment Journal*, **3**(4), 328–335.

Horton, A.A. et al., 2017. Microplastics in freshwater and terrestrial environments: Evaluating the current understanding to identify the knowledge gaps and future research priorities. *Science of the Total Environment*, **586**, 127–141.

Horton, A.A. & Dixon, S.J., 2018. Microplastics : An introduction to environmental transport processes. *Wiley Interdisciplinary Reviews*,

5(2), e1268.

Howard, A.D., 1992. Modelling channel migration and floodplain sedimentation in meandering streams. In Carling, P. A. & Petts, G. E., eds. *Lowland Floodplain Rivers: Geomorphological Perspectives*. Hoboken, NJ: John Wiley & Sons Ltd, pp. 1–41.

Howard, A.D. & Hemberger, A.T., 1991. Multivariate characterization of meandering. *Geomorphology*, **4**, 161–186.

Howard, A.J. et al., 2016. Assessing riverine threats to heritage assets posed by future climate change through a geomorphological approach and predictive modelling in the Derwent Valley Mills WHS , UK. *Journal of Cultural Heritage*, **19**, 387–394.

Hughes, M.L., McDowell, P.F. & Marcus, W.A., 2006. Accuracy assessment of georectified aerial photographs: Implications for measuring lateral channel movement in a GIS. *Geomorphology*, **74**(1–4), 1–16.

Huntington, T.G., 2006. Evidence for intensification of the global water cycle: Review and synthesis. *Journal of Hydrology*, **319**(1–4), 83–95.

Hurley, R., Woodward, J. & Rothwell, J.J., 2018. significantly reduced by catchment-wide flooding. *Nature Geoscience*, **11**(4), 251.

Ikeda, S., Parker, G. & Sawai, K., 1981. Bend theory of river meanders. Part 1. Linear development. *Journal of Fluid Mechanics*, **112**, 363–377.

Jain, V. & Tandon, S.K., 2010. Conceptual assessment of (dis)connectivity and its application to the Ganga River dispersal system. *Geomorphology*, **118**(3–4), 349–358.

James, L.A., 2018. Ten conceptual models of large-scale legacy sedimentation – A review. *Geomorphology*, **317**, 199–217.

Jerolmack, D.J. & Paola, C., 2010. Shredding of environmental signals by sediment transport. *Geophysical Research Letters*, **37**(19), 1–5.

Johnson, M.J. & Meade, R.H., 1990. Chemical weathering of fluvial sediments during alluvial storage; the Macuapanim Island point bar,

Solimoes River, Brazil. *Journal of Sedimentary Petrology*, **60**(6), 827–842.

Keeler, J. et al., 2015. Accounting for LongTerm Sediment Storage in a Watershed Scale Numerical Model for Suspended Sediment Routing. In *AGU Fall Meeting 14-18 December 2015*. San Francisco.

Kelsey, H.M., Lamberson, R. & Madej, M.A., 1987. Stochastic Model for the Long-Term Transport of Stored Sediment in a River Channel. *Water Resour. Res.*, **23**(9), 1738–1750.

Kleinhans, M.G. & Rijn, L.C. Van, 2002. Stochastic Prediction of Sediment Transport in Sand-Gravel Bed Rivers. *Journal of Hydraulic Engineering*, **128**(4), 412–425.

Konrad, C.P., 2012. Reoccupation of floodplains by rivers and its relation to the age structure of floodplain vegetation. *Journal of Geophysical Research: Biogeosciences*, **117**, G00N13.

Kuo, C.-W. & Brierley, G.J., 2013. The influence of landscape configuration upon patterns of sediment storage in a highly connected river system. *Geomorphology*, **180**–**181**, 255–266.

Lack, A.J. & Evans, D.E., 2001. *Plant Biology*, New York: Springer-Verlag.

Lancaster, S.T. & Bras, R.L., 2002. A simple model of river meandering and its comparison to natural channels. *Hydrological Processes*, **16**(1), 1–26.

Lancaster, S.T. & Casebeer, N.E., 2007. Sediment storage and evacuation in headwater valleys at the transition between debris-flow and fluvial processes. *Geology*, **35**(11), 1027–1030.

Lancaster, S.T., Underwood, E.F. & Frueh, W.T., 2010. Sediment reservoirs at mountain stream confluences: Dynamics and effects of tributaries dominated by debris-flow and fluvial processes. *Bulletin of the Geological Society of America*, **122**(11–12), 1775–1786.

Lane, E.W., 1955. Design of stable channels. *Transaction of American Society of Civil Engineers*, **120**, 1234–1260.

Lang, A. et al., 2003. Changes in sediment flux and storage within a fluvial system: some examples from the Rhine catchment. *Hydrological Processes*, **17**, 3321–3334.

Larsen, E.W., Fremier, A.K. & Girvetz, E.H., 2006. Modeling the effects of variable annual flow on river channel meander migration patterns, Sacramento River, California, USA. *Journal of the American Water Resources Association*, **42**(4), 1063–1075.

Lauer, J.W., 2012. The Importance of Off-Channel Sediment Storage in 1-D Morphodynamic Modelling. In Church, M., Biron, P. M., & Roy, A. G., eds. *Gravel-Bed Rivers: Processes, Tools, Environments*. Chichester: John Wiley & Sons Ltd, pp. 123–134.

Lauer, J.W. & Parker, G., 2008. Net local removal of floodplain sediment by river meander migration. *Geomorphology*, **96**(1–2), 123–149.

Lauer, J.W. & Willenbring, J., 2010. Steady state reach-scale theory for radioactive tracer concentration in a simple channel/floodplain system. *Journal of Geophysical Research: Earth Surface*, **115**(August 2009), 1–21.

Lawler, D.M., 1993. The measurement of river bank erosion and lateral channel change: a review. *Earth Surface Processes and Landforms*, **18**, 777–821.

Legg, N.T. et al., 2014. *The Channel Migration Toolbox: ArcGIS® Tools for Measuring Stream Channel Migration*, Olympia, Washington.

Leopold, L.B., Wolman, M.G. & Miller, J.P., 1964. *Fluvial processes in geomorphology*, Mineola, New York: Courier Dover Publications.

Lewin, J. & Macklin, M.G., 1987. Metal Mining and Floodplain Sedimentation in Britain. In Gardiner, V., ed. *International Geomorphology 1986 Proceedings of the First International Conference on Geomorphology Part 1*. John Wiley & Sons Ltd, pp. 1008–1027.

Lewin, J., Macklin, M.G. & Johnstone, E., 2005. Interpreting alluvial archives: Sedimentological factors in the British Holocene fluvial record.

Quaternary Science Reviews, **24**(16–17), 1873–1889.

Li, C. et al., 2015. A review of comminution age method and its potential application in the East China Sea to constrain the time scale of sediment source-to-sink process. *Journal of Ocean University of China*, **14**(3), 399–406.

Lyons, J., Thimble, S.W. & Paine, L.K., 2000. Grass versus trees: managing riparian areas to benefit streams of central north america. *JAWRA Journal of the American Water Resources Association*, **36**(4), 919–930.

Macklin, M.G. & Dowsett, R.B., 1989. The chemical and physical speciation of trace metals in fine grained overbank flood sediments in the Tyne basin, north-east England. *Catena*, **16**(2), 135–151.

Macklin, M.G. & Lewin, J., 1989. Sediment Transfer and Transformation of an Alluvial Valley Floor: The River South Tyne, Northumberia, U.K. *Earth Surface Processes and Landforms*, **14**, 233–246.

Malik, I., 2006. Contribution to understanding the historical evolution of meandering rivers using dendrochronological methods: Example of the Mała Panew River in southern Poland. *Earth Surface Processes and Landforms*, **31**(10), 1227–1245.

Malmon, D. V. et al., 2005. Influence of sediment storage on downstream delivery of contaminated sediment. *Water Resources Research*, **41**(5), 1–17.

Malmon, D. V., Dunne, T. & Reneau, S.L., 2002. Predicting the fate of sediment and pollutants in river floodplains. *Environmental Science and Technology*, **36**(9), 2026–2032.

Malmon, D. V, Dunne, T. & Reneau, S.L., 2003. Stochastic Theory of Particle Trajectories through Alluvial Valley Floors. *The Journal of Geology*, **111**(5), 525–542.

Martin, A.N., 2015. *Reconstructing past variations in erosion and sediment transport using uranium-series isotopes*. University of Wollongong.

Martin, Y. & Church, M., 2004. Numerical modelling of landscape evolution:

geomorphological perspectives. *Progress in Physical Geography*, **28**(3), 317–339.

Meadows, T., 2014. *Forecasting Long-Term Sediment Yield From the Upper North Fork Toutle River, Mount St Helens, Usa*. University of Nottingham.

Micheli, E.R. & Kirchner, J.W., 2002. Effects of wet meadow riparian vegetation on streambank erosion. 2. Measurements of vegetated bank strength and consequences for failure mechanics. *Earth Surface Processes and Landforms*, **27**(7), 687–697.

Miller, J.R., 1997. The role of fluvial geomorphic processes in the dispersal of heavy metals from mine sites. *Journal of Geochemical Exploration*, **58**, 101–118.

Miller, J.R. & Friedman, J.M., 2009. Influence of flow variability on floodplain formation and destruction, Little Missouri River, North Dakota. *Geological Society of America Bulletin*, **121**(5–6), 752–759.

Mitsch, W.J. & Gosselink, J.G., 2015. *Wetlands* 5th ed., Hoboken, New Jersey: Wiley.

Moody, J.A., 2017. Residence times and alluvial architecture of a sediment superslug in response to different flow regimes. *Geomorphology*, **294**, 40–57.

Moore, J.N. & Langner, H.W., 2012. Can a river heal itself? Natural attenuation of metal contamination in river sediment. *Environmental Science and Technology*, **46**, 2616–2623.

Nakamura, F. et al., 2017. Large wood, sediment, and flow regimes: Their interactions and temporal changes caused by human impacts in Japan. *Geomorphology*, **279**, 176–187.

Nakamura, F. & Kikuchi, S., 1996. Some methodological developments in the analysis of sediment transport processes using age distribution of floodplain deposits. *Geomorphology*, **16**(2), 139–145.

Nanson, G.C. & Beach, H.F., 1977. Forest succession and sedimentation on

a meandering-river floodplain northeast British Columbia, Canada. *Journal of Biogeography*, **4**(3), 229–251.

Nanson, G.C. & Croke, J.C., 1992. A genetic classification of floodplains. *Geomorphology*, **4**(6), 459–486.

Nanson, G.C. & Hickin, E.J., 1983. Channel Migration and Incision on the Beatton River. *Journal of Hydraulic Engineering*, **109**(3), 327–337.

Nicholas, A.P. et al., 1995. Sediment slugs: Large-scale fluctuations in fluvial sediment transport rates and storage volumes. *Progress in Physical Geography*, **19**(4), 500–519.

Nicoll, T.J. & Hickin, E.J., 2010. Planform geometry and channel migration of confined meandering rivers on the Canadian prairies. *Geomorphology*, **116**(1–2), 37–47.

O'Connor, J.E., Jones, M.A. & Haluska, T.L., 2003. Flood plain and channel dynamics of the Quinault and Queets Rivers, Washington, USA. *Geomorphology*, **51**(1–3), 31–59.

Oreskes, N., 1998. Evaluation (not validation) of quantitative models. *Environmental Health Perspectives*, **106**(SUPPL. 6), 1453–1460.

Owens, P.N., Petticrew, E.L. & van der Perk, M., 2010. Sediment response to catchment disturbances. *Journal of Soils and Sediments*, **10**(4), 591–596.

Parker, G. & Andrews, E.D., 1986. On the time development of meander bends. *Journal of Fluid Mechanics*, **162**, 139–156.

Parsons, A.J. et al., 2018. Virtual velocity of sand transport in water. *Earth Surface Processes and Landforms*, **43**(3), 755–761.

Pasculli, A. & Audisio, C., 2015. Cellular Automata Modelling of Fluvial Evolution: Real and Parametric Numerical Results Comparison Along River Pellice (NW Italy). *Environmental Modeling and Assessment*, **20**(5), 425–441.

Phillips, J.D., 2006. Deterministic chaos and historical geomorphology: A

review and look forward. *Geomorphology*, **76**, 109–121.

Phillips, J.D., 1991. Multiple modes of adjustment in unstable river channel cross-sections. *Journal of Hydrology*, **123**(1–2), 39–49.

Phillips, J.D., 2003. Sources of nonlinearity and complexity in geomorphic systems. *Progress in Physical Geography*, **27**(1), 1–23.

Phillips, J.D., Marden, M. & Gomez, B., 2007. Residence time of alluvium in an aggrading fluvial system. *Earth Surface Processes and Landforms*, **32**, 307–316.

Pitlick, J., 1995. Sediment Routing in Tributaries of the Redwood Creek Basin, Northwestern California. In U.S. Geological Survey Professional Paper 145-L, ed. *Geomorphic Processes and Aquatic Habitat, Redwood Creek, Northwestern California*. USGS, pp. K1–K10.

Pizzuto, J. et al., 2015. A Stochastic Model For Extracting Sediment Delivery Timescales From Sediment Budgets. In *AGU Fall Meeting 14-18 December 2015*. San Francisco.

Pizzuto, J. et al., 2014. Characteristic length scales and time-averaged transport velocities of suspended sediment in the mid-Atlantic Region, USA. *Water Resources Research*, **50**(2), 790–805.

Pizzuto, J. et al., 2017. Storage filters upland suspended sediment signals delivered from watersheds. *Geology*, **45**(2), 151–154.

Pizzuto, J. & O'Neal, M., 2009. Increased mid-twentieth century riverbank erosion rates related to the demise of mill dams, South River, Virginia. *Geology*, **37**(1), 19–22.

Pizzuto, J.E., 2014. Long-term storage and transport length scale of fine sediment: Analysis of a mercury release into a river. *Geophysical Research Letters*, **41**(16), 5875–5882.

Provansal, M. et al., 2014. Geomorphology The geomorphic evolution and sediment balance of the lower Rhône River (southern France) over the last 130 years: Hydropower dams versus other control factors. *Geomorphology*, **219**, 27–41.

Rodhe, H., 2000. Modelling Biogeochemical Cycles. In Jacobson, M. et al., eds. *Earth System Science: From Biogeochemical Cycles to Global Change*. London: International Geophysical Series: Elsevier, pp. 62–84.

Rowan, J.S. et al., 1995. Geomorphology and pollution: the environmental impacts of lead mining, Leadhills, Scotland. *Journal of Geochemical Exploration*, **51**, 57–65.

Rowan, J.S. & Franks, S.W., 2002. Heavy metal mining and flood plain response in the upper Clyde basin , Scotland. In *The structure, function and management implications of fluvial sedimentary systems*. Alice Springs, Australia: IAHS Publication, pp. 143–150.

Saaty, T.L., 1990. How to make a decision: The Analytic Hierarchy Process. *European Journal of Operational Research*, **48**(1), 9–26.

Saaty, T.L. & Vargas, L.G., 2012. *Models, methods, concepts & applications of the analytic hierarchy process* 2nd ed., Berlin: Springer Science & Business Media.

Schneider, A., 2013. *Spatial and temporal development of sediment mass balances during the initial phase of landform evolution in a small catchment*. Brandenburg University of Technology.

Schumm, S.A., 1977. *The Fluvial System*, New York: John Wiley & Sons Ltd.

Seoane, M. et al., 2015. A Geomorphological Modelling Approach for Landscape Evolution Analysis of the Macquarie Marshes , Australia. In *E-proceedings of the 36th IAHR World Congress 28 June - 3 July, 2015*. The Hague, pp. 1–8.

Singh, A., Lanzoni, S. & Foufoula-Georgiou, E., 2009. Nonlinearity and complexity in gravel bed dynamics. *Stochastic Environmental Research and Risk Assessment*, **23**(7), 967–975.

Skalak, K. et al., 2015. Age Dating Fluvial Sediment Storage Reservoirs to Construct Sediment Waiting Time Distributions. In *AGU Fall Meeting 14-18 December 2015*. San Francisco.

Skalak, K. & Pizzuto, J., 2010. The distribution and residence time of

suspended sediment stored within the channel margins of a gravel-bed bedrock river. *Earth Surface Processes and Landforms*, **35**(4), 435–446.

Slaymaker, O., Spencer, T. & Embleton-Hamann, C., 2009. *Geomorphology and Global Environmental Change*, New York: Cambridge University Press.

Smith, H.G., Blake, W.H. & Taylor, A., 2014. Modelling particle residence times in agricultural river basins using a sediment budget model and fallout radionuclide tracers. *Earth Surface Processes and Landforms*, **39**, 1944–1959.

Stockinger, M.P. et al., 2016. Tracer sampling frequency influences estimates of young water fraction and streamwater transit time distribution. *Journal of Hydrology*, **541**, 952–964.

Stolum, H.-H., 1996. River Meandering as a Self-Organization Process. *Science*, **271**(5256), 1710–1713.

Suresh, P.O. et al., 2014. Very long hillslope transport timescales determined from uranium-series isotopes in river sediments from a large, tectonically stable catchment. *Geochimica et Cosmochimica Acta*, **142**, 442–457.

Sutfin, N.A., Wohl, E.E. & Dwire, K.A., 2016. Banking carbon: A review of organic carbon storage and physical factors influencing retention in floodplains and riparian ecosystems. *Earth Surface Processes and Landforms*, **41**(1), 38–60.

Syvitski, J.P.M., 2003. Supply and flux of sediment along hydrological pathways: research for the 21st century. *Global and Planetary Change*, **39**(1–2), 1–11.

Syvitski, J.P.M. & Kettner, A., 2011. Sediment flux and the anthropocene. *Philosophical Transactions of the Royal Society A: Mathematical, Physical and Engineering Sciences*, **369**(1938), 957–975.

Thrasher, I.M. et al., 2009. Luminescence dating of glaciofluvial deposits: A review. *Earth-Science Reviews*, **97**(1–4), 133–146.

Tockner, K. & Stanford, J.A., 2002. Riverine flood plains: present state and

future trends. *Environmental Conservation*, **29**(3), 308–330.

Torres, M.A. et al., 2017. Model predictions of long-lived storage of organic carbon in river deposits. *Earth Surface Dynamics Discussions*, **5**, 711–730.

Trimble, S., 2004. Effects of riparian vegetation on stream channel stability and sediment budgets. In Bennett, S. J. & Simon, A., eds. *Riparian Vegetation and Fluvial Geomorphology - Water Science and Application*. Washington D.C.: American Geopysical Union, pp. 153–169.

Trimble, S.W., 1983. A sediment budget for Coon Creek Basin in the Driftless Area, Wisonsin, 1853-1977. *American Journal of Science*, **283**, 454–474.

Trimble, S.W., 1975. Present and prospective technology for predicting sediment yields and sources. In *Proceedings of the Sediment-Yield Workshop, USDA Sedimentation Laboratory, Oxford, Miss., Nov. 28-30, 1972*. pp. 142–152.

Trimble, S.W., 2010. Streams, Valleys and Floodplains in the Sediment Cascade. In Burt, T. & Allison, R., eds. *Sediment Cascades : An Integrated Approach*. Hoboken, NJ: John Wiley & Sons, pp. 307–343.

Tucker, G.E. et al., 2001. The Channel-Hillslope Integrated Landscape Development (CHILD) Model. In Harmon, R. S. & Doe III, W. W., eds. *Landscape Erosion and Evolution Modeling*. Dordrecht: Kluwer Academic/Plenum Publishers, pp. 349–388.

Tucker, G.E. & Hancock, G.R., 2010. Modelling landscape evolution. *Earth Surface Processes and Landforms*, **35**, 28–50.

UKCEH, 2020. Search Data | National River Flow Archive. *UK National River Flow Archive*. Available at: https://nrfa.ceh.ac.uk/data/search [Accessed April 5, 2020].

Vargas, L.G., 1990. An overview of the analytical hierarchy process and its applications. *Europeon Journal of Operational Research*, **48**, 2–4.

de Vente, J. et al., 2007. The sediment delivery problem revisited. *Progress*

in Physical Geography, **31**(2), 155–178.

Vigier, N. et al., 2001. Erosion timescales derived from U-decay series measurements in rivers. *Earth and Planetary Science Letters*, **193**(3–4), 549–563.

Vigier, N. et al., 2005. Mobility of U-series nuclides during basalt weathering: An example from the Deccan Traps (India). *Chemical Geology*, **219**(1–4), 69–91.

Vigier, N. et al., 2006. The relationship between riverine U-series disequilibria and erosion rates in a basaltic terrain. *Earth and Planetary Science Letters*, **249**, 258–273.

Voepel, H., Schumer, R. & Hassan, M.A., 2013. Sediment residence time distributions: Theory and application from bed elevation measurements. *Journal of Geophysical Research: Earth Surface*, **118**(4), 2557–2567.

Walling, D.E. et al., 2003. Storage of sediment-associated nutrients and contaminants in river channel and floodplain systems. *Applied Geochemistry*, **18**(2), 195–220.

Walling, D.E., 1983. The Sediment Delivery Problem. *Journal of Hydrology*, **65**, 209–237.

Walling, D.E. & Owens, P.N., 2003. The role of overbank floodplain sedimentation in catchment contaminant budgets. *Hydrobiologia*, **494**, 83–91.

Whitehead, P. et al., 2009. A review of the potential impacts of climate change on surface water quality. *Hydrological Sciences Journal*, **54**(1), 37–41.

Whittaker, A.C., Attal, M. & Allen, P.A., 2010. Characterising the origin, nature and fate of sediment exported from catchments perturbed by active tectonics. *Basin Research*, **22**(6), 809–828.

Van De Wiel, M.J. et al., 2007. Embedding reach-scale fluvial dynamics within the CAESAR cellular automaton landscape evolution model. *Geomorphology*, **90**(3–4), 283–301.

Van De Wiel, M.J. et al., 2011. Modelling the response of river systems to environmental change: Progress, problems and prospects for palaeo-environmental reconstructions. *Earth-Science Reviews*, **104**(1–3), 167–185.

Van De Wiel, M.J. & Coulthard, T.J., 2010. Self-organized criticality in river basins: Challenging sedimentary records of environmental change. *Geology*, **38**(1), 87–90.

Wittenberg, L. & Newson, M.D., 2005. Particle clusters in gravel-bed rivers : an experimental morphological approach to bed material transport and stability concepts. *Earth Surface Processes and Landforms*, **30**(11), 1351–1368.

Wittmann, H. & von Blanckenburg, F., 2009. Cosmogenic nuclide budgeting of floodplain sediment transfer. *Geomorphology*, **109**(3–4), 246–256.

Wohl, E., 2013. Floodplains and wood. *Earth-Science Reviews*, **123**, 194–212.

Wohl, E. et al., 2015. The natural sediment regime in rivers: Broadening the foundation for ecosystem management. *BioScience*, **65**(4), 358–371.

Wolman, M.G. & Leopold, L.B., 1957. River flood plains: some observations on their formation. In *US Geological Survey Professional Paper 282-C*. pp. 87–107.

Zalasiewicz, J. et al., 2008. Are we now living in the Anthropocene. *GSA Today*, **18**(2), 4–8.

Ziliani, L. et al., 2013. Reduced-complexity modeling of braided rivers: Assessing model performance by sensitivity analysis, calibration, and validation. *Journal of Geophysical Research: Earth Surface*, **118**(4), 2243–2262.

Ziliani, L. & Surian, N., 2012. Evolutionary trajectory of channel morphology and controlling factors in a large gravel-bed river. *Geomorphology*, **173**–**174**(November), 104–117.

Appendix 1

A: Metadata for the study sites (OS maps, aerial images and LiDAR / DTMs)

Bollin1

OS maps

- Modern 2016 OS map: OS VectorMap® Local – January 2016.
- Historic 1987 OS map: National Grid 1:10 000 Latest Version – January 1987.

Aerial photos

- Date: April 2003; Scale 1:10,000
- Number of images georeferenced: 1
- Number of ground control points for georectification: 15
- Image transformation algorithm used: 2nd order polynomial
- Root mean square error (RMSE) of transformation (metres): 3.255

LiDAR / DTMs

- LiDAR Composite Digital Terrain Model (DTM) at 2m spatial resolution.

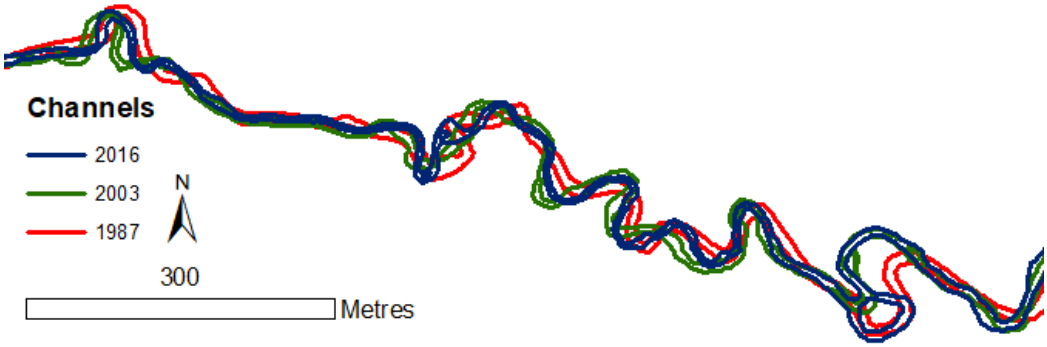

Bollin2

OS maps

- Modern 2016 OS map: OS VectorMap® Local – January 2016.
- Historic 1976 OS map: National Grid 1:10 000 1st Metric Edition – January 1976.

Aerial photos

- Date: April 2003; Scale 1:10,000
- Number of images georeferenced: 1
- Number of ground control points for georectification: 10
- Image transformation algorithm used: 2nd order polynomial
- RMSE of transformation (metres): 0.779

LiDAR / DTMs

- LiDAR Composite Digital Terrain Model (DTM) at 2m spatial resolution.

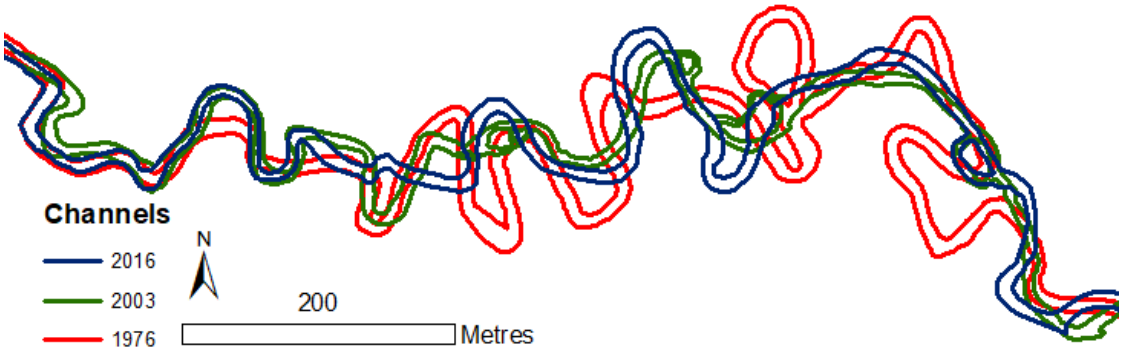

Calder

OS maps

- Modern 2016 OS map: OS Street View (April 2016).
- Historic 1988 OS map: National Grid 1:10 000 Latest Version – January 1992.

Aerial photos

- Date: 31st December 2003; Scale 1:10,000
- Number of images georeferenced: 3
- Number of ground control points for georectification: 17 (mean of all images)
- Image transformation algorithm used: 2nd order polynomial
- RMSE of transformation (metres): 3.386 (mean of all images)

LiDAR / DTMs

- LiDAR Composite Digital Terrain Model (DTM) at 2m spatial resolution.

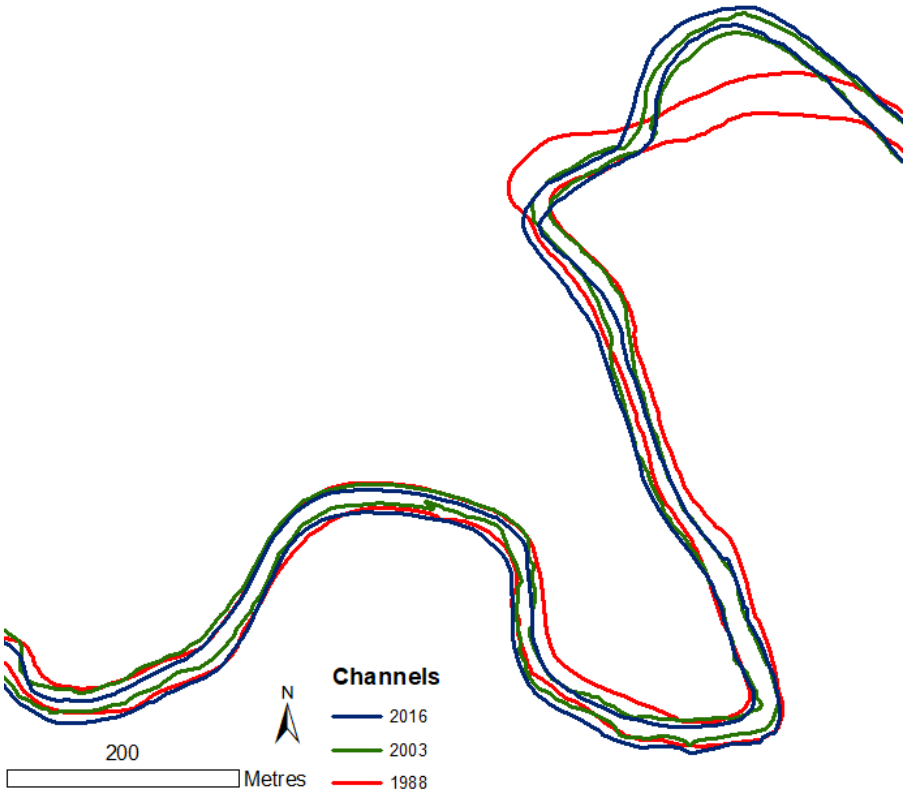

Coquet1

OS maps

- Modern 2016 OS map: OS VectorMap® Local – April 2016.
- Historic 1976 OS map: National Grid 1:2500 1st Edition – January 1976.

Aerial photos

- Date: 31st December 2002; Scale 1:10,000
- Number of images georeferenced: 1
- Number of ground control points for georectification: 21
- Image transformation algorithm used: 2nd order polynomial
- RMSE of transformation (metres): 2.542

LiDAR / DTMs

- LiDAR Composite Digital Terrain Model (DTM) at 2m spatial resolution.

Coquet2

- Modern 2016 OS map: OS VectorMap® Local – April 2016.
- Historic 1979 OS map: National Grid 1:2500 1st Edition – January 1979.

Aerial photos

- Date: 31st December 2002; Scale 1:10,000

- Number of images georeferenced: 1
- Number of ground control points for georectification: 13
- Image transformation algorithm used: 2nd order polynomial
- RMSE of transformation (metres): 3.019

LiDAR / DTMs

- OS Terrain 5 m – last amended 18 May 2013.

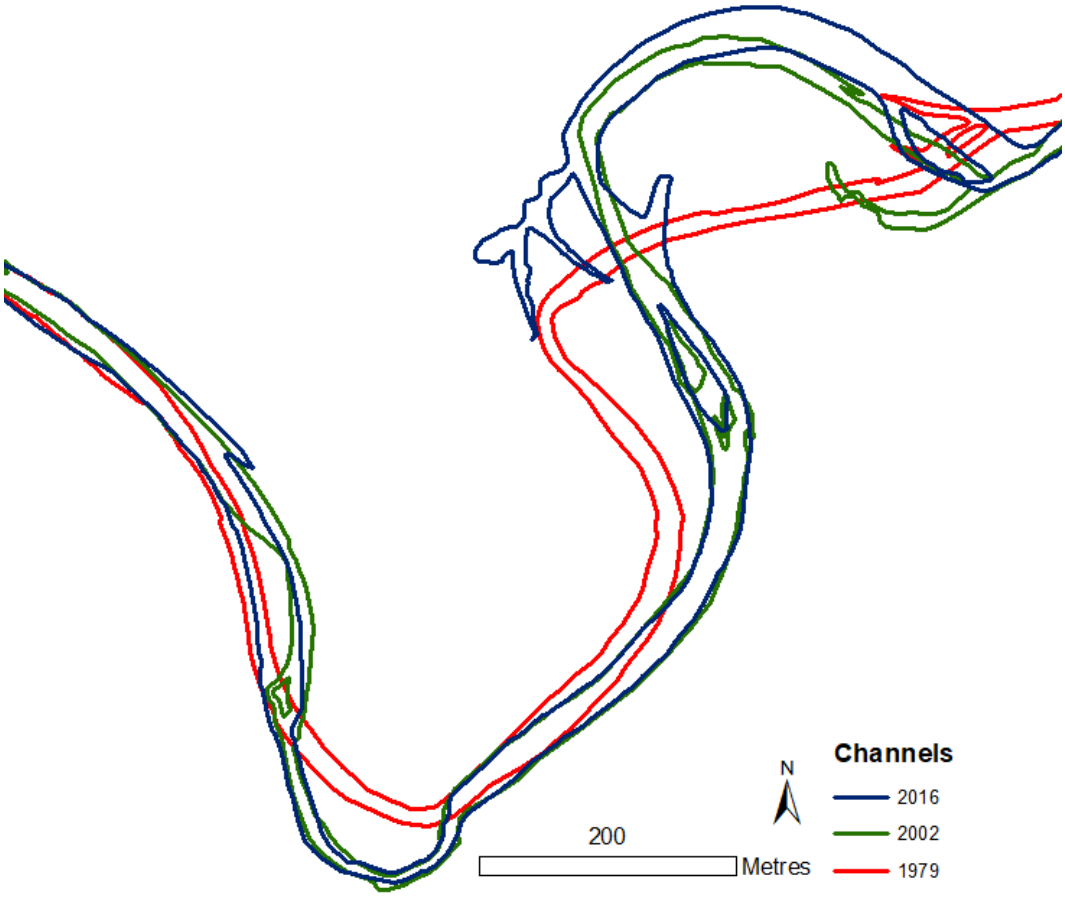

Dane

OS maps

- Modern 2016 OS map: OS Open Map Local – October 2016.
- Historic 1992 OS map: National Grid 1:10 000 Latest Version – January 1992
- Historic 1969 OS map: National Grid 1:2500 1st Edition – January 1969.

Aerial photos

- None – riverbanks were obscured by too much tree cover. Map from 1992 used instead.

LiDAR / DTMs

- LiDAR Composite Digital Terrain Model (DTM) at 2m spatial resolution.

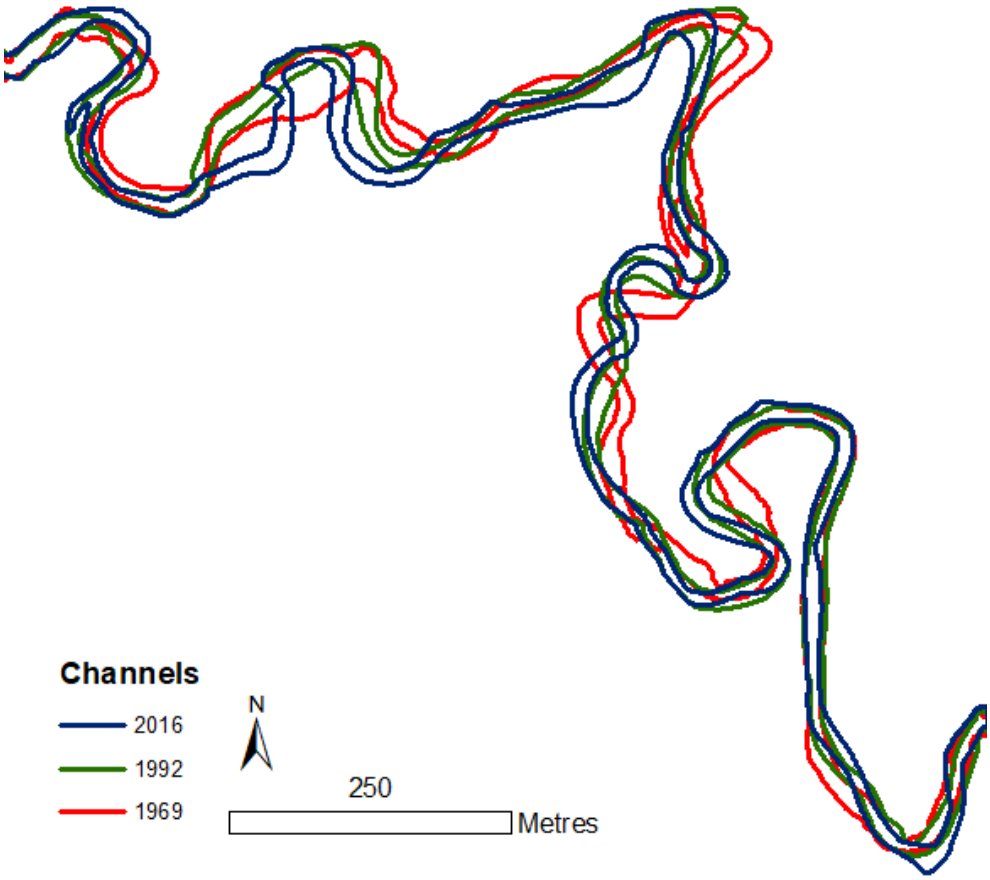

Harwood Beck

OS maps

- Modern 2016 OS map: OS VectorMap® Local – April 2016.
- Historic 1977 OS map: National Grid 1:10 000 1st Metric Edition – January 1977.

Aerial photos

- Date: 31st December 2001; Scale 1:10,000

- Number of images georeferenced: 4
- Number of ground control points for georectification: 63 (mean of all images)
- Image transformation algorithm used: 2nd order polynomial
- RMSE of transformation (metres): 1.252 (mean of all images)

LiDAR / DTMs

- LiDAR Composite Digital Terrain Model (DTM) at 2m spatial resolution.

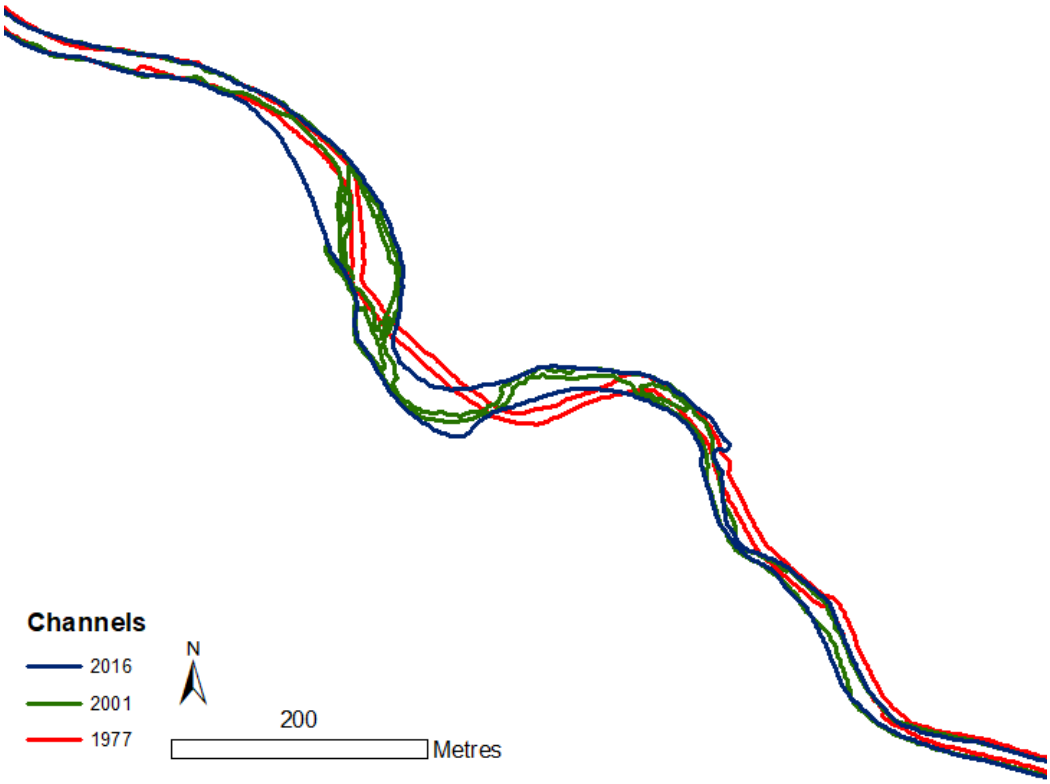

Lune

OS maps

- Modern 2016 OS map: OS VectorMap® Local – April 2016.
- Historic 1974 OS map: National Grid 1:10 000 1st Metric Edition - January 1974.

Aerial photos

- Date: 31st December 2000; Scale 1:10,000

- Number of images georeferenced: 7
- Number of ground control points for georectification: 25 (mean of all images)
- Image transformation algorithm used: 2nd and 3rd order polynomial
- RMSE of transformation (metres): 3.315 (mean of all images)

LiDAR / DTMs

- LiDAR Composite Digital Terrain Model (DTM) at 2m spatial resolution.

South Tyne1

OS maps

- Modern 2016 OS map: OS VectorMap® Local – April 2016.
- Historic 1982 OS map: National Grid 1:10 000 Latest Version – January 1982.

Aerial photos

- Date: 31st December 2003; Scale 1:10,000
- Number of images georeferenced: 3
- Number of ground control points for georectification: 15 (mean of all images)
- Image transformation algorithm used: 2nd order polynomial
- RMSE of transformation (metres): 3.668 (mean of all images)

LiDAR / DTMs

- LiDAR Composite Digital Terrain Model (DTM) at 2m spatial resolution.

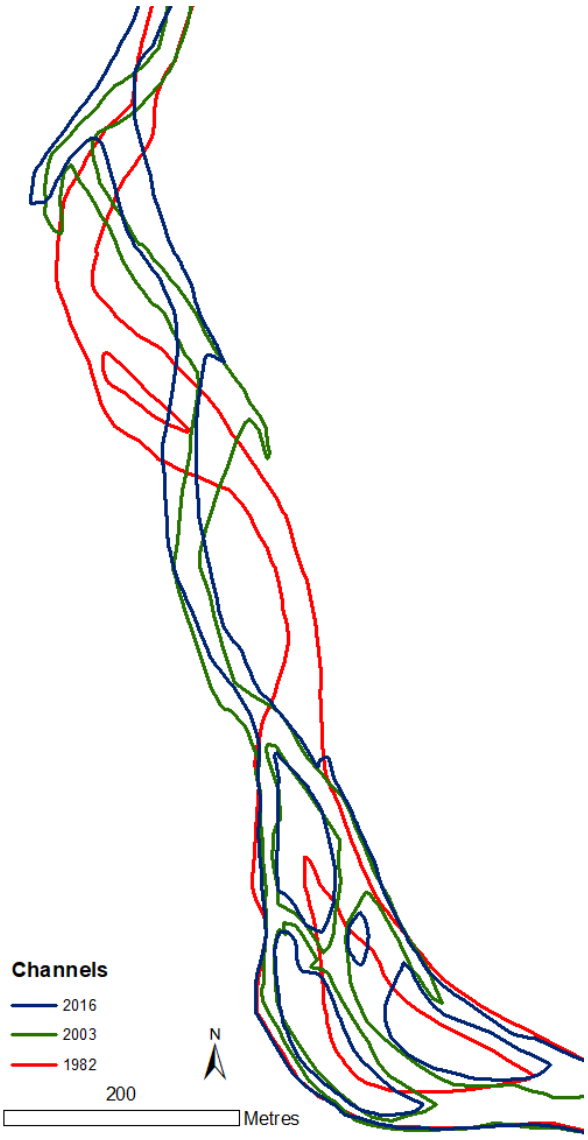

South Tyne2

OS maps

- Modern 2016 OS map: OS VectorMap® Local – April 2016.
- Historic 1982 OS map: National Grid 1:10 000 Latest Version – January 1982.

Aerial photos

- Date: 31st December 2003; Scale 1:10,000
- Number of images georeferenced: 2
- Number of ground control points for georectification: 16 (mean of all images)
- Image transformation algorithm used: 2nd order polynomial
- RMSE of transformation (metres): 4.349 (mean of all images)

LiDAR / DTMs

- LiDAR Composite Digital Terrain Model (DTM) at 2m spatial resolution.


Channels
2016
2003
1980
N
100
Metres

B: Historical channel migration polygon with centreline and locations of transects for measuring lateral migration distances

For each of the reaches, channel centrelines digitised from three historical maps and aerial images were overlaid to generate a historical meander belt area. A centreline from this polygon was digitised and transects, spaced 10 m apart from each other, were generated using the 'Transect Generation Tool' in the 'Channel Migration Toolbox' (Legg et al. 2014). When centrelines for each of the mapped and modelled river channels were digitised, lateral migration distances were calculated along each transect using the 'Transect Channel Migration Tool' (Legg et al. 2014). Annual lateral migration rates for a given time interval were calculated by dividing each of the measured distances by the number of years in the time interval of interest. Historical meander belt polygons and their centrelines, and the locations of the lateral migration measurement transects are displayed for each reach below.

Bollin1

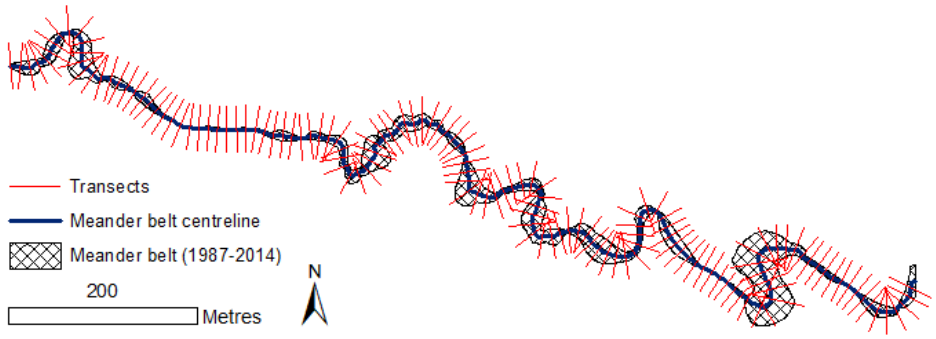

Bollin2

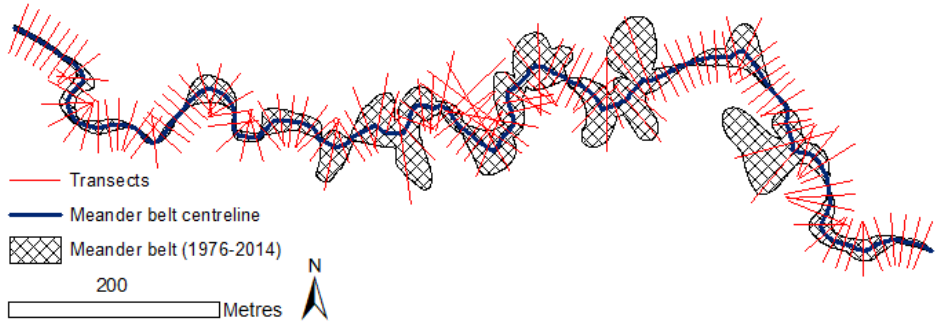

Calder

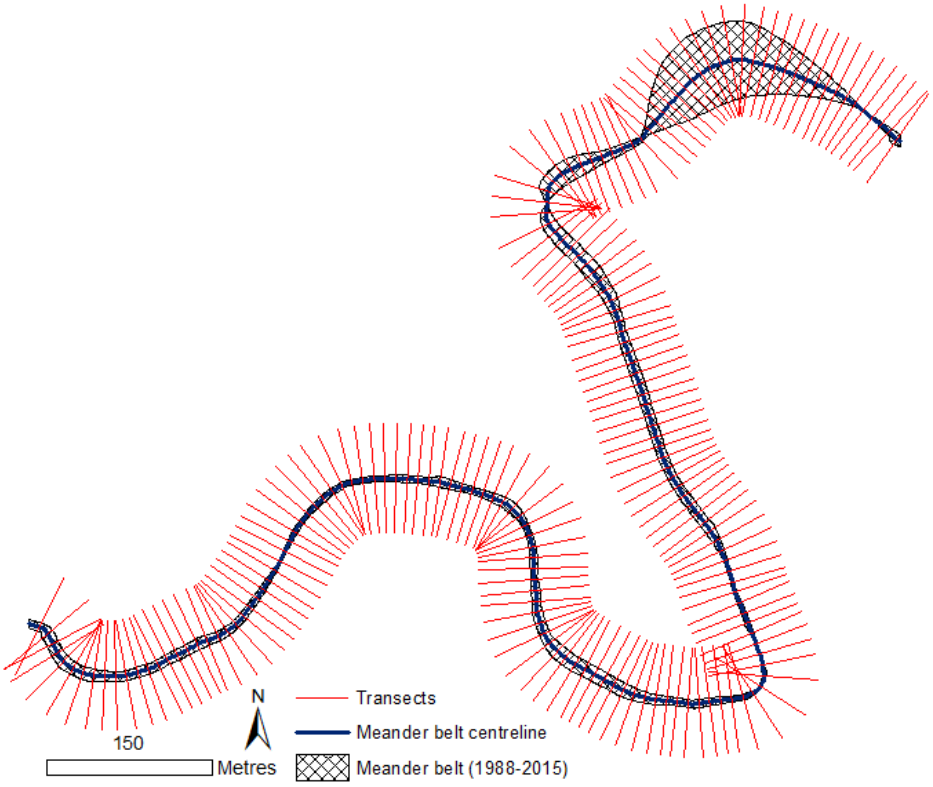

Coquet1

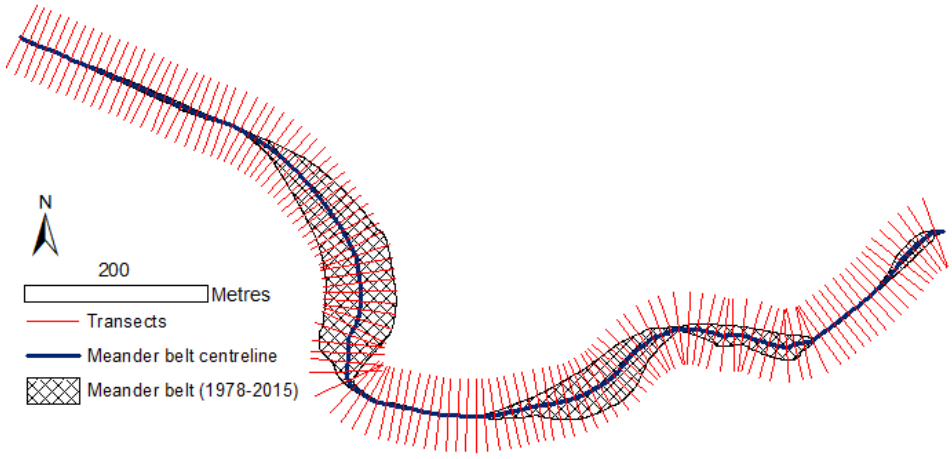

Coquet2

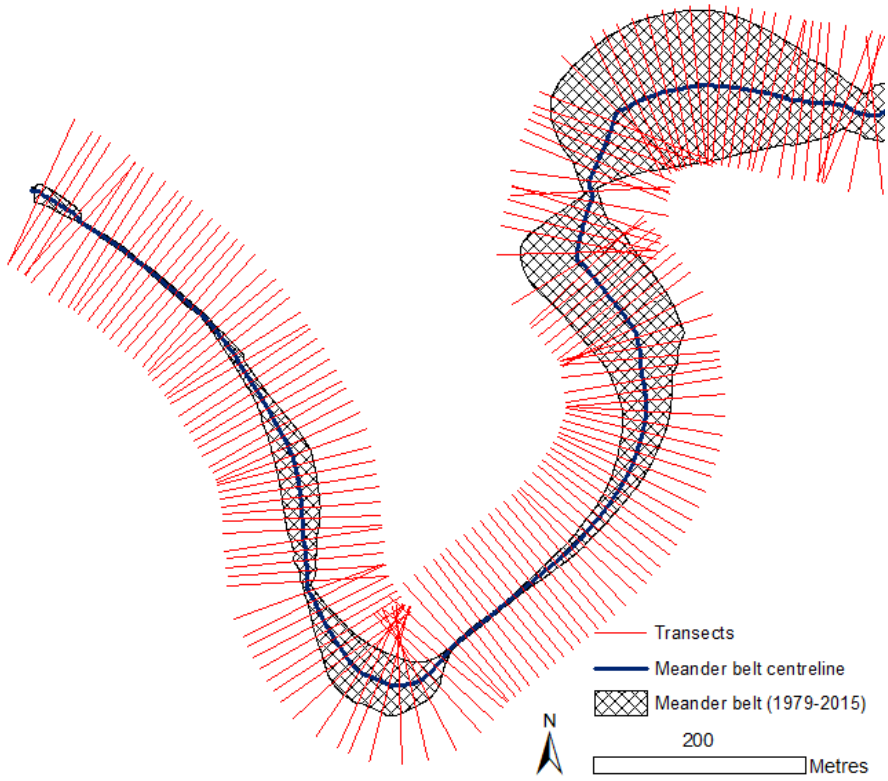

Dane

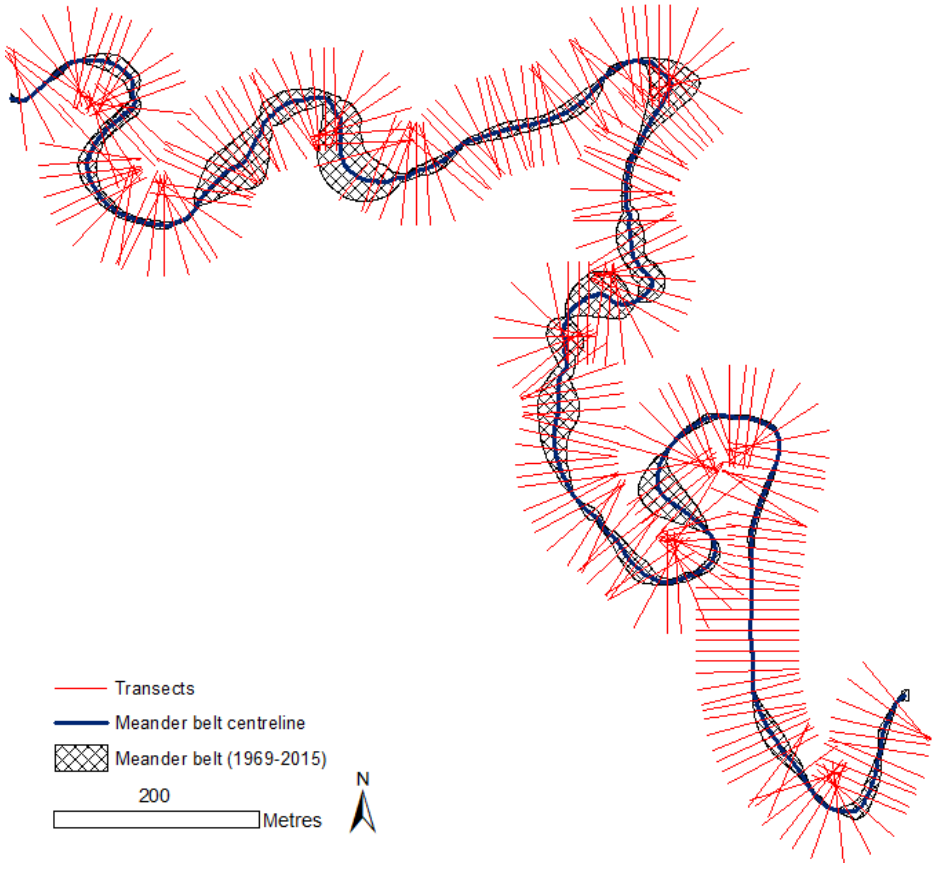

Harwood Beck

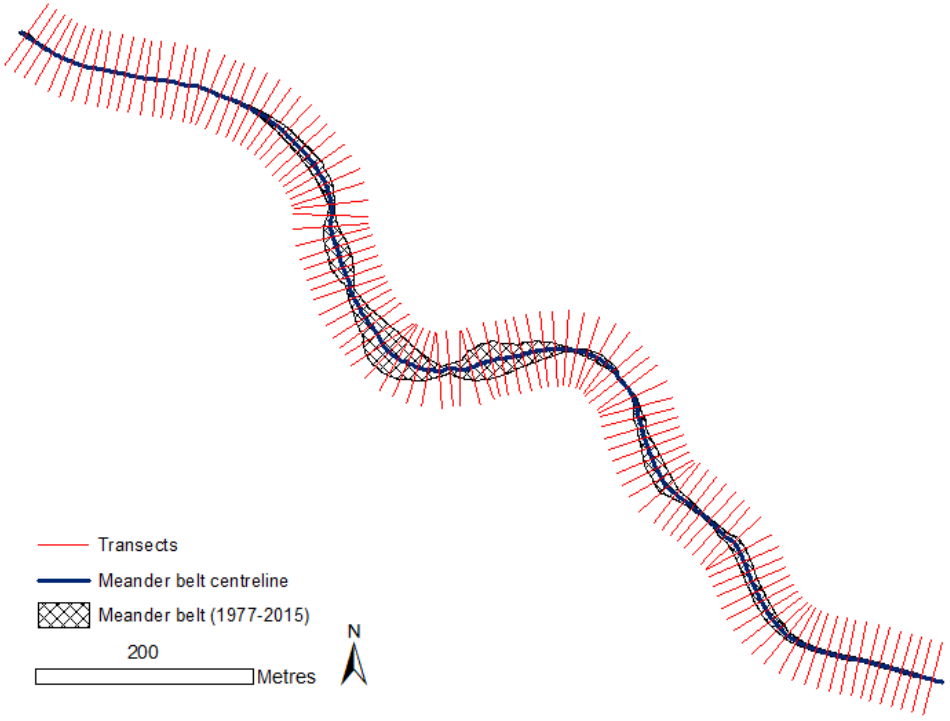

Lune

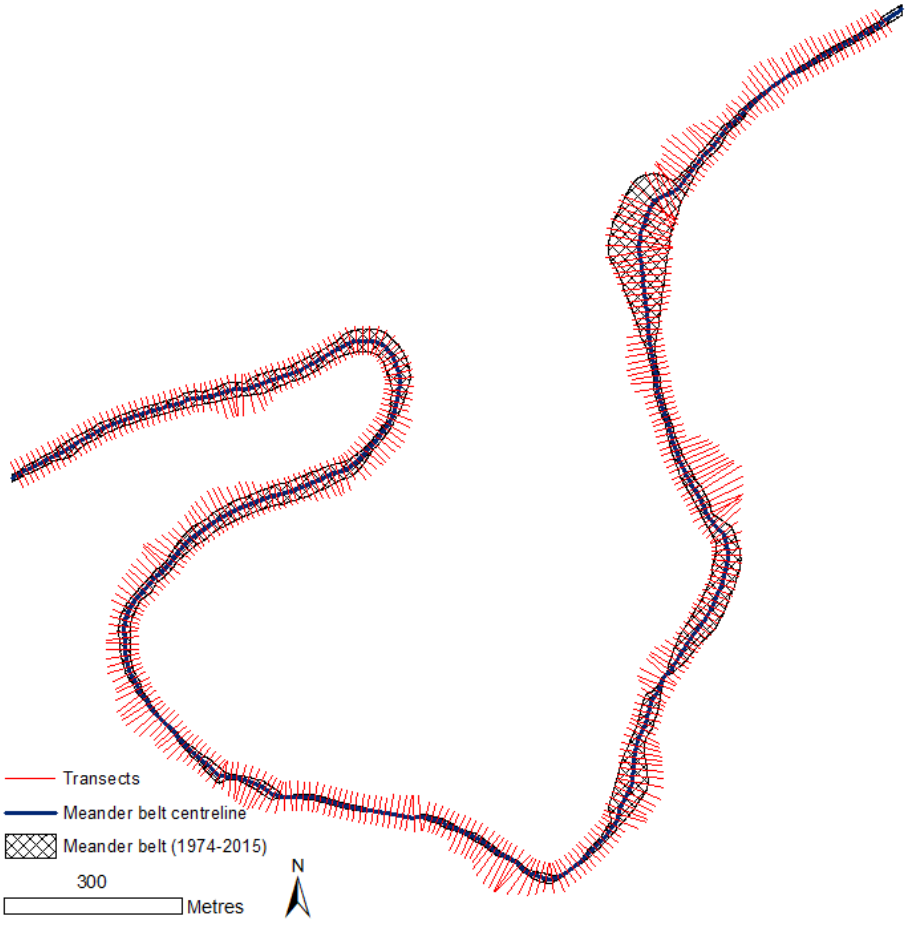

South Tyne1

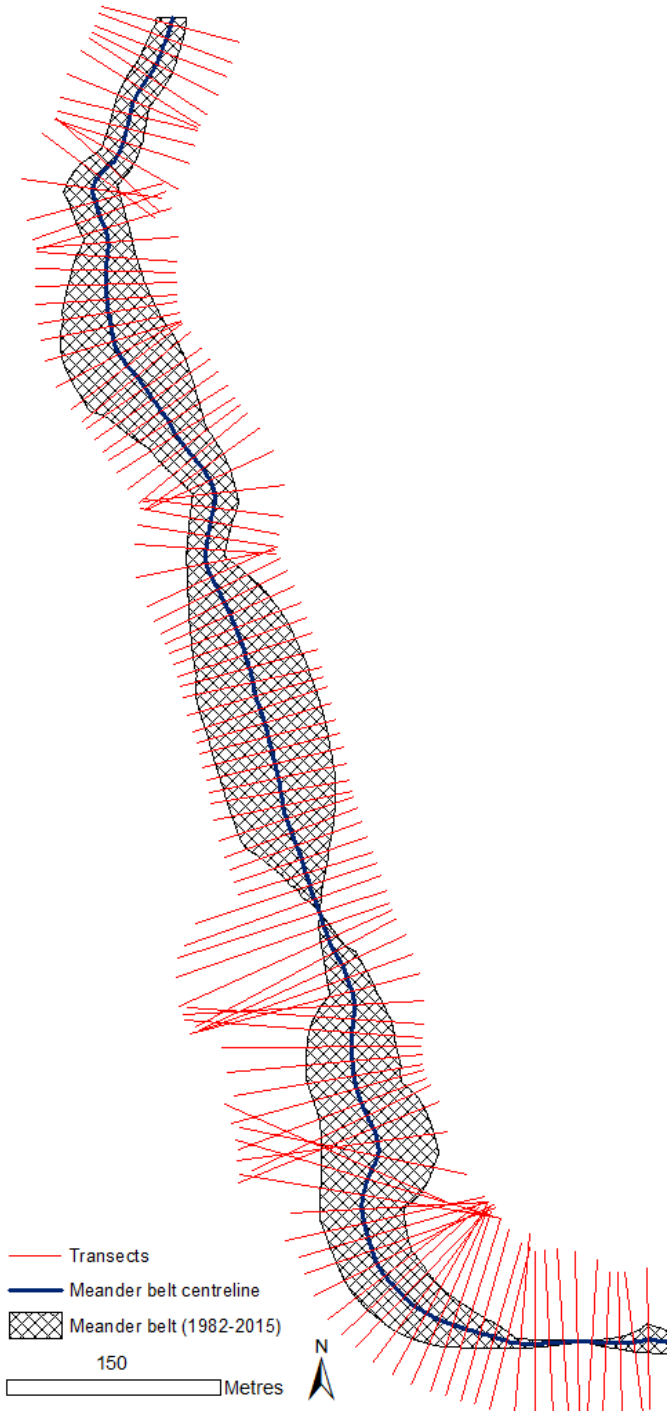
Transects
Meander belt centreline
Meander belt (1982-2015)
150
Metres
N

South Tyne2

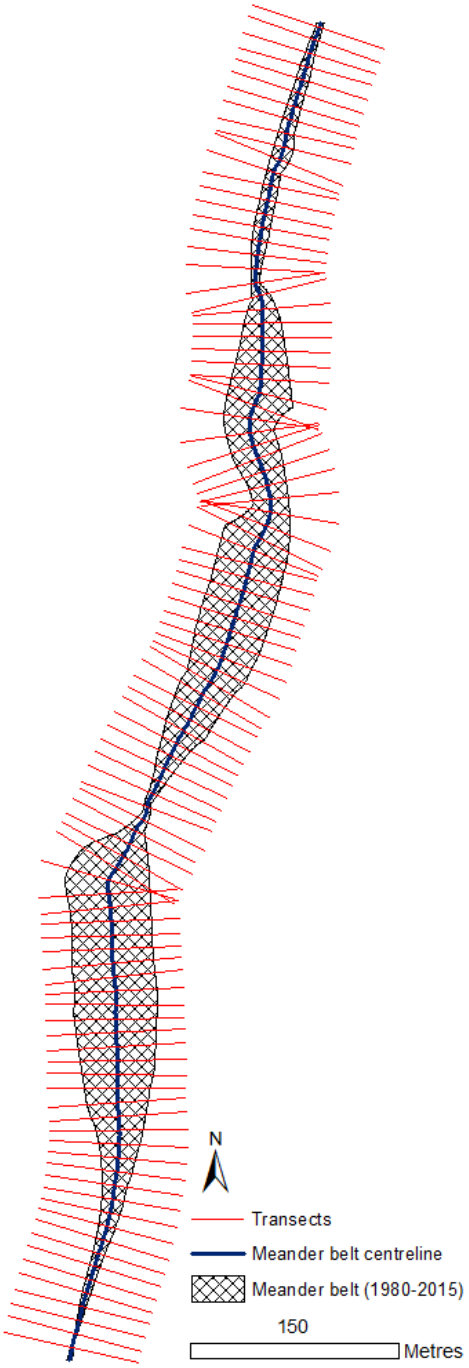
N
Transects
Meander belt centreline
Meander belt (1980-2015)
150
Metres

C: The Analytic Hierarchy Process in detail

Several criteria can be used to evaluate how accurately a model reproduces real-world phenomena. With CAESAR-Lisflood, rates of erosion, deposition and lateral migration, as well as successful reconstruction of mapped planform channel morphology, were used to evaluate how accurately each simulation reconstructed mapped historical changes. This was undertaken during model calibration for five reaches to select the single most accurate combination of parameter values from a series of simulations. After calibration of the five selected reaches, the resulting model parameter value ranges were applied to five uncalibrated reaches, and the same model evaluation criteria were used to select the single most accurate parameter value combination for each of these reaches and to quantify the overall accuracy of modelled reconstructions. In order to achieve this however, two challenges needed to be addressed:

1) How to determine an overall 'score' of model accuracy from multiple criteria, and;
2) How to do this when the selected criteria contribute different degrees of importance to the overall assessment of model accuracy.

The Analytic Hierarchy Process (AHP) is a decision-making framework whereby multiple criteria of differing importance, derived from user judgement, are compared in a pairwise manner in order to select the best outcome from a range of competing alternatives (Saaty 1990; Vargas 1990). The AHP has been applied previously in a CAESAR-Lisflood modelling context to select the most accurate simulation, based on multiple criteria of differing importance, from an ensemble of runs during model calibration (see Meadows 2014). To make a 'decision' – in this case, select the most accurate simulation from a large ensemble – the following steps should be taken:

1) Develop a hierarchical model for the decision which includes a goal, criteria and alternatives.

2) Derive priorities (weights) for the criteria, by comparing the importance of criteria in a pairwise manner with respect to the stated goal.
3) Derive local priorities by (preferences) for the alternatives.
4) Derive overall priorities (model synthesis) by combining local priorities as a weighted sum to establish the overall priority of each of the alternatives. The alternative with the highest overall priority is the 'best choice'.
5) Perform a sensitivity analysis to determine how changes in the weights of the criteria could affect the result.
6) Making a final decision based on the results of the preceding steps.

The following discussion uses the calibration of the Dane reach as a demonstration of how the AHP works. Each of the six steps will use data for this reach. See also: Mu, E. & Pereyra-Rojas, M., 2017. Understanding the analytic hierarchy process. In *Practical decision making* (pp. 7-22), Cham: SpringerBriefs in Operations Research, DOI 10.1007/978-3-319-33861-3_2 for further details and where the following step-by-step is originally taken from.

STEP 1: Developing a hierarchical model

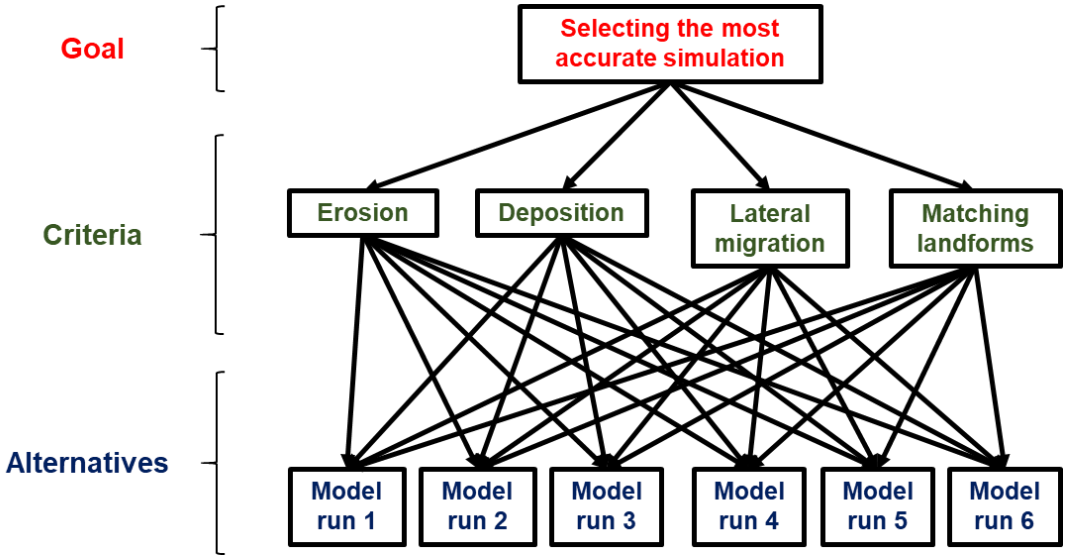

The goal and criteria specified above apply to all ten of the reaches.

For the Dane, six model runs were identified during calibration as having a 'good fit' to mapped data, based on visual comparison with historical river channel changes. Therefore, for this example, the alternatives are the six visually accurate simulations from the wider ensemble of calibration runs.

STEP 2: Deriving priorities (weights) for each criterion

Thomas Saaty, the developer of the AHP, devised a numerical scale for pairwise comparison to determine the relative importance of one criterion over another (see table below). Values from 1 to 9 are assigned to different criteria based on user judgement.

The 1-9 scale of importance for pairwise comparisons between selection criteria (modified from Saaty 1986, 2008).

Rank of importance	Definition	Explanation
1	Equal	Equal contribution of criteria to the objective
2	Weak or slight	-
3	Moderate	Slightly favouring one criterion over another
4	Moderate plus	-
5	Strong	Strongly favouring one criterion over another
6	Strong plus	-
7	Very strong	Very strongly favouring a criterion
8	Very, very strong	-
9	Extreme	Evidence favouring a criterion is of the highest degree of importance over another
Reciprocals of above	If criterion *a* has one of the above rank values assigned to it when compared with criterion *b*, then *b* has the reciprocal value when compared with *a*	-

To perform the pairwise comparison, a comparison matrix of the criteria outlined in STEP 1 needs to be created (see below).

Cells in the comparison matrix have a value or 'judgement' from the numeric scale listed in the table above. For example, if it is judged that 'erosion' is weakly/slightly more important than 'lateral migration', the erosion-lateral

migration comparison cell (where the row ‘erosion’ and column ‘lateral migration’ intersect will have a value of 2. By extension, the opposite comparison of the importance of ‘lateral migration’ relative to ‘erosion’ will produce the reciprocal of this value in the cell where the row ‘lateral migration’ and column ‘erosion’ intersect.

Other values in the comparison matrix arise due to the following:

- ‘Erosion’ is judged to be of equal importance to ‘deposition’.
- ‘Deposition’ is judged to be of weak/slight importance over ‘lateral migration’.
- Both ‘erosion’ and ‘deposition’ are judged to be of moderate importance over ‘matching landforms’.
- ‘Lateral migration’ is judged to be of weak/slight importance over ‘matching landforms’.
- Where these criteria are compared in the opposite direction, the reciprocal values occupy the remaining cells.

Once judgement values are assigned to each of the cells in the matrix, the overall priorities/weights of the criteria need to be calculated. This is achieved by normalisation – i.e. taking the sum of values in each column and dividing the values in each cell by their respective column sums.

Pairwise comparison matrix with judgement values of the relative importance of criteria over one another.

	Erosion	**Deposition**	**Lateral migration**	**Matching landforms**
Erosion	1	1	2	3
Deposition	1	1	2	3
Lateral migration	0.5	0.5	1	2
Matching landforms	0.33	0.33	0.5	1

Pairwise comparison matrix after values in each column have been summed.

	Erosion	**Deposition**	**Lateral migration**	**Matching landforms**

Erosion	1	1	2	3
Deposition	1	1	2	3
Lateral migration	0.5	0.5	1	2
Matching landforms	0.33	0.33	0.5	1
Sum	2.83	2.83	3.5	9

Pairwise comparison matrix after normalisation (normalised values in bold).

	Erosion	**Deposition**	**Lateral migration**	**Matching landforms**
Erosion	1 ÷ 2.83 = **0.353**	1 ÷ 2.83 = **0.353**	2 ÷ 3.5 = **0.364**	3 ÷ 9 = **0.333**
Deposition	1 ÷ 2.83 = **0.353**	1 ÷ 2.83 = **0.353**	2 ÷ 3.5 = **0.364**	3 ÷ 9 = **0.333**
Lateral migration	0.5 ÷ 2.83 = **0.176**	0.5 ÷ 2.83 = **0.176**	1 ÷ 3.5 = **0.182**	2 ÷ 9 = **0.222**
Matching landforms	0.33 ÷ 2.83 = **0.118**	0.33 ÷ 2.83 = **0.118**	0.5 ÷ 3.5 = **0.090**	1 ÷ 9 = **0.111**

From the normalised matrix, the overall or final priorities are calculated by taking the mean of each row.

Calculation of priorities/weights by taking the mean of each row.

	Erosion	**Deposition**	**Lateral migration**	**Matching landforms**	**Priority (weight)**
Erosion	0.353	0.353	0.364	0.333	**0.351**
Deposition	0.353	0.353	0.364	0.333	**0.351**
Lateral migration	0.176	0.176	0.182	0.222	**0.189**
Matching landforms	0.118	0.118	0.090	0.111	**0.109**

Original judgements of importance with calculated priorities.

	Erosion	**Deposition**	**Lateral migration**	**Matching landforms**	**Priority (weight)**
Erosion	1	1	2	3	**0.351**
Deposition	1	1	2	3	**0.351**

Lateral migration	0.5	0.5	1	2	**0.189**
Matching landforms	0.33	0.33	0.5	1	**0.109**

It is possible for inconsistencies to arise when judgement weights are calculated, with the chance of these occurring as the number of pairwise comparisons increases. Some inconsistency in the matrix of judgements is expected and allowed in AHP analysis.

When weights were calculated, a consistency ratio (*CR*) was determined as:

$$CR = \frac{CI}{RI}$$

where *CI* is the consistency index of the matrix in question and *RI* is the consistency index of a matrix where judgements have random values (Saaty & Vargas 2012). If $CR \leq 0.1$, the consistency in judgement values is deemed acceptable to continue analysis (Saaty & Vargas 2012).

Software packages such as the ‘‘ahp” package in R (Glur 2018) calculate automatically the priority weights from a matrix of assigned judgements, and calculate a consistency ratio value to check that consistency in the judgments is acceptable.

For the judgement values presented in the matrices above, a consistency ratio of 0.004 is calculated, indicating the judgement values are satisfactorily consistent.

STEP 3: Deriving local priorities (preferences) for the alternatives

This step involves deriving relative priorities (preferences) of the alternatives with respect to each criterion. In this case, what are the priorities of the alternatives with respect to ‘erosion’, ‘deposition’, ‘lateral migration’ and ‘matching landforms’?

The original approach (see Saaty 1990 for an example) involves performing another set of pairwise comparisons, this time with judgments for the relative importance of different alternatives to each other based on individual criteria.

Here, a similar but more streamlined approach is adopted. For each criterion, the absolute relative error between modelled and mapped datasets is calculated. The six simulations are then ranked from 1 (lowest error value) to 6 (highest error value). This is then repeated until all four criteria have been compared across the alternatives.

Absolute relative error values for each model run-criterion intersection.

	Erosion	Deposition	Lateral migration	Matching landforms
Model run 1	0.448	0.799	0.48	0.114
Model run 2	0.346	0.793	0.413	0.108
Model run 3	0.514	0.687	0.369	0.117
Model run 4	0.289	0.804	0.388	0.113
Model run 5	0.509	0.857	0.481	0.117
Model run 6	0.601	0.825	0.532	0.12

Ranks (by column) of each simulation based on the magnitude of error for each criterion. The ranks are used here as local priorities for the subsequent steps in the AHP analysis.

	Erosion	Deposition	Lateral migration	Matching landforms
Model run 1	3	3	4	2
Model run 2	2	2	3	1
Model run 3	5	1	1	5
Model run 4	1	4	2	3
Model run 5	4	6	5	4
Model run 6	6	5	6	6

STEP 4: Deriving overall priorities (model synthesis)

For each alternative, the overall priority is calculated as follows:

1) Multiplying the local priority of each model run-criterion intersection in the second matrix of STEP 3 by the corresponding priority/weight values calculated in STEP 2 (see last matrix in STEP 2).
2) Taking the sum of these newly calculated products to give an overall priority for each model run.

This is illustrated below:

Local priorities calculated in STEP 3 with weights calculated in STEP 2.

	Erosion	**Deposition**	**Lateral migration**	**Matching landforms**
Criteria weights (from STEP 2)	*0.351*	*0.351*	*0.189*	*0.109*
Model run 1	3	3	4	2
Model run 2	2	2	3	1
Model run 3	5	1	1	5
Model run 4	1	4	2	3
Model run 5	4	6	5	4
Model run 6	6	5	6	6

Synthesis of the model produced by calculating overall priorities.

	Erosion	**Deposition**	**Lateral migration**	**Matching landforms**	**Overall priority (row sums)**
Model run 1	3 × 0.351 = 1.053	3 × 0.351 = 1.053	4 × 0.189 = 0.756	2 × 0.109 = 0.218	3.08
Model run 2	2 × 0.351 = 0.702	2 × 0.351 = 0.702	3 × 0.189 = 0.567	1 × 0.109 = 0.109	2.08
Model run 3	5 × 0.351 = 1.755	1 × 0.351 = 0.351	1 × 0.189 = 0.189	5 × 0.109 = 0.545	2.84
Model run 4	1 × 0.351 = 0.351	4 × 0.351 = 1.404	2 × 0.189 = 0.378	3 × 0.109 = 0.327	2.46
Model run 5	4 × 0.351 = 1.404	6 × 0.351 = 2.106	5 × 0.189 = 0.945	4 × 0.109 = 0.436	4.891
Model run 6	6 × 0.351 = 2.106	5 × 0.351 = 1.755	6 × 0.189 = 1.134	6 × 0.109 = 0.654	5.649

STEP 5: Sensitivity analysis

Based on the results of STEP 4, Model run 2 would be judged to be the most accurate of the six simulations because it has the smallest overall priority

value of all the alternatives. However, before a final decision can be made as to which simulation is the most accurate, a sensitivity analysis needs to be undertaken.

The overall weights will be affected by the weights given to the respective criteria. Even if the following assumptions are adhered to:

1) 'Erosion' and 'deposition' are always of equal importance;
2) 'Erosion' and 'deposition' are always more important than 'lateral migration' and 'matching landforms';
3) 'Lateral migration' is always slightly/weakly less important than 'erosion' and 'deposition' – i.e. 1 rank lower;

there are seven combinations of overall priorities that could be calculated in STEP 4 (model synthesis).

Therefore, before a final decision is made, it is useful to carry out a 'what-if' analysis to determine how the final results would have changed if the weights of the criteria had been different. Scenarios with the six other combinations of criteria weights are presented below:

Pairwise comparison matrices for each of the other scenarios where the three assumptions described above apply.

	Erosion	Deposition	Lateral migration	Matching landforms	Priority (weight)
Erosion	1	1	2	4	0.364
Deposition	1	1	2	4	0.364
Lateral migration	0.5	0.5	1	2	0.182
Matching landforms	0.25	0.25	0.5	1	0.091

	Erosion	Deposition	Lateral migration	Matching landforms	Priority (weight)
Erosion	1	1	2	5	0.372
Deposition	1	1	2	5	0.372
Lateral migration	0.5	0.5	1	2	0.176

Matching landforms	0.2	0.2	0.5	1	0.079

	Erosion	**Deposition**	**Lateral migration**	**Matching landforms**	**Priority (weight)**
Erosion	1	1	2	6	0.379
Deposition	1	1	2	6	0.379
Lateral migration	0.5	0.5	1	2	0.172
Matching landforms	0.17	0.17	0.5	1	0.07

	Erosion	**Deposition**	**Lateral migration**	**Matching landforms**	**Priority (weight)**
Erosion	1	1	2	7	0.384
Deposition	1	1	2	7	0.384
Lateral migration	0.5	0.5	1	2	0.168
Matching landforms	0.14	0.14	0.5	1	0.064

	Erosion	**Deposition**	**Lateral migration**	**Matching landforms**	**Priority (weight)**
Erosion	1	1	2	8	0.388
Deposition	1	1	2	8	0.388
Lateral migration	0.5	0.5	1	2	0.165
Matching landforms	0.12	0.12	0.5	1	0.059

	Erosion	**Deposition**	**Lateral migration**	**Matching landforms**	**Priority (weight)**
Erosion	1	1	2	9	0.392
Deposition	1	1	2	9	0.392
Lateral migration	0.5	0.5	1	2	0.162
Matching landforms	0.11	0.11	0.5	1	0.055

Model synthesis results when new priority weights are used.

	Erosion	Deposition	Lateral migration	Matching landforms	Overall priority (row sums)
Criteria weights	*0.364*	*0.364*	*0.182*	*0.091*	**-**
Model run 1	3 × 0.364 = 1.092	3 × 0.364 = 1.092	4 × 0.182 = 0.728	2 × 0.091 = 0.182	3.094
Model run 2	2 × 0.364 = 0.728	2 × 0.364 = 0.728	3 × 0.182 = 0.546	1 × 0.091 = 0.091	2.093
Model run 3	5 × 0.364 = 1.82	1 × 0.364 = 0.364	1 × 0.182 = 0.182	5 × 0.091 = 0.455	2.821
Model run 4	1 × 0.364 = 0.364	4 × 0.364 = 1.456	2 × 0.182 = 0.364	3 × 0.091 = 0.273	2.457
Model run 5	4 × 0.364 = 1.456	6 × 0.364 = 2.184	5 × 0.182 = 0.91	4 × 0.091 = 0.364	4.914
Model run 6	6 × 0.364 = 2.184	5 × 0.364 = 1.82	6 × 0.182 = 1.092	6 × 0.091 = 0.546	5.642

	Erosion	Deposition	Lateral migration	Matching landforms	Overall priority (row sums)
Criteria weights	*0.372*	*0.372*	*0.176*	*0.079*	**-**
Model run 1	3 × 0.372 = 1.116	3 × 0.372 = 1.116	4 × 0.176 = 0.704	2 × 0.079 = 0.158	3.094
Model run 2	2 × 0.372 = 0.744	2 × 0.372 = 0.744	3 × 0.176 = 0.528	1 × 0.079 = 0.079	2.095
Model run 3	5 × 0.372 = 1.86	1 × 0.372 = 0.372	1 × 0.176 = 0.176	5 × 0.079 = 0.395	2.803
Model run 4	1 × 0.372 = 0.372	4 × 0.372 = 1.488	2 × 0.176 = 0.352	3 × 0.079 = 0.237	2.449
Model run 5	4 × 0.372 = 1.488	6 × 0.372 = 2.232	5 × 0.176 = 0.88	4 × 0.079 = 0.316	4.916
Model run 6	6 × 0.372 = 2.232	5 × 0.372 = 1.86	6 × 0.176 = 1.056	6 × 0.079 = 0.474	5.622

	Erosion	Deposition	Lateral migration	Matching landforms	Overall priority (row sums)
Criteria weights	*0.379*	*0.379*	*0.172*	*0.07*	**-**
Model run 1	3 × 0.379 = 1.137	3 × 0.379 = 1.137	4 × 0.172 = 0.688	2 × 0.07 = 0.14	3.102
Model run 2	2 × 0.379 = 0.758	2 × 0.379 = 0.758	3 × 0.172 = 0.516	1 × 0.07 = 0.07	2.102
Model run 3	5 × 0.379 = 1.895	1 × 0.379 = 0.379	1 × 0.172 = 0.172	5 × 0.07 = 0.35	2.796
Model run 4	1 × 0.379 = 0.379	4 × 0.379 = 1.516	2 × 0.172 = 0.344	3 × 0.07 = 0.21	2.449
Model run 5	4 × 0.379 = 1.516	6 × 0.379 = 2.274	5 × 0.172 = 0.86	4 × 0.07 = 0.28	4.93
Model run 6	6 × 0.379 = 2.274	5 × 0.379 = 1.895	6 × 0.172 = 1.032	6 × 0.07 = 0.42	5.621

	Erosion	Deposition	Lateral migration	Matching landforms	Overall priority (row sums)
Criteria weights	*0.384*	*0.384*	*0.168*	*0.064*	**-**
Model run 1	3 × 0.384 = 1.152	3 × 0.384 = 1.152	4 × 0.168 = 0.672	2 × 0.064 = 0.128	3.104
Model run 2	2 × 0.384 = 0.768	2 × 0.384 = 0.768	3 × 0.168 = 0.504	1 × 0.064 = 0.064	2.104
Model run 3	5 × 0.384 = 1.92	1 × 0.384 = 0.384	1 × 0.168 = 0.168	5 × 0.064 = 0.32	2.792
Model run 4	1 × 0.384 = 0.384	4 × 0.384 = 1.536	2 × 0.168 = 0.336	3 × 0.064 = 0.192	2.448
Model run 5	4 × 0.384 = 1.536	6 × 0.384 = 2.304	5 × 0.168 = 0.84	4 × 0.064 = 0.256	4.936
Model run 6	6 × 0.384 = 2.304	5 × 0.384 = 1.92	6 × 0.168 = 1.008	6 × 0.064 = 0.384	5.616

	Erosion	Deposition	Lateral migration	Matching landforms	Overall priority (row sums)
Criteria weights	*0.388*	*0.388*	*0.165*	*0.059*	**-**
Model run 1	3 × 0.388 = 1.164	3 × 0.388 = 1.164	4 × 0.165 = 0.66	2 × 0.059 = 0.118	3.106
Model run 2	2 × 0.388 = 0.776	2 × 0.388 = 0.776	3 × 0.165 = 0.495	1 × 0.059 = 0.059	2.106
Model run 3	5 × 0.388 = 1.94	1 × 0.388 = 0.388	1 × 0.165 = 0.165	5 × 0.059 = 0.295	2.788
Model run 4	1 × 0.388 = 0.388	4 × 0.388 = 1.552	2 × 0.165 = 0.33	3 × 0.059 = 0.177	2.447
Model run 5	4 × 0.388 = 1.552	6 × 0.388 = 2.328	5 × 0.165 = 0.825	4 × 0.059 = 0.236	4.941
Model run 6	6 × 0.388 = 2.328	5 × 0.388 = 1.94	6 × 0.165 = 0.99	6 × 0.059 = 0.354	5.612

	Erosion	Deposition	Lateral migration	Matching landforms	Overall priority (row sums)
Criteria weights	*0.392*	*0.392*	*0.162*	*0.055*	**-**
Model run 1	3 × 0.392 = 1.176	3 × 0.392 = 1.176	4 × 0.162 = 0.648	2 × 0.055 = 0.11	3.11
Model run 2	2 × 0.392 = 0.784	2 × 0.392 = 0.784	3 × 0.162 = 0.486	1 × 0.055 = 0.055	2.109
Model run 3	5 × 0.392 = 1.96	1 × 0.392 = 0.392	1 × 0.162 = 0.162	5 × 0.055 = 0.275	2.789
Model run 4	1 × 0.392 = 0.392	4 × 0.392 = 1.568	2 × 0.162 = 0.324	3 × 0.055 = 0.165	2.449
Model run 5	4 × 0.392 = 1.568	6 × 0.392 = 2.352	5 × 0.162 = 0.81	4 × 0.055 = 0.22	4.95
Model run 6	6 × 0.392 = 2.352	5 × 0.392 = 1.96	6 × 0.162 = 0.972	6 × 0.055 = 0.33	5.614

STEP 6: Making a final decision

Once the preceding steps have been completed, a final decision can be made (in this case, which model out of the ensemble of calibration runs should be selected). To do this, it is important to compare the overall priorities from the model synthesis stage (STEP 4), taking into account the sensitivity analysis conducted in STEP 5.

The table below summarises how this was done for the model selection.

Summary of overall priorities for each model run. Total of seven values for each simulation for each scenario where 'erosion' and 'deposition' are jointly most important, both are always 1 rank higher than 'lateral migration', and all three of these criteria are more important than 'matching landforms'. Overall priority scores are ranked 1-6 (by row). The model ranked '1' the most times is selected as the most accurate.

Model run 1		Model run 2		Model run 3		Model run 4		Model run 5		Model run 6	
Overall priority	Rank	Overall priority	Rank	Overall priority	Rank	Overall priority	Rank	Overall priority	Rank	Overall priority	Rank
3.08	4	2.08	1	2.84	3	2.46	2	4.891	5	5.649	6
3.094	4	2.093	1	2.821	3	2.457	2	4.914	5	5.642	6
3.094	4	2.095	1	2.803	3	2.449	2	4.916	5	5.622	6
3.102	4	2.102	1	2.796	3	2.449	2	4.93	5	5.621	6
3.104	4	2.104	1	2.792	3	2.448	2	4.936	5	5.616	6
3.106	4	2.106	1	2.788	3	2.447	2	4.941	5	5.612	6
3.11	4	2.109	1	2.789	3	2.449	2	4.95	5	5.614	6

Based on the above table, Model run 2 has the lowest overall priority consistently, and is therefore selected from the other calibration runs as the most accurate for this reach.

This 6-step AHP procedure is repeated until the single most accurate parameter value combination has been identified for all ten reaches.

D: Testing for (un)even channel-floodplain sediment exchange

Extra simulations were run for four of the reaches (Coquet1, Coquet2, Dane and Lune) to test if the grainsize distribution of recorded sediment fluxes at the reach outlet was similar to the grainsize distribution of sediment entering the top of the reach. If the input and output distributions are similar, this demonstrates that the CAESAR-Lisflood model does conserve mass across the full range of grainsizes. If these distributions are unequal however, there is a risk that uneven sediment exchange is going on, affecting river channel changes in the process. To determine whether (un)even sediment exchange between the channel and floodplain is occurring, the saved output discharge/sediment flux file from the end of the original Coquet1, Coquet2, Dane and Lune calibration simulations was input into a set of new model runs along these reaches. The grainsize distributions of input and output sediment fluxes were compared for selected days. Generally, it would appear that output sediment fluxes balance with input sediment fluxes, suggesting that uneven channel-floodplain exchange is not occurring. Note the time-series presented for each reach includes the full historic flow series that overlaps with the map record (i.e. the spin-up and calibration periods together).

Coquet1

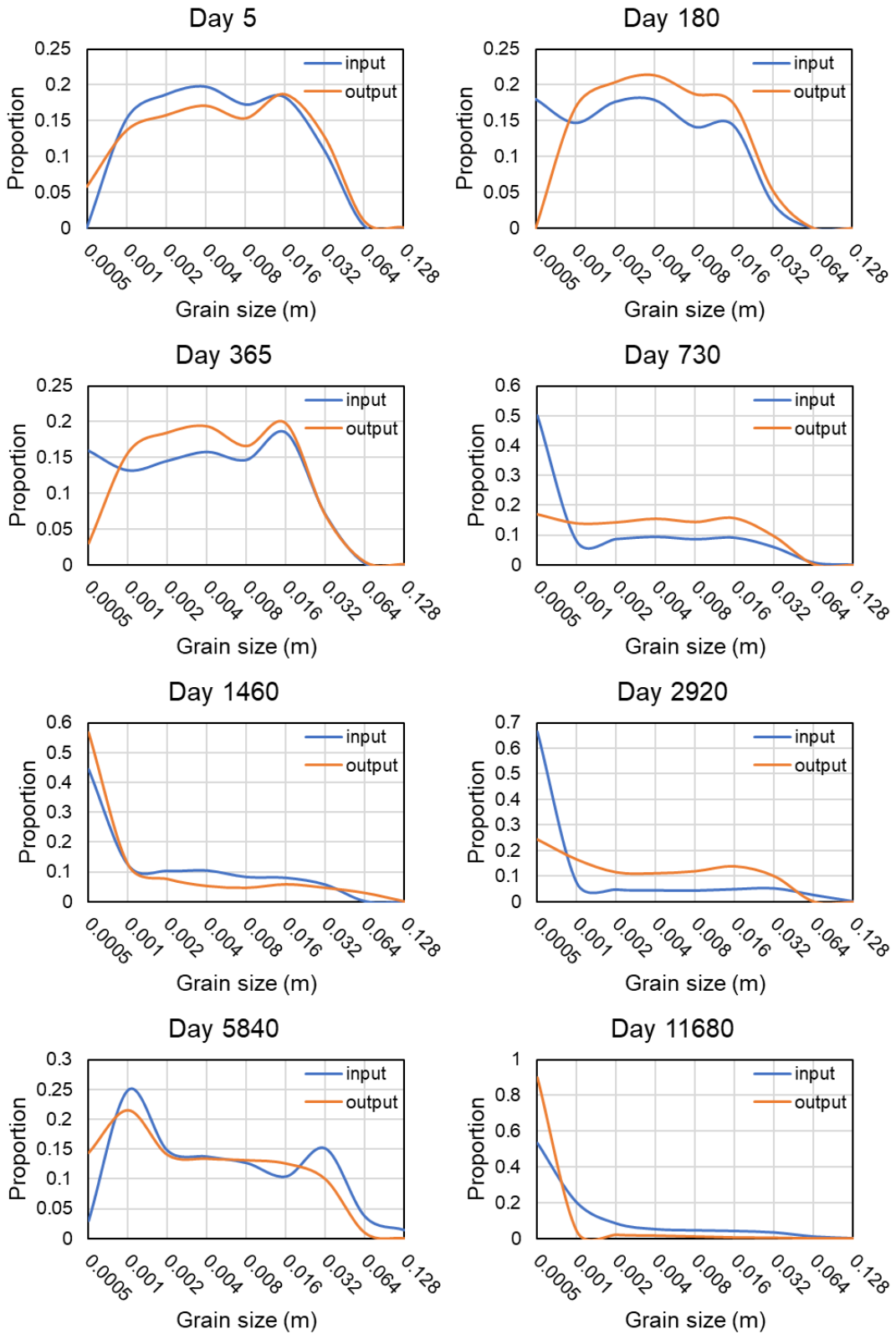
Day 5
Day 180
Day 365
Day 730
Day 1460
Day 2920
Day 5840
Day 11680
input
output
Proportion
Grain size (m)
0.0005
0.001
0.002
0.004
0.008
0.016
0.032
0.064
0.128

Coquet2

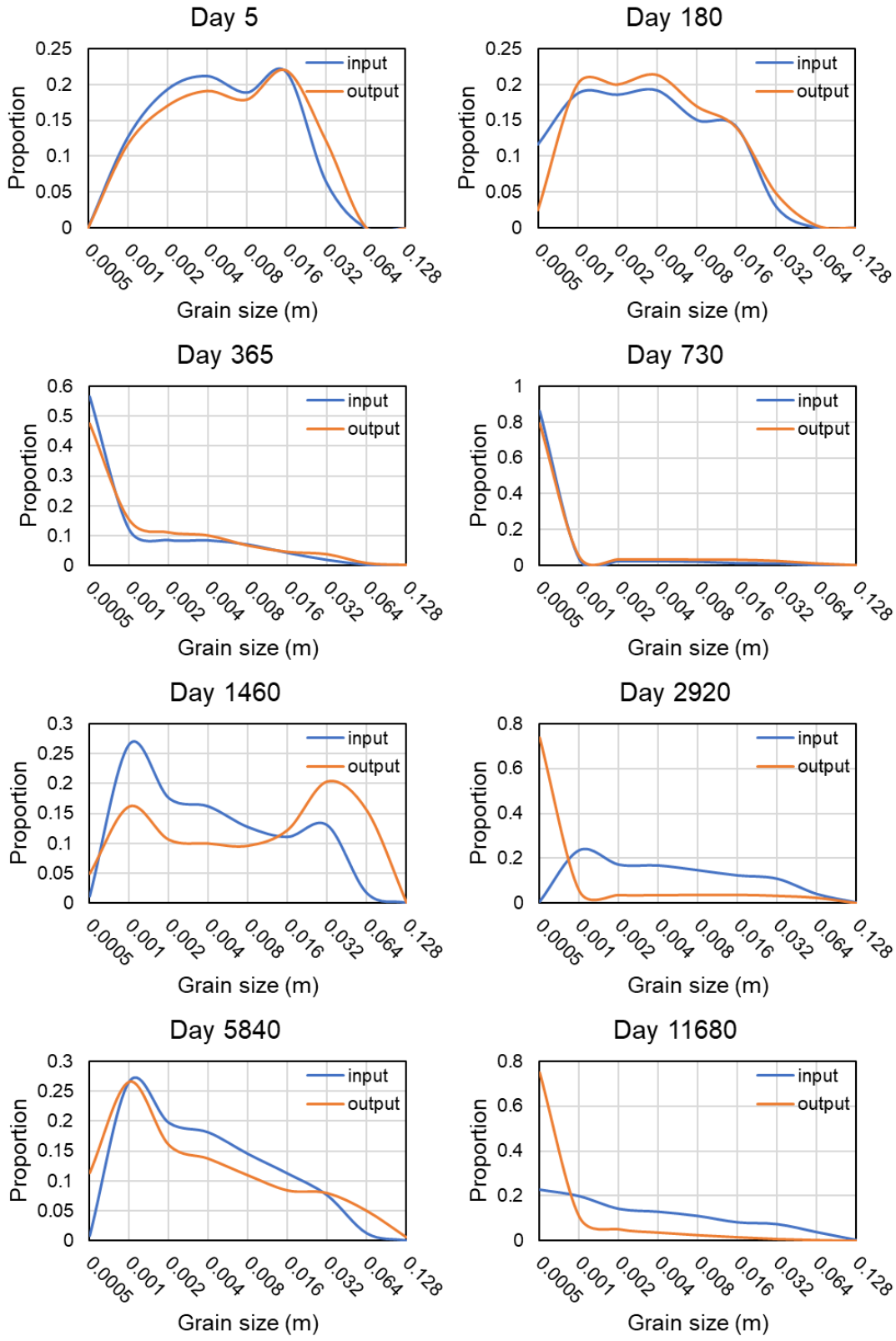
Day 5
Day 180
Day 365
Day 730
Day 1460
Day 2920
Day 5840
Day 11680
input
output
Proportion
Grain size (m)
0.0005
0.001
0.002
0.004
0.008
0.016
0.032
0.064
0.128

Dane

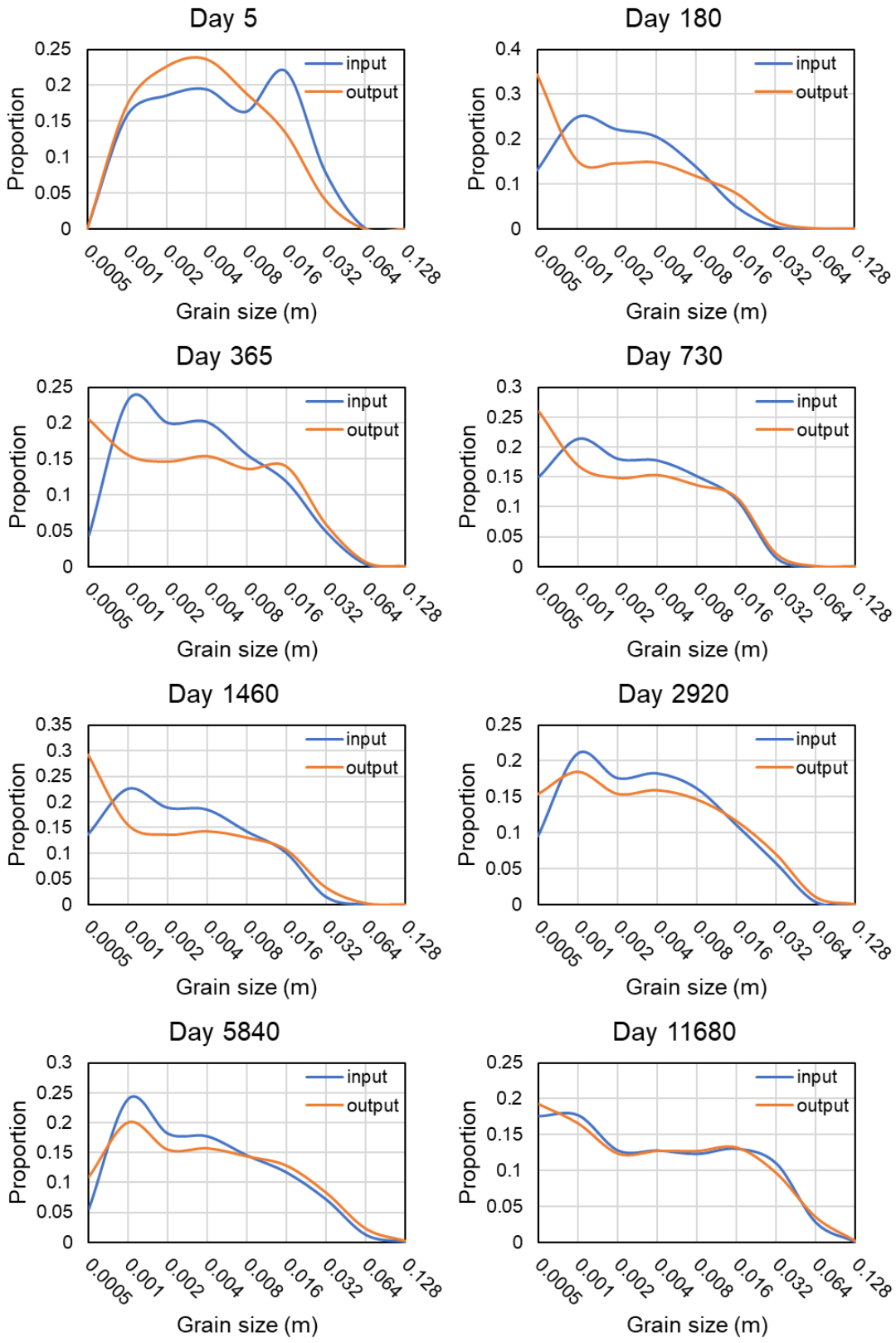
Day 5
Day 180
Day 365
Day 730
Day 1460
Day 2920
Day 5840
Day 11680
input
output
Proportion
Grain size (m)
0.0005
0.001
0.002
0.004
0.008
0.016
0.032
0.064
0.128

Lune

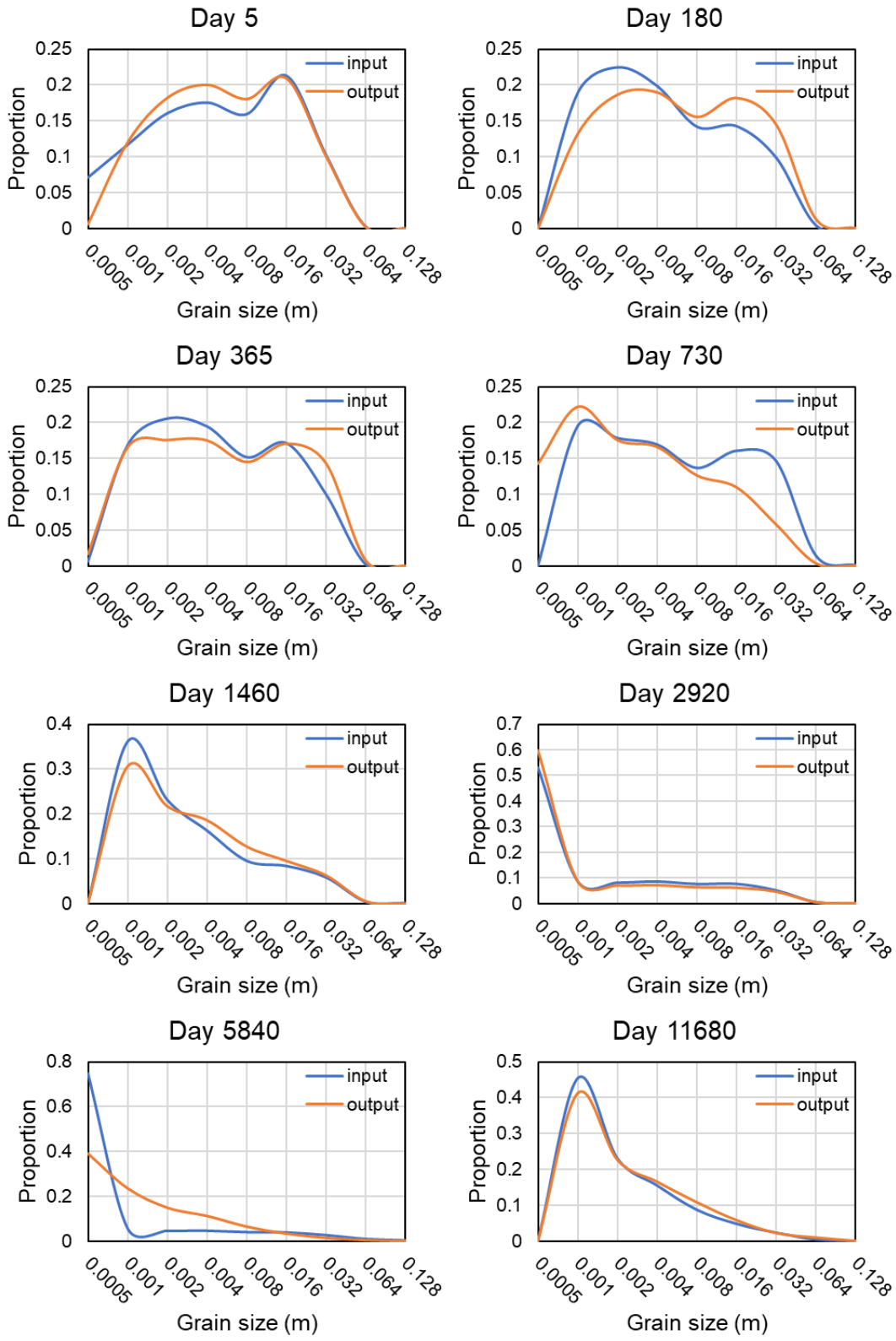
Day 5
Day 180
Day 365
Day 730
Day 1460
Day 2920
Day 5840
Day 11680
input
output
Proportion
Grain size (m)
0.0005
0.001
0.002
0.004
0.008
0.016
0.032
0.064
0.128

Appendix 2

A: Difference between input and output sediment fluxes for the Coquet2 reach (the 1000-year simulations in Chapter 4)

From Chapter 4, section 4.3.1: “To drive the model, a 25-year historical daily flow record (01/01/1988 – 31/12/2012), obtained from gauges close to the reaches, was repeated 40 times to make up a 1000-year long input file. For the Dane and Coquet1, no input sediments were supplied with the input flow series. An option to recirculate sediments was applied so that while there would be no sediment inputs into the reach initially, subsequent timesteps would include bedload and suspended sediment fluxes. For Coquet2, initial 1000-year runs revealed progressively decreasing sediment outputs with time – until virtually no sediments at all were being transported for some simulations. As this is unrealistic, a 25-year period of recorded sediment fluxes (between 50 and 75 years after the start of the simulation) from the initial forest, grass and unvegetated runs was repeated 40 times and included with the input flow series to drive the analysed simulations.”

When the analysed simulations finished, the input sediment fluxes were subtracted from output fluxes to creating a time-series of differences over 1000 years. Linear regressions for the forest, grass and unvegetated cover simulations (presented below) possessed slope and y-intercept values that did not differ significantly from zero – based on one-sample t-testing.

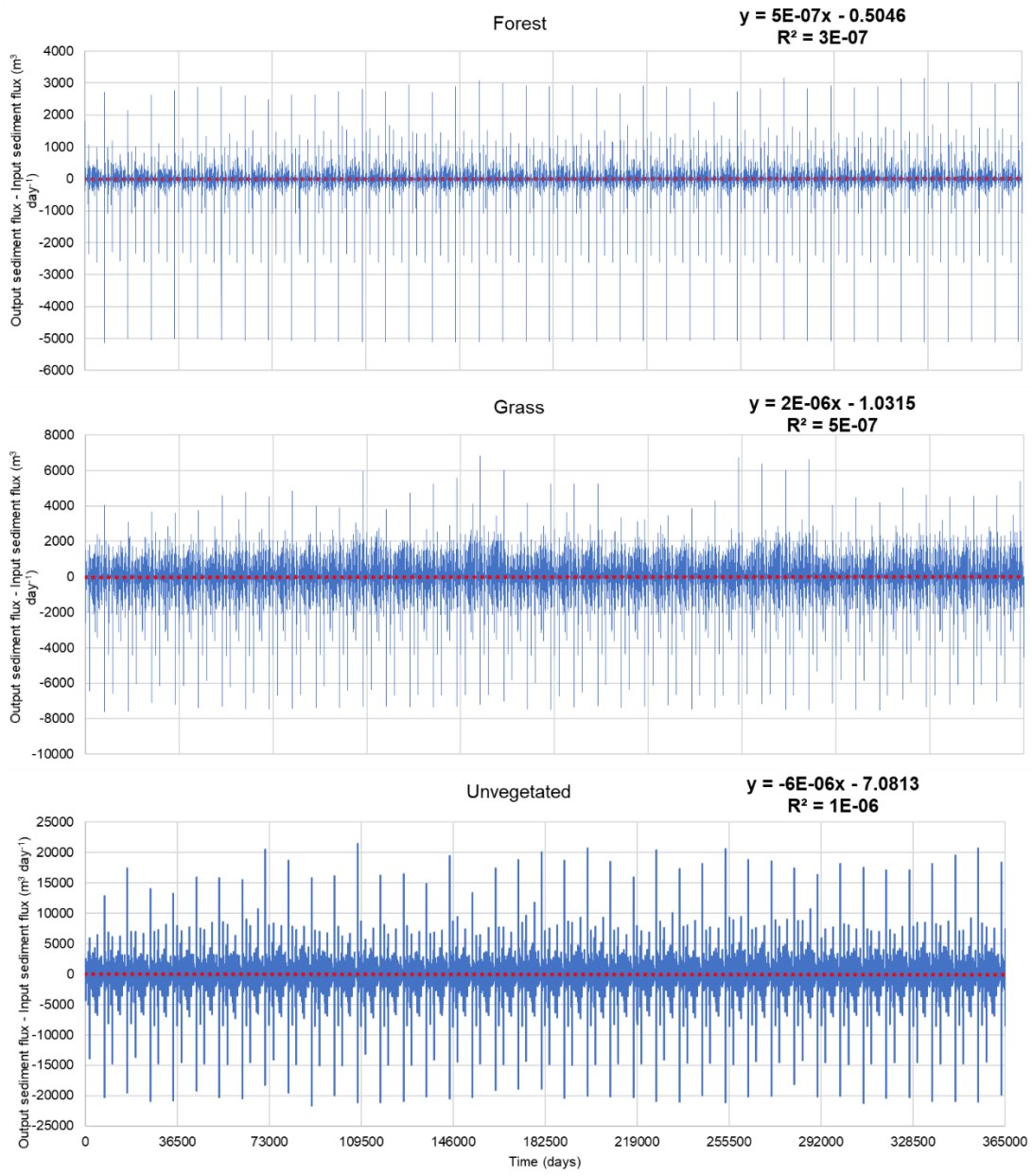

Slope t-test results

T- value = -0.48; p-value = 0.681, therefore accept the null hypothesis: mean = 0

y-intercept t-test results

T- value = -1.36; p-value = 0.306, therefore accept the null hypothesis: mean = 0

B: Storage time distributions of Chapter 4 with curves fitted by non-linear regression

Coquet1 Forest Cover

10-year

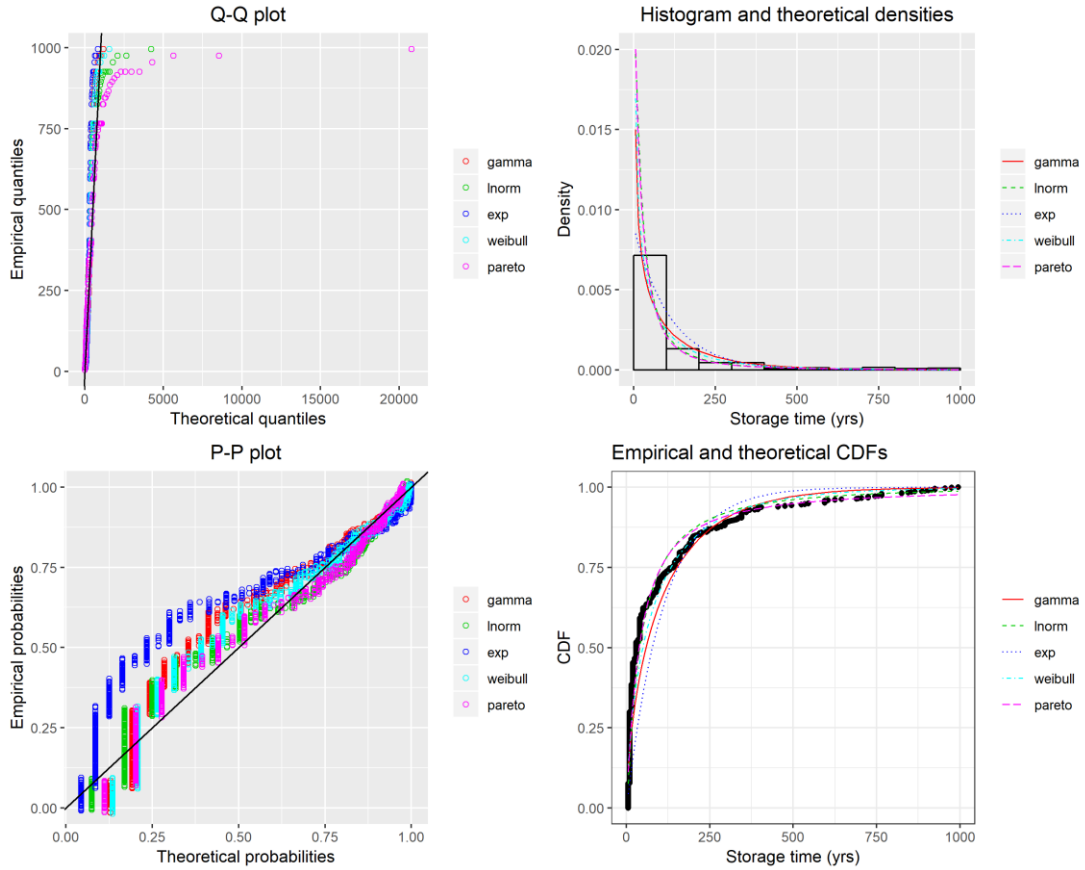

Diagnostic plots for evaluating model fits. Clockwise from top left: Quantile-Quantile plot, Histogram and fitted curves, Probability-Probability plot, and empirical cumulative distribution function with fitted curves.

	gamma	exponential	Weibull	lognormal	Pareto
CvM	7.281	23.033	4.679	3.325	2.686
AD	40.097	134.416	28.525	20.242	18.745
KS	0.179	0.292	0.140	0.135	0.125
AIC	9906.378	10104.063	9827.205	9640.683	9725.038
BIC	9915.944	10108.846	9836.772	9650.249	9734.604

*CvM = Cramer-von-Mises test, AD = Anderson-Darling test, KS = Kolmogorov-Smirnov test, AIC = Akaike's Information Criterion, BIC =

Bayesian Information Criterion. Highlighted cells indicate the best-fit model according to the test statistic scores (3 decimal places).

20-year

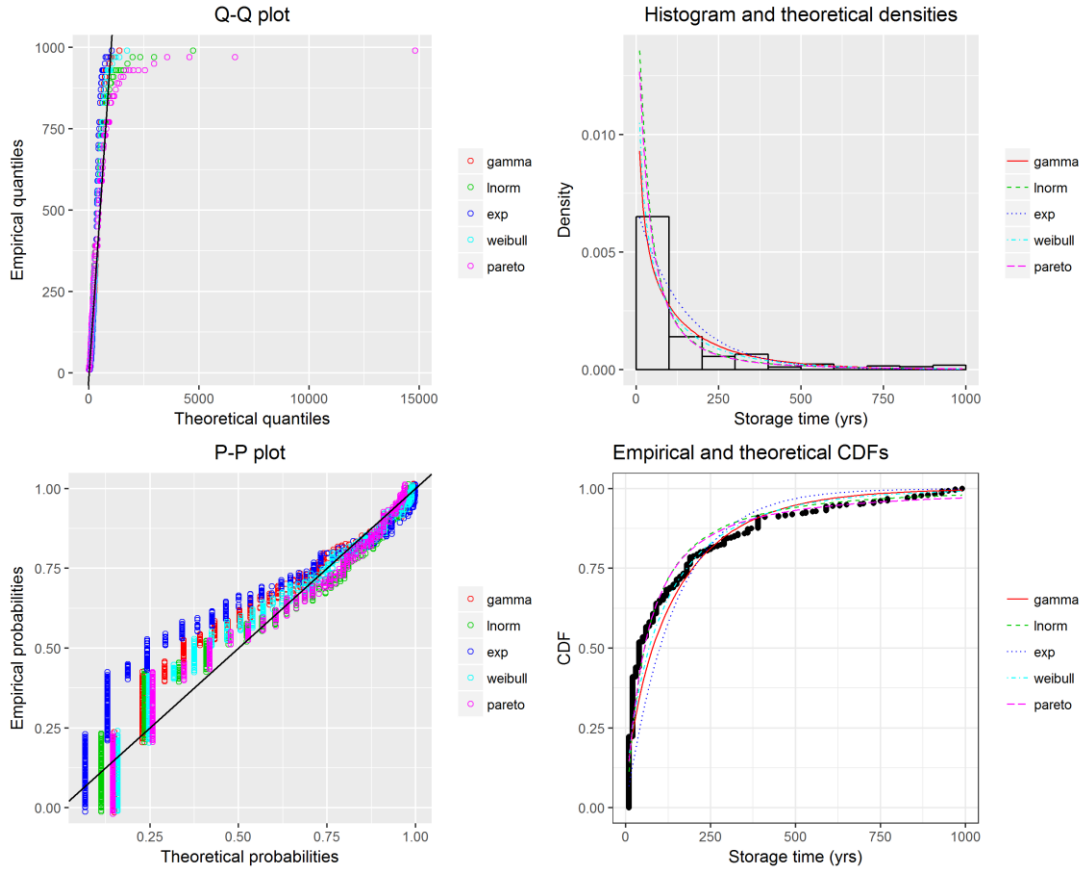

Diagnostic plots for evaluating model fits. Clockwise from top left: Quantile-Quantile plot, Histogram and fitted curves, Probability-Probability plot, and empirical cumulative distribution function with fitted curves.

	gamma	exponential	Weibull	lognormal	Pareto
CvM	4.547	13.034	3.174	2.581	2.189
AD	26.499	78.871	20.302	17.248	15.654
KS	0.182	0.281	0.163	0.176	0.153
AIC	7579.087	7680.402	7538.973	7425.800	7493.342
BIC	7588.019	7684.868	7547.905	7434.733	7502.274

*CvM = Cramer-von-Mises test, AD = Anderson-Darling test, KS = Kolmogorov-Smirnov test, AIC = Akaike's Information Criterion, BIC = Bayesian Information Criterion. Highlighted cells indicate the best-fit model according to the test statistic scores (3 decimal places).

50-year

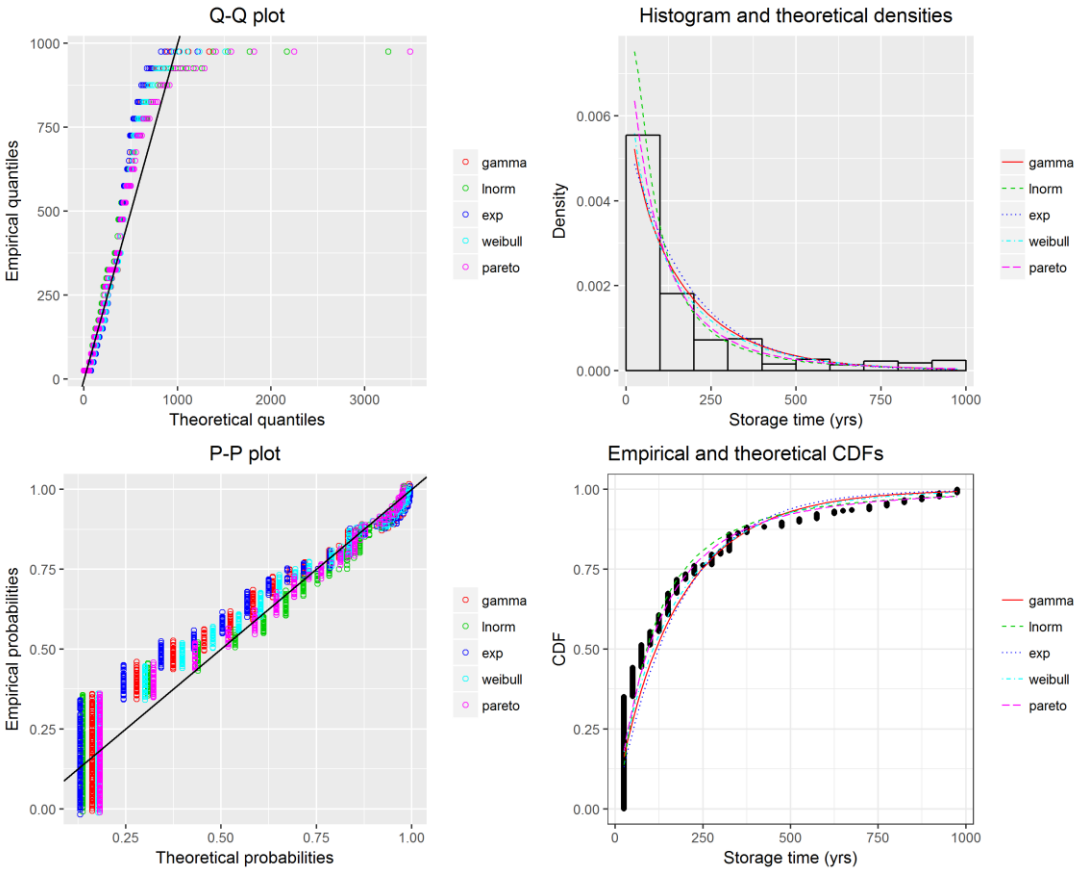

Diagnostic plots for evaluating model fits. Clockwise from top left: Quantile-Quantile plot, Histogram and fitted curves, Probability-Probability plot, and empirical cumulative distribution function with fitted curves.

	gamma	exponential	Weibull	lognormal	Pareto
CvM	3.126	4.341	2.538	2.515	2.097
AD	20.410	27.727	17.434	18.157	15.255
KS	0.189	0.221	0.179	0.214	0.183
AIC	5661.051	5666.769	5649.887	5567.976	5629.631
BIC	5669.305	5670.896	5658.141	5576.229	5637.885

*CvM = Cramer-von-Mises test, AD = Anderson-Darling test, KS = Kolmogorov-Smirnov test, AIC = Akaike's Information Criterion, BIC = Bayesian Information Criterion. Highlighted cells indicate the best-fit model according to the test statistic scores (3 decimal places).

100-year

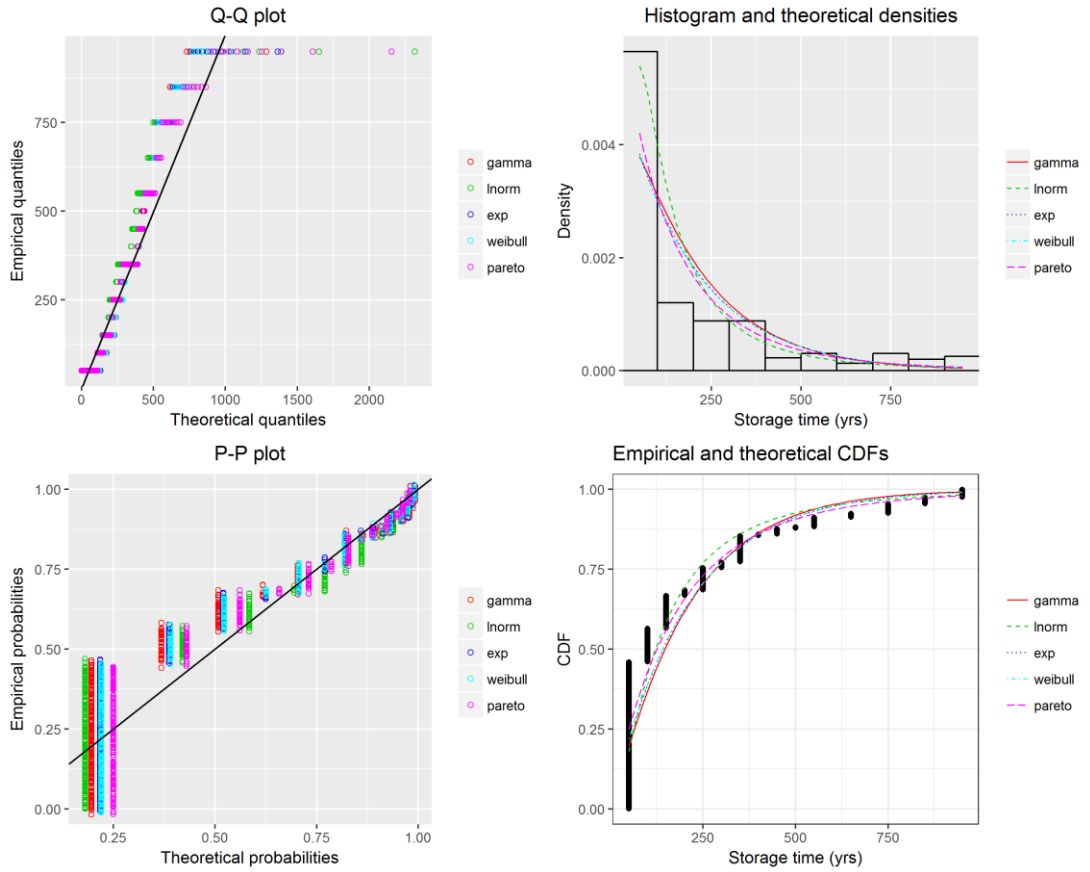

Diagnostic plots for evaluating model fits. Clockwise from top left: Quantile-Quantile plot, Histogram and fitted curves, Probability-Probability plot, and empirical cumulative distribution function with fitted curves.

	gamma	exponential	Weibull	lognormal	Pareto
CvM	5.014	4.492	4.423	4.429	3.879
AD	29.584	26.696	26.334	27.715	23.749
KS	0.264	0.243	0.239	0.279	0.249
AIC	5057.082	5057.476	5059.417	4960.352	5050.528
BIC	5065.065	5061.467	5067.399	4968.334	5058.511

*CvM = Cramer-von-Mises test, AD = Anderson-Darling test, KS = Kolmogorov-Smirnov test, AIC = Akaike's Information Criterion, BIC = Bayesian Information Criterion. Highlighted cells indicate the best-fit model according to the test statistic scores (3 decimal places).

Coquet1 Grass Cover

10-year

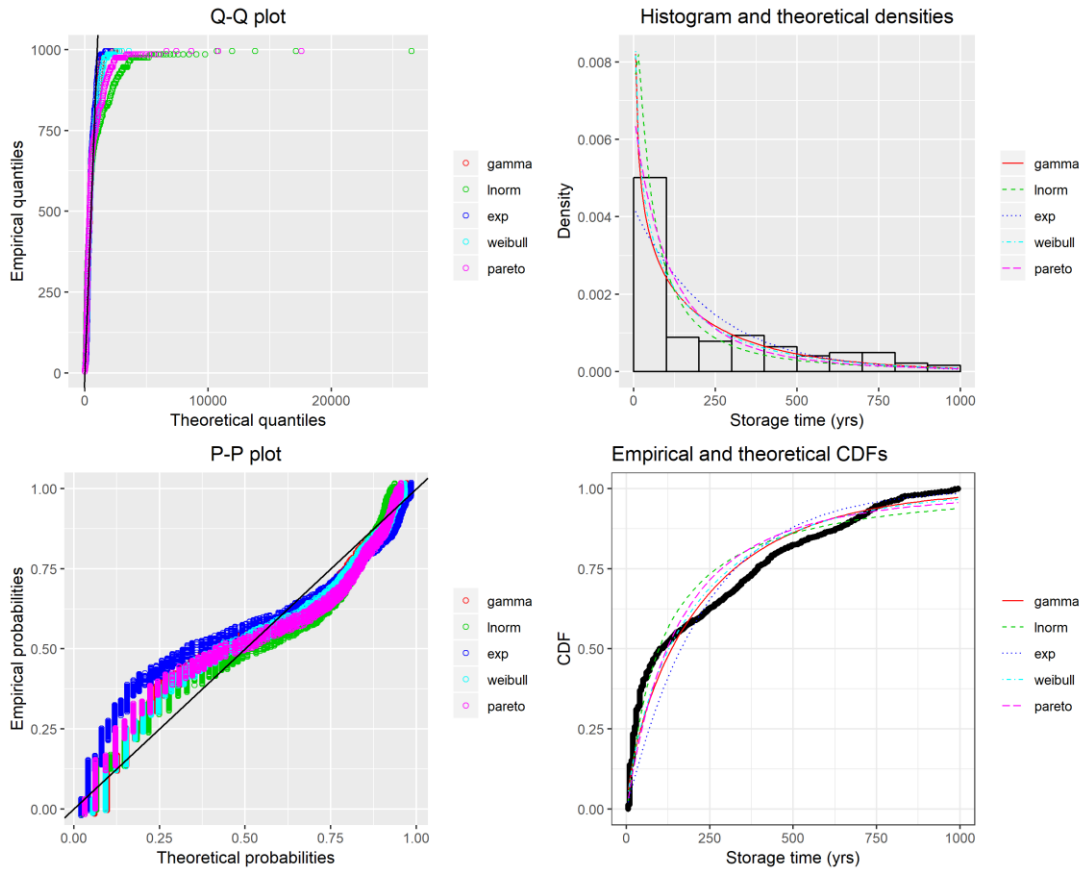

Diagnostic plots for evaluating model fits. Clockwise from top left: Quantile-Quantile plot, Histogram and fitted curves, Probability-Probability plot, and empirical cumulative distribution function with fitted curves.

	gamma	exponential	Weibull	lognormal	Pareto
CvM	17.875	54.629	17.232	17.407	26.809
AD	110.486	362.629	107.997	112.966	167.919
KS	0.128	0.214	0.123	0.114	0.147
AIC	60922.781	61445.507	60906.701	60948.745	61252.956
BIC	60935.714	61451.974	60919.634	60961.678	61265.889

*CvM = Cramer-von-Mises test, AD = Anderson-Darling test, KS = Kolmogorov-Smirnov test, AIC = Akaike's Information Criterion, BIC = Bayesian Information Criterion. Highlighted cells indicate the best-fit model according to the test statistic scores (3 decimal places).

20-year

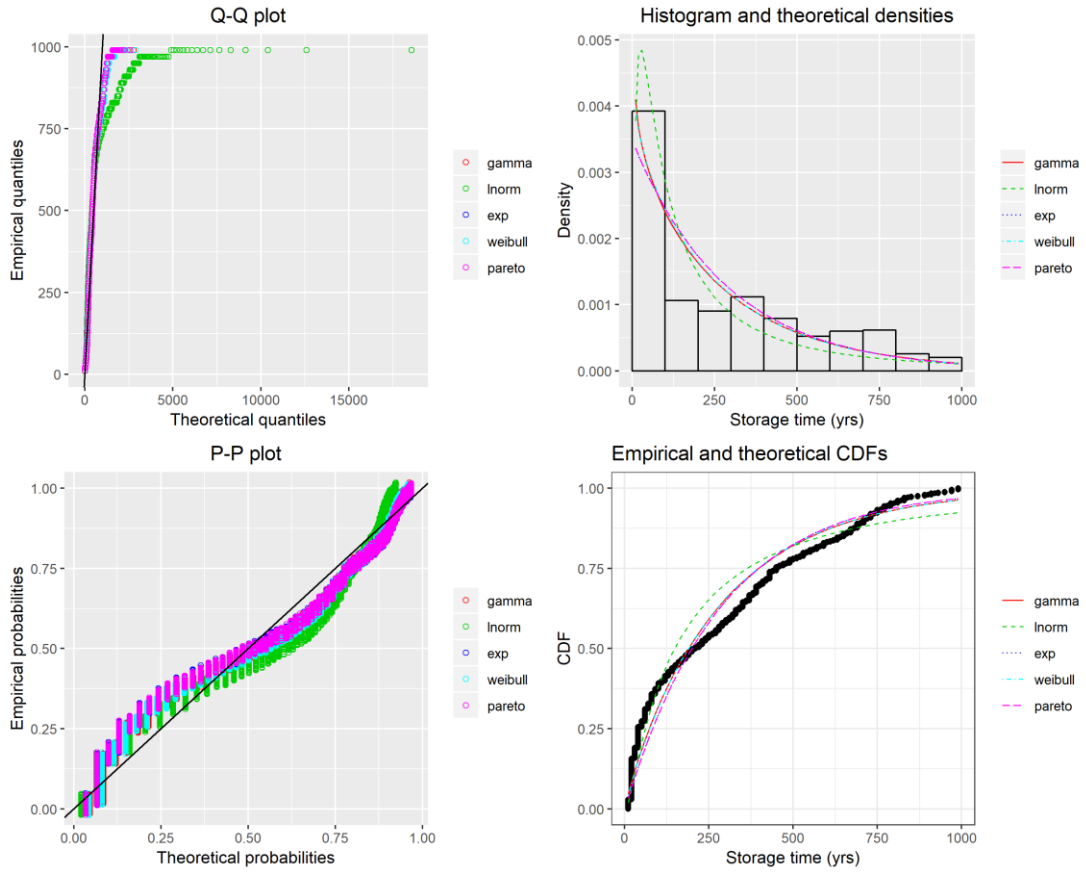

Diagnostic plots for evaluating model fits. Clockwise from top left: Quantile-Quantile plot, Histogram and fitted curves, Probability-Probability plot, and empirical cumulative distribution function with fitted curves.

	gamma	exponential	Weibull	lognormal	Pareto
CvM	10.268	14.215	11.078	16.087	14.213
AD	68.547	96.175	73.613	101.833	96.172
KS	0.102	0.126	0.107	0.127	0.126
AIC	50031.340	50064.063	50043.178	50380.385	50066.063
BIC	50043.804	50070.295	50055.641	50392.849	50078.527

*CvM = Cramer-von-Mises test, AD = Anderson-Darling test, KS = Kolmogorov-Smirnov test, AIC = Akaike's Information Criterion, BIC = Bayesian Information Criterion. Highlighted cells indicate the best-fit model according to the test statistic scores (3 decimal places).

50-year

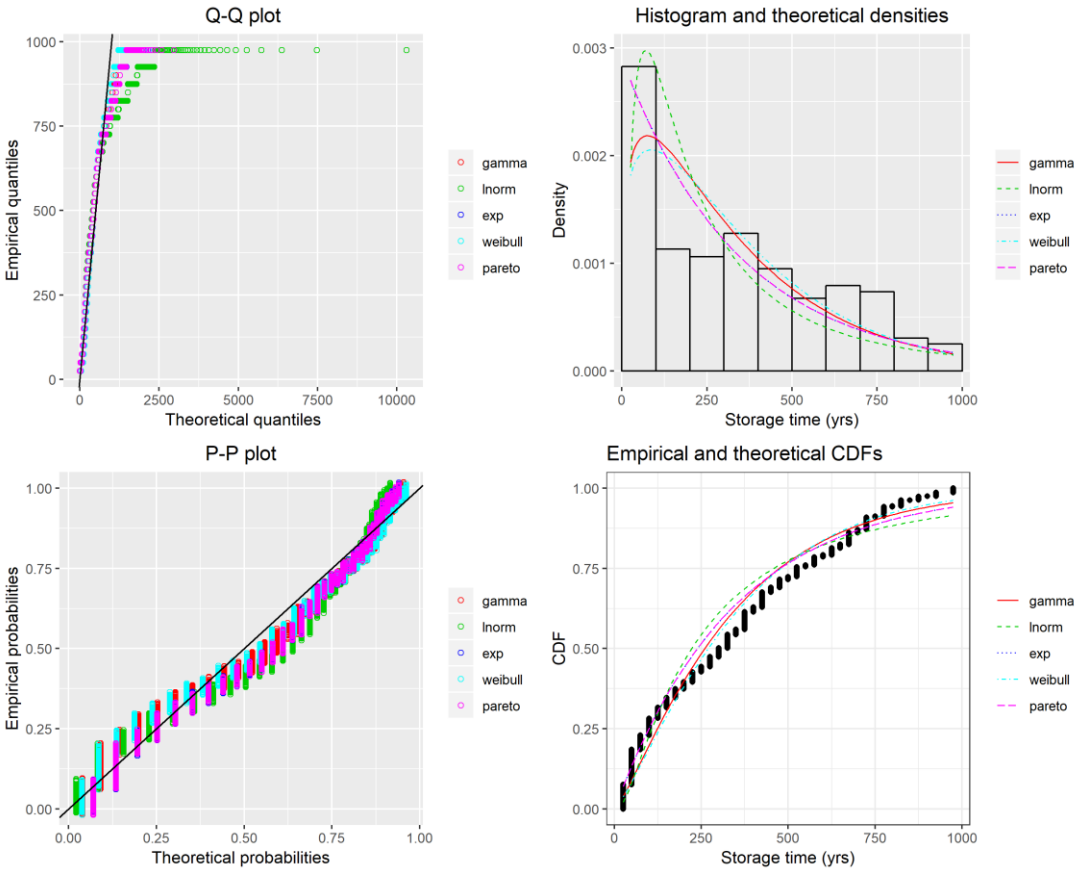

Diagnostic plots for evaluating model fits. Clockwise from top left: Quantile-Quantile plot, Histogram and fitted curves, Probability-Probability plot, and empirical cumulative distribution function with fitted curves.

	gamma	exponential	Weibull	lognormal	Pareto
CvM	6.492	7.206	6.145	12.788	7.218
AD	43.709	45.915	43.511	79.614	45.963
KS	0.094	0.109	0.099	0.137	0.109
AIC	38029.407	38124.975	37990.272	38418.104	38126.976
BIC	38041.271	38130.908	38002.136	38429.969	38138.841

*CvM = Cramer-von-Mises test, AD = Anderson-Darling test, KS = Kolmogorov-Smirnov test, AIC = Akaike's Information Criterion, BIC = Bayesian Information Criterion. Highlighted cells indicate the best-fit model according to the test statistic scores (3 decimal places).

100-year

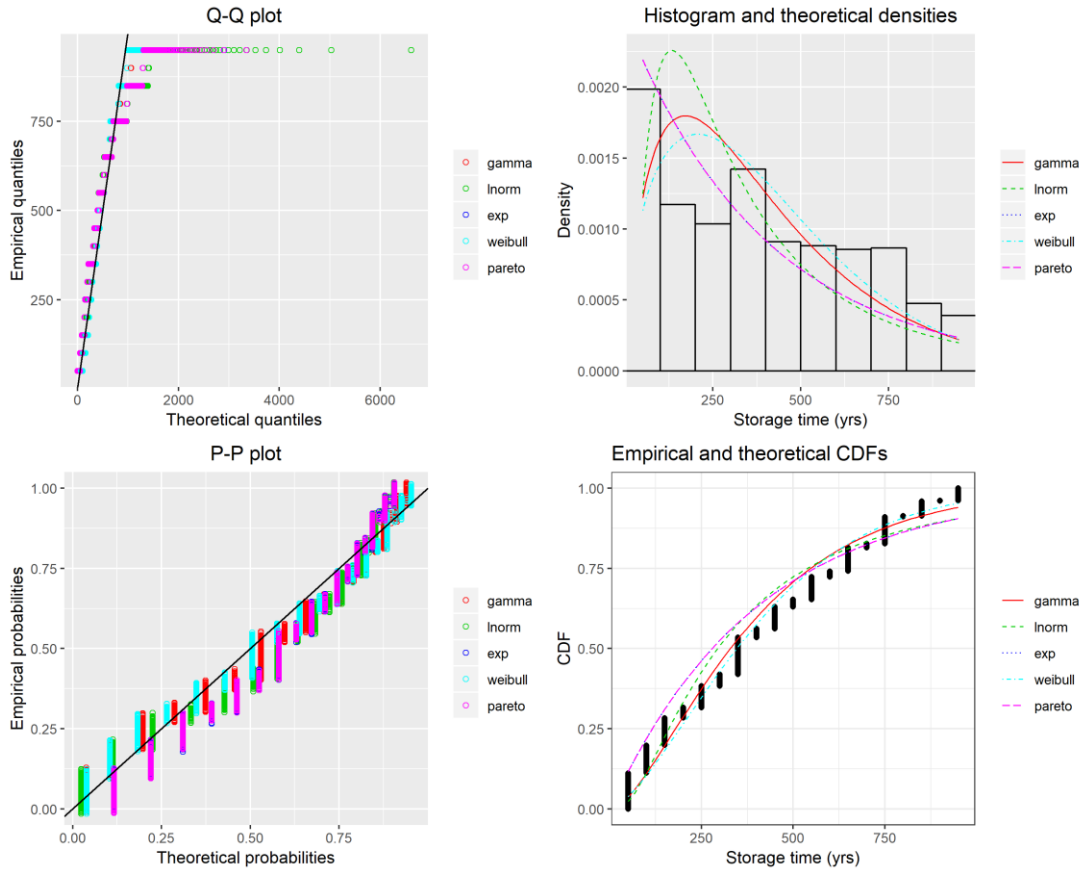

Diagnostic plots for evaluating model fits. Clockwise from top left: Quantile-Quantile plot, Histogram and fitted curves, Probability-Probability plot, and empirical cumulative distribution function with fitted curves.

	gamma	exponential	Weibull	lognormal	Pareto
CvM	4.866	12.221	4.018	9.228	12.245
AD	34.747	74.212	30.985	61.744	74.312
KS	0.111	0.161	0.101	0.157	0.161
AIC	27948.157	28262.678	27880.881	28234.052	28264.679
BIC	27959.377	28268.289	27892.102	28245.273	28275.899

*CvM = Cramer-von-Mises test, AD = Anderson-Darling test, KS = Kolmogorov-Smirnov test, AIC = Akaike's Information Criterion, BIC = Bayesian Information Criterion. Highlighted cells indicate the best-fit model according to the test statistic scores (3 decimal places).

Coquet1 Unvegetated Cover

10-year

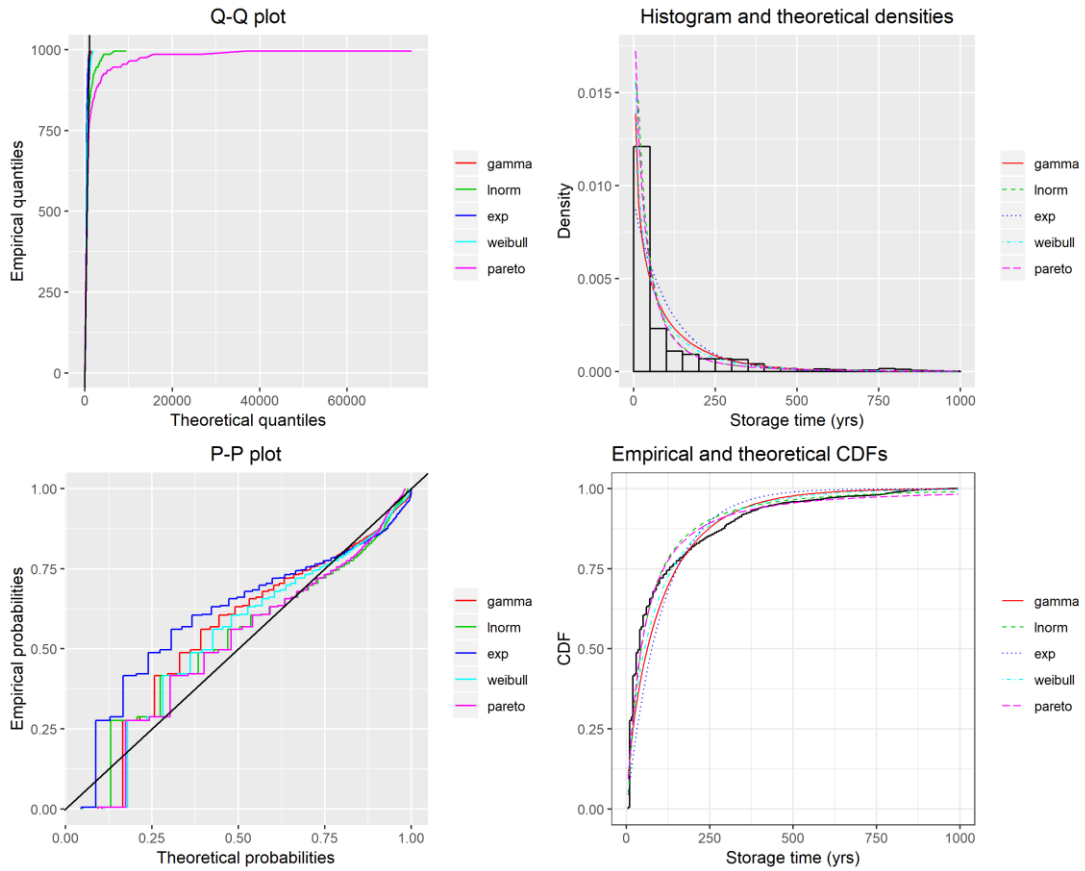

Diagnostic plots for evaluating model fits. Clockwise from top left: Quantile-Quantile plot, Histogram and fitted curves, Probability-Probability plot, and empirical cumulative distribution function with fitted curves.

	gamma	exponential	Weibull	lognormal	Pareto
CvM	156.808	379.726	107.604	75.869	63.833
AD	882.891	2145.256	673.526	534.006	483.257
KS	0.169	0.255	0.174	0.146	0.168
AIC	213971.390	216295.576	212696.716	208639.915	210829.412
BIC	213987.093	216303.427	212712.418	208655.617	210845.114

*CvM = Cramer-von-Mises test, AD = Anderson-Darling test, KS = Kolmogorov-Smirnov test, AIC = Akaike's Information Criterion, BIC = Bayesian Information Criterion. Highlighted cells indicate the best-fit model according to the test statistic scores (3 decimal places).

20-year

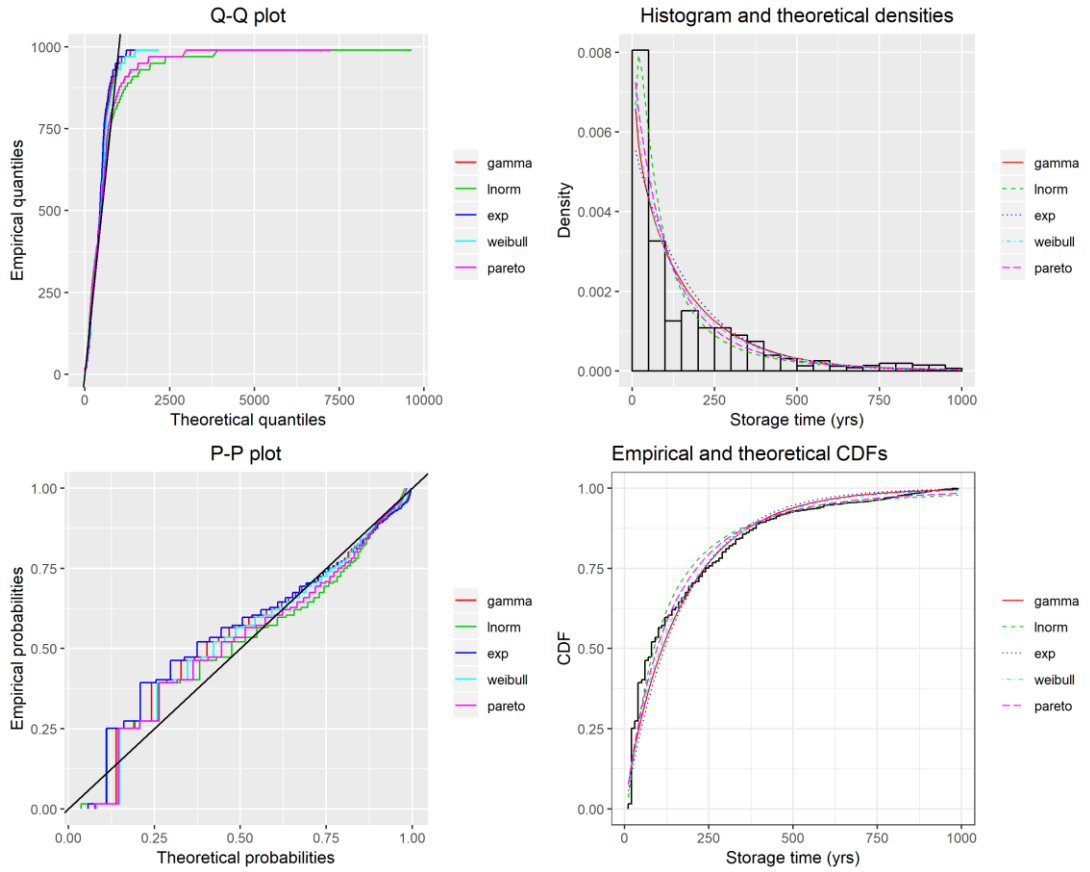

Diagnostic plots for evaluating model fits. Clockwise from top left: Quantile-Quantile plot, Histogram and fitted curves, Probability-Probability plot, and empirical cumulative distribution function with fitted curves.

	gamma	exponential	Weibull	lognormal	Pareto
CvM	47.945	73.798	37.689	34.691	32.281
AD	300.855	440.044	253.846	243.961	229.185
KS	0.152	0.184	0.136	0.139	0.129
AIC	135351.849	135511.175	135171.518	133862.550	134963.559
BIC	135366.467	135518.484	135186.136	133877.168	134978.178

*CvM = Cramer-von-Mises test, AD = Anderson-Darling test, KS = Kolmogorov-Smirnov test, AIC = Akaike's Information Criterion, BIC = Bayesian Information Criterion. Highlighted cells indicate the best-fit model according to the test statistic scores (3 decimal places).

50-year

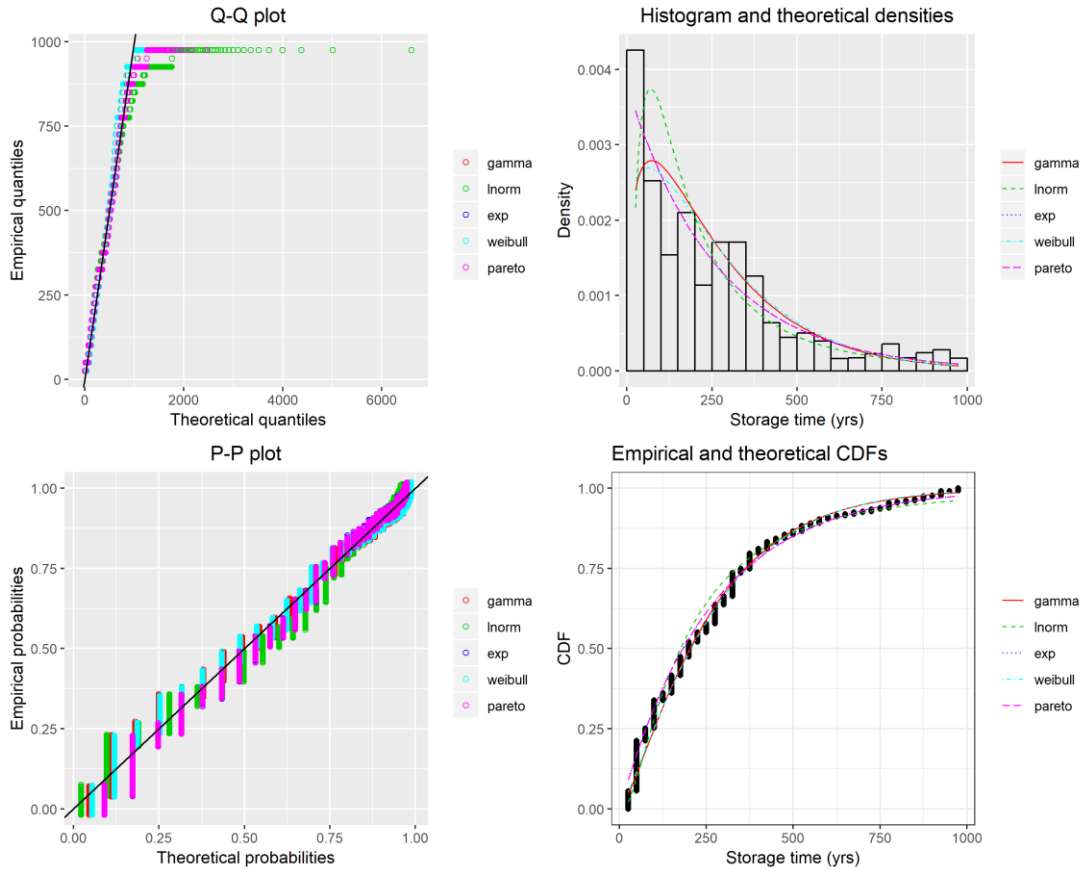

Diagnostic plots for evaluating model fits. Clockwise from top left: Quantile-Quantile plot, Histogram and fitted curves, Probability-Probability plot, and empirical cumulative distribution function with fitted curves.

	gamma	exponential	Weibull	lognormal	Pareto
CvM	5.873	8.909	5.316	11.861	8.911
AD	46.936	71.646	44.652	76.888	71.658
KS	0.102	0.117	0.093	0.116	0.117
AIC	74539.442	74866.360	74592.415	74646.071	74868.478
BIC	74552.737	74873.008	74605.709	74659.365	74881.773

*CvM = Cramer-von-Mises test, AD = Anderson-Darling test, KS = Kolmogorov-Smirnov test, AIC = Akaike's Information Criterion, BIC = Bayesian Information Criterion. Highlighted cells indicate the best-fit model according to the test statistic scores (3 decimal places).

100-year

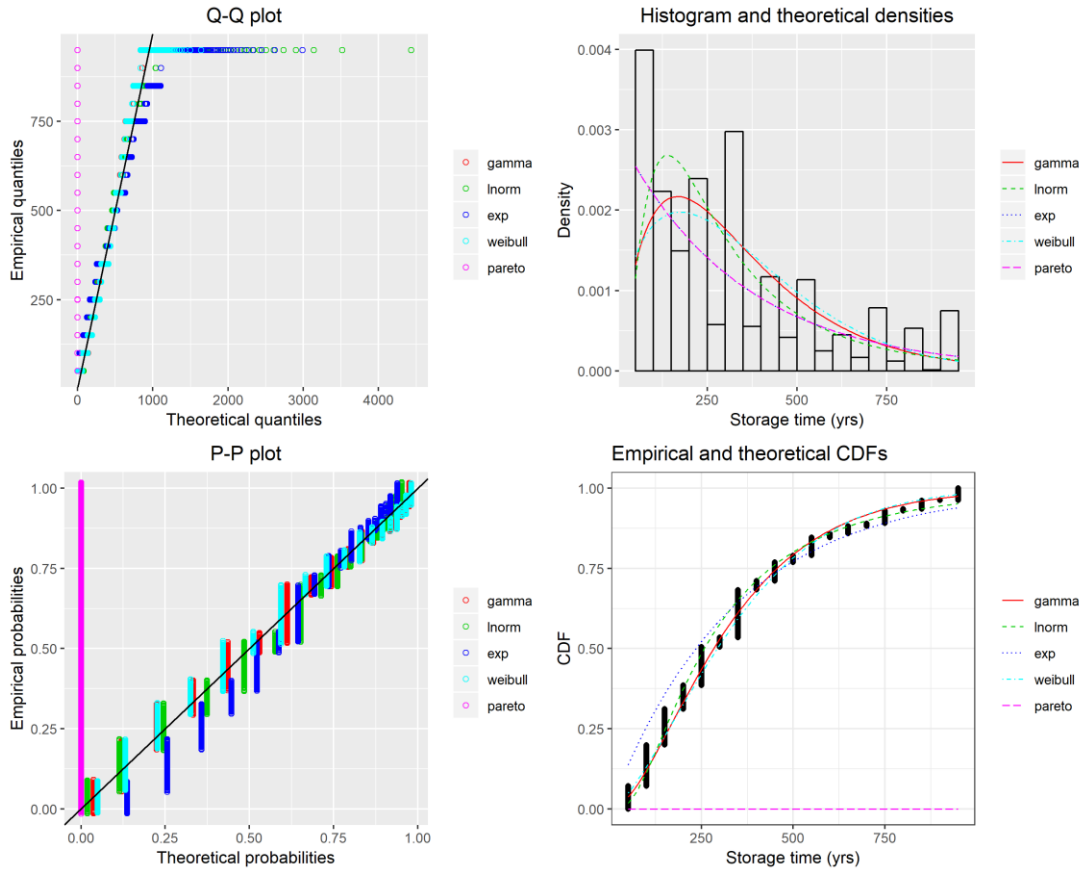

Diagnostic plots for evaluating model fits. Clockwise from top left: Quantile-Quantile plot, Histogram and fitted curves, Probability-Probability plot, and empirical cumulative distribution function with fitted curves.

	gamma	exponential	Weibull	lognormal	Pareto
CvM	3.687	22.160	4.048	5.539	1146.333
AD	26.067	137.460	28.258	38.126	Inf
KS	0.087	0.184	0.089	0.118	1
AIC	46168.224	46943.431	46218.329	46284.257	46945.431
BIC	46180.509	46949.574	46230.616	46296.543	46957.717

*CvM = Cramer-von-Mises test, AD = Anderson-Darling test, KS = Kolmogorov-Smirnov test, AIC = Akaike's Information Criterion, BIC = Bayesian Information Criterion. Highlighted cells indicate the best-fit model according to the test statistic scores (3 decimal places).

Coquet2 Forest Cover

10-year

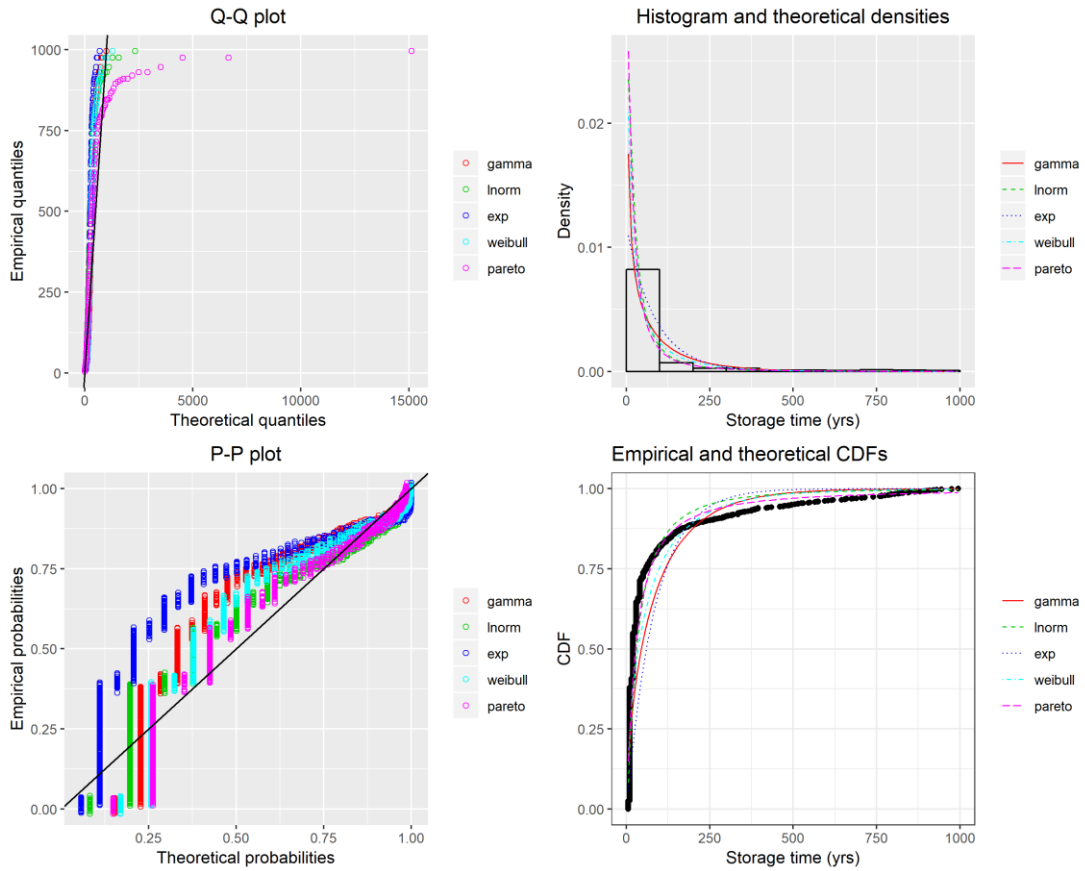

Diagnostic plots for evaluating model fits. Clockwise from top left: Quantile-Quantile plot, Histogram and fitted curves, Probability-Probability plot, and empirical cumulative distribution function with fitted curves.

	gamma	exponential	Weibull	lognormal	Pareto
CvM	26.714	61.162	18.101	11.976	10.882
AD	139.389	326.819	102.980	73.013	68.913
KS	0.239	0.353	0.231	0.183	0.237
AIC	15750.662	16099.061	15520.385	14948.736	15115.205
BIC	15761.254	16104.357	15530.978	14959.329	15125.798

*CvM = Cramer-von-Mises test, AD = Anderson-Darling test, KS = Kolmogorov-Smirnov test, AIC = Akaike's Information Criterion, BIC = Bayesian Information Criterion. Highlighted cells indicate the best-fit model according to the test statistic scores (3 decimal places).

20-year

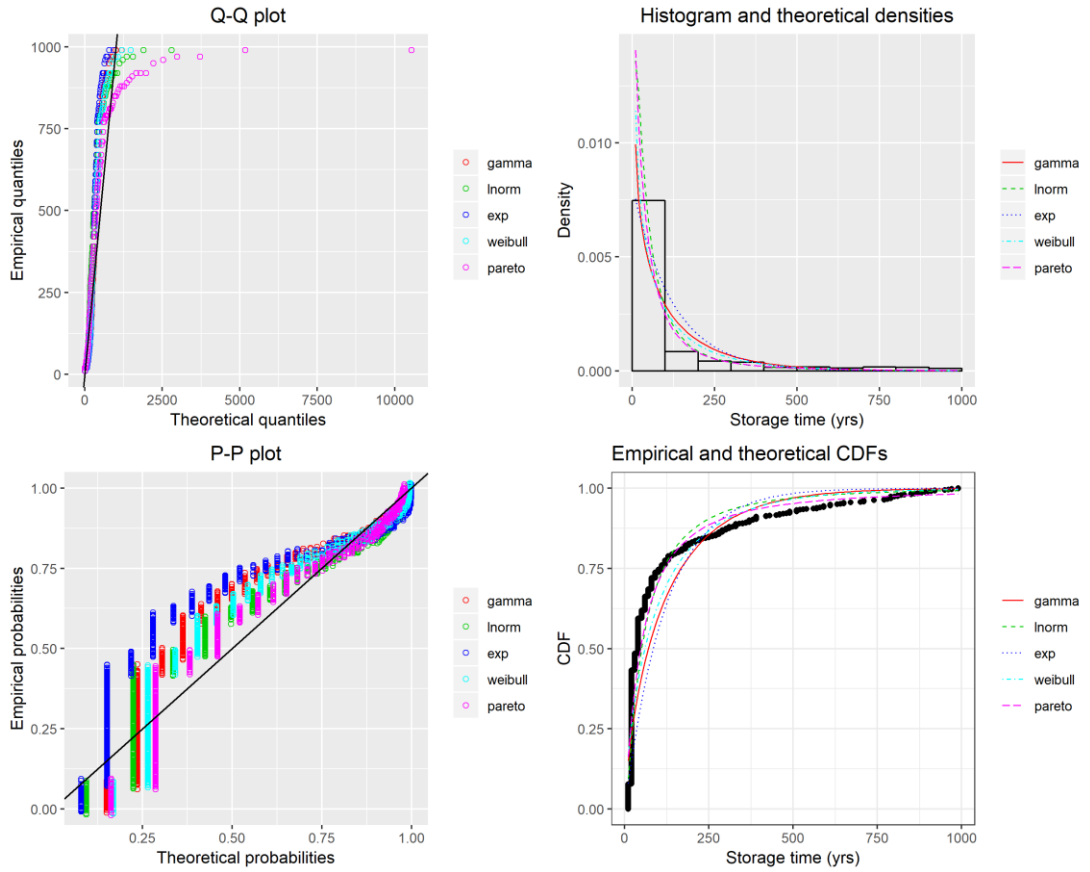

Diagnostic plots for evaluating model fits. Clockwise from top left: Quantile-Quantile plot, Histogram and fitted curves, Probability-Probability plot, and empirical cumulative distribution function with fitted curves.

	gamma	exponential	Weibull	lognormal	Pareto
CvM	14.943	27.873	10.912	7.789	7.091
AD	78.600	146.548	61.423	45.187	43.811
KS	0.231	0.315	0.191	0.208	0.208
AIC	11341.457	11447.661	11250.306	10929.186	11071.496
BIC	11351.244	11452.554	11260.093	10938.973	11081.283

*CvM = Cramer-von-Mises test, AD = Anderson-Darling test, KS = Kolmogorov-Smirnov test, AIC = Akaike's Information Criterion, BIC = Bayesian Information Criterion. Highlighted cells indicate the best-fit model according to the test statistic scores (3 decimal places).

50-year

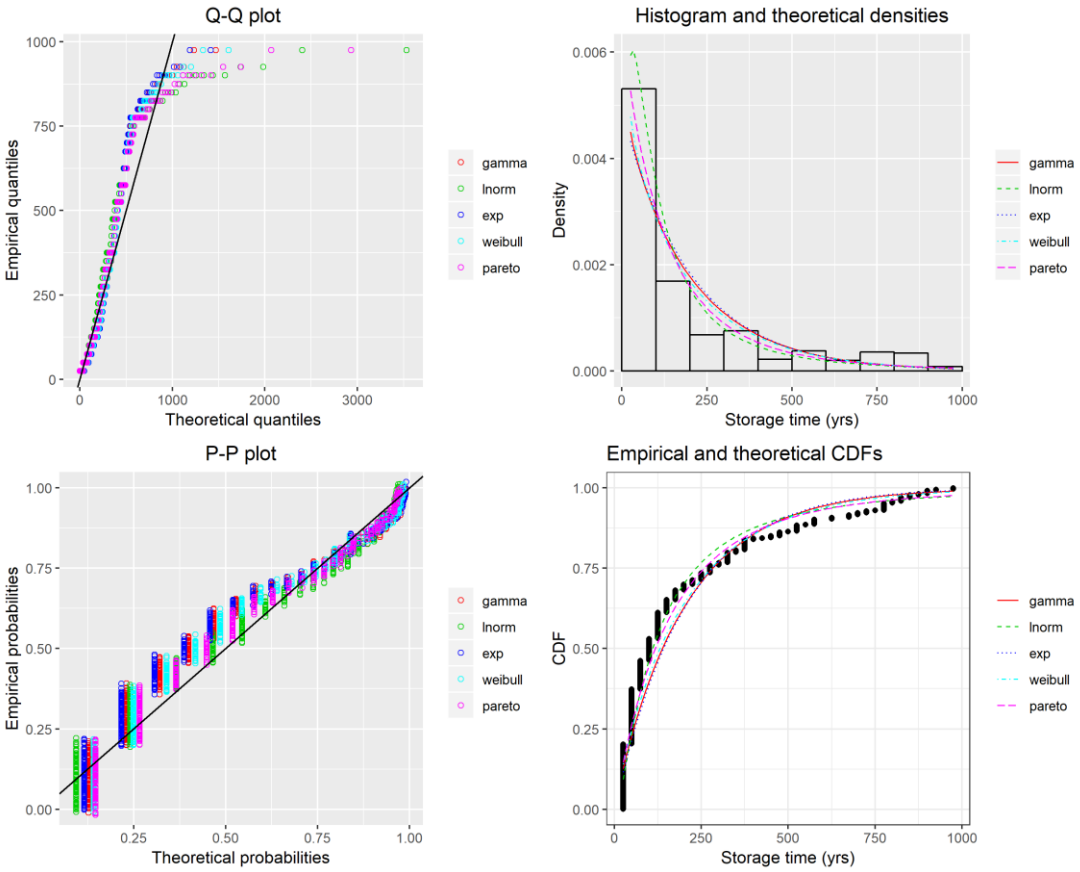

Diagnostic plots for evaluating model fits. Clockwise from top left: Quantile-Quantile plot, Histogram and fitted curves, Probability-Probability plot, and empirical cumulative distribution function with fitted curves.

	gamma	exponential	Weibull	lognormal	Pareto
CvM	2.677	3.155	2.073	1.247	1.382
AD	16.319	18.654	13.659	9.715	10.599
KS	0.145	0.157	0.141	0.133	0.146
AIC	6361.062	6360.359	6355.493	6276.571	6342.756
BIC	6369.503	6364.579	6363.934	6285.012	6351.197

*CvM = Cramer-von-Mises test, AD = Anderson-Darling test, KS = Kolmogorov-Smirnov test, AIC = Akaike's Information Criterion, BIC = Bayesian Information Criterion. Highlighted cells indicate the best-fit model according to the test statistic scores (3 decimal places).

100-year

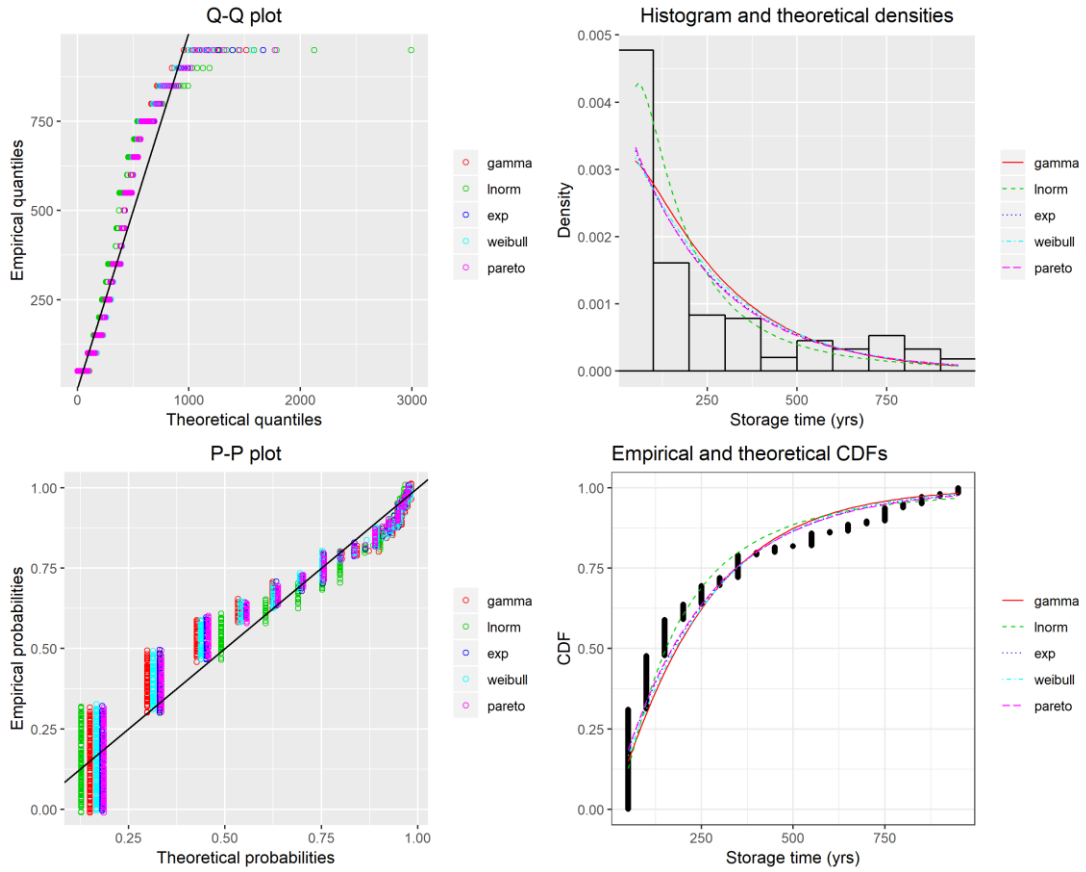

Diagnostic plots for evaluating model fits. Clockwise from top left: Quantile-Quantile plot, Histogram and fitted curves, Probability-Probability plot, and empirical cumulative distribution function with fitted curves.

	gamma	exponential	Weibull	lognormal	Pareto
CvM	2.687	2.097	2.365	1.922	2.007
AD	17.312	14.422	15.613	14.352	14.059
KS	0.179	0.182	0.167	0.185	0.186
AIC	5187.621	5191.481	5192.128	5127.099	5193.343
BIC	5195.594	5195.468	5200.101	5135.072	5201.316

*CvM = Cramer-von-Mises test, AD = Anderson-Darling test, KS = Kolmogorov-Smirnov test, AIC = Akaike's Information Criterion, BIC = Bayesian Information Criterion. Highlighted cells indicate the best-fit model according to the test statistic scores (3 decimal places).

Coquet2 Grass Cover

10-year

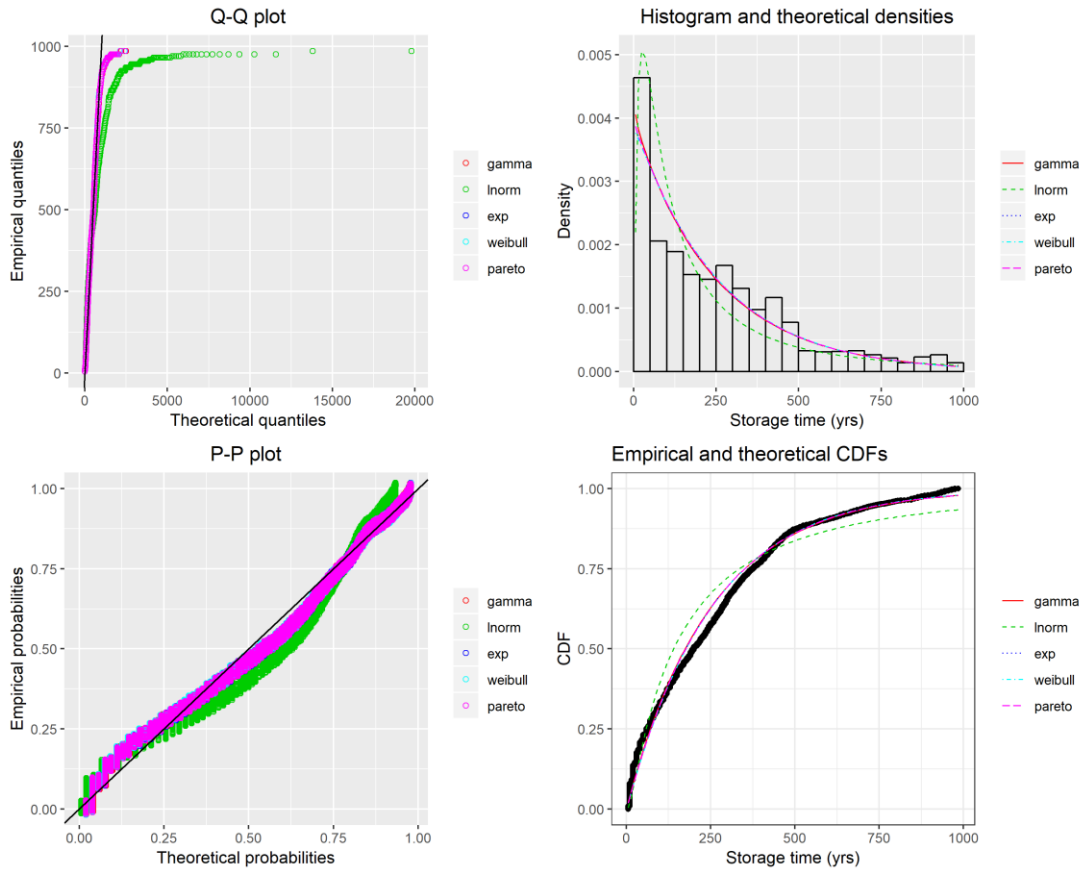

Diagnostic plots for evaluating model fits. Clockwise from top left: Quantile-Quantile plot, Histogram and fitted curves, Probability-Probability plot, and empirical cumulative distribution function with fitted curves.

	gamma	exponential	Weibull	lognormal	Pareto
CvM	8.038	8.151	8.181	31.806	8.138
AD	54.278	57.066	58.658	192.267	57.027
KS	0.061	0.065	0.067	0.114	0.065
AIC	103205.954	103206.130	103207.343	104529.955	103208.133
BIC	103219.902	103213.104	103221.291	104543.903	103222.081

*CvM = Cramer-von-Mises test, AD = Anderson-Darling test, KS = Kolmogorov-Smirnov test, AIC = Akaike's Information Criterion, BIC = Bayesian Information Criterion. Highlighted cells indicate the best-fit model according to the test statistic scores (3 decimal places).

20-year

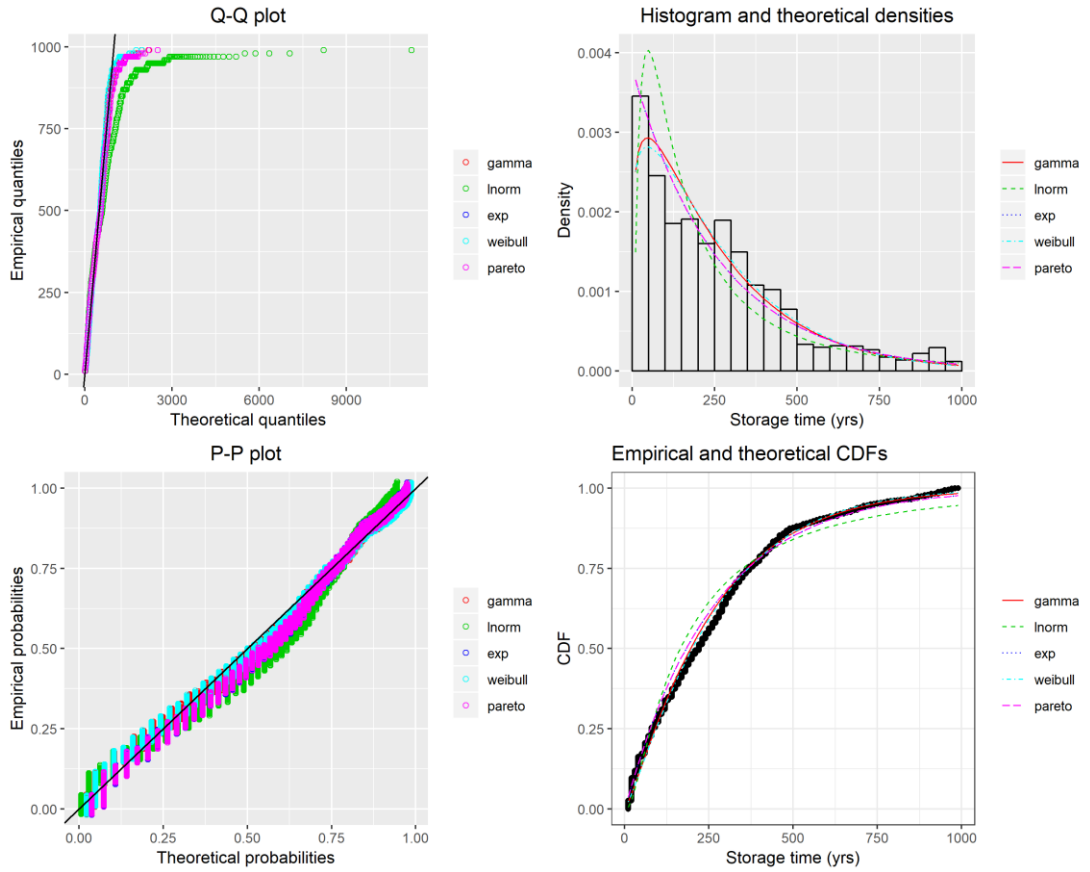

Diagnostic plots for evaluating model fits. Clockwise from top left: Quantile-Quantile plot, Histogram and fitted curves, Probability-Probability plot, and empirical cumulative distribution function with fitted curves.

	gamma	exponential	Weibull	lognormal	Pareto
CvM	4.378	8.578	3.381	21.861	8.536
AD	30.610	48.366	26.736	132.314	48.199
KS	0.057	0.072	0.058	0.107	0.072
AIC	90248.028	90398.327	90214.256	91209.946	90400.329
BIC	90261.699	90405.163	90227.929	91223.618	90414.001

*CvM = Cramer-von-Mises test, AD = Anderson-Darling test, KS = Kolmogorov-Smirnov test, AIC = Akaike's Information Criterion, BIC = Bayesian Information Criterion. Highlighted cells indicate the best-fit model according to the test statistic scores (3 decimal places).

50-year

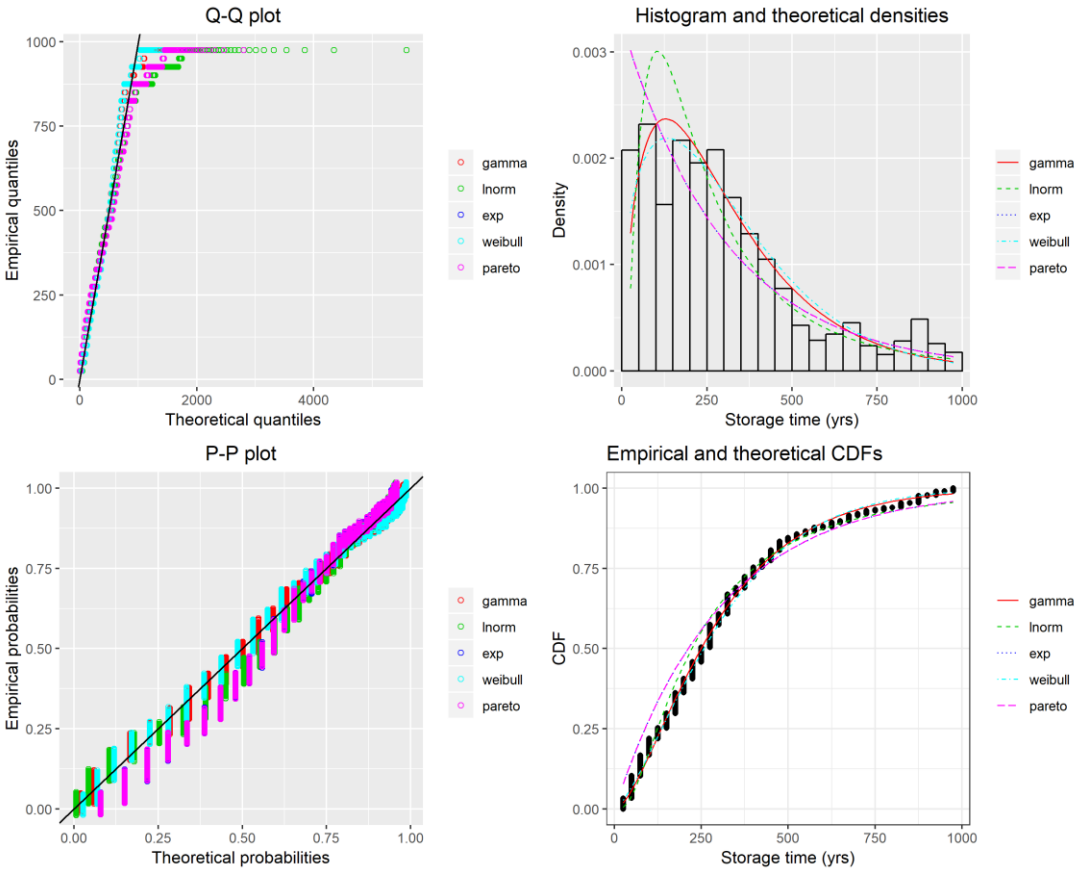

Diagnostic plots for evaluating model fits. Clockwise from top left: Quantile-Quantile plot, Histogram and fitted curves, Probability-Probability plot, and empirical cumulative distribution function with fitted curves.

	gamma	exponential	Weibull	lognormal	Pareto
CvM	1.844	22.587	1.837	8.614	22.603
AD	15.517	133.928	16.099	52.996	133.996
KS	0.057	0.138	0.053	0.098	0.138
AIC	63537.882	64266.687	63560.594	63907.232	64268.688
BIC	63550.827	64273.159	63573.538	63920.176	64281.632

*CvM = Cramer-von-Mises test, AD = Anderson-Darling test, KS = Kolmogorov-Smirnov test, AIC = Akaike's Information Criterion, BIC = Bayesian Information Criterion. Highlighted cells indicate the best-fit model according to the test statistic scores (3 decimal places).

100-year

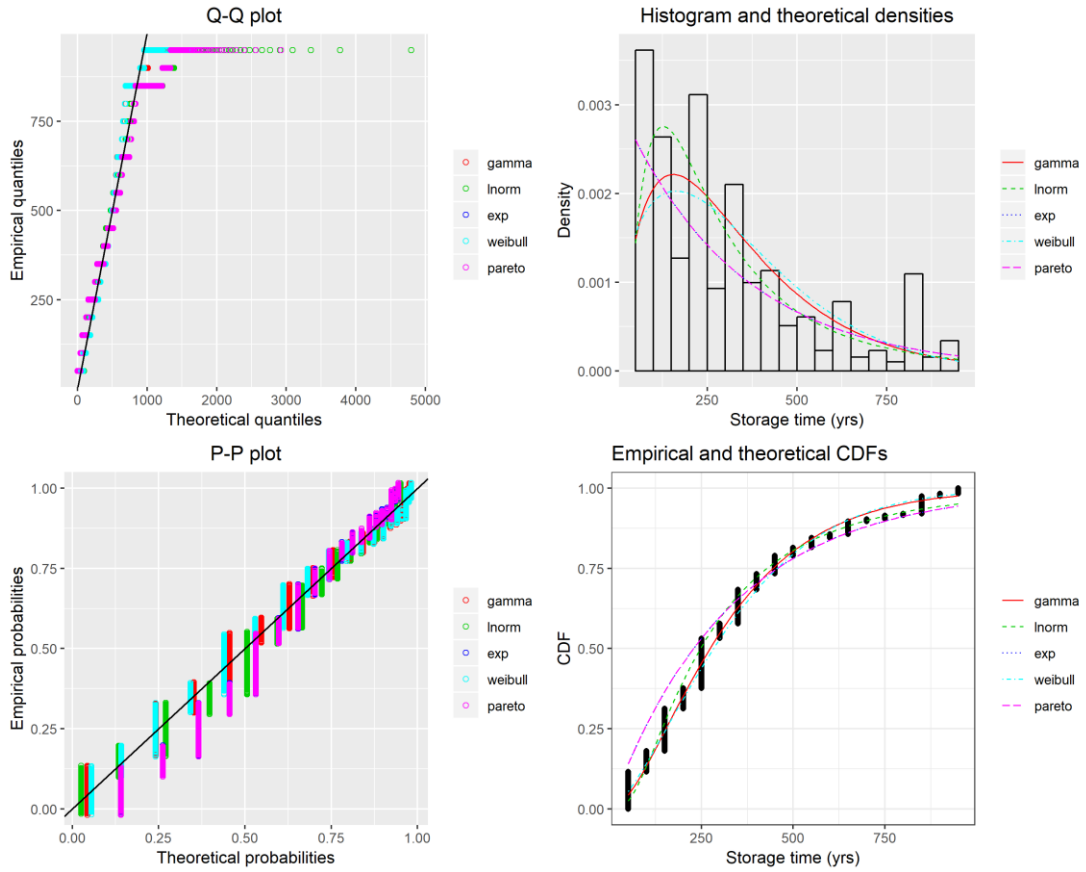

Diagnostic plots for evaluating model fits. Clockwise from top left: Quantile-Quantile plot, Histogram and fitted curves, Probability-Probability plot, and empirical cumulative distribution function with fitted curves.

	gamma	exponential	Weibull	lognormal	Pareto
CvM	3.414	22.670	3.859	6.814	22.626
AD	29.163	135.251	30.225	54.615	135.071
KS	0.079	0.185	0.092	0.129	0.185
AIC	47930.798	48642.415	47961.286	48130.914	48644.492
BIC	47943.163	48648.597	47973.651	48143.279	48656.857

*CvM = Cramer-von-Mises test, AD = Anderson-Darling test, KS = Kolmogorov-Smirnov test, AIC = Akaike's Information Criterion, BIC = Bayesian Information Criterion. Highlighted cells indicate the best-fit model according to the test statistic scores (3 decimal places).

Coquet2 Unvegetated Cover

10-year

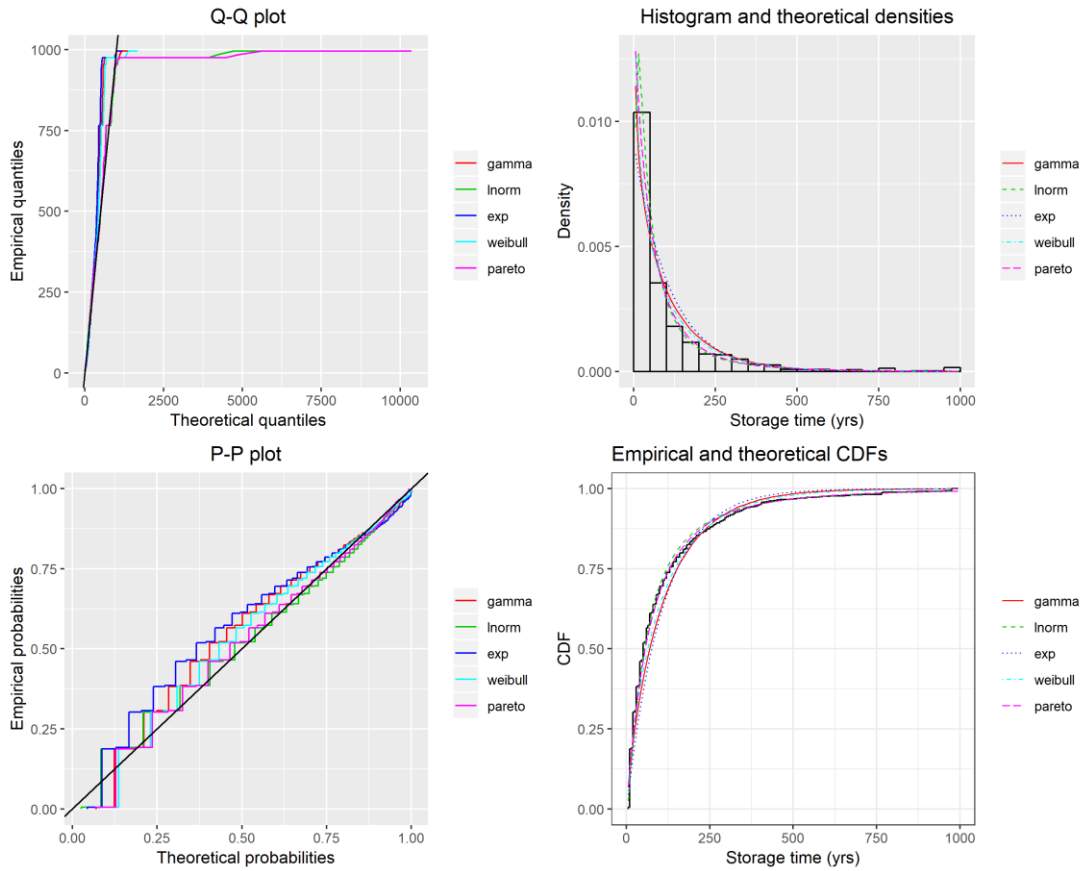

Diagnostic plots for evaluating model fits. Clockwise from top left: Quantile-Quantile plot, Histogram and fitted curves, Probability-Probability plot, and empirical cumulative distribution function with fitted curves.

	gamma	exponential	Weibull	lognormal	Pareto
CvM	85.188	161.182	52.581	26.105	26.396
AD	522.654	899.583	385.838	237.861	253.587
KS	0.118	0.156	0.131	0.104	0.122
AIC	262552.489	263211.742	261744.816	257970.066	260253.299
BIC	262568.583	263219.789	261760.909	257986.159	260269.393

*CvM = Cramer-von-Mises test, AD = Anderson-Darling test, KS = Kolmogorov-Smirnov test, AIC = Akaike's Information Criterion, BIC = Bayesian Information Criterion. Highlighted cells indicate the best-fit model according to the test statistic scores (3 decimal places).

20-year

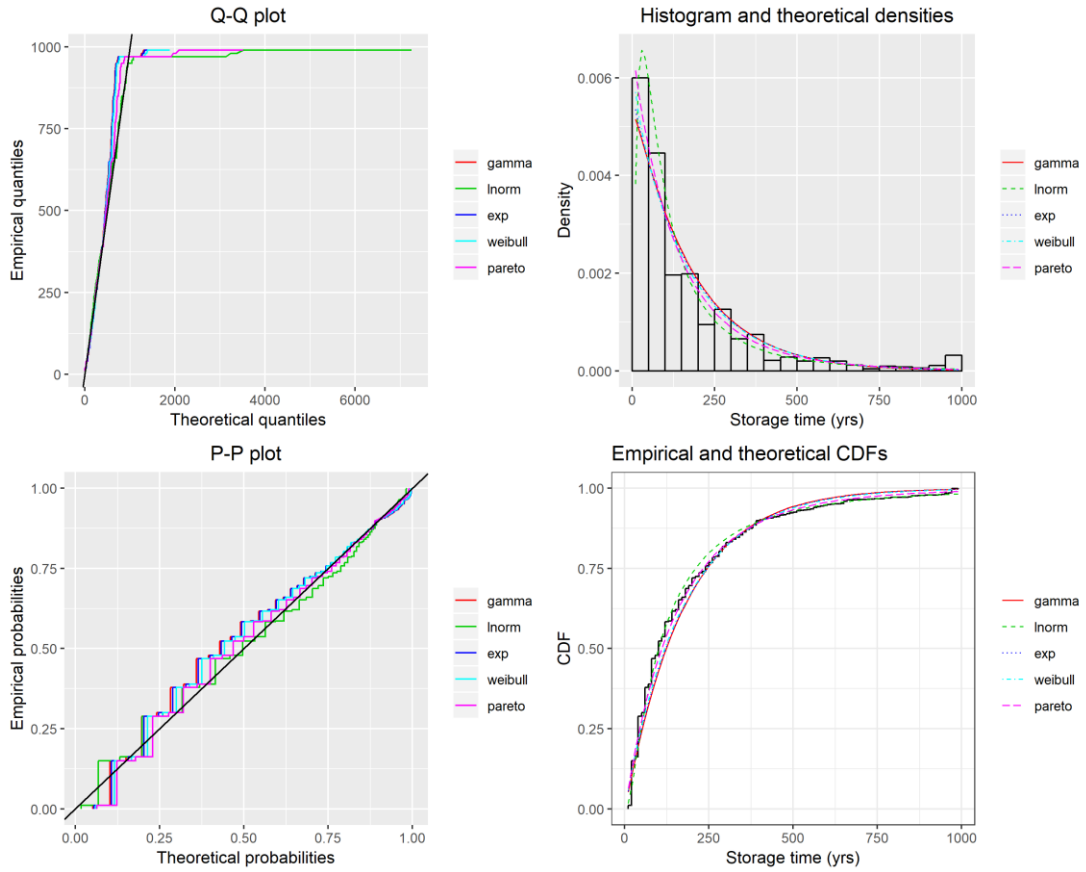

Diagnostic plots for evaluating model fits. Clockwise from top left: Quantile-Quantile plot, Histogram and fitted curves, Probability-Probability plot, and empirical cumulative distribution function with fitted curves.

	gamma	exponential	Weibull	lognormal	Pareto
CvM	27.844	25.143	20.471	11.104	12.754
AD	178.026	167.038	149.289	91.073	117.156
KS	0.109	0.104	0.104	0.091	0.112
AIC	148313.553	148317.510	148299.466	146936.365	148094.378
BIC	148328.341	148324.904	148314.253	146951.152	148109.166

*CvM = Cramer-von-Mises test, AD = Anderson-Darling test, KS = Kolmogorov-Smirnov test, AIC = Akaike's Information Criterion, BIC = Bayesian Information Criterion. Highlighted cells indicate the best-fit model according to the test statistic scores (3 decimal places).

50-year

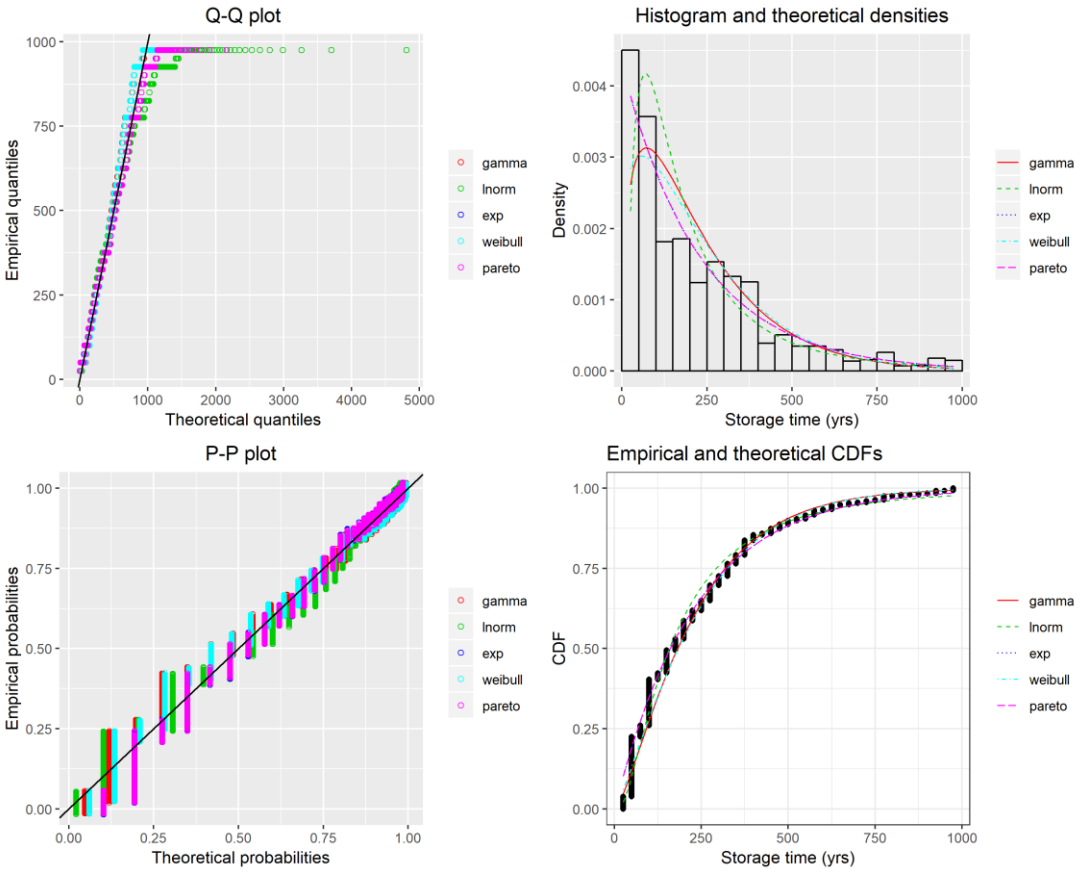

Diagnostic plots for evaluating model fits. Clockwise from top left: Quantile-Quantile plot, Histogram and fitted curves, Probability-Probability plot, and empirical cumulative distribution function with fitted curves.

	gamma	exponential	Weibull	lognormal	Pareto
CvM	9.666	11.358	8.831	9.925	11.359
AD	67.006	94.448	64.503	68.449	94.459
KS	0.128	0.155	0.120	0.122	0.155
AIC	70440.984	70854.045	70553.700	70233.016	70856.145
BIC	70454.206	70860.656	70566.923	70246.238	70869.367

*CvM = Cramer-von-Mises test, AD = Anderson-Darling test, KS = Kolmogorov-Smirnov test, AIC = Akaike's Information Criterion, BIC = Bayesian Information Criterion. Highlighted cells indicate the best-fit model according to the test statistic scores (3 decimal places).

100-year

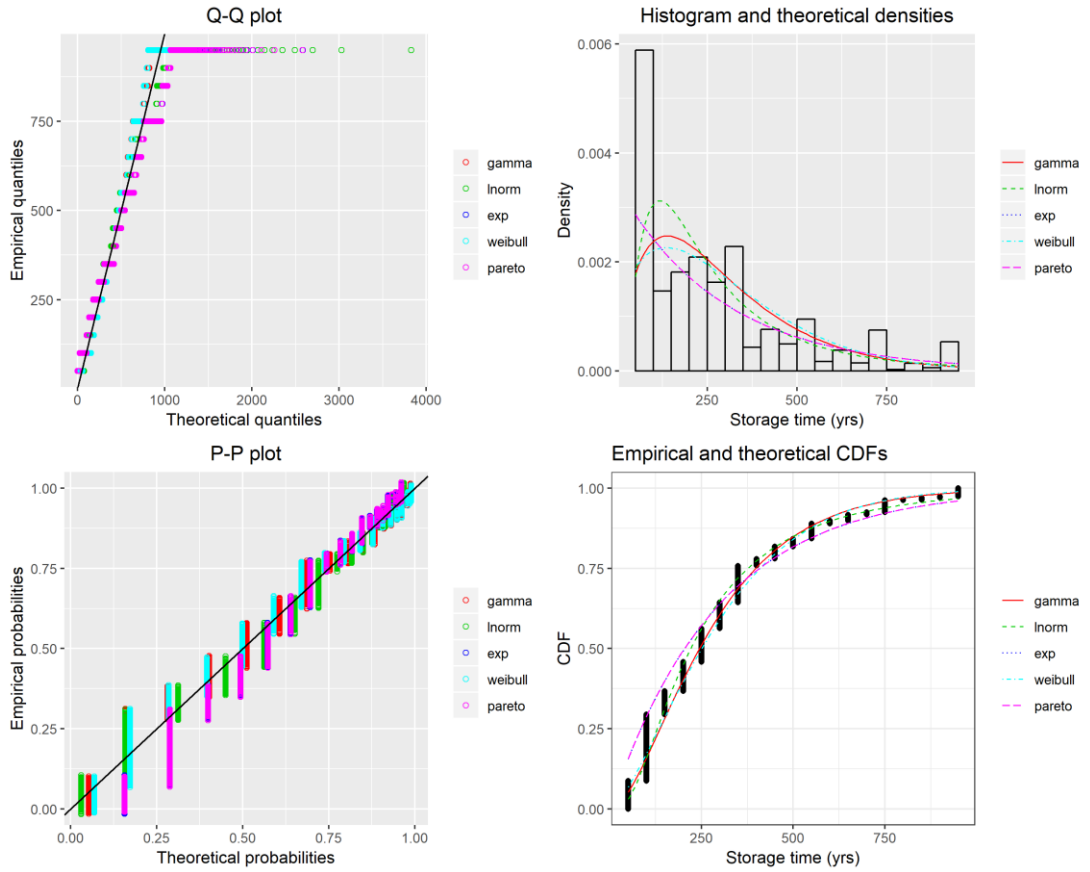

Diagnostic plots for evaluating model fits. Clockwise from top left: Quantile-Quantile plot, Histogram and fitted curves, Probability-Probability plot, and empirical cumulative distribution function with fitted curves.

	gamma	exponential	Weibull	lognormal	Pareto
CvM	5.342	18.590	5.412	6.810	18.583
AD	37.796	120.115	38.917	44.690	120.082
KS	0.135	0.200	0.122	0.136	0.200
AIC	42571.369	43213.103	42660.087	42545.752	43215.104
BIC	42583.531	43219.184	42672.248	42557.914	43227.266

*CvM = Cramer-von-Mises test, AD = Anderson-Darling test, KS = Kolmogorov-Smirnov test, AIC = Akaike's Information Criterion, BIC = Bayesian Information Criterion. Highlighted cells indicate the best-fit model according to the test statistic scores (3 decimal places).

Dane Forest Cover

10-year

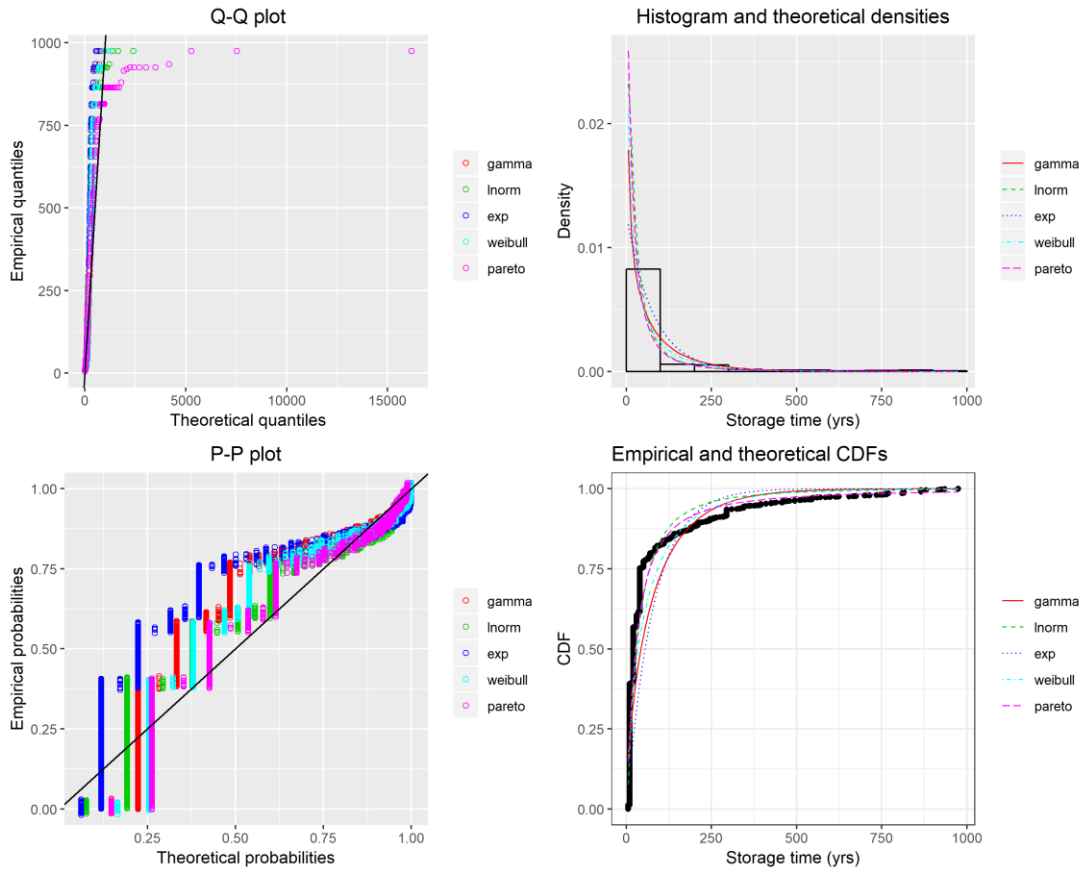

Diagnostic plots for evaluating model fits. Clockwise from top left: Quantile-Quantile plot, Histogram and fitted curves, Probability-Probability plot, and empirical cumulative distribution function with fitted curves.

	gamma	exponential	Weibull	lognormal	Pareto
CvM	49.619	101.827	34.853	23.873	22.409
AD	256.916	533.544	196.037	147.698	139.925
KS	0.267	0.355	0.242	0.199	0.249
AIC	28064.789	28552.892	27686.761	26644.952	26994.301
BIC	28076.559	28558.777	27698.532	26656.723	27006.072

*CvM = Cramer-von-Mises test, AD = Anderson-Darling test, KS = Kolmogorov-Smirnov test, AIC = Akaike's Information Criterion, BIC = Bayesian Information Criterion. Highlighted cells indicate the best-fit model according to the test statistic scores (3 decimal places).

20-year

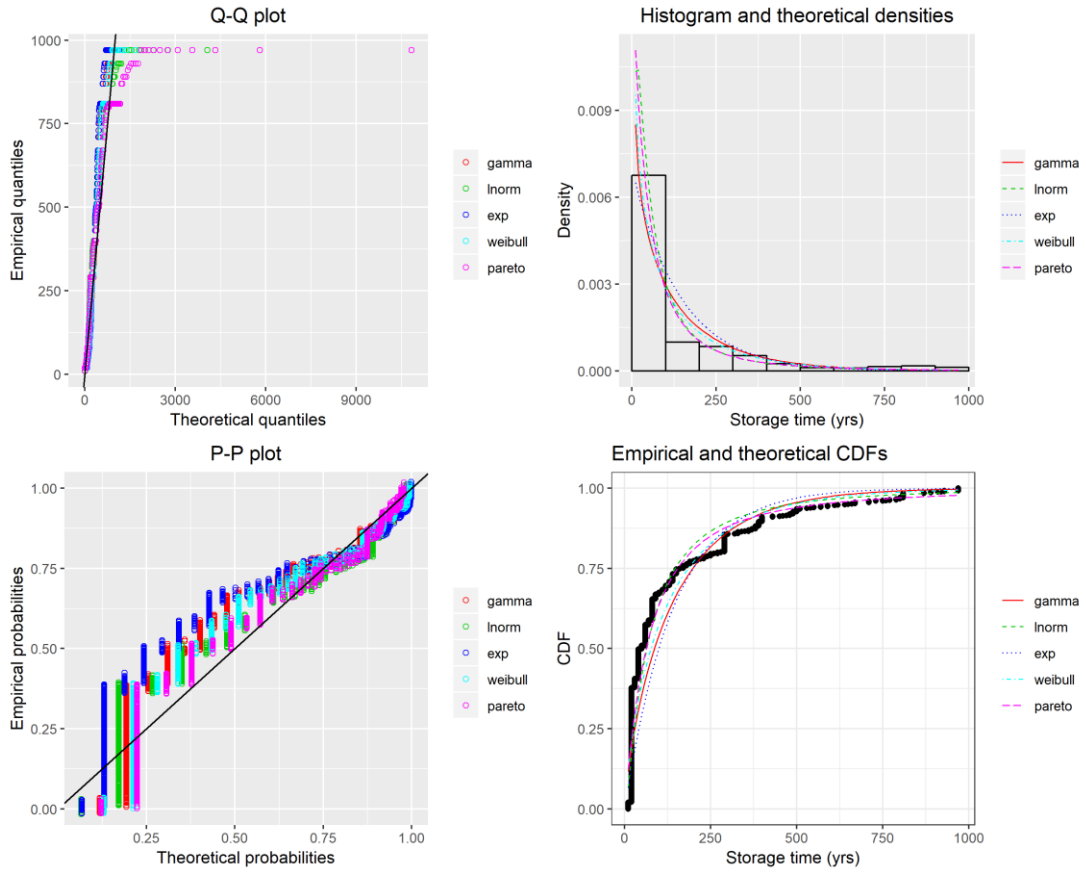

Diagnostic plots for evaluating model fits. Clockwise from top left: Quantile-Quantile plot, Histogram and fitted curves, Probability-Probability plot, and empirical cumulative distribution function with fitted curves.

	gamma	exponential	Weibull	lognormal	Pareto
CvM	14.874	25.993	11.409	9.287	8.019
AD	83.221	144.734	68.079	59.752	53.649
KS	0.189	0.255	0.192	0.207	0.202
AIC	16239.146	16325.084	16164.975	15833.703	16031.233
BIC	16249.589	16330.305	16175.417	15844.146	16041.675

*CvM = Cramer-von-Mises test, AD = Anderson-Darling test, KS = Kolmogorov-Smirnov test, AIC = Akaike's Information Criterion, BIC = Bayesian Information Criterion. Highlighted cells indicate the best-fit model according to the test statistic scores (3 decimal places).

50-year

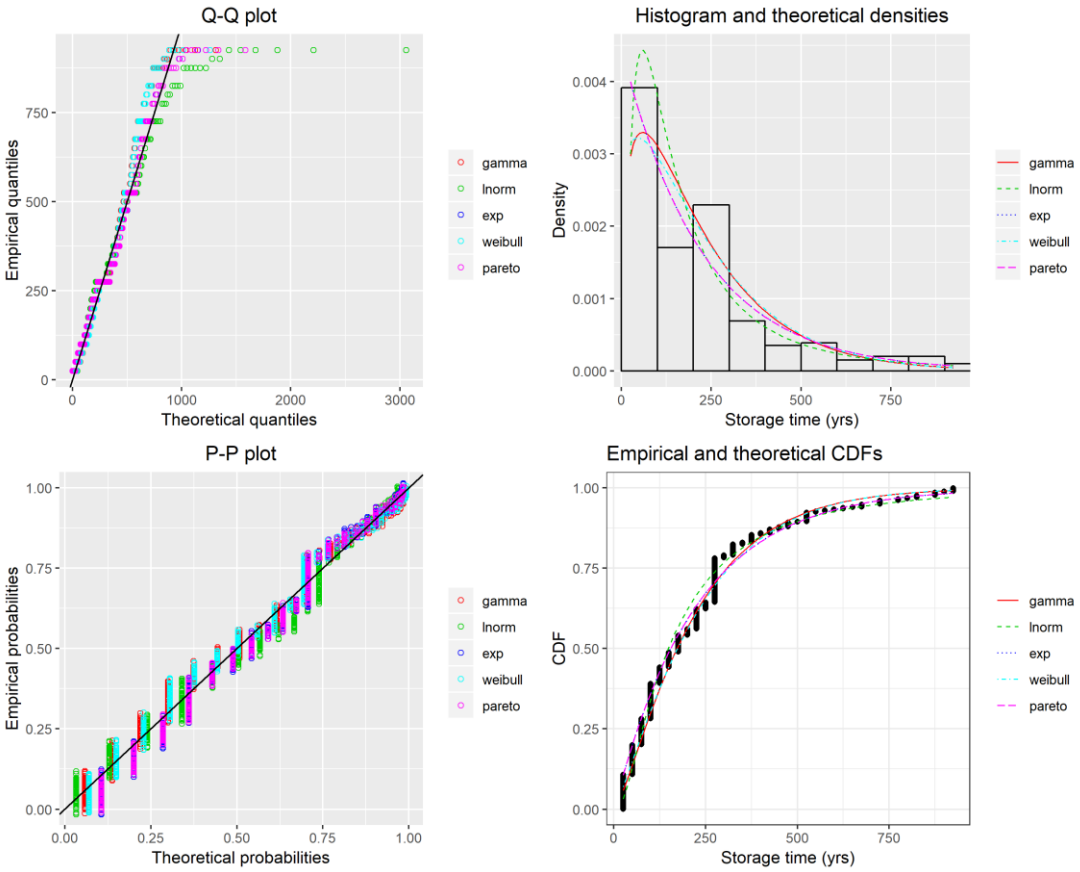

Diagnostic plots for evaluating model fits. Clockwise from top left: Quantile-Quantile plot, Histogram and fitted curves, Probability-Probability plot, and empirical cumulative distribution function with fitted curves.

	gamma	exponential	Weibull	lognormal	Pareto
CvM	0.657	0.993	0.635	0.952	0.987
AD	4.794	7.659	4.814	6.660	7.629
KS	0.092	0.106	0.087	0.105	0.106
AIC	7574.838	7604.809	7583.425	7572.961	7606.811
BIC	7583.608	7609.195	7592.195	7581.731	7615.581

*CvM = Cramer-von-Mises test, AD = Anderson-Darling test, KS = Kolmogorov-Smirnov test, AIC = Akaike's Information Criterion, BIC = Bayesian Information Criterion. Highlighted cells indicate the best-fit model according to the test statistic scores (3 decimal places).

100-year

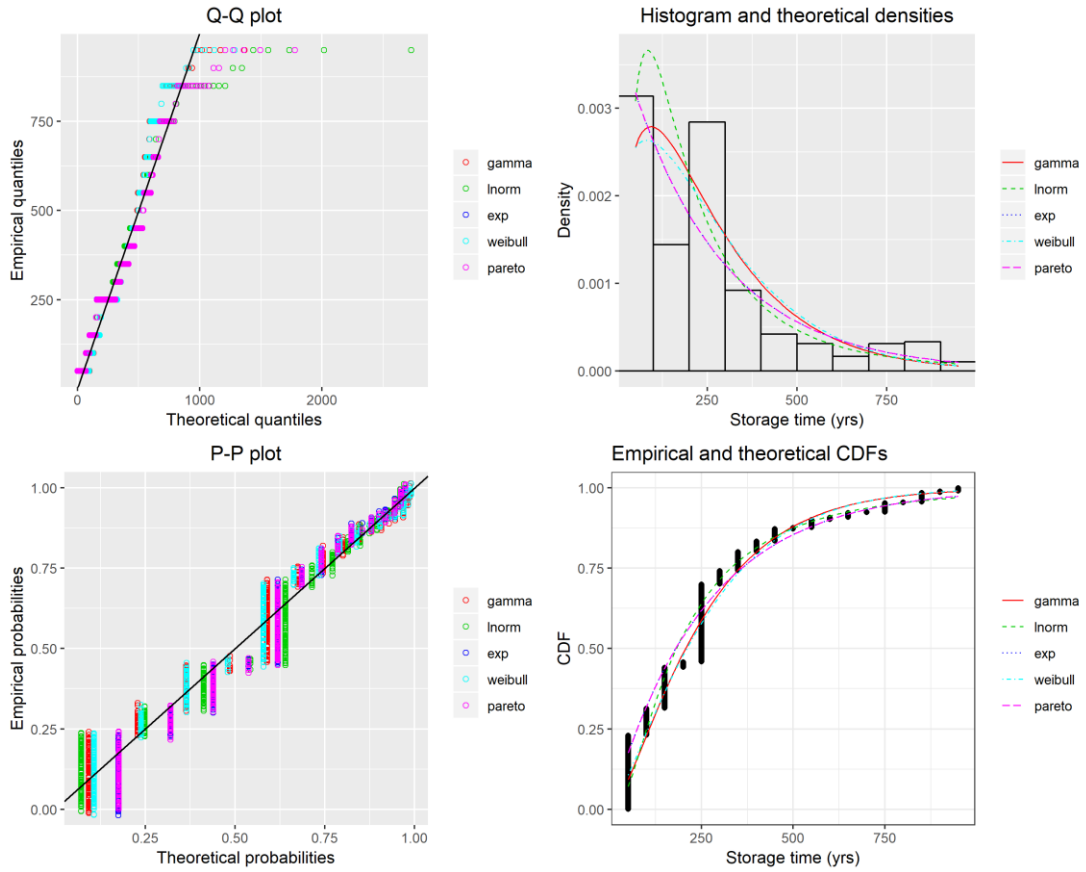

Diagnostic plots for evaluating model fits. Clockwise from top left: Quantile-Quantile plot, Histogram and fitted curves, Probability-Probability plot, and empirical cumulative distribution function with fitted curves.

	gamma	exponential	Weibull	lognormal	Pareto
CvM	1.441	2.234	1.401	2.002	2.234
AD	10.573	14.573	10.080	14.037	14.571
KS	0.138	0.175	0.123	0.182	0.175
AIC	6222.948	6271.469	6233.192	6213.971	6273.469
BIC	6231.287	6275.639	6241.531	6222.310	6281.809

*CvM = Cramer-von-Mises test, AD = Anderson-Darling test, KS = Kolmogorov-Smirnov test, AIC = Akaike's Information Criterion, BIC = Bayesian Information Criterion. Highlighted cells indicate the best-fit model according to the test statistic scores (3 decimal places).

Dane Grass Cover

10-year

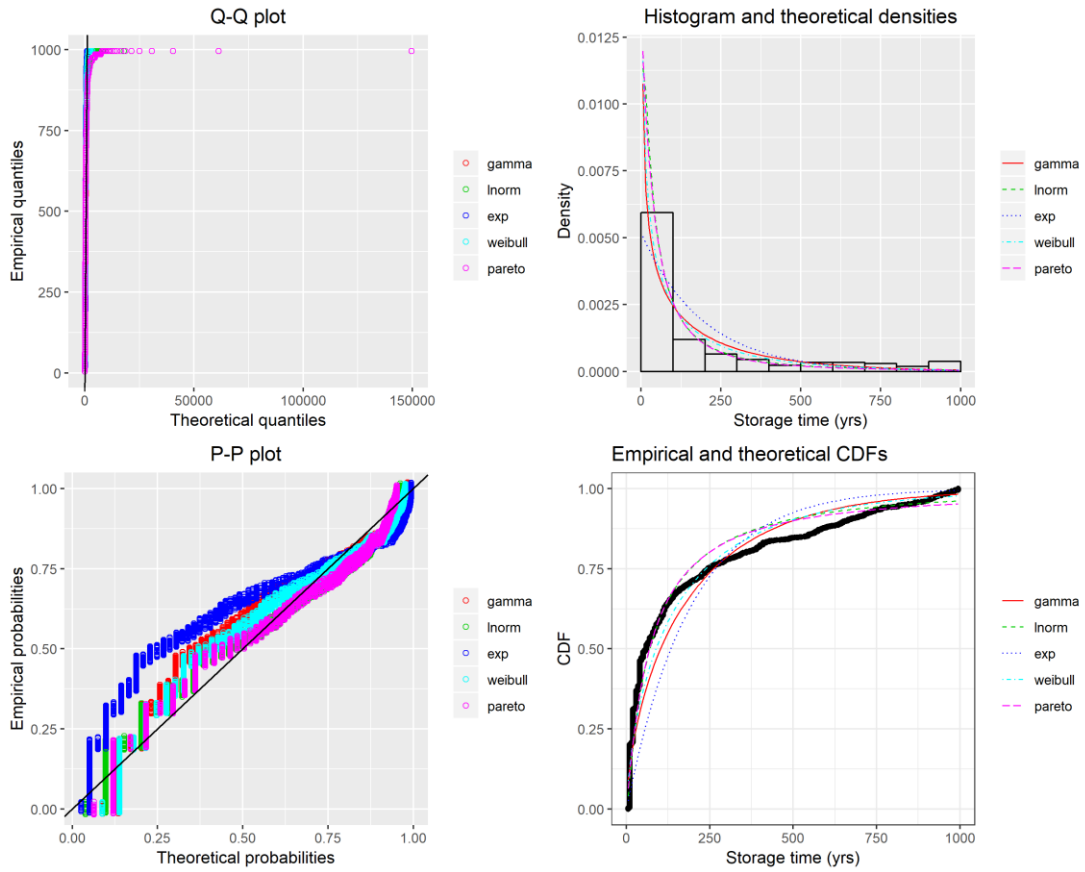

Diagnostic plots for evaluating model fits. Clockwise from top left: Quantile-Quantile plot, Histogram and fitted curves, Probability-Probability plot, and empirical cumulative distribution function with fitted curves.

	gamma	exponential	Weibull	lognormal	Pareto
CvM	27.342	97.716	18.197	12.041	10.766
AD	162.820	611.981	122.529	93.488	87.879
KS	0.159	0.275	0.136	0.109	0.116
AIC	56374.670	57299.749	56143.971	55553.438	55990.176
BIC	56387.527	57306.178	56156.828	55566.296	56003.033

*CvM = Cramer-von-Mises test, AD = Anderson-Darling test, KS = Kolmogorov-Smirnov test, AIC = Akaike's Information Criterion, BIC = Bayesian Information Criterion. Highlighted cells indicate the best-fit model according to the test statistic scores (3 decimal places).

20-year

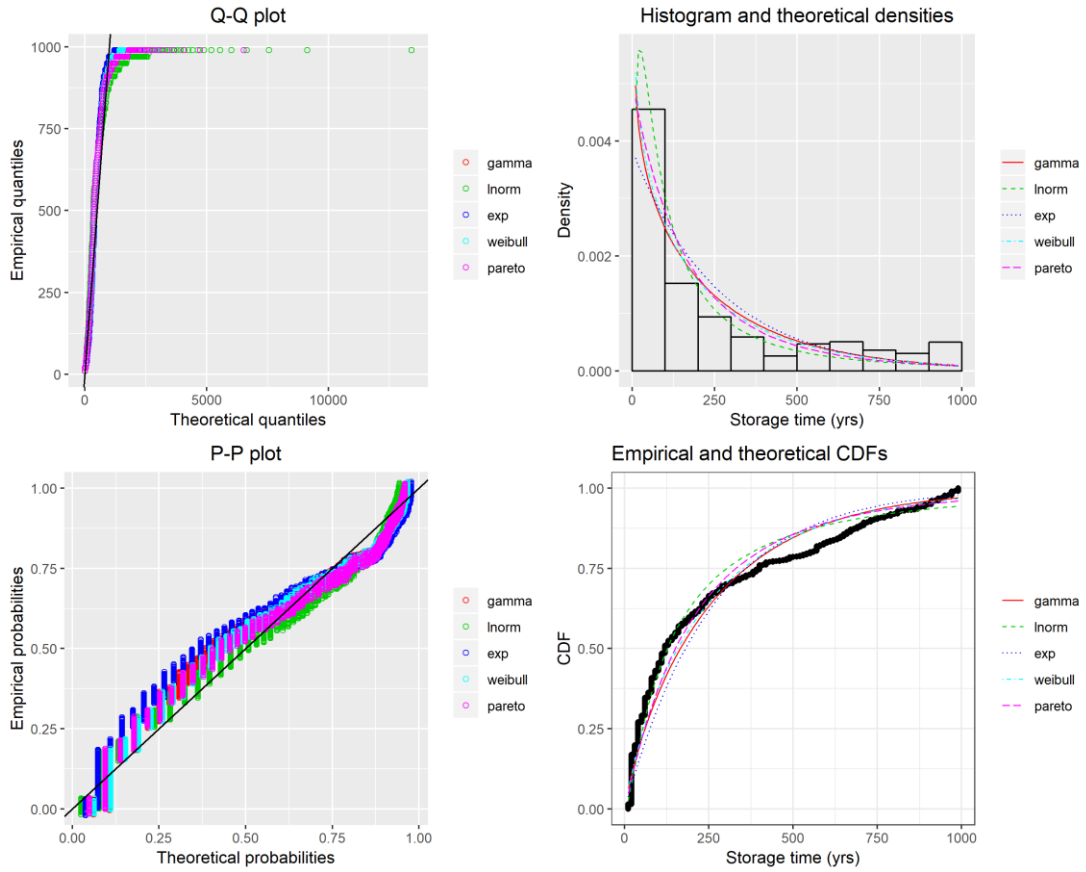

Diagnostic plots for evaluating model fits. Clockwise from top left: Quantile-Quantile plot, Histogram and fitted curves, Probability-Probability plot, and empirical cumulative distribution function with fitted curves.

	gamma	exponential	Weibull	lognormal	Pareto
CvM	9.868	20.165	7.871	5.598	8.215
AD	65.619	123.659	56.548	47.459	59.449
KS	0.102	0.144	0.095	0.092	0.095
AIC	41147.839	41229.971	41116.580	40975.343	41156.467
BIC	41159.945	41236.024	41128.686	40987.449	41168.573

*CvM = Cramer-von-Mises test, AD = Anderson-Darling test, KS = Kolmogorov-Smirnov test, AIC = Akaike's Information Criterion, BIC = Bayesian Information Criterion. Highlighted cells indicate the best-fit model according to the test statistic scores (3 decimal places).

50-year

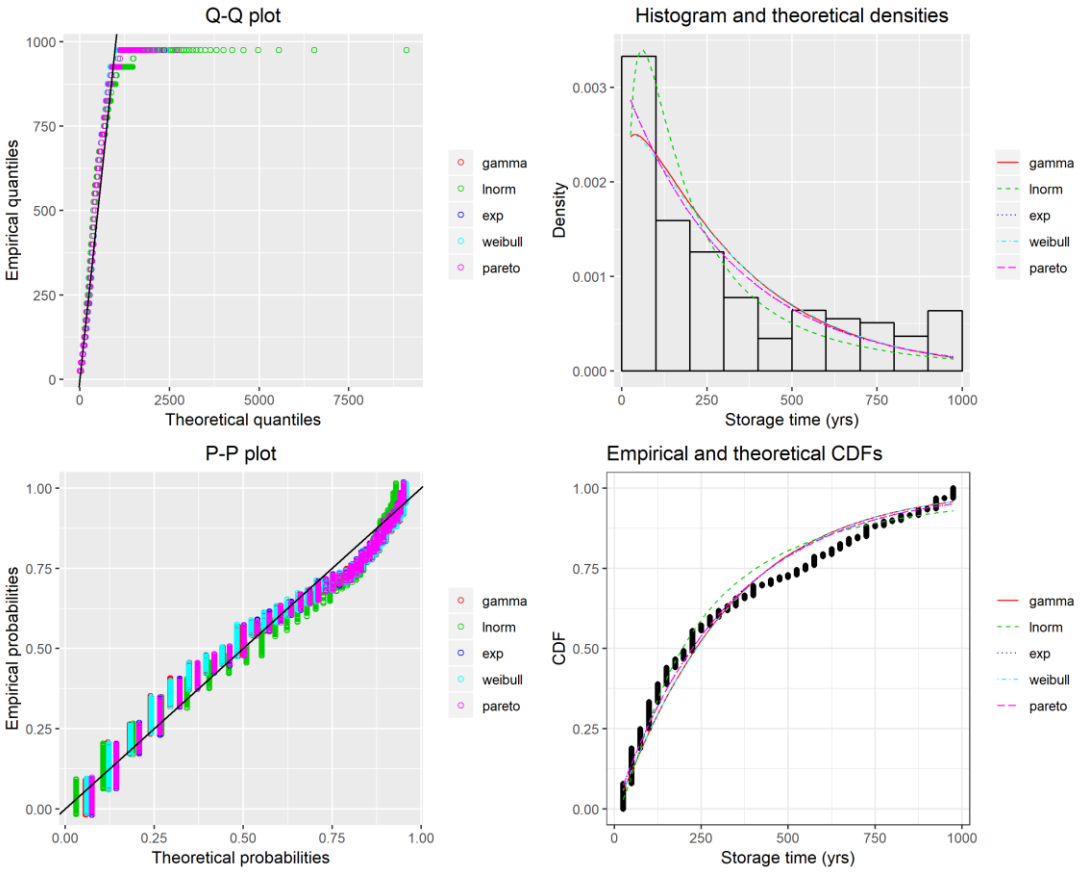

Diagnostic plots for evaluating model fits. Clockwise from top left: Quantile-Quantile plot, Histogram and fitted curves, Probability-Probability plot, and empirical cumulative distribution function with fitted curves.

	gamma	exponential	Weibull	lognormal	Pareto
CvM	4.682	2.983	4.607	3.899	2.982
AD	32.265	25.294	31.786	30.943	25.274
KS	0.094	0.075	0.093	0.088	0.075
AIC	31134.914	31154.784	31139.001	31181.149	31156.785
BIC	31146.395	31160.524	31150.482	31192.629	31168.265

*CvM = Cramer-von-Mises test, AD = Anderson-Darling test, KS = Kolmogorov-Smirnov test, AIC = Akaike's Information Criterion, BIC = Bayesian Information Criterion. Highlighted cells indicate the best-fit model according to the test statistic scores (3 decimal places).

100-year

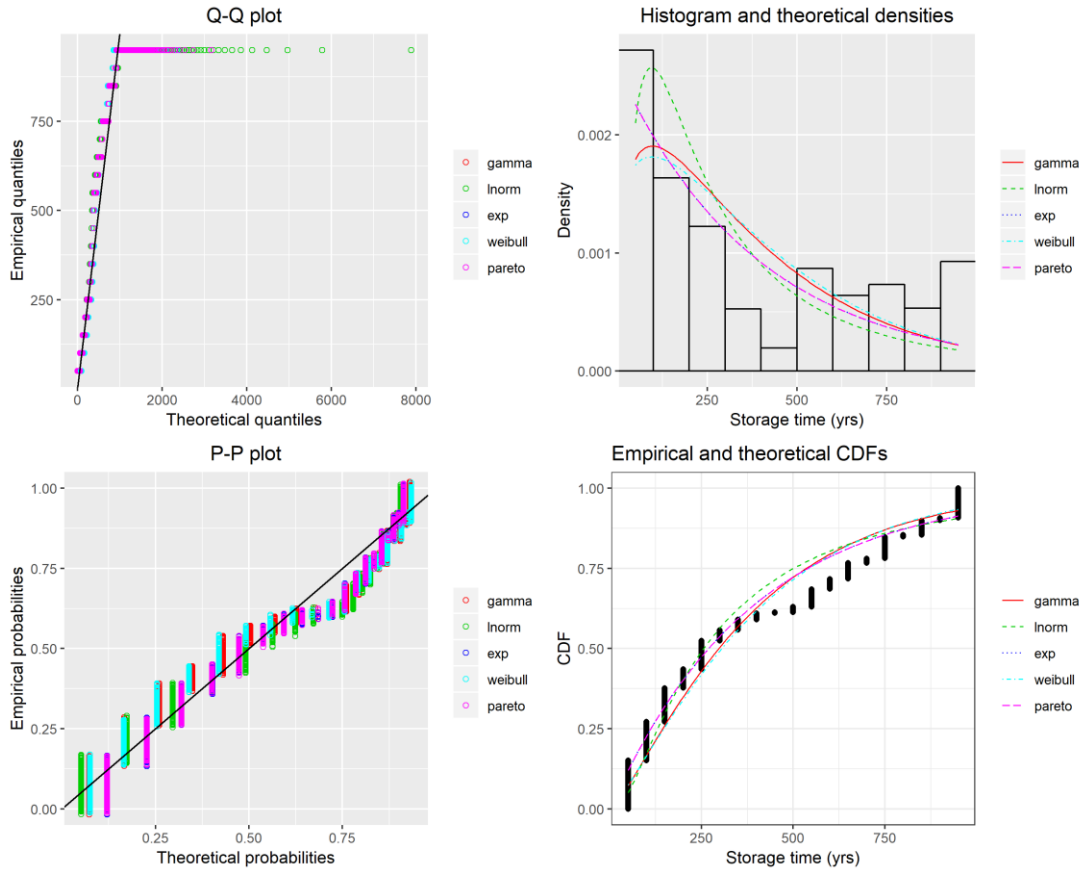

Diagnostic plots for evaluating model fits. Clockwise from top left: Quantile-Quantile plot, Histogram and fitted curves, Probability-Probability plot, and empirical cumulative distribution function with fitted curves.

	gamma	exponential	Weibull	lognormal	Pareto
CvM	6.163	4.494	6.457	5.955	4.496
AD	42.637	37.257	43.620	45.596	37.270
KS	0.131	0.127	0.125	0.149	0.127
AIC	23488.969	23566.814	23485.351	23559.601	23568.814
BIC	23499.836	23572.248	23496.219	23570.469	23579.682

*CvM = Cramer-von-Mises test, AD = Anderson-Darling test, KS = Kolmogorov-Smirnov test, AIC = Akaike's Information Criterion, BIC = Bayesian Information Criterion. Highlighted cells indicate the best-fit model according to the test statistic scores (3 decimal places).

Dane Unvegetated Cover

10-year

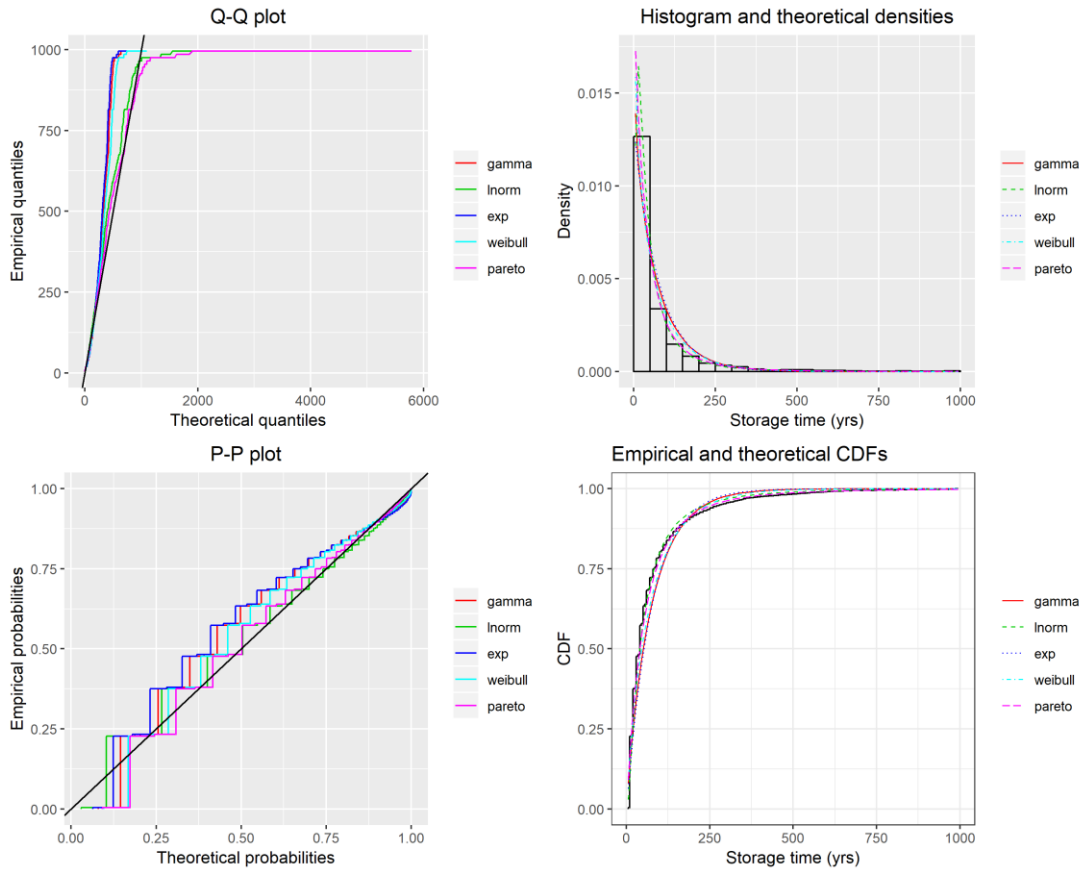

Diagnostic plots for evaluating model fits. Clockwise from top left: Quantile-Quantile plot, Histogram and fitted curves, Probability-Probability plot, and empirical cumulative distribution function with fitted curves.

	gamma	exponential	Weibull	lognormal	Pareto
CvM	177.473	226.356	124.331	57.465	75.191
AD	1059.738	1275.379	852.875	476.245	624.808
KS	0.144	0.164	0.164	0.123	0.169
AIC	341113.261	341361.538	340065.447	332127.735	337032.026
BIC	341130.009	341369.913	340082.196	332144.484	337048.775

*CvM = Cramer-von-Mises test, AD = Anderson-Darling test, KS = Kolmogorov-Smirnov test, AIC = Akaike's Information Criterion, BIC = Bayesian Information Criterion. Highlighted cells indicate the best-fit model according to the test statistic scores (3 decimal places).

20-year

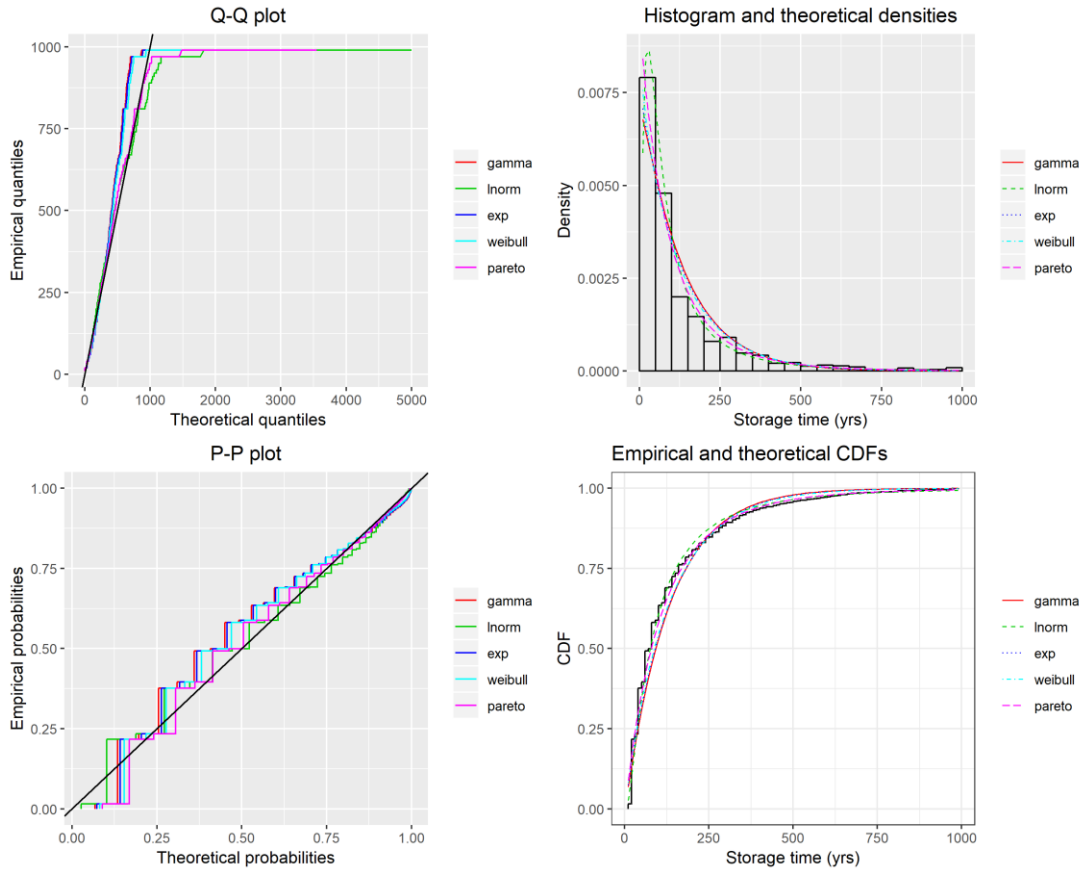

Diagnostic plots for evaluating model fits. Clockwise from top left: Quantile-Quantile plot, Histogram and fitted curves, Probability-Probability plot, and empirical cumulative distribution function with fitted curves.

	gamma	exponential	Weibull	lognormal	Pareto
CvM	68.226	62.135	52.286	27.026	35.302
AD	414.663	390.254	354.218	211.517	289.599
KS	0.133	0.126	0.138	0.115	0.153
AIC	201428.565	201442.359	201394.873	198303.716	200826.821
BIC	201444.064	201450.108	201410.372	198319.214	200842.319

*CvM = Cramer-von-Mises test, AD = Anderson-Darling test, KS = Kolmogorov-Smirnov test, AIC = Akaike's Information Criterion, BIC = Bayesian Information Criterion. Highlighted cells indicate the best-fit model according to the test statistic scores (3 decimal places).

50-year

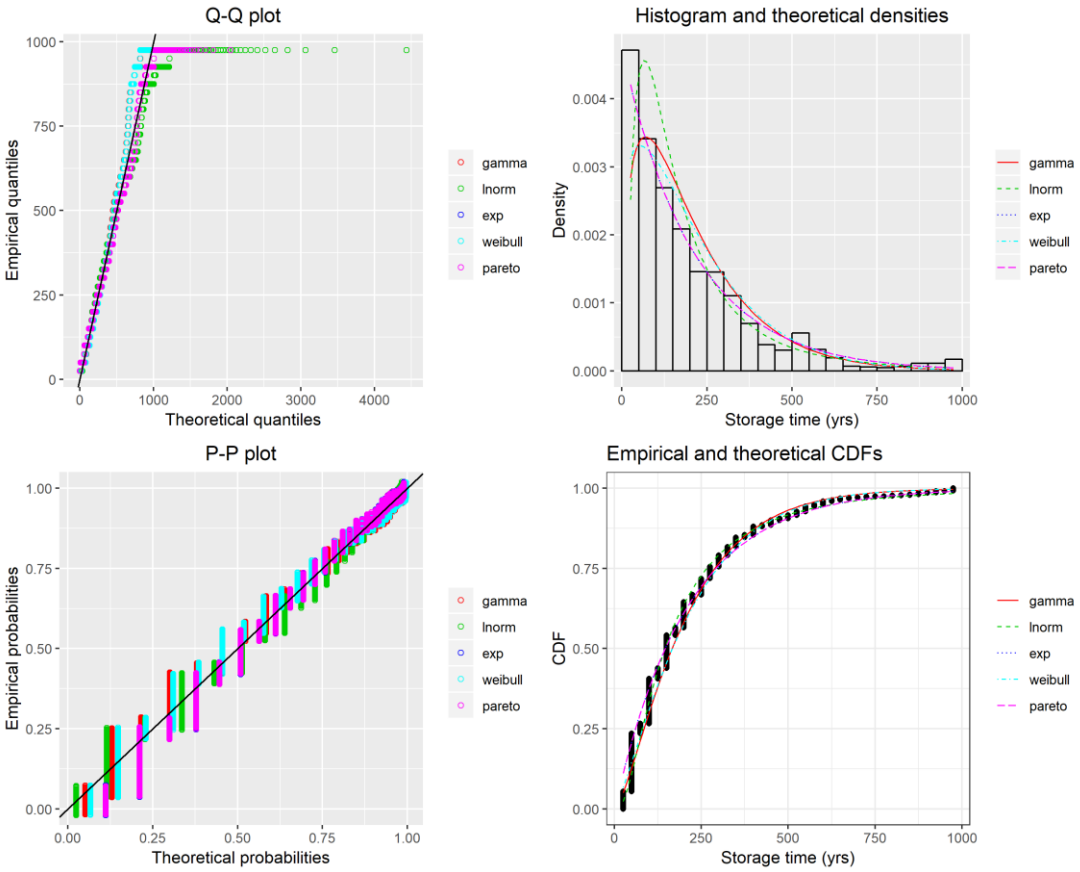

Diagnostic plots for evaluating model fits. Clockwise from top left: Quantile-Quantile plot, Histogram and fitted curves, Probability-Probability plot, and empirical cumulative distribution function with fitted curves.

	gamma	exponential	Weibull	lognormal	Pareto
CvM	11.815	20.162	11.698	11.163	20.152
AD	82.287	154.796	85.839	78.510	154.746
KS	0.105	0.156	0.097	0.121	0.156
AIC	101788.894	102496.787	102007.163	101403.526	102498.788
BIC	101802.885	102503.782	102021.154	101417.518	102512.779

*CvM = Cramer-von-Mises test, AD = Anderson-Darling test, KS = Kolmogorov-Smirnov test, AIC = Akaike's Information Criterion, BIC = Bayesian Information Criterion. Highlighted cells indicate the best-fit model according to the test statistic scores (3 decimal places).

100-year

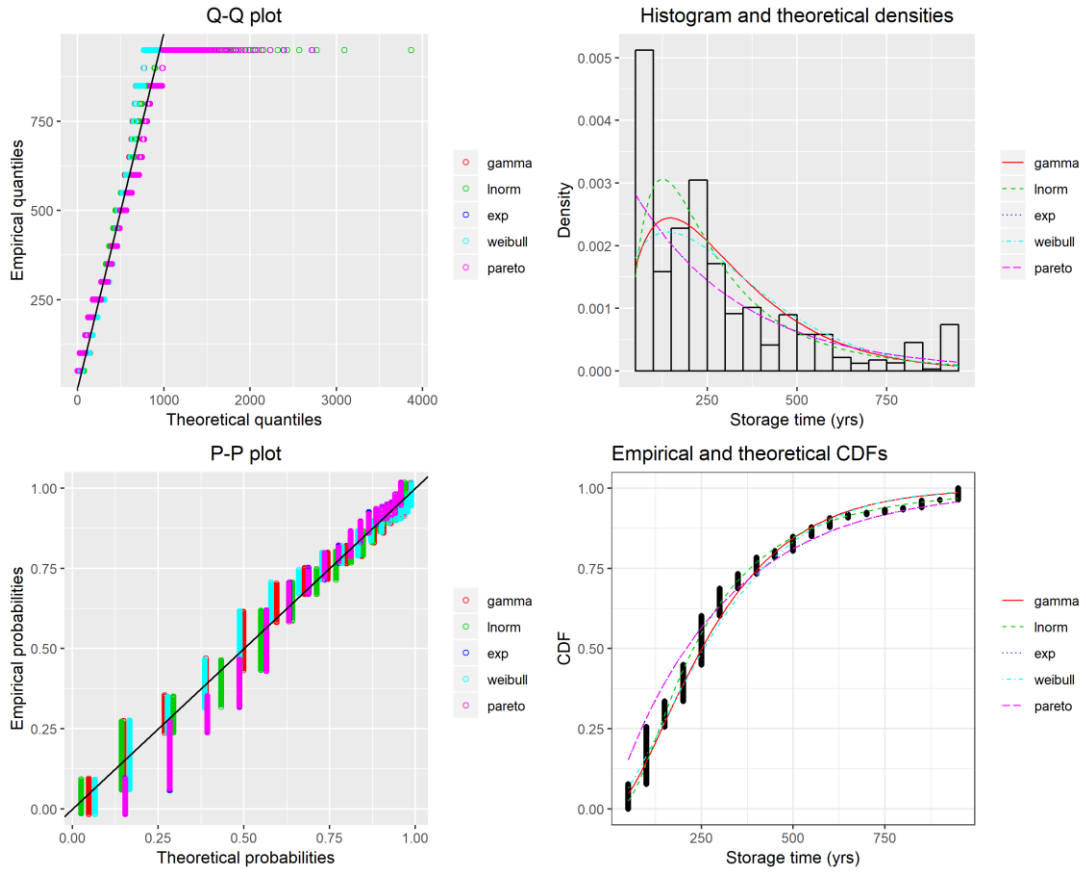

Diagnostic plots for evaluating model fits. Clockwise from top left: Quantile-Quantile plot, Histogram and fitted curves, Probability-Probability plot, and empirical cumulative distribution function with fitted curves.

	gamma	exponential	Weibull	lognormal	Pareto
CvM	7.002	28.911	8.364	6.515	28.895
AD	47.484	178.399	55.794	44.745	178.333
KS	0.107	0.207	0.114	0.113	0.207
AIC	56930.788	57869.050	57094.873	56832.003	57871.051
BIC	56943.528	57875.420	57107.613	56844.743	57883.791

*CvM = Cramer-von-Mises test, AD = Anderson-Darling test, KS = Kolmogorov-Smirnov test, AIC = Akaike's Information Criterion, BIC = Bayesian Information Criterion. Highlighted cells indicate the best-fit model according to the test statistic scores (3 decimal places).

C: Probability of floodplain reoccupation by the channel (Chapter 4 simulations)

The probability of floodplain reoccupation by the channel is another indicator of sediment storage time dynamics. Similar to the erosion hazard, which is calculated by dividing the storage time distribution by the age distribution, the probability of floodplain reoccupation is a measure of how likely a sediment deposit will be eroded based on age.

For each channel change time-series, including the four different time-steps of analysis tested in Chapter 4, the frequency of erosion events for each grid cell was calculated over 1000 years. Cells that recorded an erosion frequency value of 0 were excluded from the analysis since these areas of floodplain did not incur any reoccupation by the channel (these include cells that were classed as channel cells throughout the simulation or cells where new floodplain was formed, but remained unvisited by the channel for the remainder of time). The ages of each of the cells with an erosion frequency > 0 after 1000 years were grouped into 100-year bins and normalised to make probability values for each 100-year age class. Linear regressions of the probability of reoccupation against age were undertaken to determine whether reoccupation decayed with age, and if the decay was exponentially or as a power law function.

All forest cover datasets and all unvegetated datasets measured at 10-year time-steps) showed power law decaying reoccupation probability with floodplain age. All grass cover datasets (except Dane 10-year) and all unvegetated datasets (except for 10-year time-steps) showed exponentially decaying reoccupation probability with floodplain age.

Forest

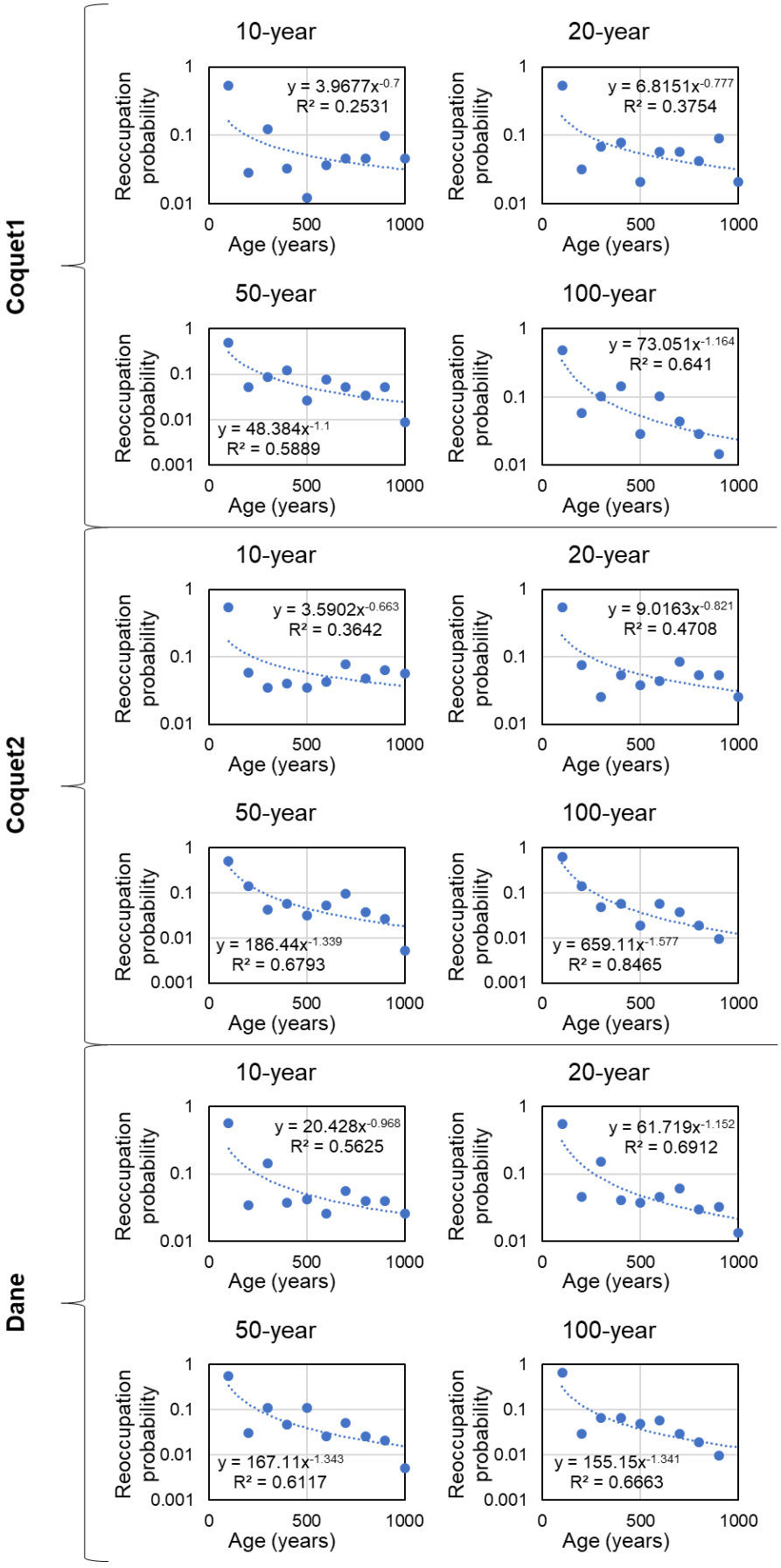
Coquet1
10-year
y = 3.9677x-0.7
R² = 0.2531
20-year
y = 6.8151x-0.777
R² = 0.3754
50-year
y = 48.384x-1.1
R² = 0.5889
100-year
y = 73.051x-1.164
R² = 0.641
Coquet2
10-year
y = 3.5902x-0.663
R² = 0.3642
20-year
y = 9.0163x-0.821
R² = 0.4708
50-year
y = 186.44x-1.339
R² = 0.6793
100-year
y = 659.11x-1.577
R² = 0.8465
Dane
10-year
y = 20.428x-0.968
R² = 0.5625
20-year
y = 61.719x-1.152
R² = 0.6912
50-year
y = 167.11x-1.343
R² = 0.6117
100-year
y = 155.15x-1.341
R² = 0.6663
Reoccupation probability
Age (years)

Grass

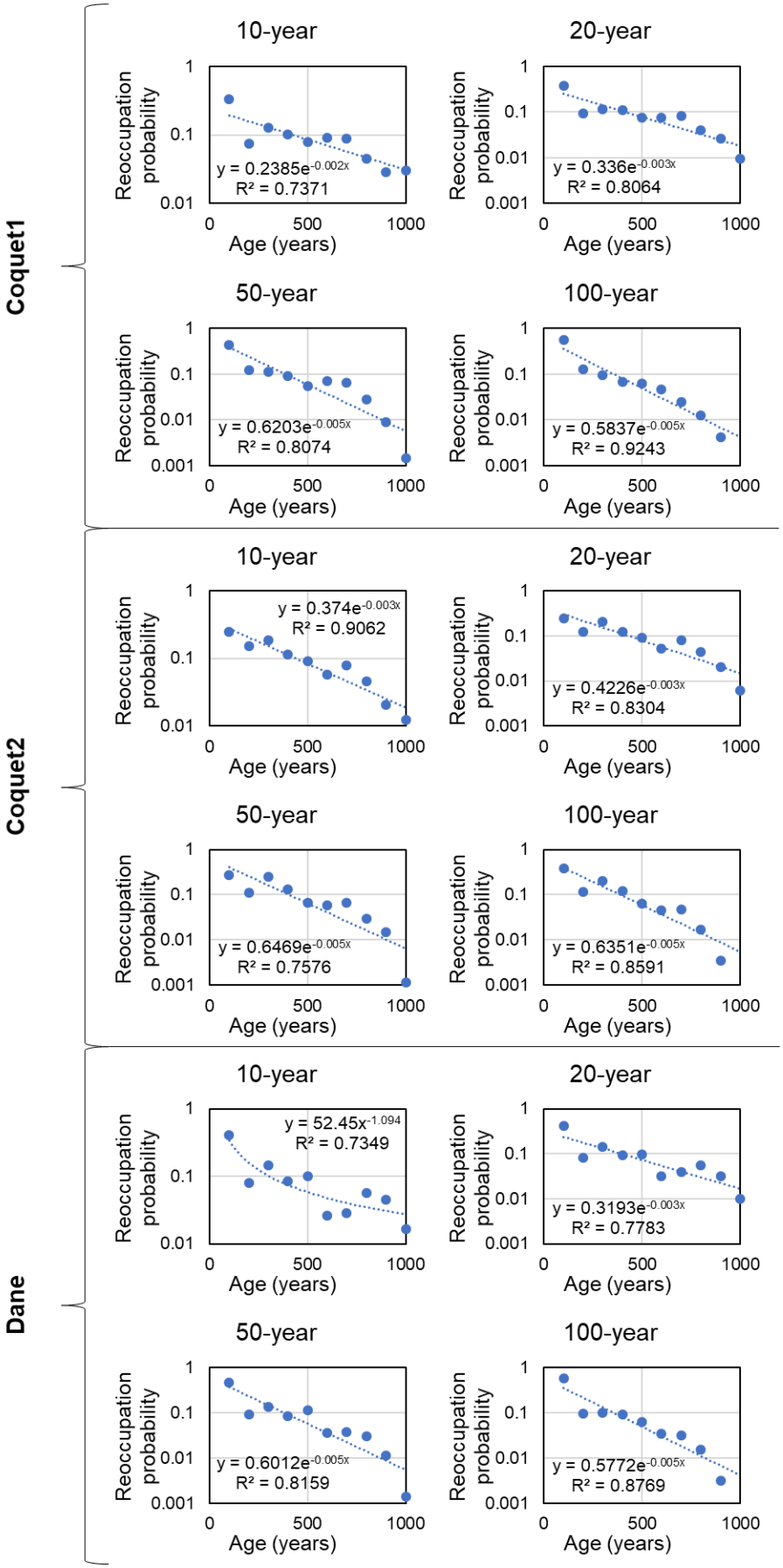
Coquet1
10-year
y = 0.2385e-0.002x
R² = 0.7371
20-year
y = 0.336e-0.003x
R² = 0.8064
50-year
y = 0.6203e-0.005x
R² = 0.8074
100-year
y = 0.5837e-0.005x
R² = 0.9243
Coquet2
10-year
y = 0.374e-0.003x
R² = 0.9062
20-year
y = 0.4226e-0.003x
R² = 0.8304
50-year
y = 0.6469e-0.005x
R² = 0.7576
100-year
y = 0.6351e-0.005x
R² = 0.8591
Dane
10-year
y = 52.45x-1.094
R² = 0.7349
20-year
y = 0.3193e-0.003x
R² = 0.7783
50-year
y = 0.6012e-0.005x
R² = 0.8159
100-year
y = 0.5772e-0.005x
R² = 0.8769
Reoccupation probability
Age (years)

Unvegetated

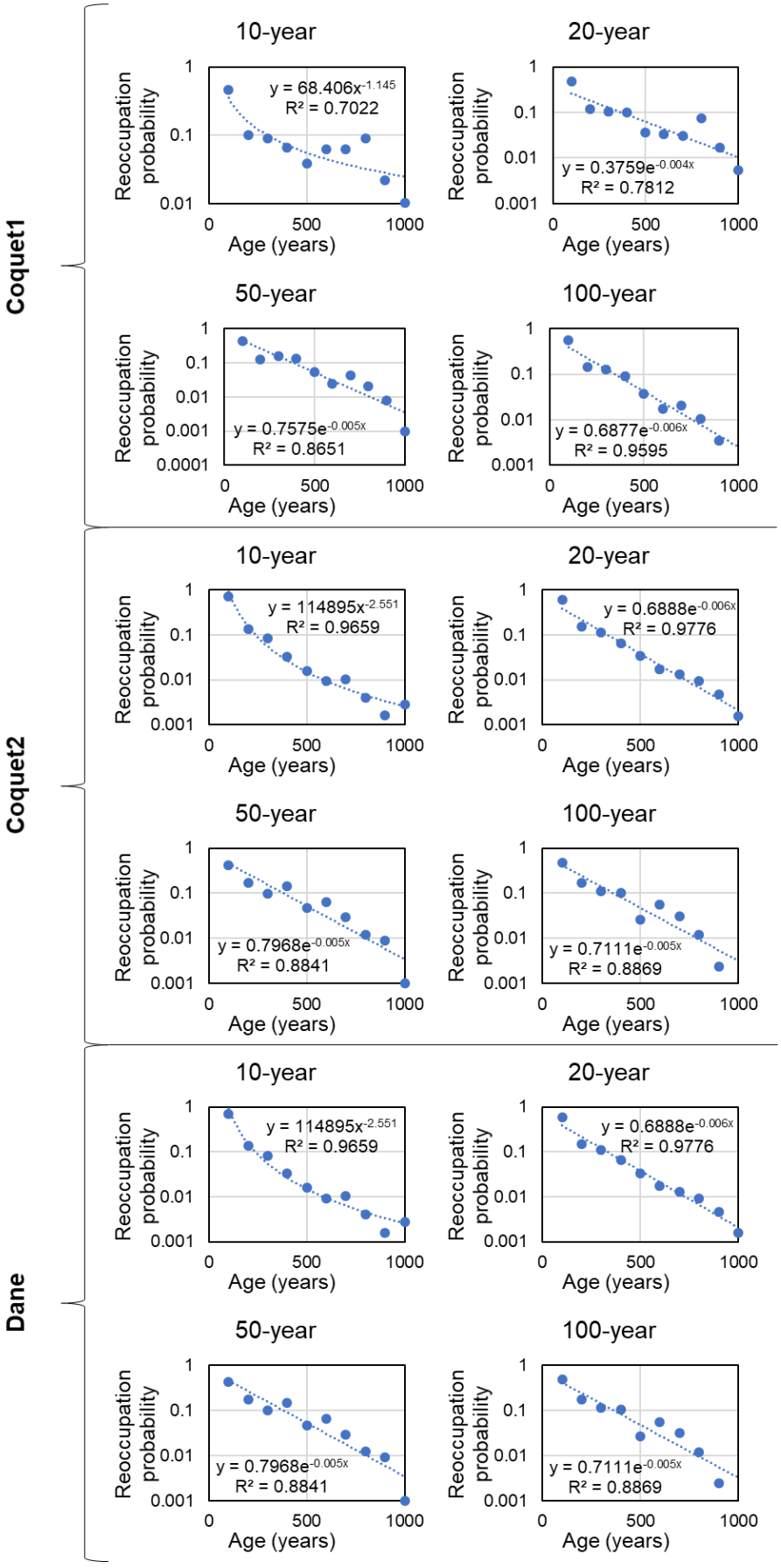

Appendix 3

A: Age and storage time distributions after 250, 500, 750 and 1000 years of simulation

For each of the fifteen simulations (three reaches multiplied by five scenarios), age and storage time inverse cumulative distribution functions were modelled for the first 250, 500, 750 and 1000 years of simulation. Changes in curvature indicate changes in the population of ages retained within and eroding from storage. Convex curvature indicates older ages dominate the distribution while concave indicates the opposite. “Steps”, where there is no overall curvature, indicate that no erosion occurred. An inflection point between the types of curvature identifies the timing of any changes in sediment storage behaviour. By modelling a full distribution at four different timescales, it should be possible to more easily identify any changes in the distribution curvature and the timing of these changes. It should also be possible to track changes in the median (horizontal dashed line) age and median storage time through time, with a reduction in median age for example, indicating that sediment of older ages has begun to be eroded proportionally more than before. For each of the following pages, the age and storage time distributions are displayed on the top and bottom plots, respectively.

Coquet1 Decreasing flow magnitudes scenario

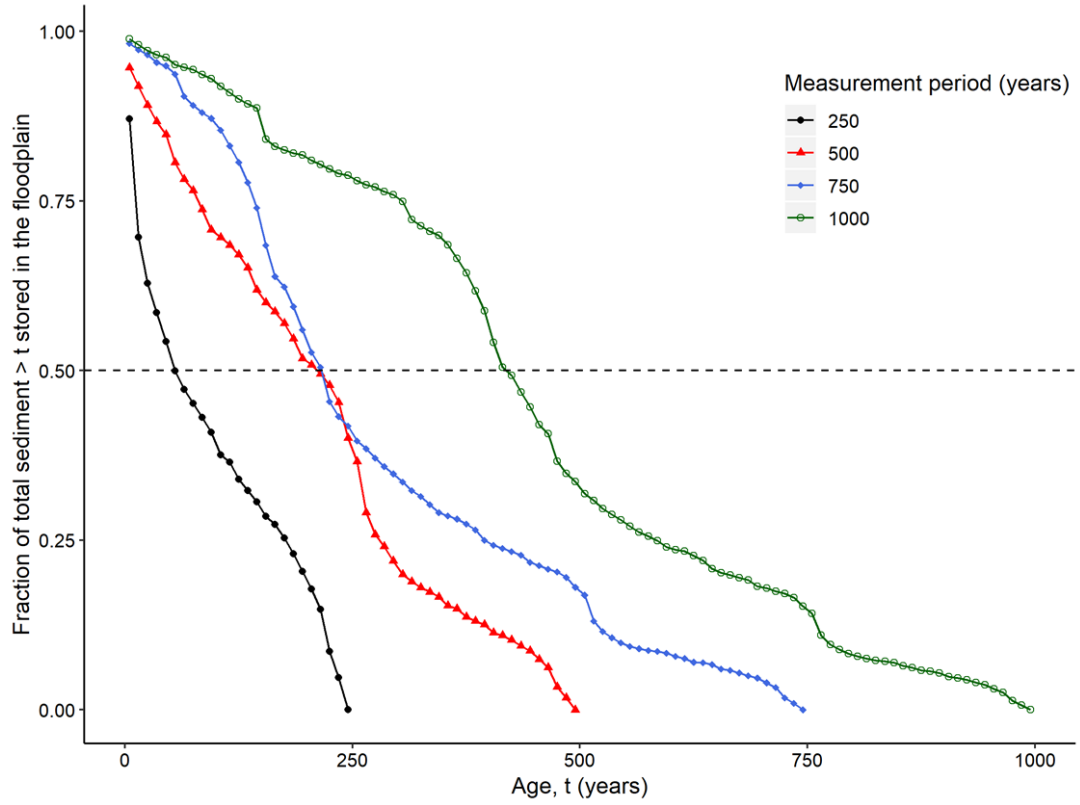

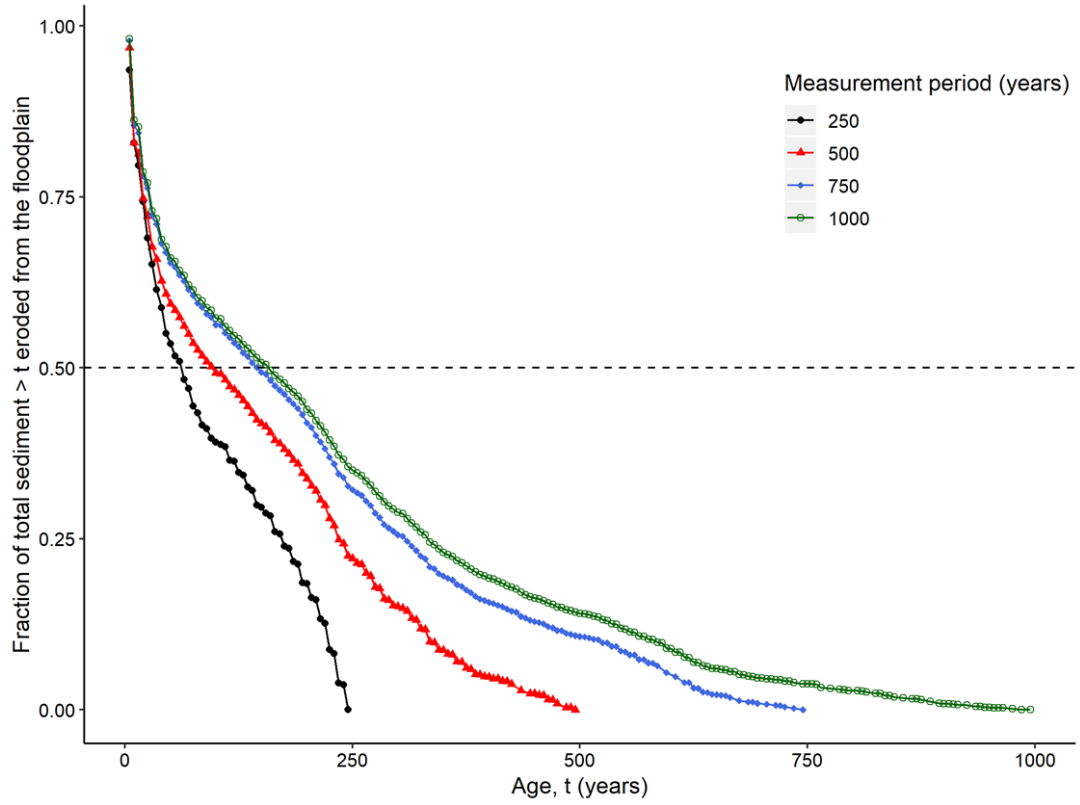

Coquet1 Increasing flow magnitudes scenario

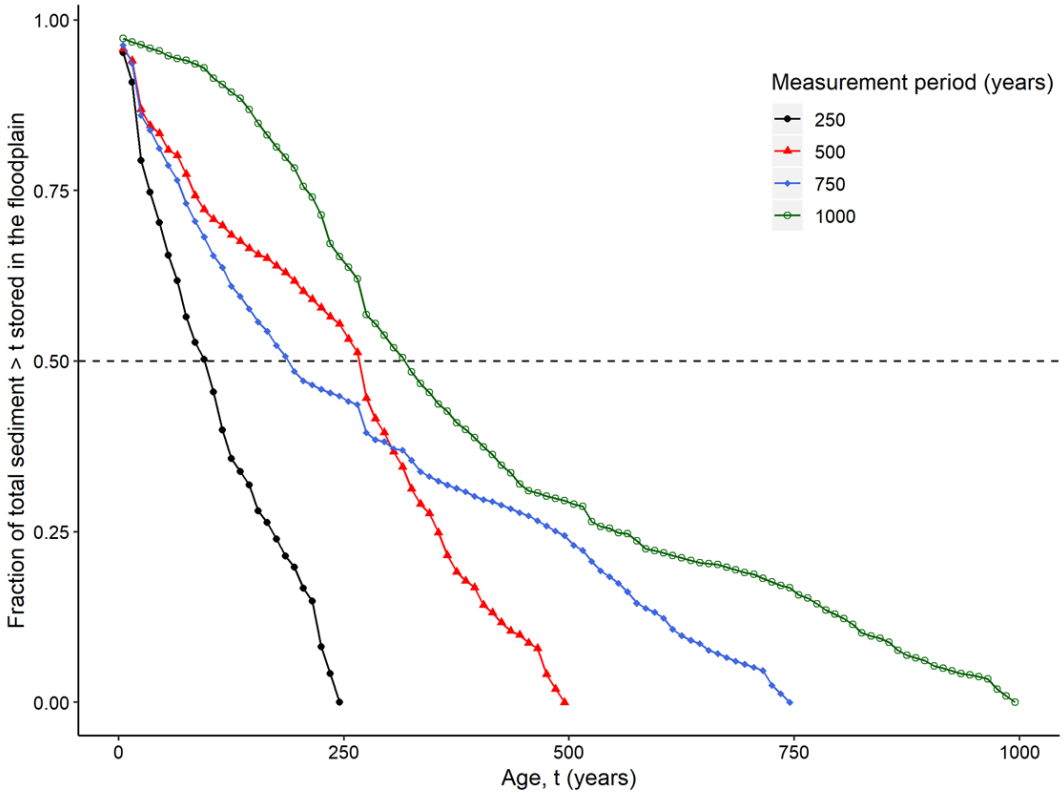

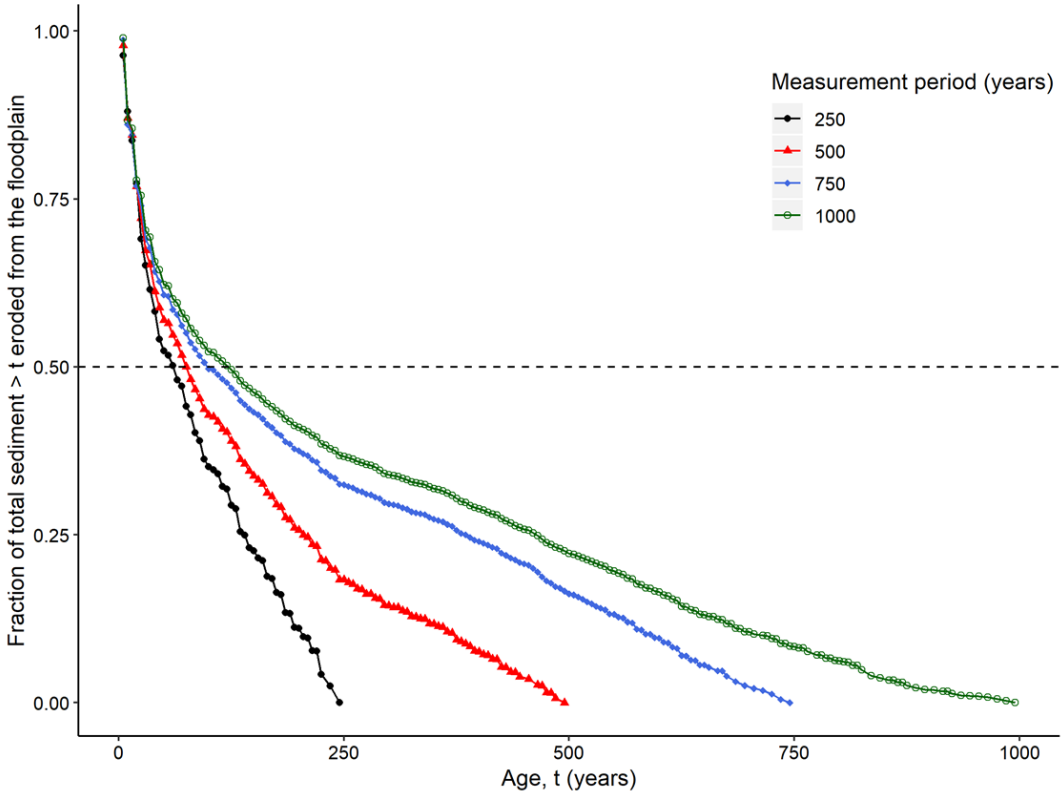

Coquet1 Forest to grass scenario

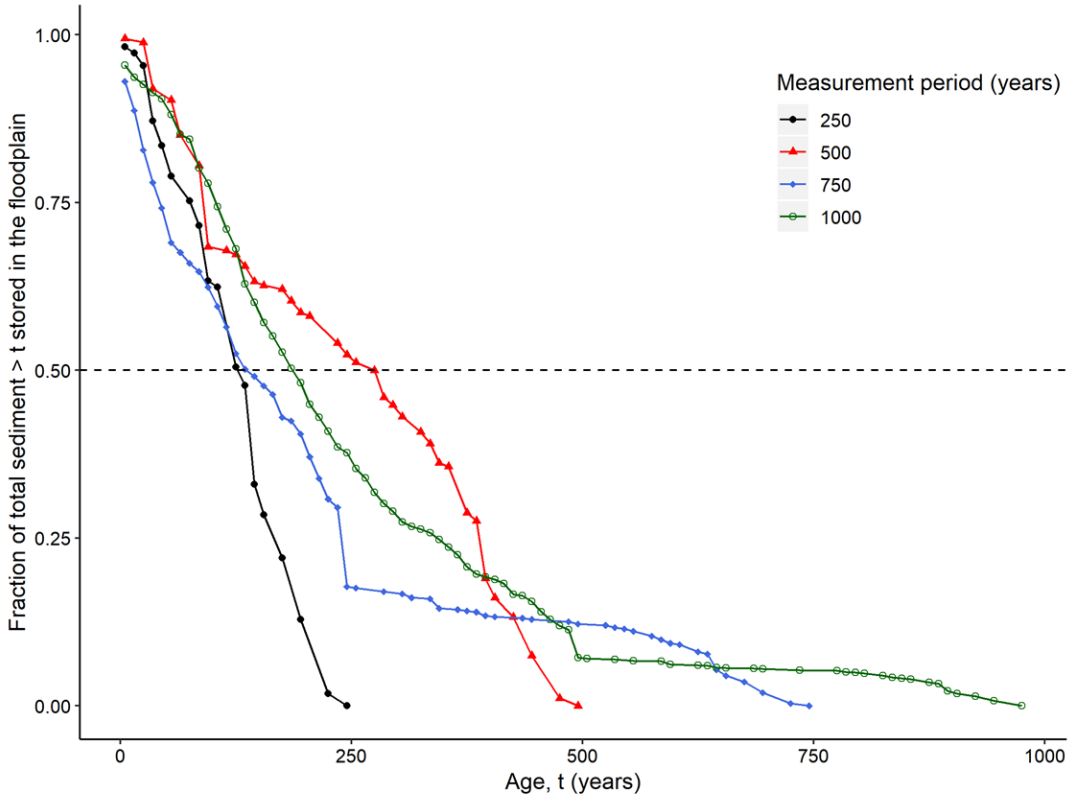

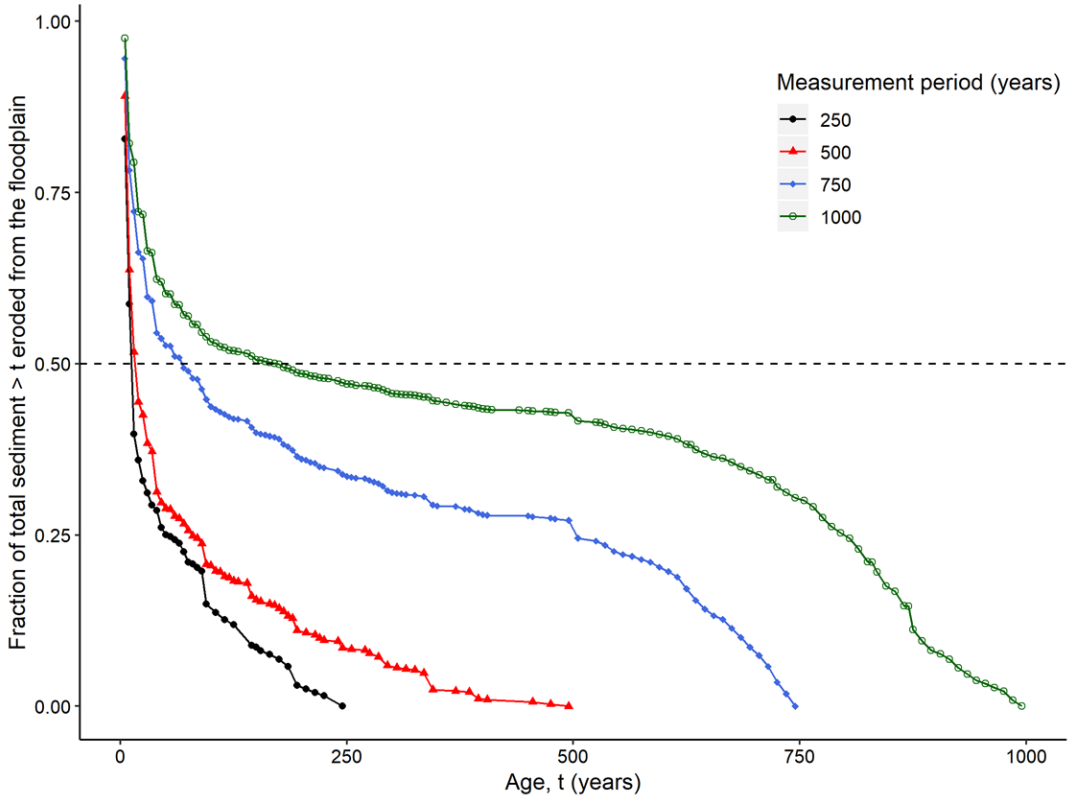

Coquet1 Unvegetated to grass scenario

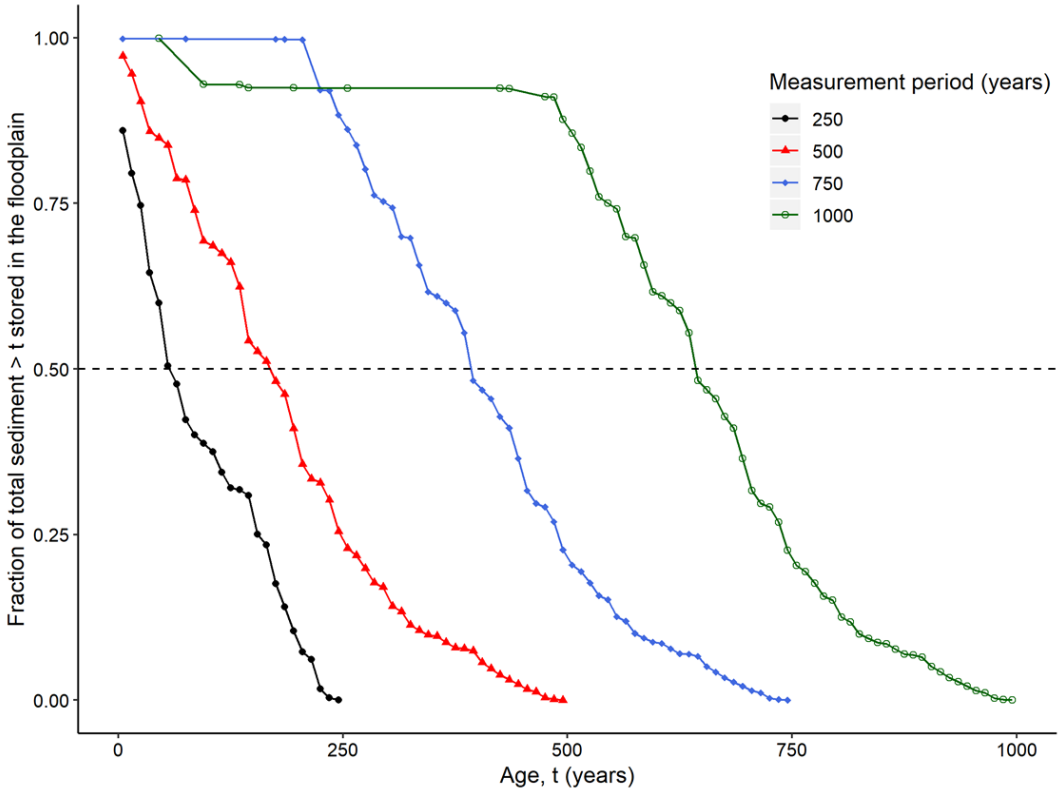

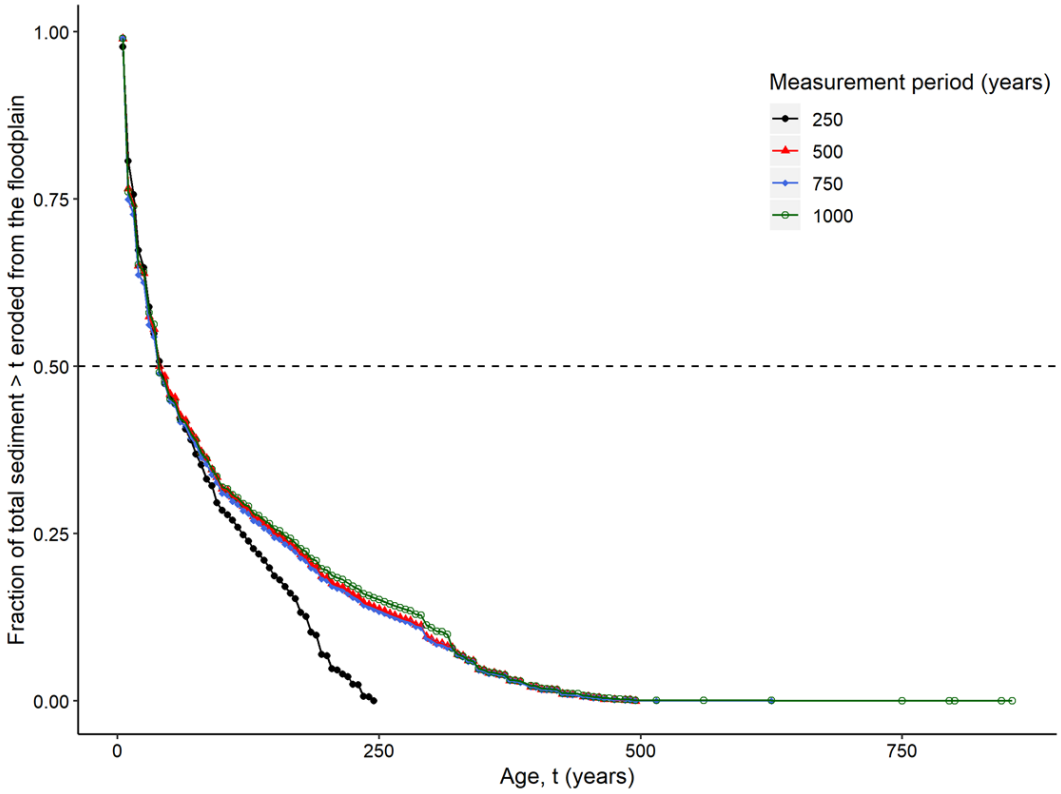

Coquet1 Grass to forest scenario

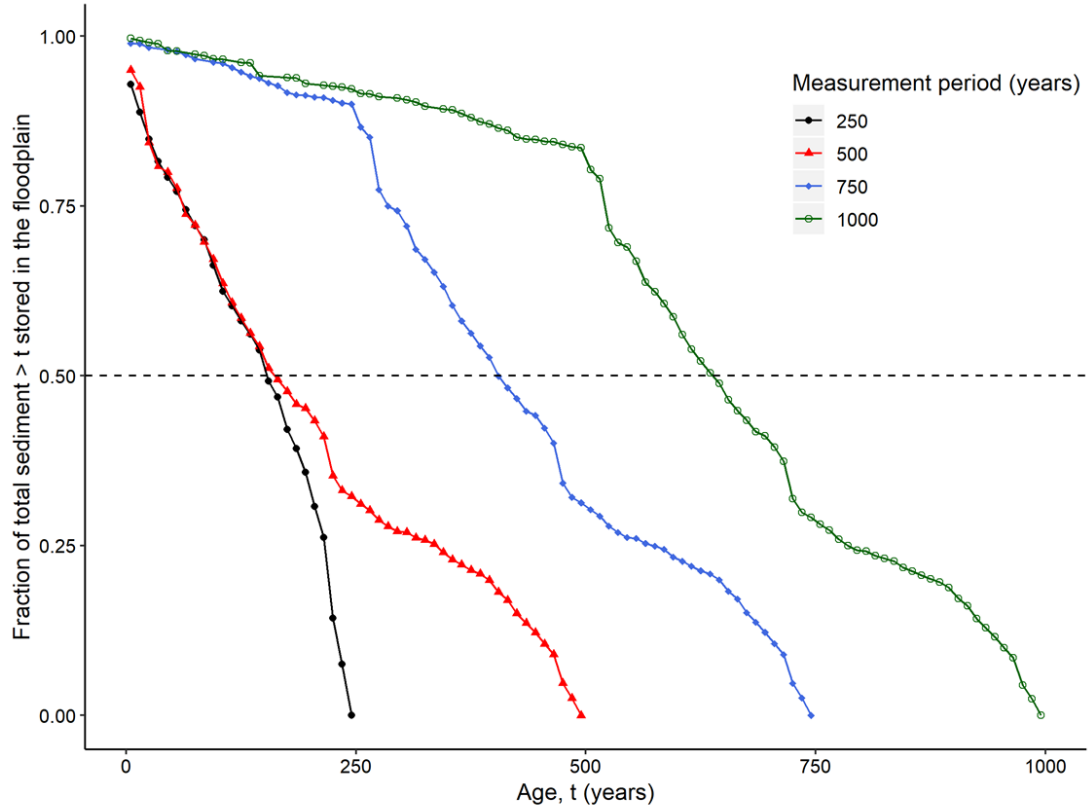

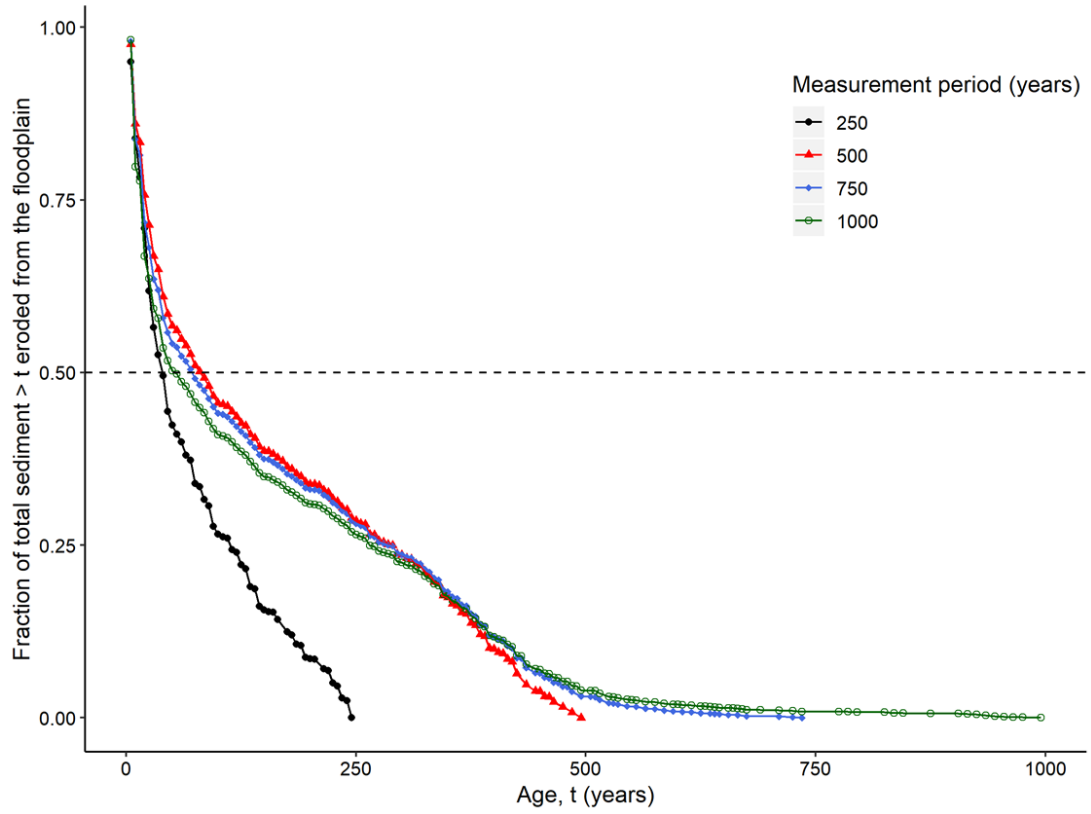

Coquet2 Decreasing flow magnitudes scenario

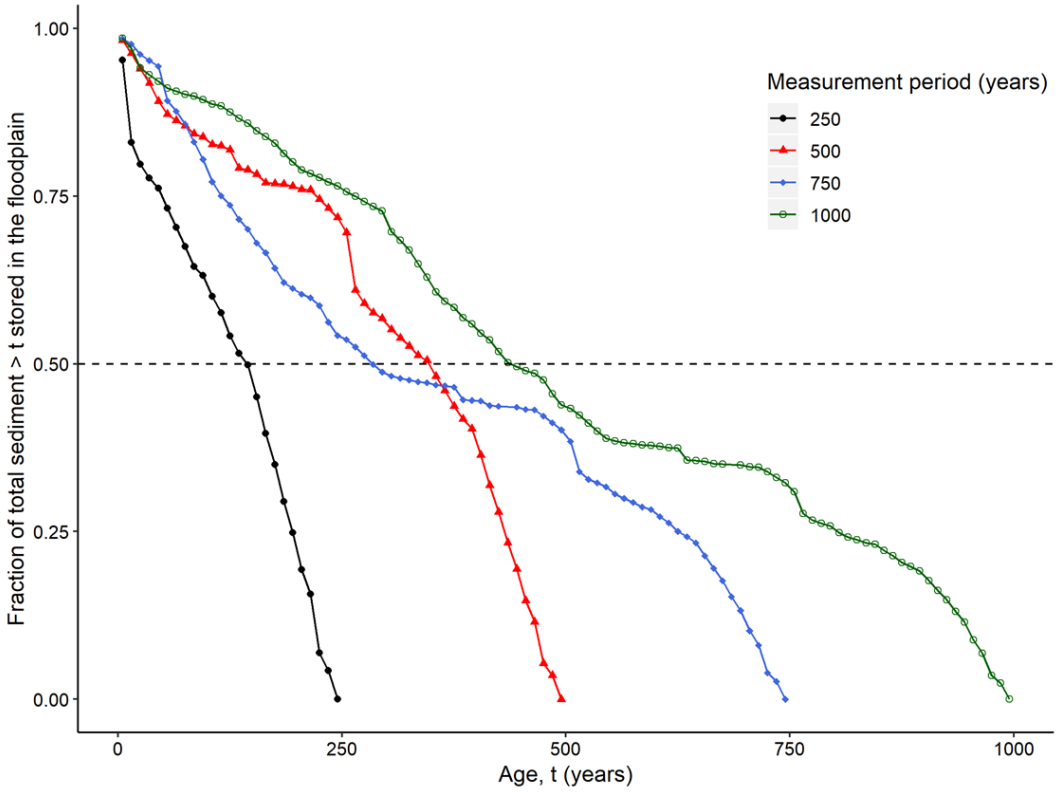

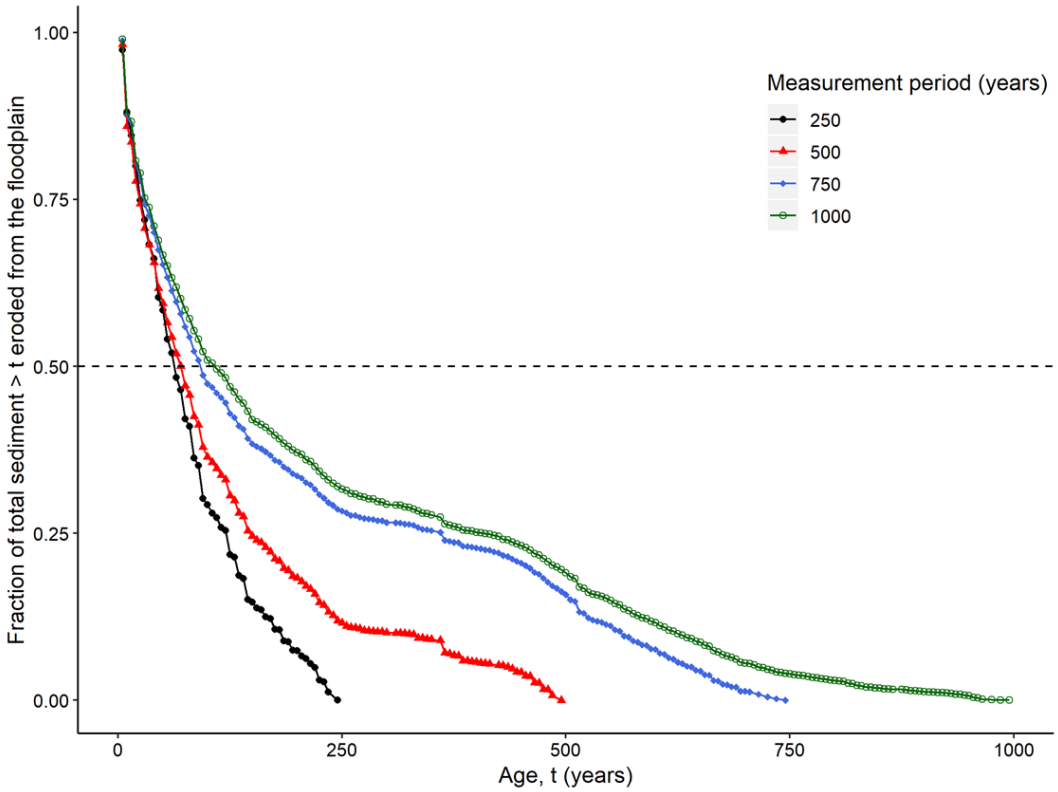

Coquet2 Increasing flow magnitudes scenario

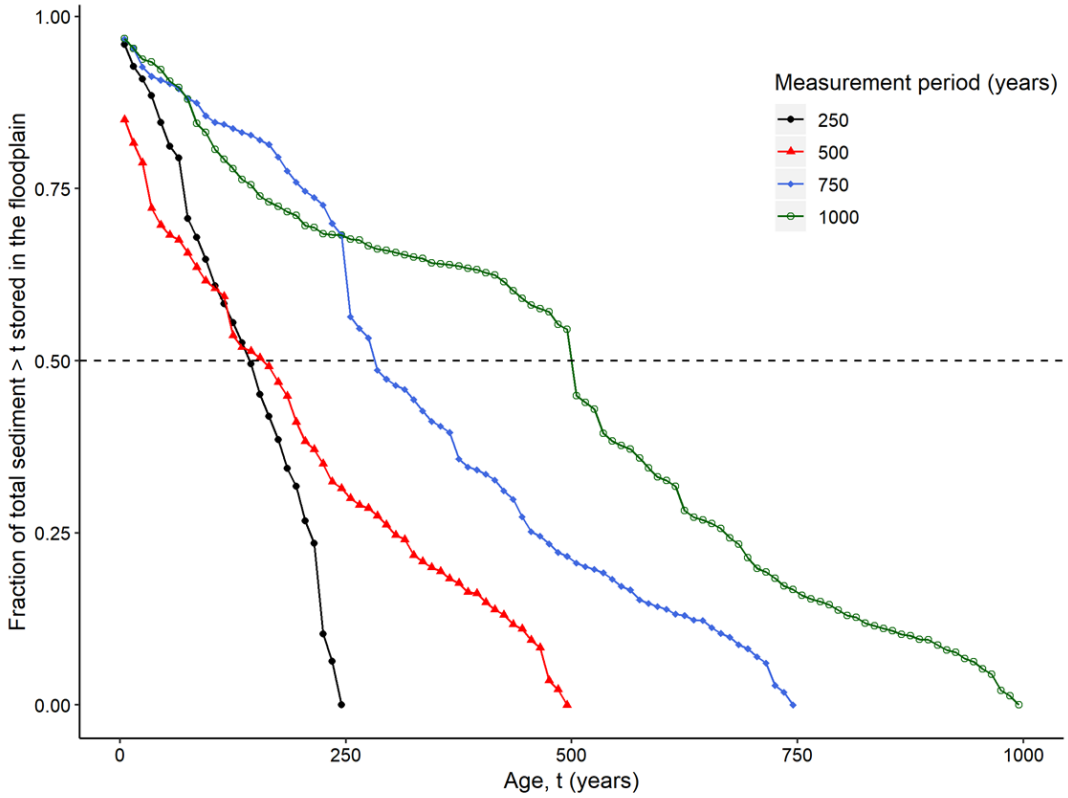

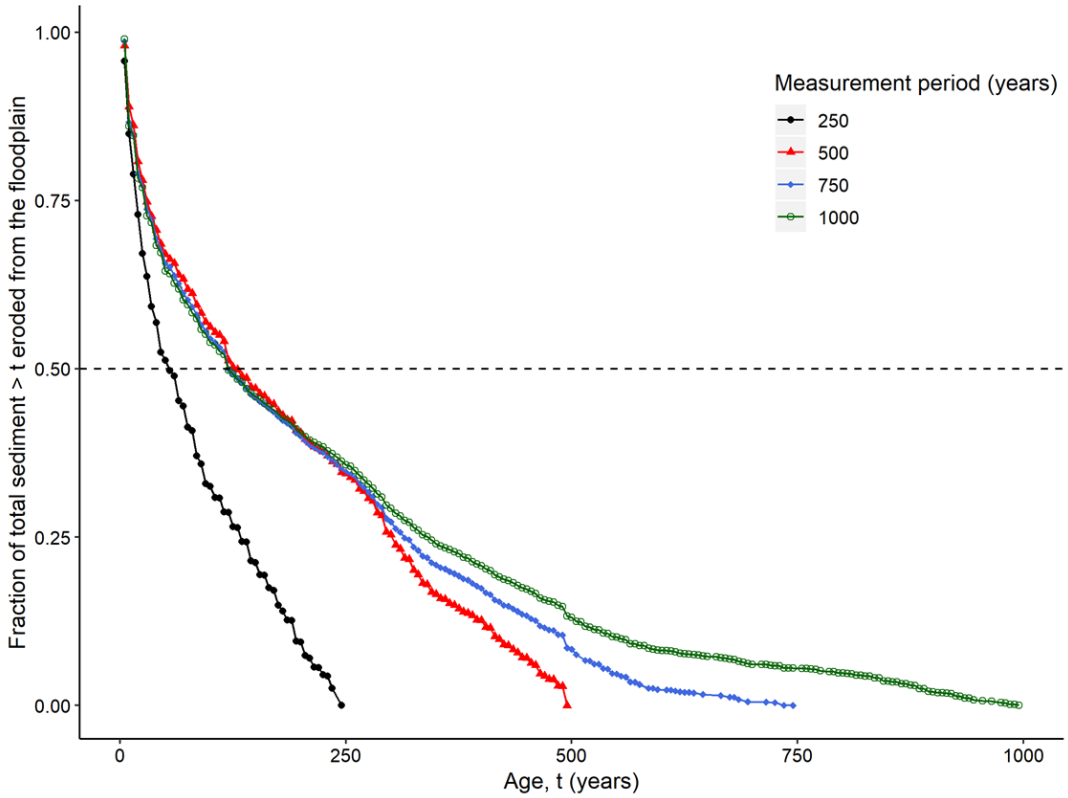

Coquet2 Forest to grass scenario

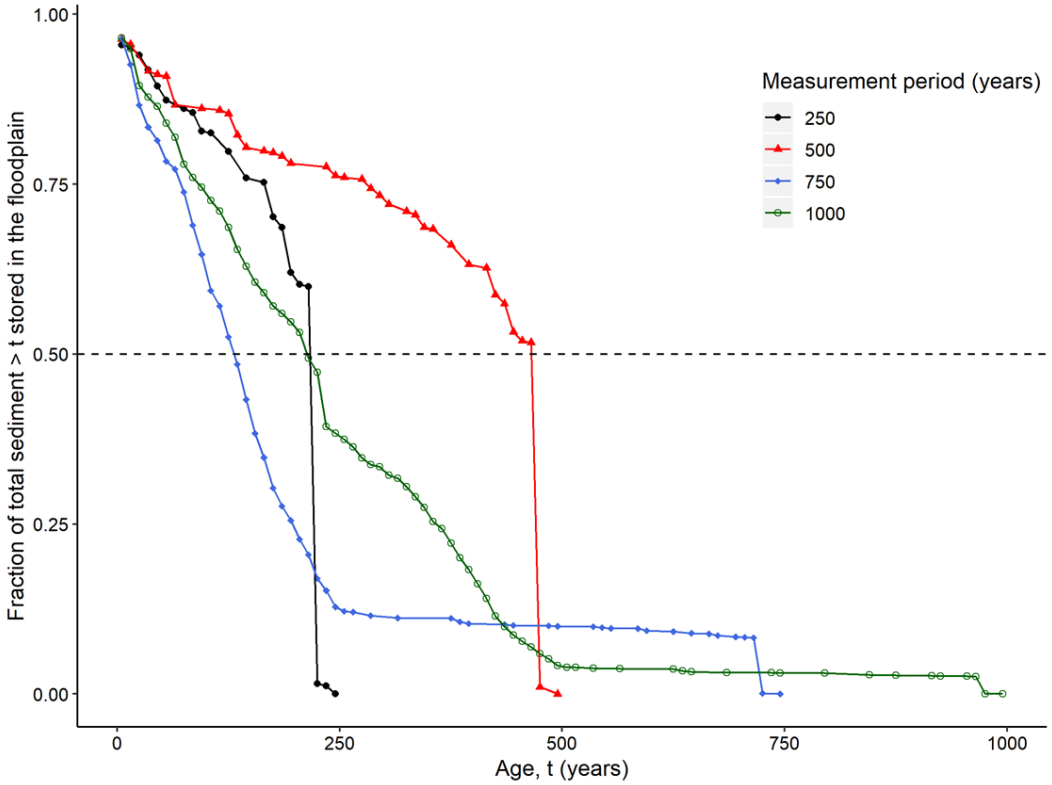

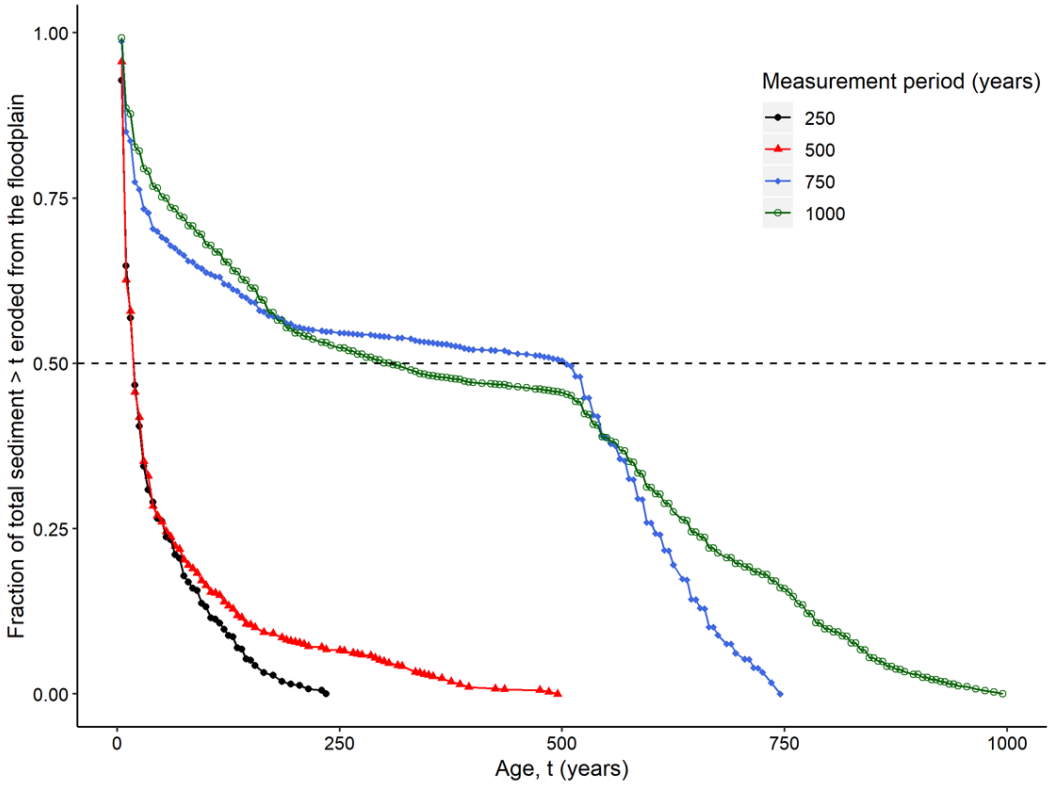

Coquet2 Unvegetated to grass scenario

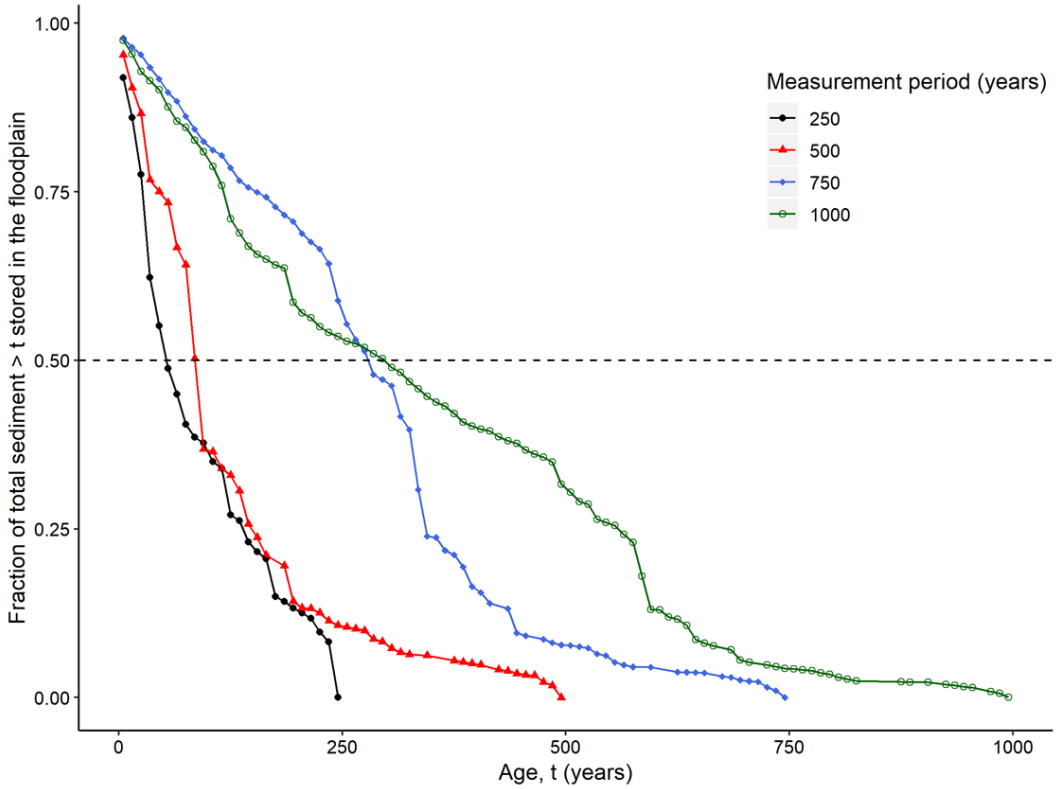

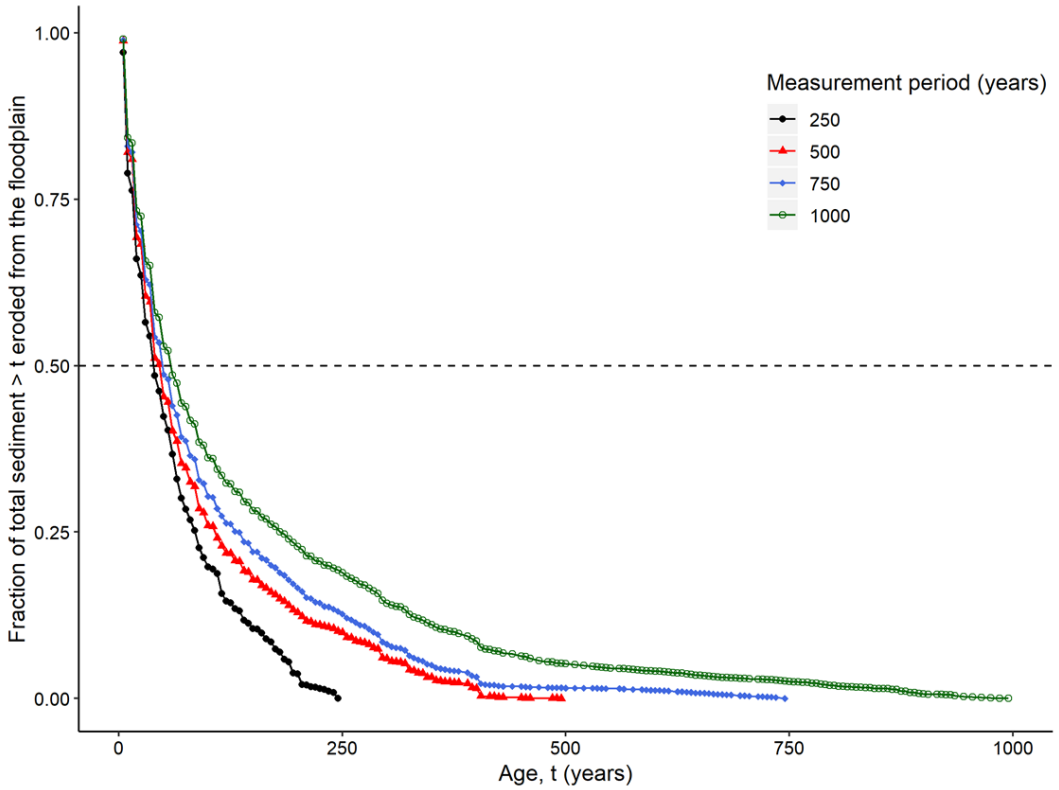

Coquet2 Grass to forest scenario

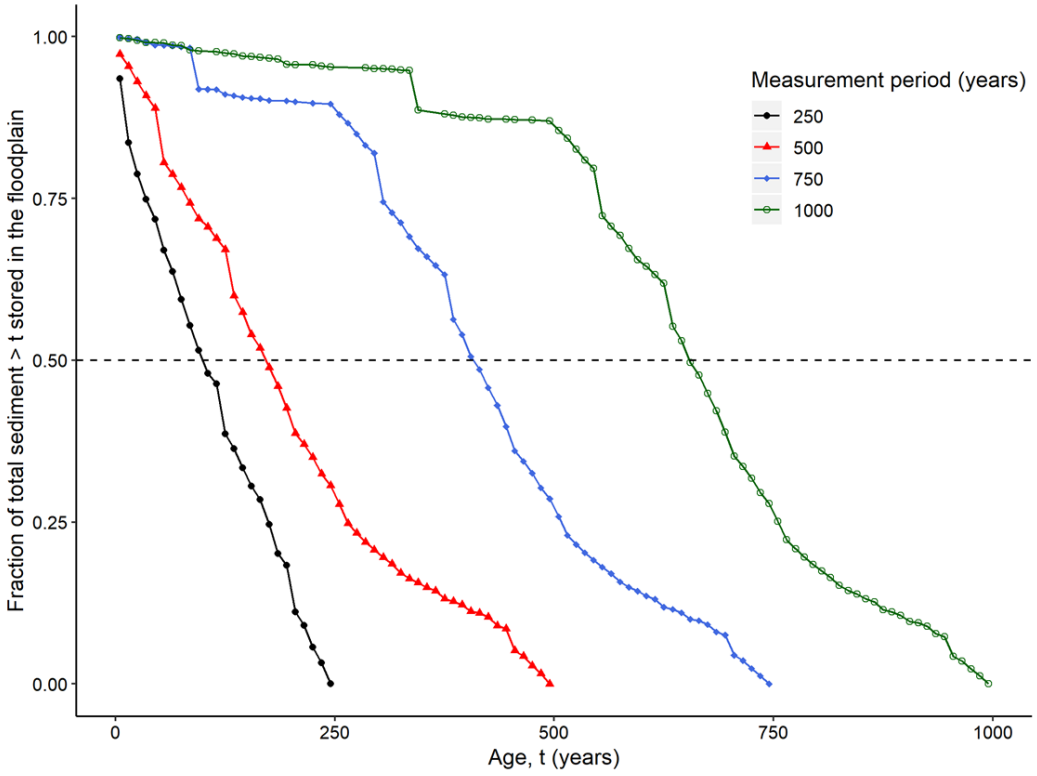

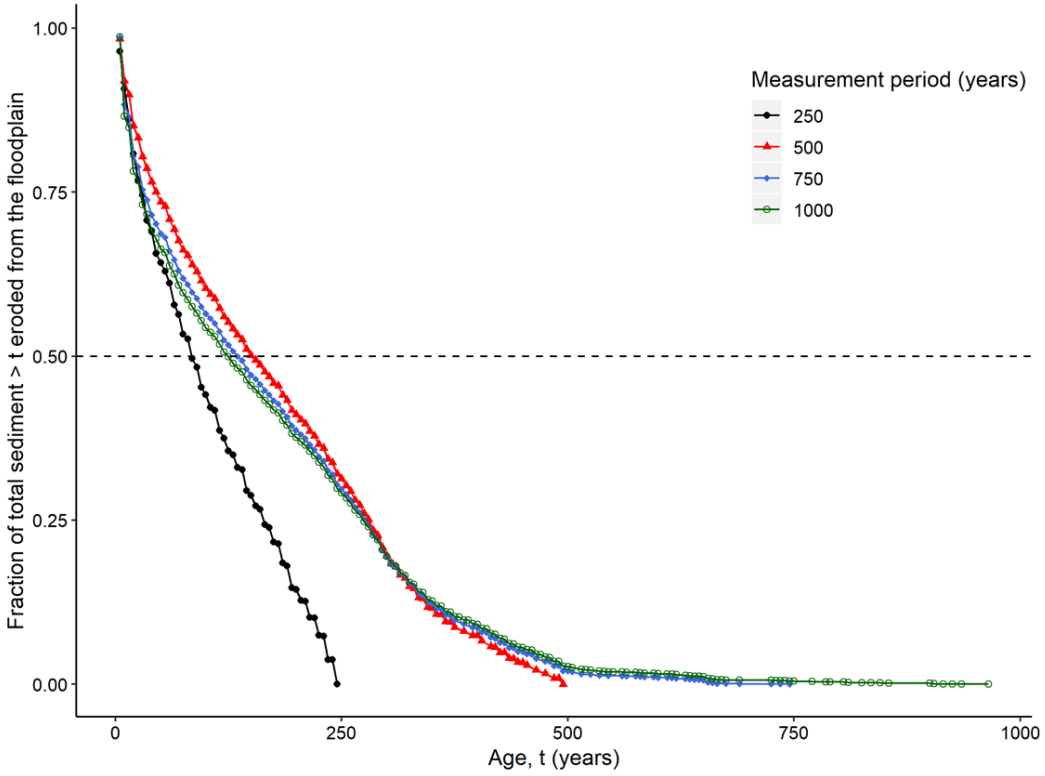

Dane Decreasing flow magnitudes scenario

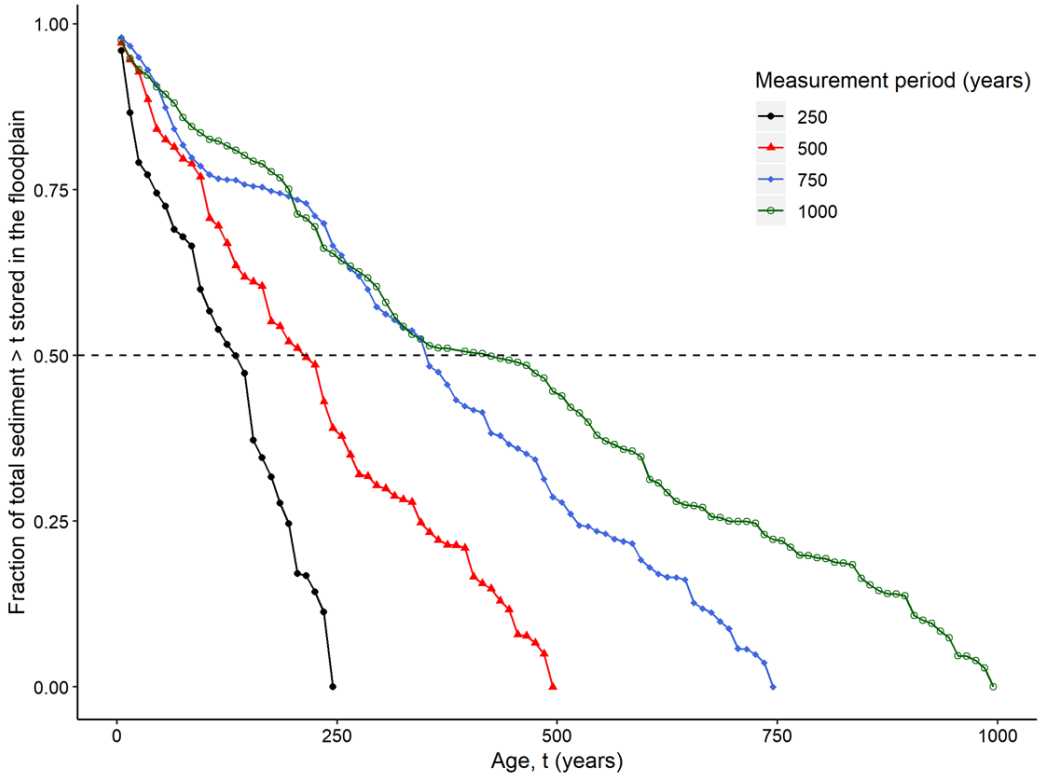

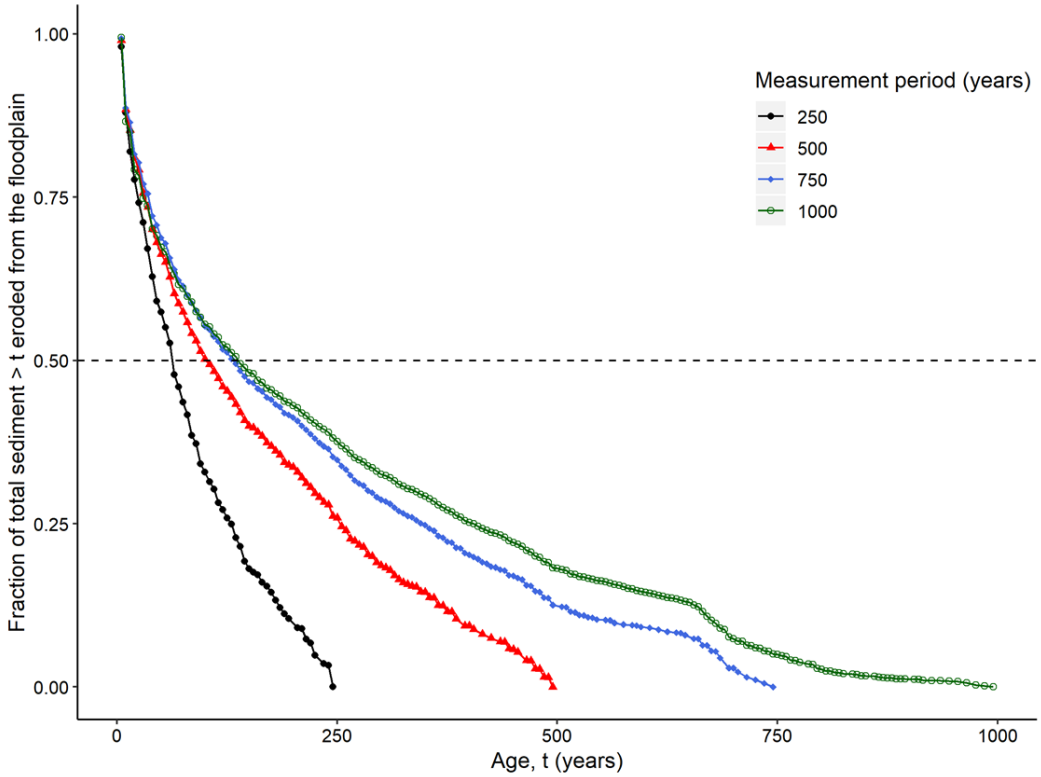

Dane Increasing flow magnitudes scenario

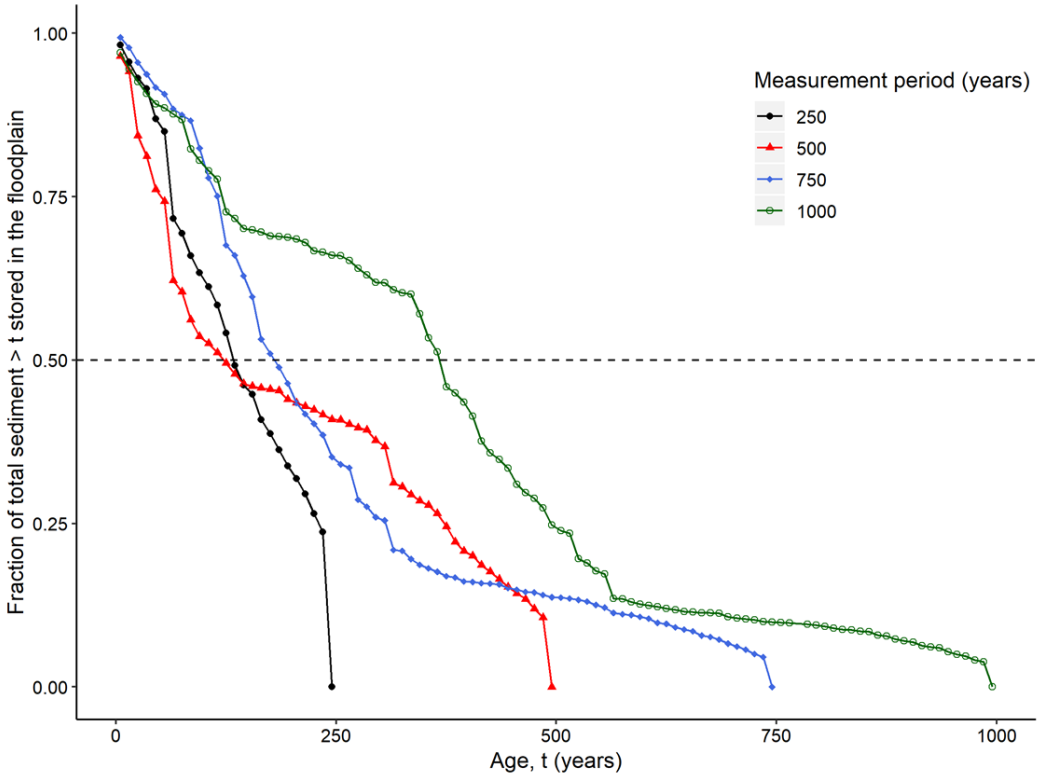

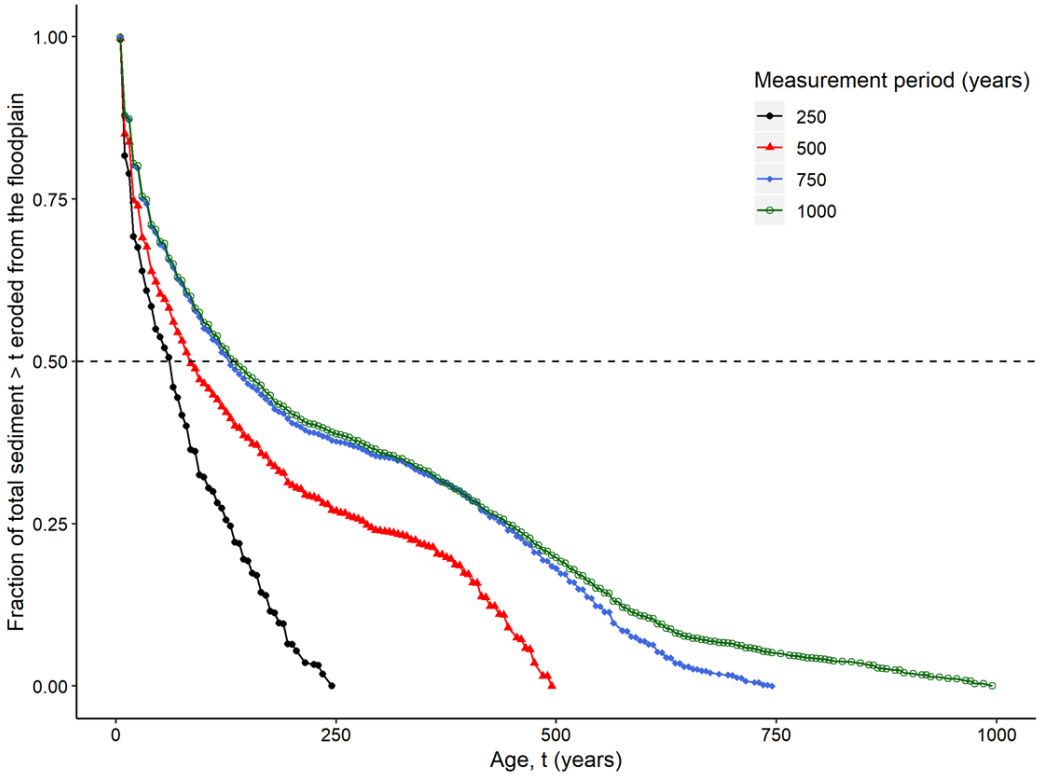

Dane Forest to grass scenario

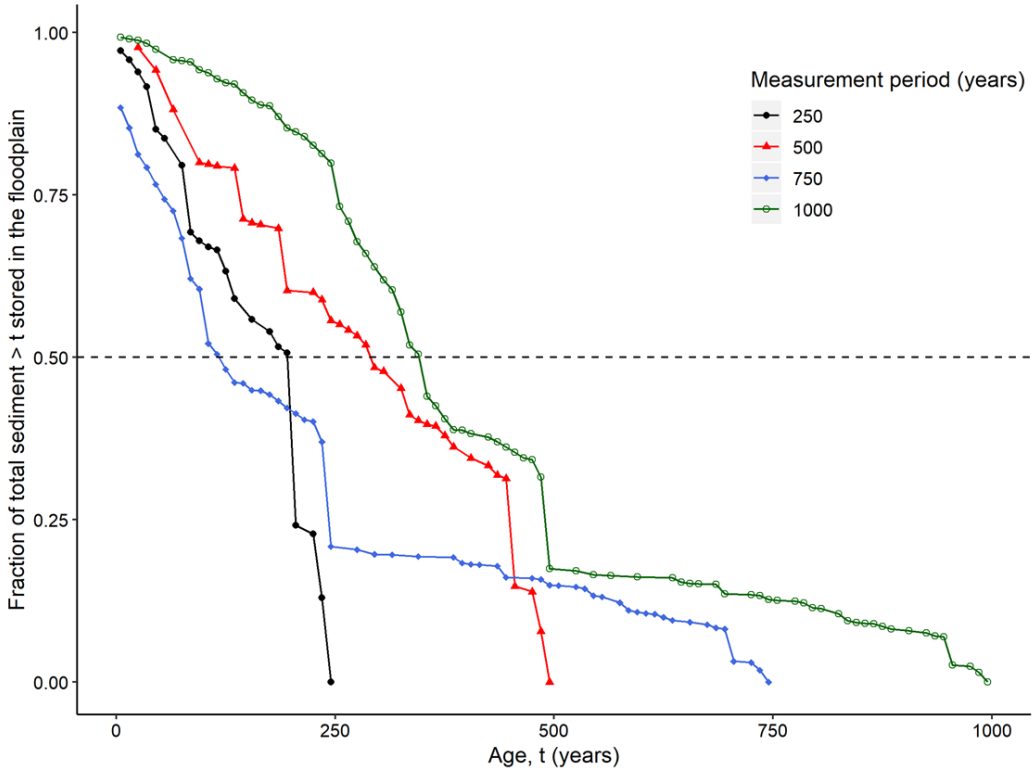

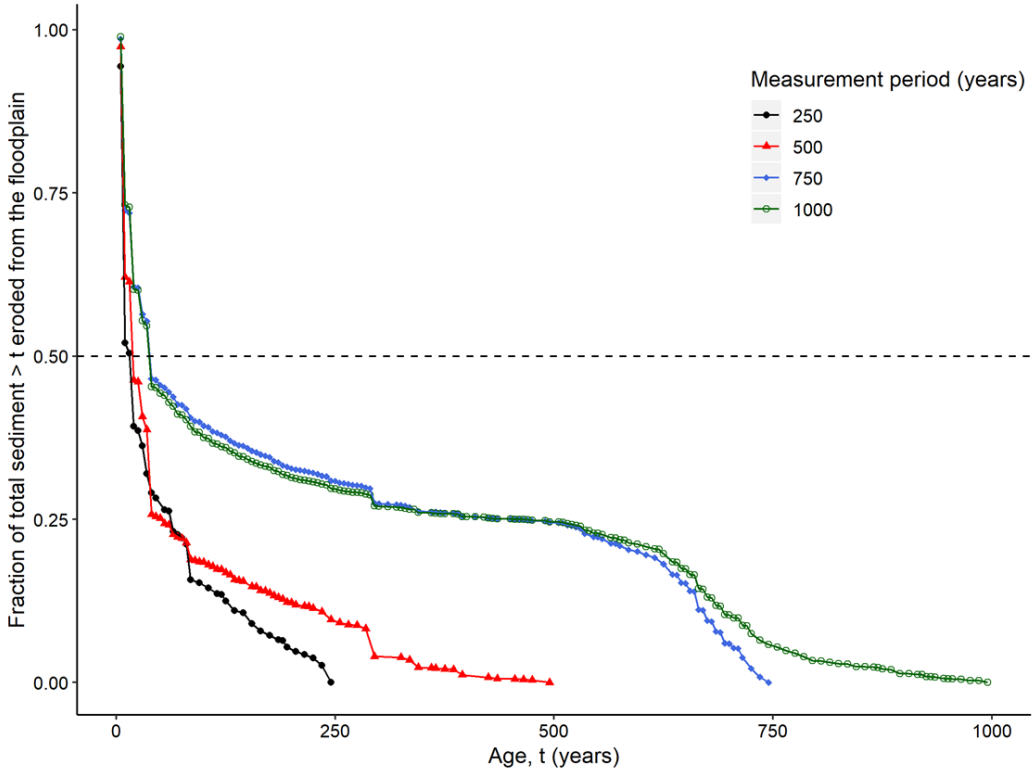

Dane Unvegetated to grass scenario

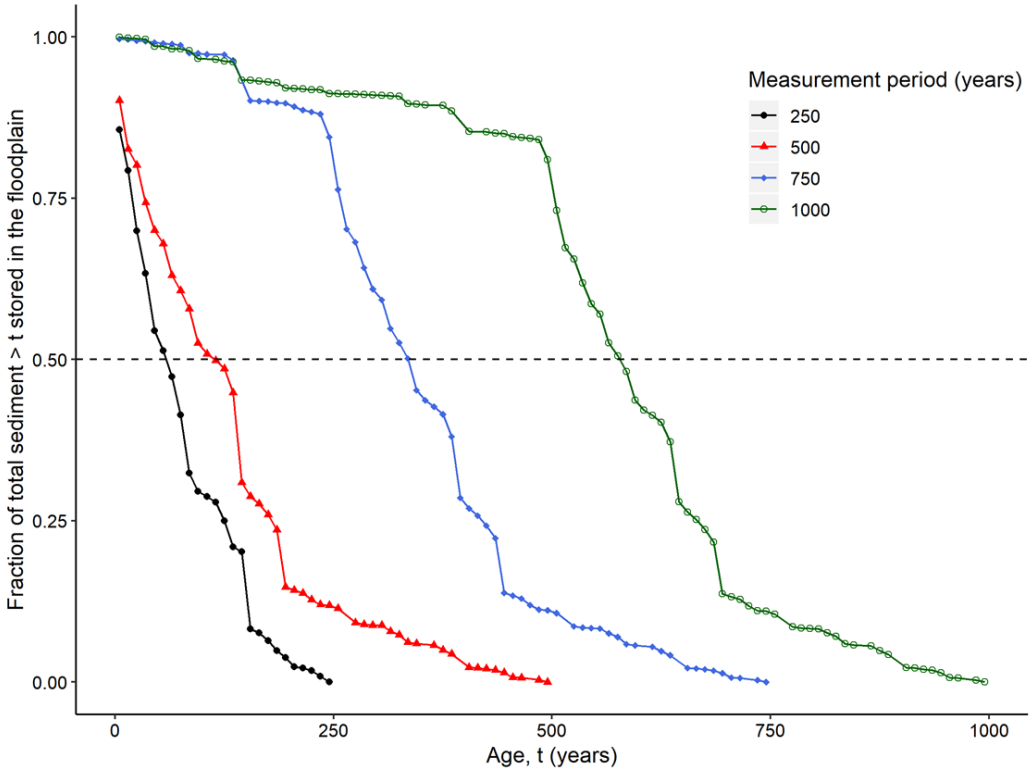

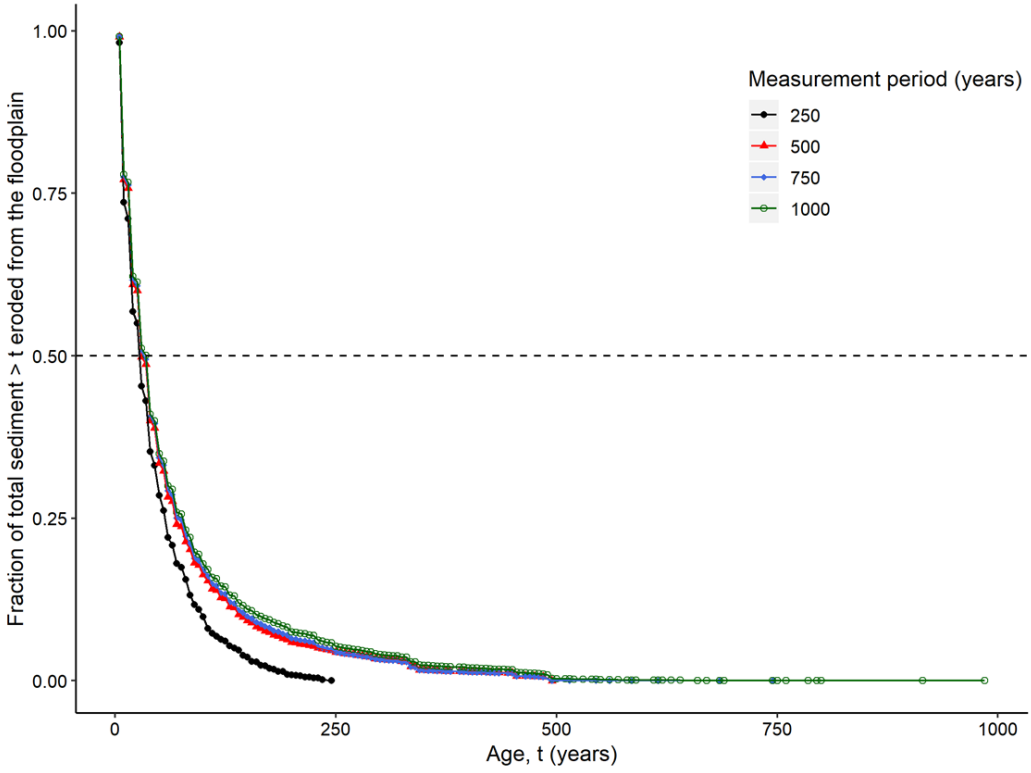

Dane Grass to forest scenario

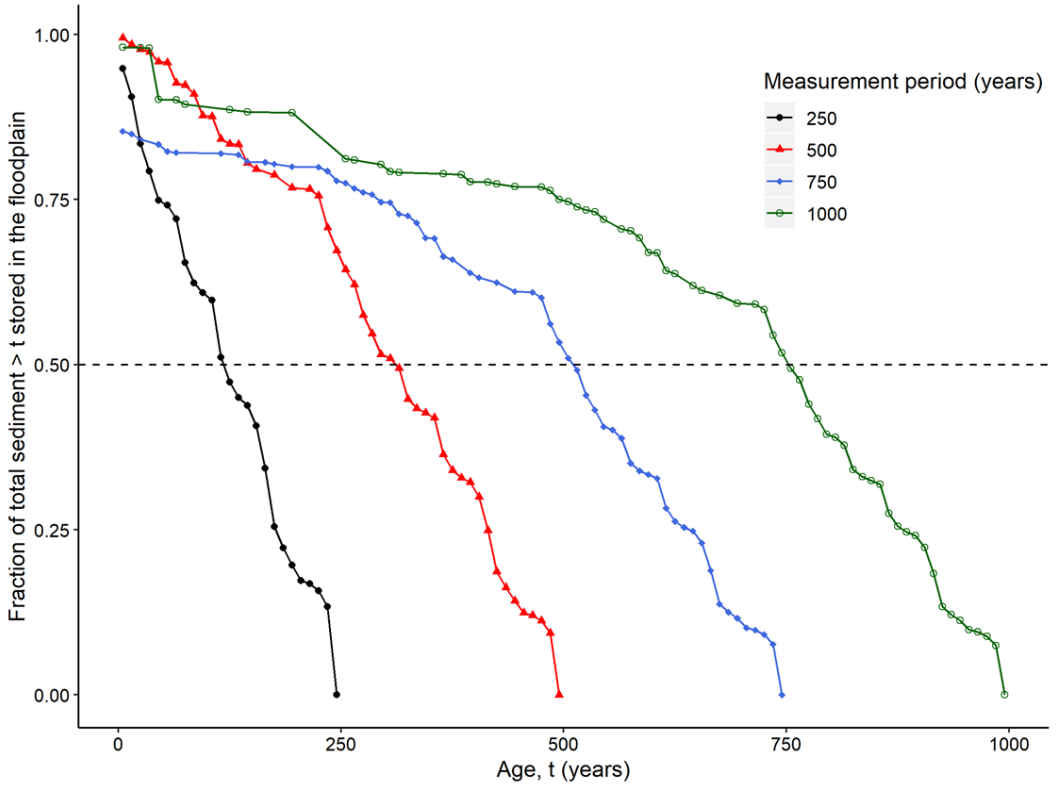

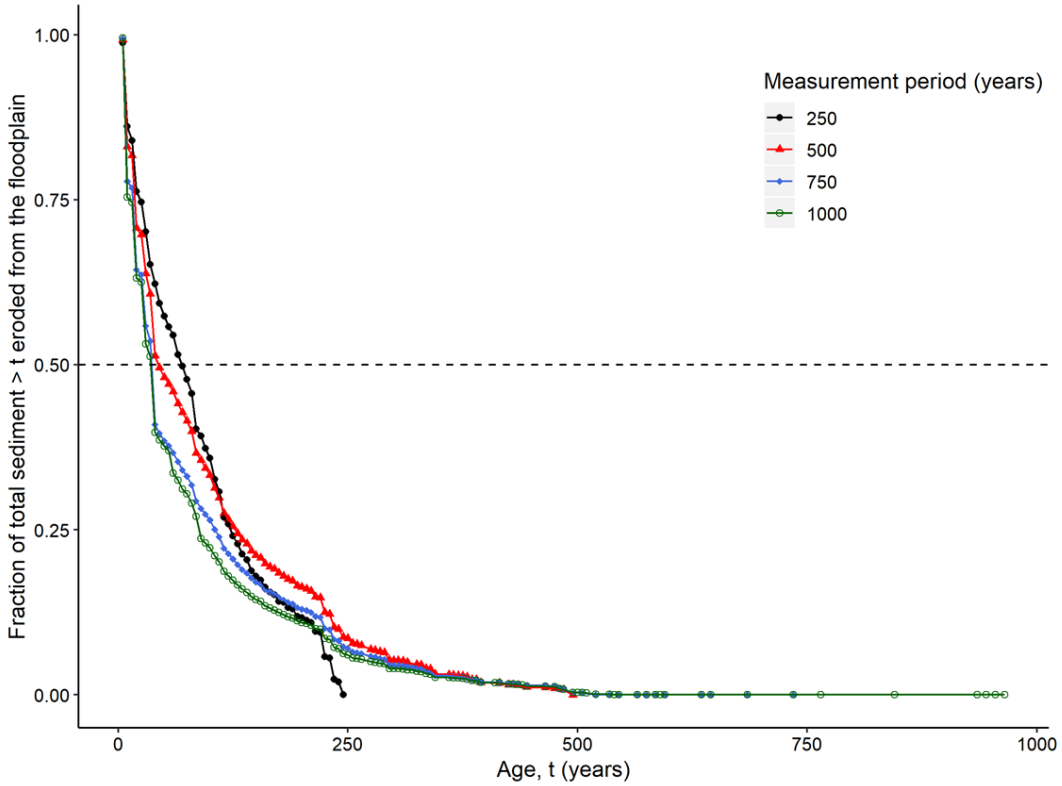

B: Age histograms and cumulative distribution functions for all simulations with best-fit distribution curves

The age distributions from the fifteen simulations of Chapter 5 were found to be best fit by either Weibull or Gaussian functions. The following two figures show the PDFs and CDFs of the floodplain surface ages after 1000 years of simulation, with the fitted Weibull or Gaussian function as a red curve. Best-fit functions were determined via comparison of goodness-of-fit statistics (Cramer-von-Mises, Anderson-Darling test, Kolmogorov-Smirnov test, Akaike's Information Criterion and Bayesian Information Criterion) with other non-linear functions (exponential, Pareto, lognormal and Gamma) using the "fitdistrplus" library (Delignette-Muller et al. 2019) in R.

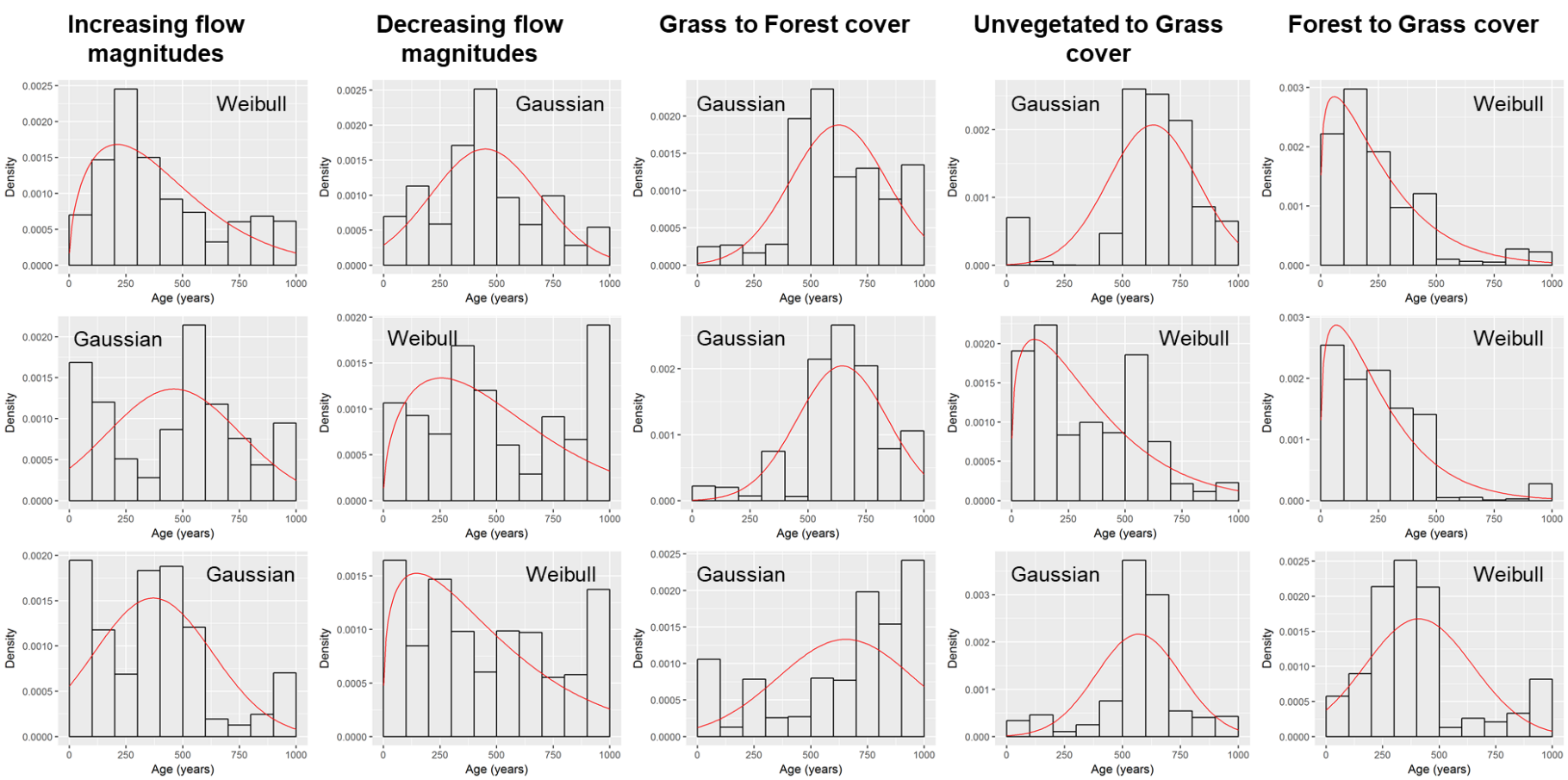
Increasing flow magnitudes
Decreasing flow magnitudes
Grass to Forest cover
Unvegetated to Grass cover
Forest to Grass cover
Weibull
Gaussian
Gaussian
Gaussian
Weibull
Gaussian
Weibull
Gaussian
Weibull
Gaussian
Gaussian
Weibull
Gaussian
Weibull
Density
Age (years)

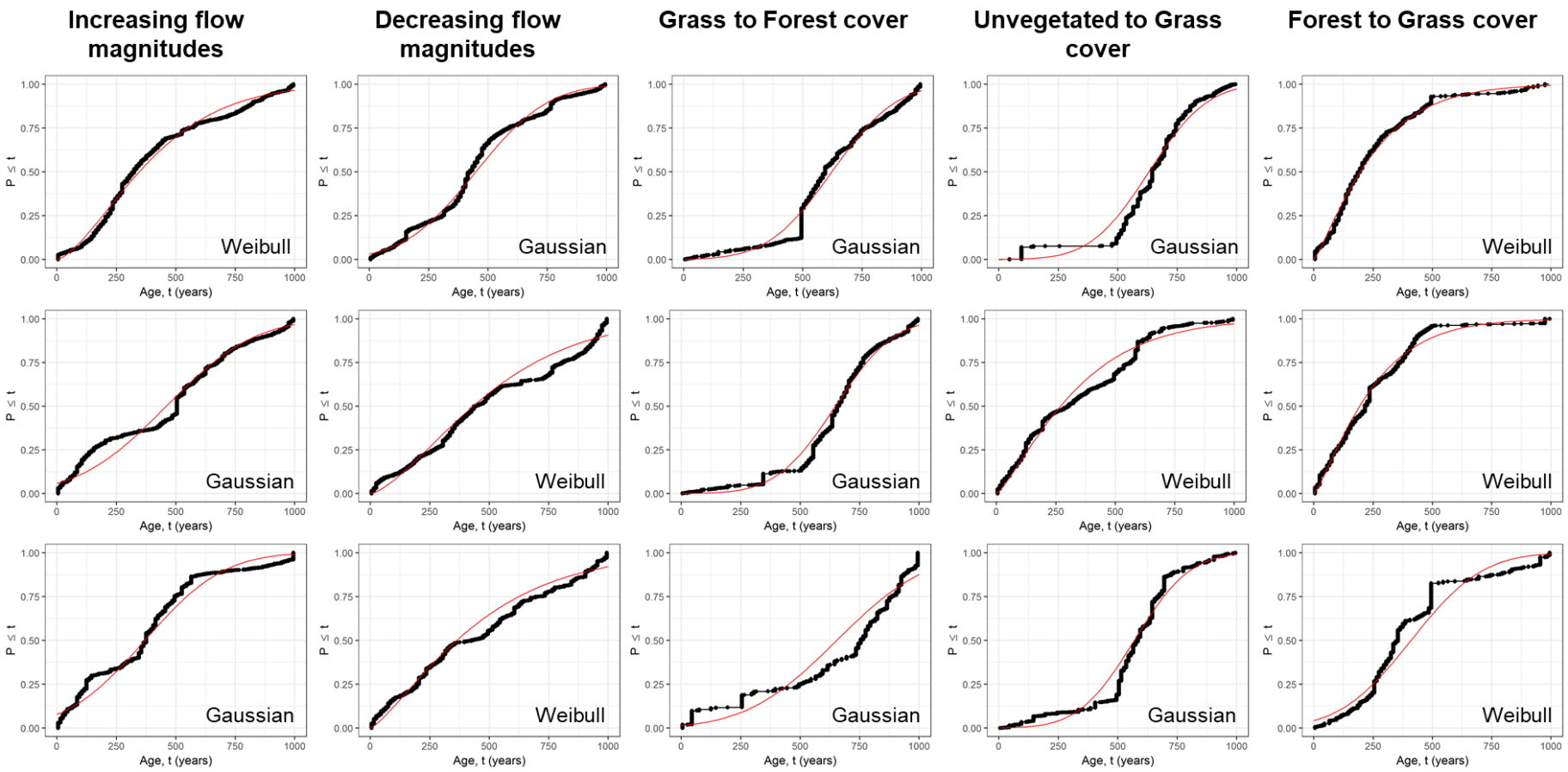
Increasing flow magnitudes
Decreasing flow magnitudes
Grass to Forest cover
Unvegetated to Grass cover
Forest to Grass cover
P ≤ t
Age, t (years)
Weibull
Gaussian
Gaussian
Gaussian
Weibull
Gaussian
Weibull
Gaussian
Weibull
Gaussian
Gaussian
Gaussian
Weibull
Gaussian
Weibull